

**Strategies for Peptide-Induced Formation
of
Noble-Metal Nanoparticles
and Investigation of their Antibacterial Efficacy**

Inauguraldissertation

zur

Erlangung der Würde eines Doktors der Philosophie

vorgelegt der

Philosophisch-Naturwissenschaftlichen Fakultät

der Universität Basel

von

Conelious Pfumbidzai

Aus Chipinge (Zimbabwe)

Basel, 2011

Genehmigt von der Philosophisch-Naturwissenschaftlichen Fakultät der Universität Basel auf
Antrag von:

Prof. Dr. Helma Wennemers

Prof. Dr. Marcel Mayor

Basel, den 18. Oktober 2011

Prof. Dr. Martin Spiess

Dekan

Die vorliegende Arbeit wurde unter der Anleitung von Prof. Dr. Helma Wennemers in der Zeit von Oktober 2007 bis Oktober 2011 am Departement Chemie der Philosophisch-Naturwissenschaftlichen Fakultät der Universität Basel durchgeführt.

Teile dieser Arbeit wurden auf folgenden Veranstaltungen vorgestellt:

Vorträge

2010 Swiss Chemical Society Fall Meeting, ETHZ, Switzerland

2009 Bachem Research Sponsors, University of Basel, Switzerland

 Revolutionary Catalysis Meeting, University of Basel, Switzerland

2008 Revolutionary Catalysis Meeting, University of Amsterdam, Netherlands

 Revolutionary Catalysis Meeting, University of Cambridge, UK

Posterpräsentationen

2011 Platform of the Swiss Academy of Sciences, Rigi-Workshop, Switzerland

2010 National Centre of Competence in Research, University of Basel, Switzerland

2009 Swiss Chemical Society Meeting, Ecole Polytechnique Fédérale de Lausanne, Switzerland

 Swiss Nano2009 Workshop on Nanoscience, University of Basel, Switzerland

Teile dieser Arbeit wurden bereits publiziert:

C. Pfumbidzai, G. Upert, O. Braissant, A. U. Daniels, H. Wennemers, “Peptide Sequence-Activity Relationships in the Controlled Generation of Stable Silver Nanoparticles in Different Sizes in Solution: Exceptional Antibacterial Activity”, (*In preparation*).

K. Belser, T. V. Slenters, C. Pfumbidzai, G. Upert, L. Mirolo, K. M. Fromm, H. Wennemers, “Silver Nanoparticle Formation in Different Sizes Induced by Peptides Identified within Split-and-Mix Libraries”, *Angew. Chem. Int. Ed.*, **2009**, 48, 3661. (*qualified as an important scientific paper*)

FÜR MEINE LIEBEN ELTERN, ANNA, LAYLA UND NOYA

ACKNOWLEDGEMENTS

Special thanks to my supervisor Professor Dr. Helma Wenemmers for giving me the opportunity to carry out my PhD studies in the fascinating realm of noble metal nanoparticles under her guidance and support. Her advice in the challenges of nano-research, as well as the freedom and trust that she bestowed on me were invaluable in the successful completion of my PhD studies. I am additionally thankful for the opportunity and financial support which she provided that enabled me to attend and deliver presentations at national and international conferences. My sincere gratitude also goes to Prof. Dr. Marcel Mayor for having accepted the role of external examiner for my PhD thesis defence.

I profoundly thank Dr. Kirsten Belser for helping me kick-start the research in silver nanoparticles. I gratefully acknowledge my coworkers Dr. Gregory Upert, Ludmila Sachno, Pia Feinäugle, Paolo Clerici, Dr. Francelin Bouillere, Philipp Raschle, Dr. Benjamin Hankeln, Jörg Duschmale, Roman Erdmann, Christiane Siebler, Dr. Jin Gao, Matthias Messerer, Dr. Rolf Kramer, Carsten Kroll, Dr. Gaetano Angelici, Patrick Wilhelm, Dr. Yukihiro Arakawa, Annette Bahlinger, Robert Kastl, Alexander Kaeslin for their help and friendship. Many thanks to Dr. Gregory Upert, Ludmila Sachno and Pia Feinäugle for our interesting scientific discussions in nanoscience research.

In addition, I am very thankful to Dr. Michel Calame, Dr. Gregory Upert, Dr. Yukihiro Arakawa, Pia Feinäugle and Ludmila Sachno for their help in proof-reading my thesis.

My sincere gratitude to Prof. Dr. Christian Schönenberger and his team Dr. Michel Calame, Jon Agustsson and Dr. Claire Barrett for precious collaboration in the analyses of AgNPs. In addition, I acknowledge Prof. Dr. Alma U. Daniels and Dr. Olivier Braissant for the successful collaboration in the antibacterial studies of AgNPs. Furthermore, I am very thankful to Dr. Marc Creus and Narasimha Rao Uda for the collaboration also in the antibacterial studies of AgNPs.

The scientific and technical staff helped me to use different analytical techniques and analysis methods. Notably, Dr Laurent Marot, for XPS measurements and the analysis of the results; and all coworkers at the ZMB Basel including Daniel Mathys, Evi Bieler, Marcel Düggelein, Gianni Morson for the SEM facilities. I am thankful for their help.

My life is really fascinating because of the love and care from my lovely wife Anna Baumann. I will always cherish her unwavering commitment, patience and support in uplifting my spirit during my PhD studies. Furthermore, I extend my sincere gratitude to my parents-in-law Roland Baumann and Monica Alder for their social, financial and moral support during the pursuit of my PhD studies.

My parents have been always a source of inspiration and their constant advice and unconditional support in various forms gave me the energy and courage to work towards the success of my PhD research.

I extend my sincere gratitude to the University of Basel and department of Chemistry, the European Union Revolutionary Catalysis Project and Bachem for funding my PhD research.

Finally, like in every research, I experienced challenges but thanks be to God that his divine help was always there for me to overcome the challenges as well as helping me to keep focused without losing hope.

CONTENTS

I. INTRODUCTION.....	1
1.0 General Introduction to Metal-Nanoparticles	1
1.1 Application of Silver Nanoparticles	2
1.1.1 Silver Nanoparticles as Catalysts	3
1.1.2 Silver Nanoparticles as Antibacterial Agents	5
1.1.3 AgNPs in Cancer Therapy	7
1.1.4 Application of AgNPs in Electronic Devices	9
1.2 Synthesis of AgNPs	10
1.2.1 Top-down Strategy for the Generation of AgNPs	11
1.2.1.1 Chemical Vapor Deposition	11
1.2.1.2 Laser Ablation	12
1.2.2 Bottom-up Strategy for the Generation of AgNPs	13
1.2.2.1 Photochemical Method of Generating AgNPs	20
1.2.2.2 Chemical Method of Generating AgNPs	23
1.2.2.2.1 Phage Display Libraries and Biomimetic Synthesis of AgNPs.....	29
1.3 Combinatorial Chemistry	36
1.3.1 One-Bead-One-Compound Synthesis	37
1.3.2 Encoded Split-and-Mix Synthesis	38
1.3.3 Screening Encoded Combinatorial Libraries	40
II. OBJECTIVE.....	42
III. REFERENCES	43
IV. RESULTS AND DISCUSSION	48
4.1 Preliminary Experiments to the Generation of Silver Nanoparticles	48
4.2 Split-and-Mix Synthesis of Encoded Library 1	50
4.3 Combinatorial Screening of Encoded Split-and-Mix Library 1	51
4.4 Ag-Nanoparticle Formation by Immobilised Peptides 2a-4b	53
4.5 Do the Free N-termini on Immobilized Peptides 2c-4c Influence the Formation of AgNPs ?	57

4.6 Ag-Nanoparticle Formation by Peptides 2d-4e in Solution Phase.....	59
4.6.1 Influence of pH on the Generation of AgNPs	61
4.6.2 Influence of Peptide Concentration on the Generation of AgNPs	67
4.6.3 The Role of the Linker in AgNP Formation.....	73
4.6.4 Could the free N-termini on Peptides Influence the Formation of AgNPs in Solution? ..	76
4.6.5 The Generation of AgNPs Without Sodium Ascorbate	79
4.6.6 Investigation of the Influence of Dehydroascorbate on the Generation of AgNPs	83
4.6.7 The Generation of AgNPs in the Presence of Inorganic Salts.....	89
4.6.8 Generation of AgNPs in Solution in the Presence of Other Peptides Identified Within the Combinatorial Screening of Library 1	96
4.7 Attachment of AgNPs on Glass Support	98
V. ANTIBACTERIAL STUDIES	101
VI. SUMMARY AND OUTLOOK.....	107
6.0 Summary	107
6.1 Outlook.....	108
VII. SPLIT-AND-MIX LIBRARY 2	110
7.1 Combinatorial Screening of Ac-Library 2 Without a Reducing Agent.....	111
7.2 Ag-Nanoparticle Formation by Peptides Immobilized on Solid Support.....	112
7.3 Combinatorial Screening of Ac-Library 2 in the Presence of Sodium Ascorbate.....	114
7.4 Ag-Nanoparticle Formation by Peptides Immobilized on Solid Support	116
7.5 Ag-Nanoparticle Formation by Peptides in Solution Phase	118
7.6 Combinatorial Screening of NH ₂ -Library 2 Without a Reducing Agent	121
7.7 Combinatorial Screening of NH ₂ -Library 2 in the Presence of Sodium Ascorbate.....	122
VIII. REFERENCES	126
IX. PLATINUM NANOPARTICLES	129
9.0 Platinum Nanoparticles (PtNPs).....	129
9.1 Combinatorial Screening of Encoded Split-and-Mix Library 2	129

X. REFERENCES	133
XI. EXPERIMENTAL.....	134
11.0 General Aspects.....	134
11.1 Analytical Equipments	134
11.2 Preparation of Amine-Terminated Glass Slides	140
11.3 AgNPs on the Surface of Tentagel Beads or Glass Slides.....	140
11.4 Biological Assays	141
11.5 General Protocols for Solid-Phase Peptide Synthesis	141
11.5.1 Functionalisation of Rink Amide AM resin.....	141
11.6 General Protocol for Ion Exchange of Peptides	143
11.7 Peptides Prepared by Solid-Phase Synthesis.....	144
11.8 Ag-Nanoparticle Formation by Solid Supported Peptides	150
11.9 Ag ⁺ Uptake Studies of Solid Supported Peptides.....	150
11.10 Solution Phase Experiments of AgNP Formation in the Presence of Peptides	151
11.11 Synthesis of Library 1.....	151
11.12 Synthesis of Library 2	155
11.13 Combinatorial Screening Experiments (AgNPs).....	157
11.14 Combinatorial Screening Experiments (PtNPs)	159
XII. ABBREVIATIONS.....	160
XIII. REFERENCES	162

I.

INTRODUCTION

1.0 General Introduction to Metal-Nanoparticles

The idea of manipulating materials at the nanoscale was first laid out in 1959 by the physicist Richard Feynman.¹ However, due to lack of advanced instrumentation, it took many decades to put this idea to practical use. The last 20 years have seen the advent of sophisticated instruments that are able to investigate and manipulate matter at the nanoscale. This has greatly enhanced the understanding of the nanoscale world.

Nanoparticles are generally regarded as materials which have at least one dimension falling within the nanoscale range (1-100 nm in diameter).^{2a-e} At this nanoscale level the ratio between the surface and inner atoms become significant. Hence the quantum effects and surface atoms with partial coordination strongly influence the physical, biological and chemical properties of these nanoparticles. These unique properties that are dependent on the size and shape of the nanoparticle greatly differ from the bulk material.^{2a-e}

In the last two decades, there has been a rapid increase in research especially on noble metal nanoparticles of different size, shape and stability for multiple applications: imaging, catalysis, electronics and the development of antimicrobial coatings.^{2a-e} Among the noble metals, gold and silver nanoparticles have gained enormous interest for their multiple applications. The fields of application of such noble metal nanoparticles include photography, catalysis, biological labeling and bioactivity, optoelectronics and surface-enhanced Raman scattering (SERS) detection.^{2e}

Metal nanoparticles display surface plasmon resonance (SPR) absorption bands in the UV-Visible region.^{2a-e} For Cu-, Ag- and AuNPs the plasmon frequencies occur in the visible region making it easier to control nanoparticles, for example in the case of their use as bioimaging agents.² In addition SPR allows better monitoring of nanoparticles during their application like in bio-

imaging.³ Surface Plasmon Resonance arises when the metal nanoparticle which has a size smaller than the wavelength of light interact with the oscillating electromagnetic field of light. The energy from the incident electromagnetic field, forces electrons in the conduction band of atoms to move back and forth with respect to the nanoparticle positive lattice (plasmon oscillations) (Figure 1). At a characteristic frequency the movement is most intense and the process resonant (surface plasmon resonance).^{2c} This frequency depends on the nature of the metal and the nanoparticle size, shape, chemical surrounding, adsorbed species on the surface and dielectric constant.

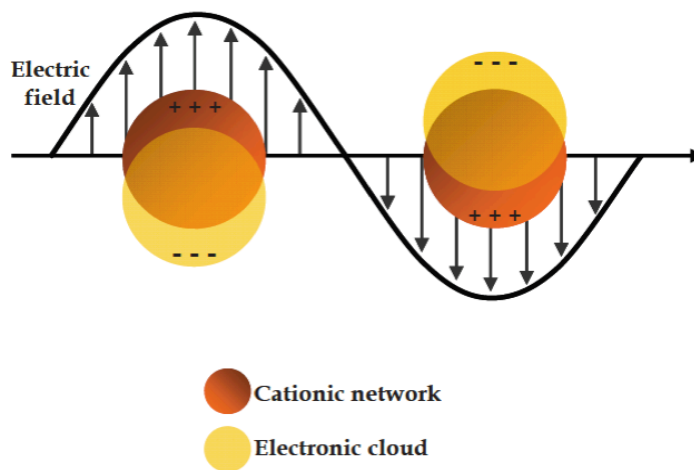


Figure 1: Schematic representation of surface plasmon (electron cloud) oscillation under the effect of an electromagnetic field

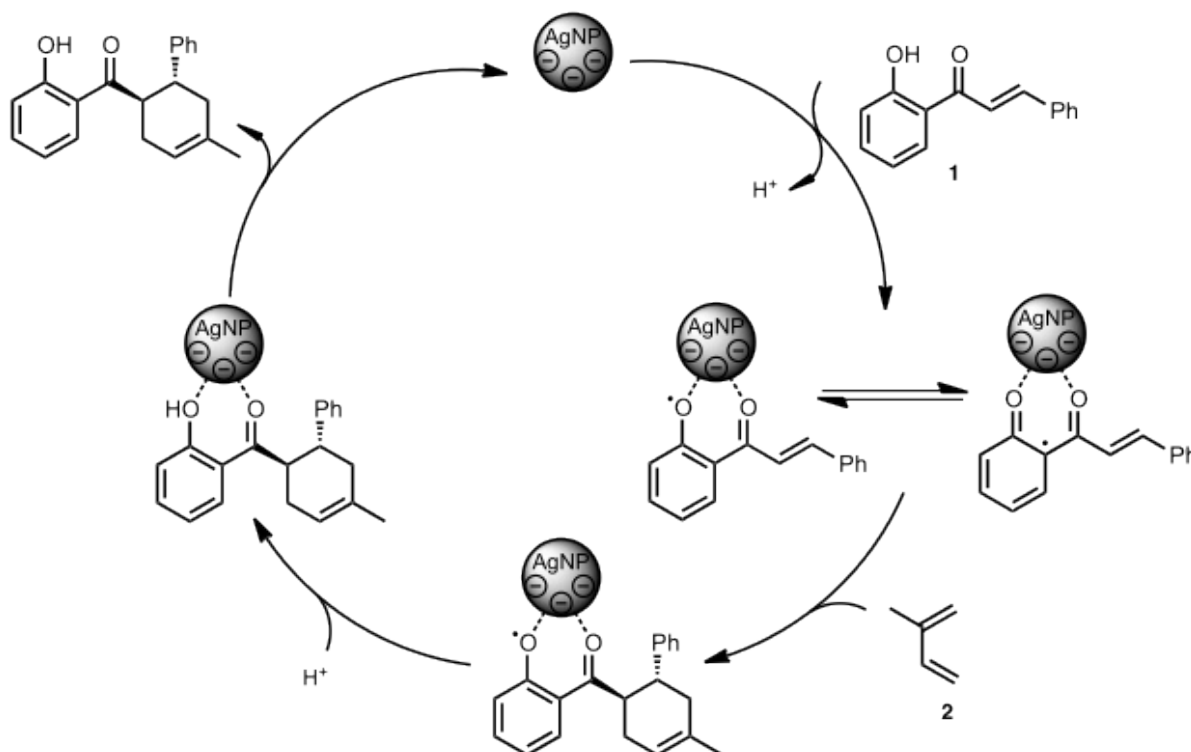
Silver nanoparticles (AgNPs) have great properties such as high extinction coefficients, sharp extinction bands, high ratio of scattering to extinction and excellent field enhancement.² Similar to other noble metal nanoparticles like gold or platinum nanoparticles, AgNPs possess very high surface to volume ratio.^{2c} Since their first synthesis, AgNPs have found their way into many different areas of science where the properties of AgNPs are utilized.⁴

1.1 Application of Silver Nanoparticles

This section highlights some of the most recent applications of AgNPs such as in catalysis, antimicrobial agents, cancer therapy and electronics.

1.1.1 Silver Nanoparticles as Catalysts

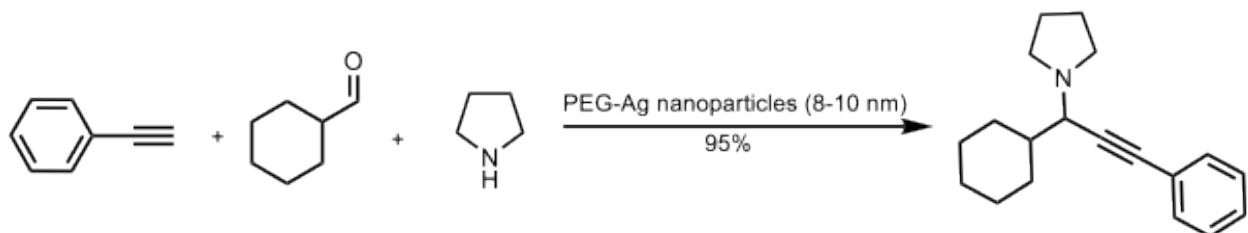
AgNPs possess a very high surface to volume ratio, which is crucial for applications as catalysts.² Porco et al. used silica-supported AgNPs as solid and recyclable catalysts for the Diels-Alder cycloadditions of 2'-hydroxychalcones and dienes in high yield and turnover number.⁵



Scheme 1: Generalized mechanism for AgNP-catalysed cycloadditions of 2'-hydroxychalcones and dienes⁵

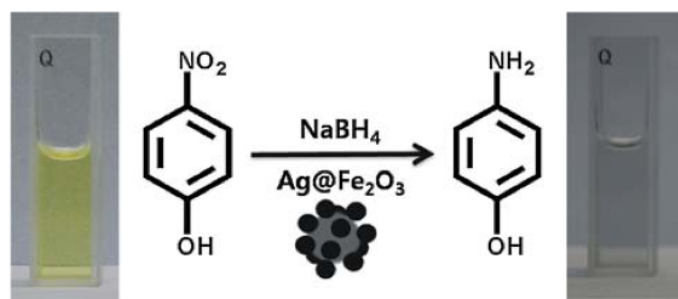
The synthetic challenges involved in this reaction are that the dienophile, 2'-hydroxychalcone **1** shows poor reactivity and it resists traditional Lewis acid promoted conditions.⁵ Such a behaviour could be due to its electron-rich nature and the tendency of undesired cyclisations to form flavanones. Furthermore, the requisite diene **2** has been found to undergo olefin isomerization and polymerization under acidic conditions which complicates chemical synthesis efforts.⁵ However, in the presence of AgNPs which may serve as catalysts by acting as electron reservoirs and shuttle electrons to the reaction site through high selective activation of 2'-hydroxychalcones for cyclo-additions (Scheme 1).⁵

The versatility of AgNPs as catalysts is also shown in many catalytic reactions which have been published.⁶⁻⁹ For example Yan et al. applied AgNPs in the catalysis of the three-component coupling reaction of aldehyde, alkyne and amine with good to excellent yields in one reaction vessel thus saving time and materials (Scheme 2).⁶



Scheme 2: AgNP-catalysed three-component coupling reaction of aldehyde, alkyne and amine⁶

In order to address the problem of AgNP contamination by undesired products during the reduction of nitro groups, Shin et al. supported AgNPs on Fe_2O_3 (Scheme 3).⁷ By choosing the reduction of 4-nitrophenol as a reaction model, the authors reported that AgNPs supported on Fe_2O_3 could be separated from the product, 4-aminophenol after the AgNPs catalysed the reduction process. Furthermore, the catalyst could be successfully recycled and reused in 21 successive reactions with conversions of 100% within 3 min periods.



Scheme 3: Schematic representation of the performance of $\text{Fe}_2\text{O}_3@AgNPs$ as catalysts in the reduction of 4-nitrophenol to 4-aminophenol by NaBH_4 ⁷

In another study Liu et al. reported the use of AgNPs in the catalytic oxidation of CO .⁸ In addition, Hamal et al. published the photo-degradation of gaseous acetaldehyde catalysed by AgNPs.⁹

1.1.2 Silver Nanoparticles as Antibacterial Agents

The current upsurge in research on AgNPs for antibacterial applications is prompted by the rapid increase in microorganisms' resistance to conventional chemical agents.^{10a,b} At the same time as the old antibiotics are losing their effectiveness, the supply of new drugs is declining. Only two completely new classes of antibiotics have been introduced over the past 30 years.^{10b} The new classes of antibiotics approved in the last 30 years are the oxazolidinone linezolid (Zyvox, Pfizer) and the lipopeptide daptomycin (Cubicin, Cubist Pharmaceuticals) approved in 2000 and 2003 respectively (Figure 2).^{10b}

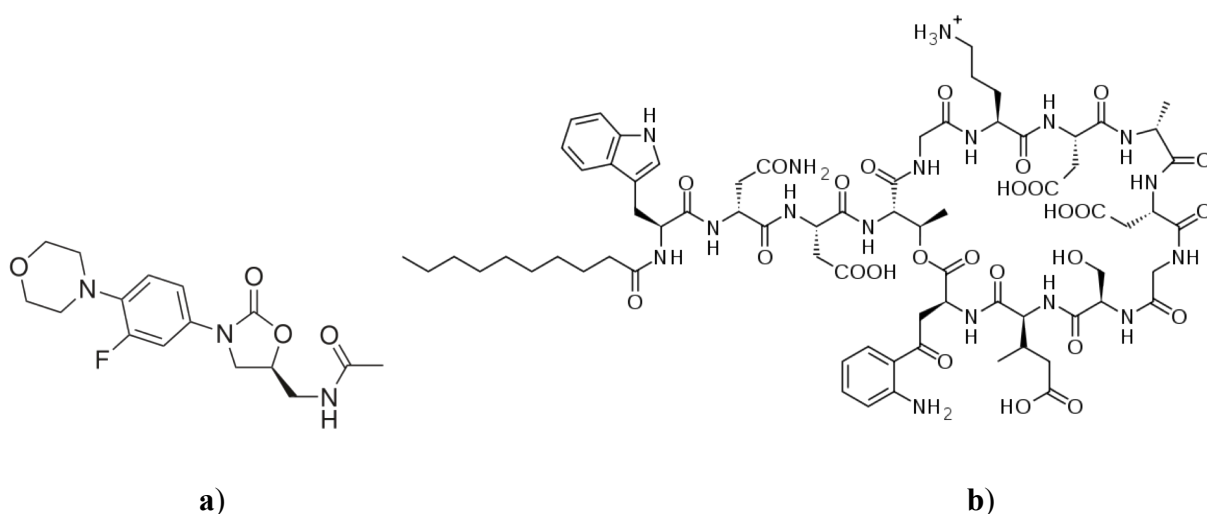


Figure 2: Two completely new classes of antibiotics oxazolidinone linezolid (a) and lipopeptide daptomycin (b) approved over the past 30 years^{10b}

This poses an urgent and important need for an alternative and efficient way to combat microbial infection before it gets out of control. One approach has been the resurgence of ionic silver containing drugs such as silver sulfadiazine and Elastoplast[®] Silver Healing[™] bandages for use as antibiotics which have been previously used for decades.^{11a,b} Unfortunately, such drugs have limited application as antimicrobial agents since they become easily inactivated upon reaction with bio-fluids.¹² In addition, the salts of silver interfere negatively with antimicrobial activity of these drugs. Recent studies indicate that many of these limitations can be overcome by using silver nanoparticles (AgNPs) which even show enhanced antimicrobial activity over ionic silver.^{11a,b} The exact mechanism of how AgNPs out-perform Ag⁺-salts in the antibacterial action is still

yet to be explored. The properties of AgNPs can be manipulated to fit dimensions which enable the nanoparticles to pass through biological membranes and affect cell physiology which has been a challenge for the conventional chemical antimicrobial agents.^{11b} The dimensions of AgNPs play a major role in their antimicrobial activity and studies showed smaller nanoparticles to have greater antimicrobial effect than larger ones.¹¹

Samsung's washing machines and refrigerators are some of the earliest consumer products where AgNPs were incorporated to kill bacteria and to prevent biofilm formation. Samsung claims that the washing machine achieves 99.9% sterilization and kills about 650 different types of bacteria. Equally important, Samsung states that the washing machine coats AgNPs onto the fabrics, which maintain antibacterial activity for up to a month.¹³

In another study Elechiguerra et al. demonstrated that AgNPs undergo a size-dependent interaction with HIV-1 with sizes of 1-10 nm attaching to the virus surface.¹⁴ Due to this interaction, AgNPs inhibited the virus from binding to host cells. Figure 3 shows the regular spatial arrangement of the attached AgNPs. Silver nanoparticles were speculated to interact with HIV-1 virus via preferential binding to the gp120 glycoprotein knobs. This hypothesis was based on the center-to-center distance between the AgNPs and the fact that the exposed sulfur-bearing residues of the glycoprotein knobs would be attractive sites for nanoparticle binding.¹⁴

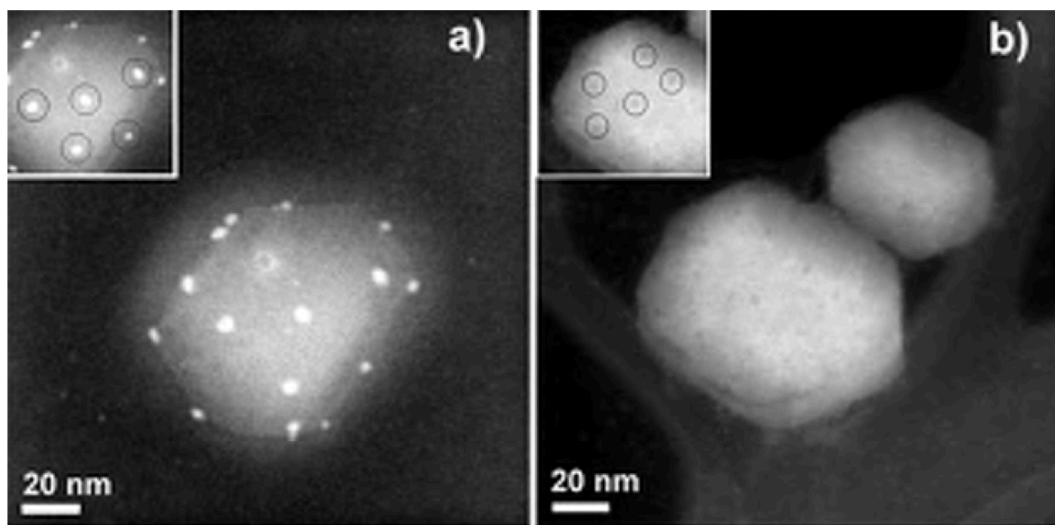


Figure 3: High angle annular dark field (HAADF) scanning transmission electron microscope image of HIV-1 virus in the presence (a) and absence (b) of silver nanoparticles¹⁴

1.1.3 AgNPs in Cancer Therapy

Recently, silver nanoparticles have been reported to have a potential to revolutionize cancer therapy.¹⁵ Cancer is an important cause of mortality worldwide and the number of people who are affected is increasing.¹⁶ There are various types of cancer and among them breast cancer is one of the major causes of death in women.¹⁷ A wide range of drugs such as doxorubicin, cisplatin, and bleomycin are currently used in the treatment of breast cancer however they display limitations like health side effects and they are not as efficient as expected.¹⁸ For this reason, it is of great interest to find novel therapeutic agents against cancer. Recent *in vitro* studies by Franco-Molina et al. showed anti-tumour activity of AgNPs through induction of apoptosis in breast cancer cells, human breast adenocarcinoma cell line (MCF) without affecting the viability of normal cells, peripheral blood mononuclear (PBM) (Figure 4).¹⁶

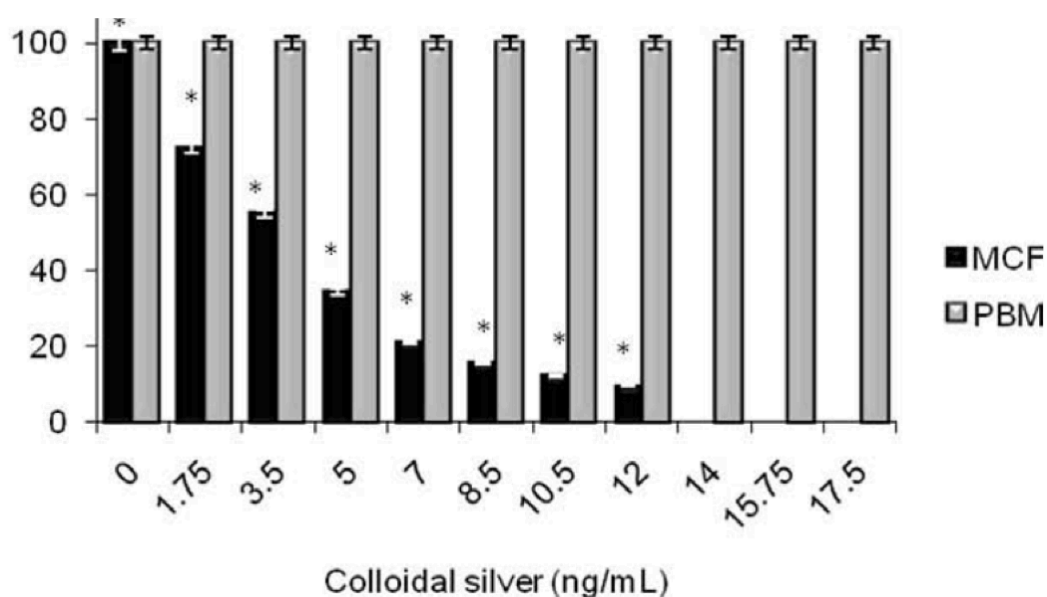


Figure 4: Cell viability of MCF-7 cell line and PBMC treated with AgNPs¹⁶

The anticancer effect of AgNPs was also reported by Asharani et al. who exposed normal human lung fibroblast cells (IMR-90) and cancerous human glioblastoma cells (U251) to different doses of AgNPs *in vitro*.¹⁹ AgNP treated cells exhibited chromosome instability and mitotic arrest in human cells. There was efficient recovery from arrest in normal human fibroblasts whereas the cancer cells ceased to proliferate. Asharani et al. theorised that the uptake of AgNPs occurred mainly through endocytosis, accompanied by a time dependent increase in exocytosis rate (Figure

5).¹⁹ Toxicity of AgNPs is mediated through intracellular calcium (Ca^{2+}) channels along with significant alterations in cell morphology and surface damages. Exposure of AgNPs to the cells resulted in the down regulation of major actin binding protein, filamin.¹⁹ The nanoparticles induced stress which resulted in an increase (up regulation) in the number of metallothionein and heme oxygenase-1 genes. Cancer cells were susceptible to damage without recovery from AgNP stress. Silver nanoparticles were found to be acting through intracellular calcium channels and chromosomal damages, either directly or through activation of catabolic enzymes. The signaling cascades are believed to play key roles in cytoskeleton deformations and ultimately to inhibit cell proliferation (Figure 5).¹⁹

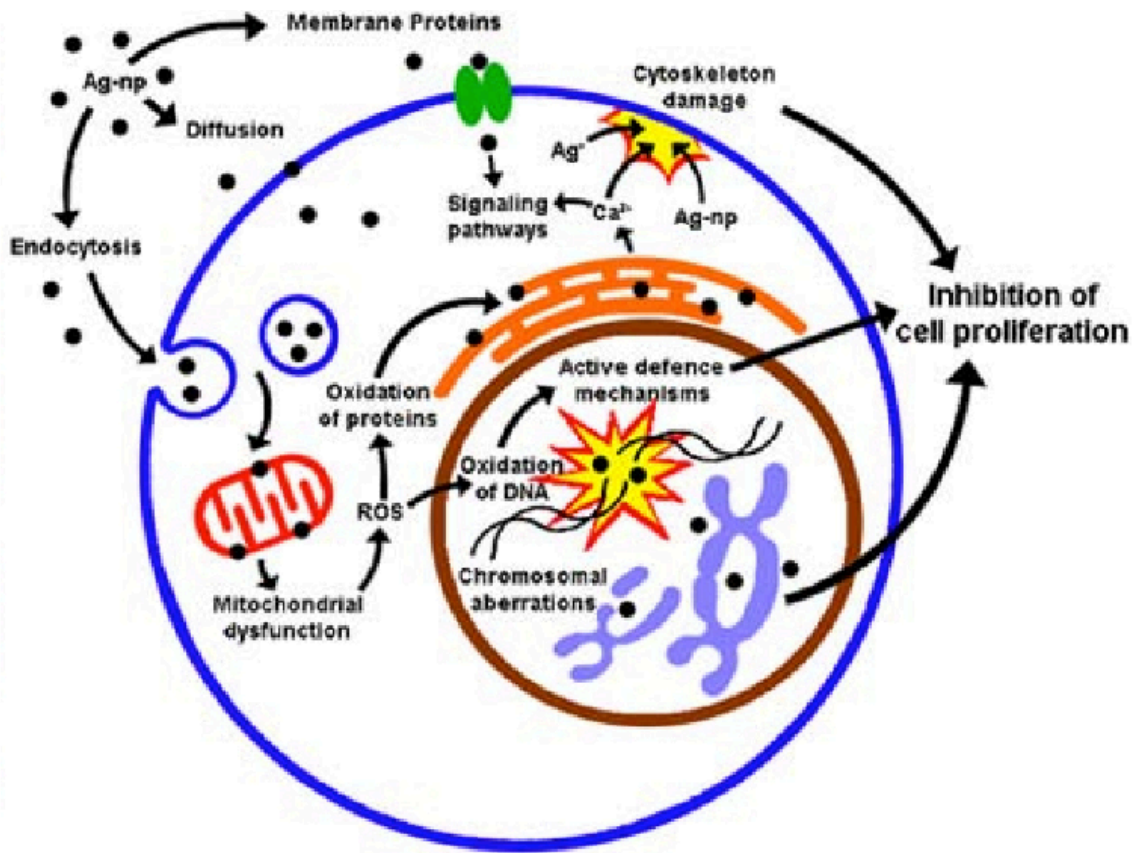


Figure 5: The proposed mechanism of AgNP toxicity based on the experimental data obtained by Asharani et al.¹⁹

1.1.4 Application of AgNPs in Electronic Devices

AgNPs are used in various electronics due to the nanoparticles' high electrical and thermal conductivity along with their enhanced optical properties. Direct ink writing is associated with problems such as nozzle clogging. In addressing this problem, Lewis et al. demonstrated the omni-directional printing of flexible, stretchable and bridging microelectrodes using concentrated AgNP inks which could readily flow through micro-nozzles in air without clogging the nozzle (Figure 6).²⁰

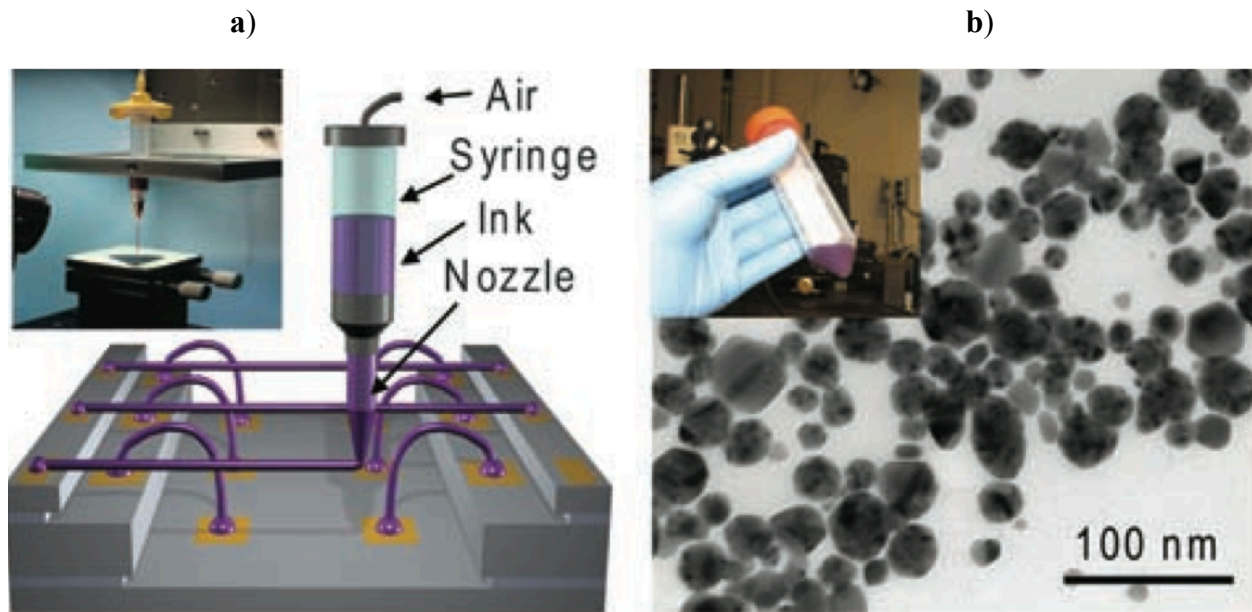


Figure 6: Schematic diagram illustrating omni-directional printing and optical image of apparatus used (a). Transmission electron microscopy image of the synthesized silver nanoparticles and optical image of the concentrated ink (b)²⁰

Also, recently Chan et al. published a direct approach to optimise the performance of organic field-effect transistors (OFETs).²¹ Their finding has potential to address the general severe degradation of organic electronic memory devices.²¹ Chan et al. found that the memory window of OFETs widens with increasing AgNPs layer thickness (Figure 7). A maximum window of 90 V was achieved for 5 nm AgNPs and the on/off current ratio decreased from 10^5 to 10 when the AgNPs layer thickness increased from 1 to 10 nm (Figure 7).²¹

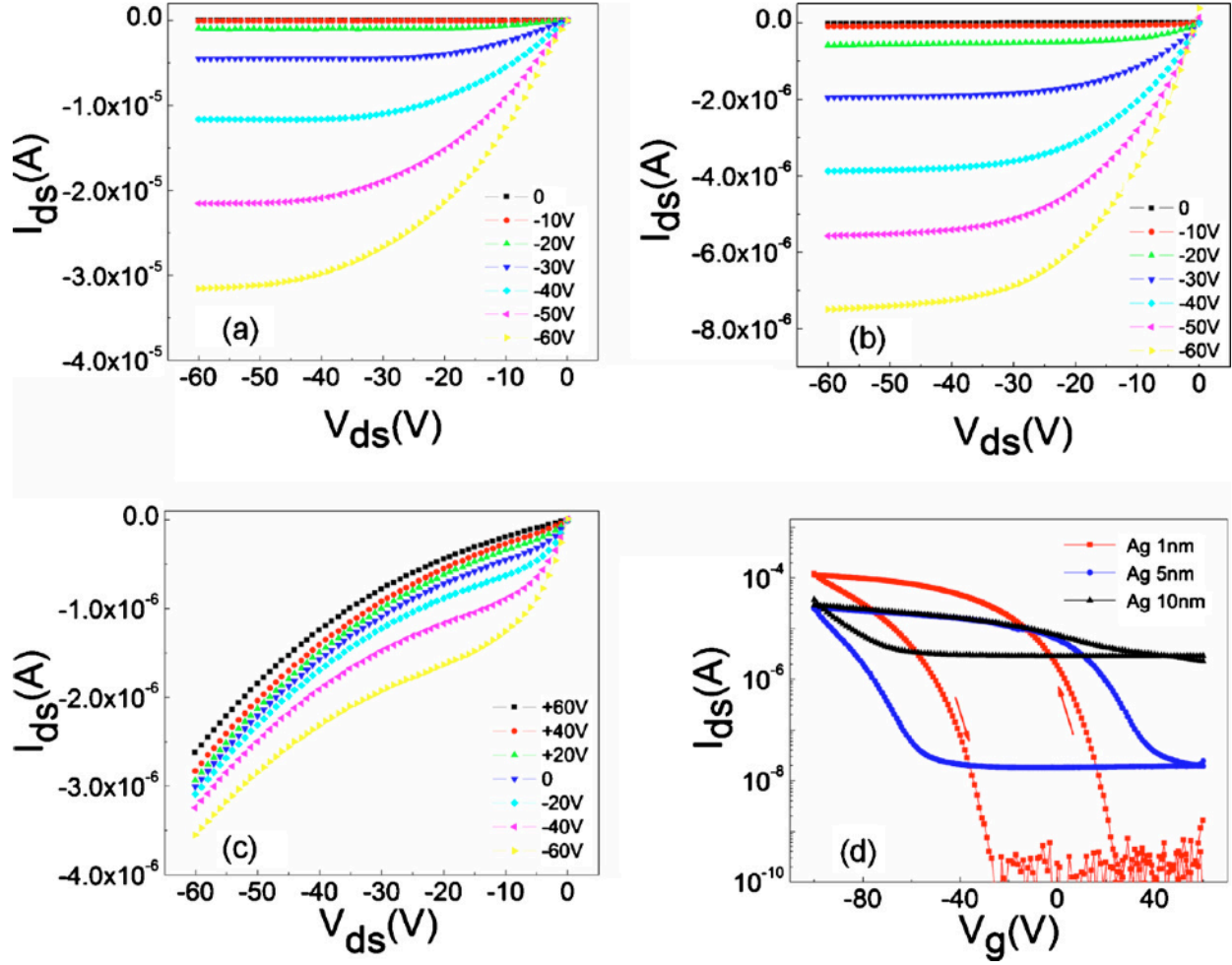


Figure 7: The output characteristics of the transistor memory with AgNPs thickness of 1 nm (a), 5 nm (b) and 10 nm (c). The transfer characteristics of the transistor memory with AgNPs thickness 1–10 nm (d)²¹

1.2 Synthesis of AgNPs

The design and control of AgNPs is crucial in achieving the appropriate properties required for many of their different applications. The size, shape, crystallinity, composition and structure (hollow versus solid) of AgNPs are known to strongly depend on the method of preparation.^{2a-e} As a result of such many properties of AgNPs that need control during their generation, for decades the controlled synthesis of AgNPs of the required characteristics is still a big challenge.^{2a-e} There are mainly two approaches for the generation of AgNPs which are the top-down and the bottom up approaches.²²

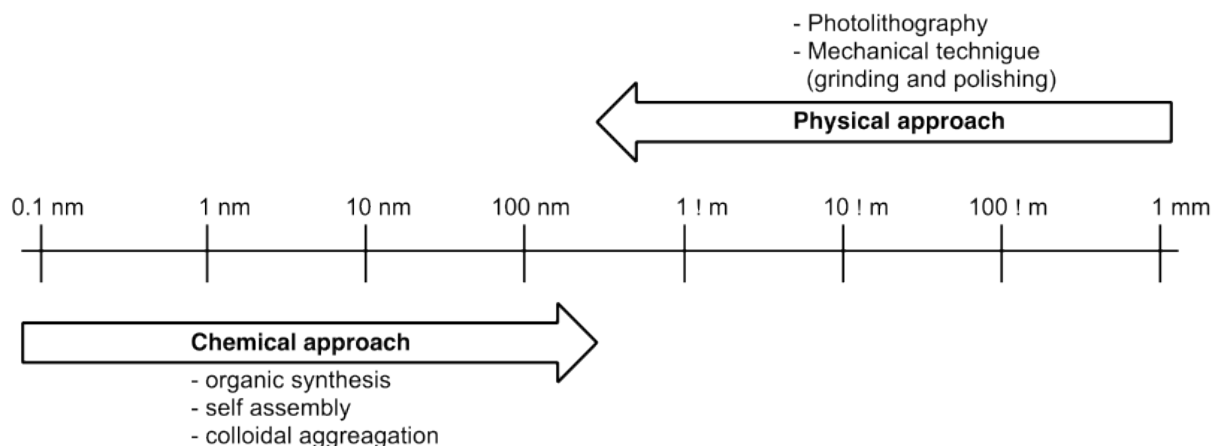


Figure 8: The physical approach versus the chemical approach of AgNP formation²²

1.2.1 Top-down Strategy for the Generation of AgNPs

Richard Feynman has advanced the idea of the top-down approach in his 1959 lecture when he stated “there is plenty of room at the bottom”.¹ The principle behind the top-down approach is to take a bulk piece of silver and then modify it into the desired morphologies of AgNPs. Cutting, grinding and etching are typical fabrication techniques, which have been developed to work on the nanoscale. The size of the nanoparticles which can be produced with top-down techniques are in the range 10 - 100 nm.²² This approach offers precise control over the size and shape, however, the point-by-point or layer-by-layer processing makes this approach time-consuming. Another drawback of this technique is the generation of imperfections on the surface of nanoparticles. Such defects can have a significant impact on the physical properties and surface chemistry of the nanoparticles. The top-down approach contributes in less than 4% in AgNP research due to the resulting imperfections.^{2b} Even though there are problems connected with the top-down approach, this is the method of choice to generate highly complex nanoparticles. Methods of generating AgNPs through the top-down approach include chemical vapour deposition and laser ablation.

1.2.1.1 Chemical Vapour Deposition

The dispersion of Ag⁰ in a homogeneous nanocrystalline form onto a matrix where nanoparticles are generated has been a long challenge. Pal et al. addressed this problem by depositing AgNPs embedded in diamond-like-carbon matrix (DLC) onto glass substrates using capacitatively

coupled (13.56 MHz) plasma chemical vapour deposition technique.²³ Crystalline AgNPs were deposited by using premixed methane and argon gas mixtures in four different proportions of argon (50%, 60%, 70% and 80%) in the gas mixture. The plasma was generated between two circular aluminum discs. One of the aluminum discs was mounted on the top side of the chamber to hold a 1.0 mm thick piece of silver of the same diameter. The second aluminum disc was placed at the bottom of the chamber to hold the glass substrates where the AgNPs were deposited. The size of AgNPs was found to increase from 11 to 36 nm with an increase in the concentration of Argon (Figure 9).²³ It was also observed that films deposited with different amount of argon in the plasma contained AgNPs with nearly spherical shape. Furthermore, the size distribution of AgNPs was narrower for the films deposited with lower concentration of argon in the plasma than those deposited with higher amount of argon in the plasma (Figure 9).

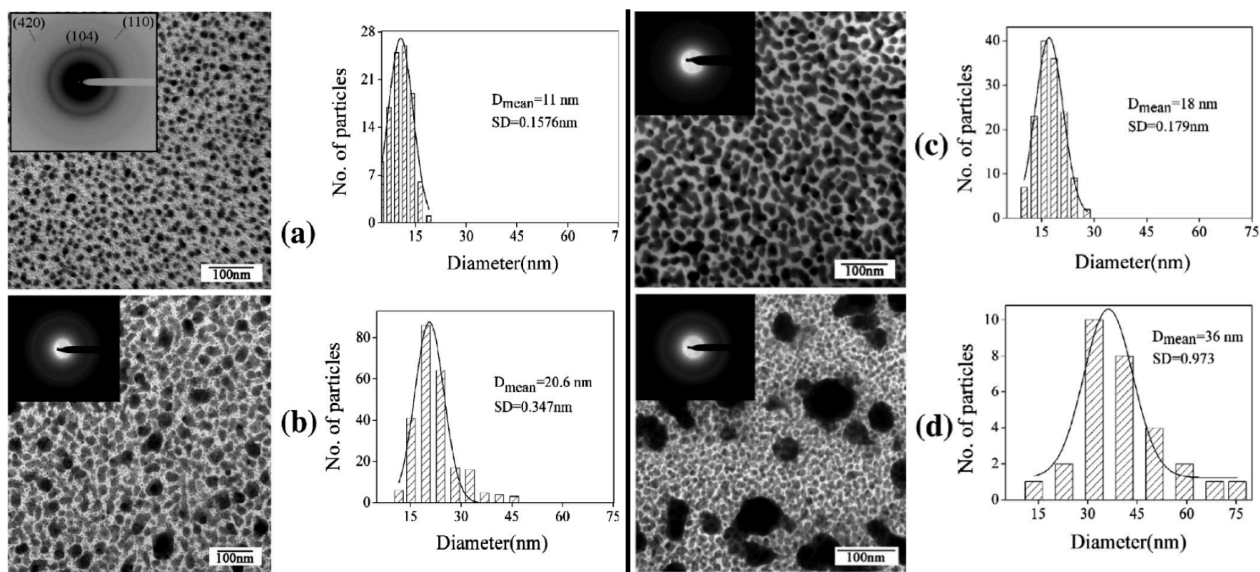


Figure 9: TEM micrographs and corresponding histogram of four representative nAg-DLC films deposited with different amount of argon in methane and argon gas mixtures: (a) 50%, (b) 60%, (c) 70% and (d) 80%. Insets also show the diffraction patterns of AgNPs²³

1.2.1.2 Laser Ablation

Henglein et al. introduced laser ablation of metallic silver as a novel method of AgNP preparation without a stabilizer as additive.^{24a,b} Laser ablation and irradiation of pulses of 1 064 nm wavelength were employed on Ag foil immersed in water in a quartz cell (Figure 10). This procedure was followed by irradiation of pulses of the same wavelength on the solution of

AgNPs without Ag foil to reduce the mean size of AgNPs through fragmentation. The AgNPs generated were reported to be of average size of 20 nm but highly polydisperse.

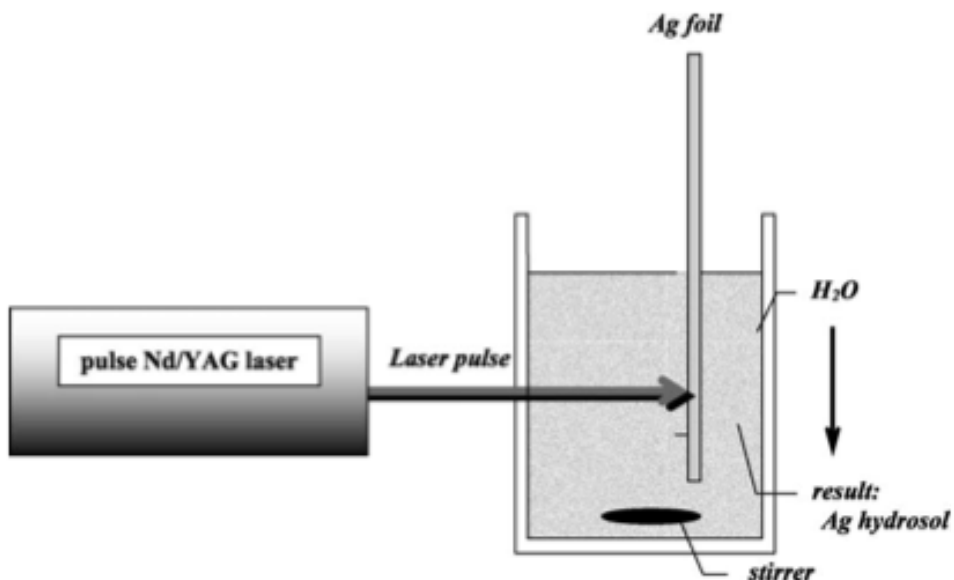


Figure 10: Schematic depiction of laser ablation^{24a}

When the liquid was changed from water to organic solvents like methanol or acetone, the nanoparticles were unstable and precipitated completely overnight at room temperature. Figure 10 show a schematic depiction of the ablation procedure.^{24a} Many research groups later modified Hanglein's procedure in order to control the size, dispersity and stability of nanoparticles. Some of the modifications include addition of additives like SDS,²⁵⁻²⁶ cetyl trimethyl ammonium bromide (CTAB)²⁷ and polyvinylpyrrolidone (PVP).²⁸

1.2.2 Bottom-up Strategy for the Generation of AgNPs

Jean-Marie Lehn pioneered the bottom-up approach when he stated “there is plenty of room at the top”.²⁹ The bottom-up approach is also referred to as self-assembly. It involves the construction of a structure atom-by-atom, molecule-by-molecule or cluster-by-cluster. This approach is simple and flexible, and the building blocks can be designed precisely to facilitate the assembly of nanostructures with tailorable features. The size of the nanostructures that can be obtained with a chemical approach spans the full range of the nanoscale.^{2b}

An advantage of the bottom-up approach is the possibility of obtaining nanoparticles with less defects and more homogeneous chemical compositions. This is due to mechanisms utilized in the synthesis of nanoparticles that reduce the Gibbs free energy, so that the produced nanoparticles are in a state closer to a thermodynamic equilibrium.²²

Depending on the method of choice in generating AgNPs through the bottom up approach, there are several factors which could influence the generation of AgNPs. Such factors include the Ag⁺-salt, solvent, type of stabilizer and type of reducing agent for Ag⁺-ions.

Silver salts (Ag⁺-salts)

The Ag-salt should dissociate into Ag⁺-ions for the reduction of the resulting Ag⁺-ions to take place followed by the formation of AgNPs. In the general and specific formation of AgNPs, AgNO₃ is the most widely used Ag⁺-salt and accounting for almost 83% of the reported AgNP studies (Figure 11).^{2b} Lee and coworkers reported that the wide spread use of AgNO₃ is attributed to its low cost and chemical stability when compared to other types of Ag-salts.³⁰

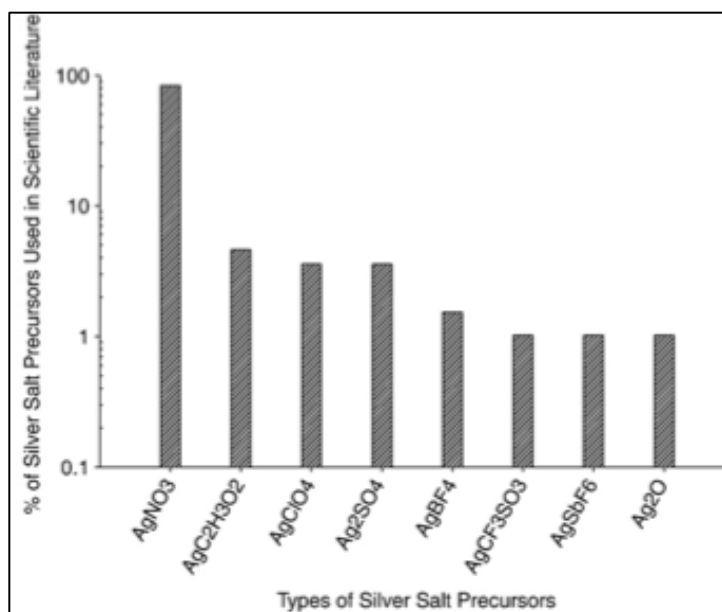


Figure 11: Analysis of silver salt precursors reported in studies of silver nanoparticle synthesis^{2b}

Solvents

Solvents play critical roles of solubilizing Ag^+ -salts and other substrates included in the synthesis of AgNPs.

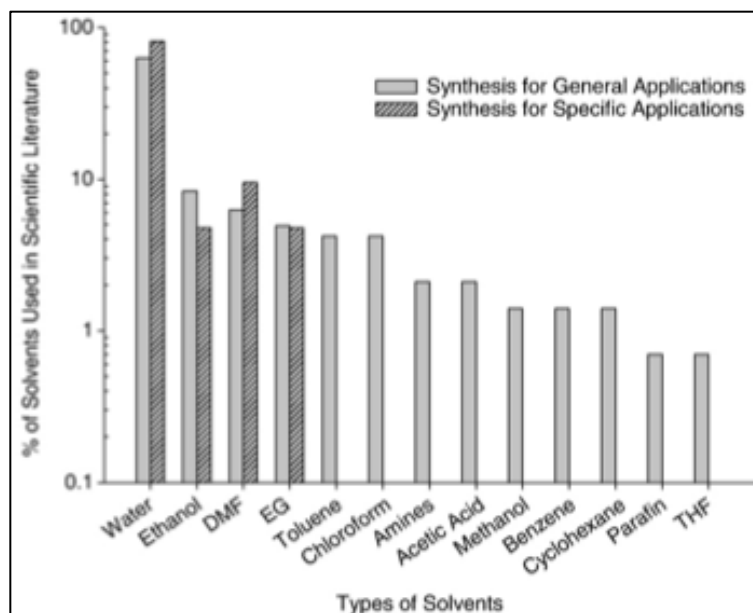


Figure 12: Analysis of solvents reported in studies of silver nanoparticle synthesis^{2b}

More than 80% of the processes of synthesizing AgNPs use water as the predominant solvent. (Figure 12).^{2b} However, the limitation of using water as the solvent is the difficulty in removing the AgNP stabilizer from the surface of the synthesised nanoparticles. Organic solvents make it easier to purify AgNPs after their synthesis.^{31a,b}

Stabilizing agents

The role of a stabilizing agent in AgNP synthesis is to protect the nanoparticles and prevent them from aggregation and also to control the size and shape of the final AgNP products. A stabilizing agent blocks the aggregation of AgNPs by producing a protective shell around the forming nanoparticles. Figure 13 shows some of the commonly used stabilizers.^{2b}

Olenin and coworkers reported that the agglomeration of AgNPs is mainly caused by high surface energy and high thermodynamic instability of the nanoparticle surface.³² The stabilization

methods can be classified in four categories which are the electrostatic, steric, electrosteric and stabilization by a ligand or a solvent.

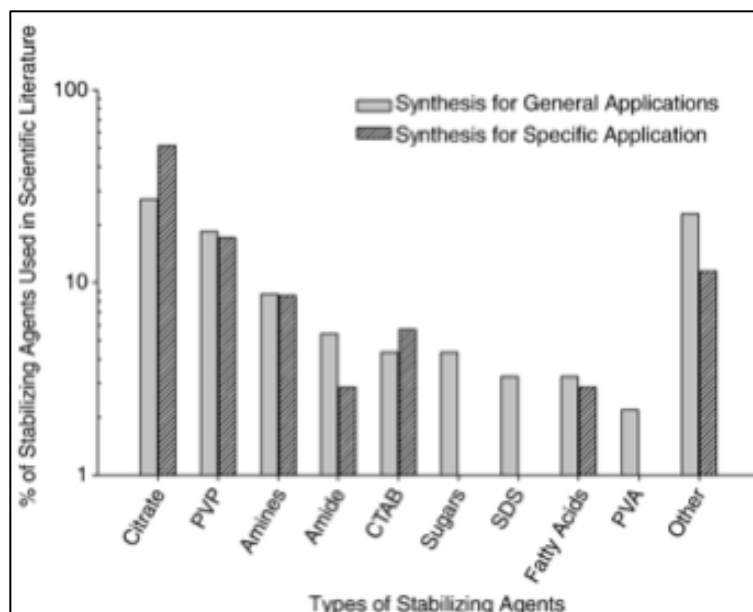


Figure 13: Analysis of stabilizing agents reported in studies of silver nanoparticle synthesis

Electrostatic stabilization

Electrostatic stabilization is achieved by addition of ionic compounds like halides, carboxylates, or polyoxoanions in the generation of AgNPs.³³ An electrical double-layer around the nanoparticle develops through adsorption of these ionic compounds and their related counterions. Nanoparticle stabilization is established by Coulombic repulsion between the particles. The control of thermal motion or ionic strength is a very important consideration in stabilizing nanoparticles by electrostatic repulsion approach.³³

Steric stabilization

Steric stabilization involves the use of macromolecules such as polymers, dendrimers or peptides.³⁴ These macromolecules generate a protective layer on the surface of the nanoparticles (Figure 14). Aggregation of nanoparticles is prevented by the restriction in motion of the adsorbed molecules in the inter-particle space which results in a decrease in entropy and therefore an increase in free energy. Unlike the electrostatic stabilization which is mainly used in aqueous solutions, steric stabilization can be used in the aqueous or organic phase.

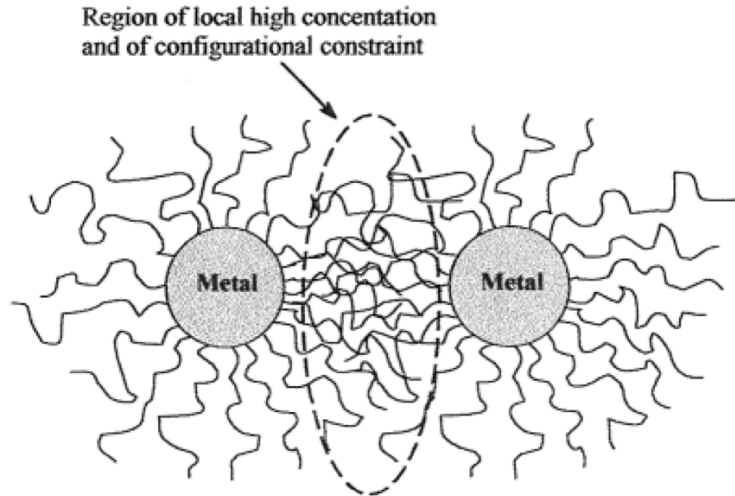


Figure 14: Schematic representation of steric stabilisation of metal nanoparticles³⁴

Electrosteric stabilization

The electrosteric stabilization of nanoparticles involves the combination of both the electrostatic and steric stabilization methods. Ionic surfactants are generally used for the electrosteric stabilization of nanoparticles.³⁵ These stabilizing compounds bear a polar head-group able to generate an electric double layer and a lyophobic side chain able to provide steric repulsion. A schematic illustration for an electrostatically or sterically stabilized metal nanoparticle.

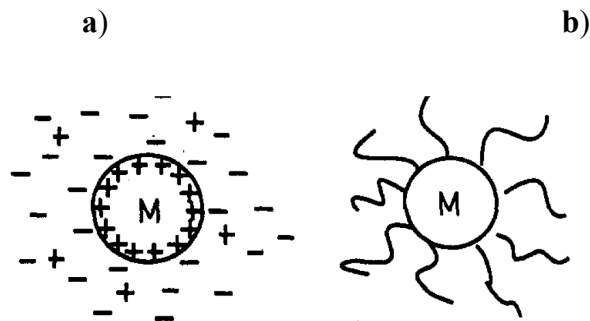


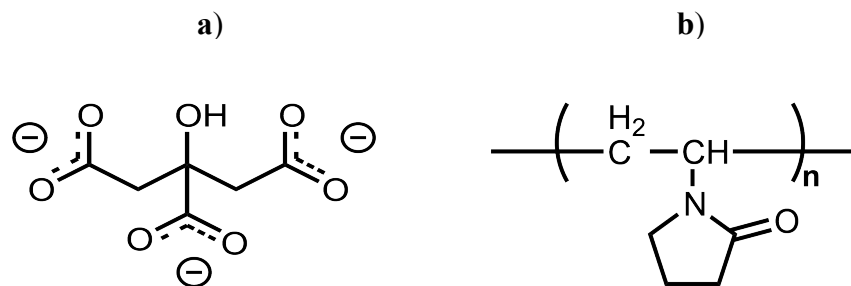
Figure 15: A schematic illustration for (a) an electrostatically stabilized metal nanoparticle (M) particle (one stabilized by the adsorption of ions and the resultant electrical double layer) and (b) a sterically stabilized metal particle (one stabilized by the adsorption of polymer chains)³⁵

Ligand stabilization

Ligands coordinate to nanoparticles their preventing them from aggregation. Examples of ligands that are used in the synthesis of nanoparticles include phosphines, thiols, amines or carbon monoxide and solvents such as tetrahydrofuran or thioethers.³⁶ Balan et al. reported that the stability, reactivity, solubility, particle shape and size could all be determined by the concentration of a given type of a stabilizing agent.³⁷ Prior findings by Wang and coworkers had also shown that smaller sizes of AgNPs are generated by increasing the concentration of the carboxylate stabilizer.³⁸

Overall the selection of the stabilizing agent for AgNPs depends on the intended application. A typical example of stabilizer is polyisopropylacrylamide (PNIPAM), a polymer with interesting properties for AgNP formation.³⁸ The polymer is commonly used as a temperature-sensitive agent and it possesses a lower critical solution temperature (LCST). Guo et al. reported that below the LCST the polymer is hydrophilic and soluble in aqueous solution whereas at temperatures above the LCST the polymer becomes hydrophobic, insoluble and aggregates in solution.³⁹ Hence these properties make AgNPs capped by PNIPAM to be used for combined surface plasmon and thermal switching applications.³⁹

Another area of AgNP application where the use of a stabilizer could play a great influence is in catalysis. Some stabilizers like sodium dodecyl sulfate (SDS) or cetyl trimethylammonium bromide (CTAB) decreases the adsorption of reactants to the AgNP surface thereby affecting the catalytic efficiency.⁴⁰ Citrate and PVP are the most widely used stabilizers for AgNPs (Figure 13).^{2b} The advantages of the citrate are its ability to act as a stabilizer of AgNPs as well as capable of reducing Ag^+ -ions during the synthesis of nanoparticles.⁴¹ The great interest in the use of PVP in stabilizing AgNPs is due to the nitrogen in PVP back bone which forms coordinate bonds with silver to form the protection layer in the case of particles with diameter lower than 50 nm. Figure 16 shows general structures of citrate and PVP molecules. For larger particles (diameters > 500 nm) both nitrogen and oxygen of PVP are found to form coordinate bonds with silver for the stabilization to be effective.⁴² Such form of electrostatic interactions determine the shape and size of anisotropy during the growth of AgNPs.⁴³



Scheme 16: Structural scheme of citrate (a) and PVP (b) molecules. In the scheme n represents the polymerization number (b)

Reducing agents for Ag⁺-ion

The Lee-Meisel⁴⁴ method which employs sodium citrate as the Ag⁺-ion reducing agent and the Creighton⁴⁵ method which uses sodium borohydride (NaBH₄) as the reducing agent are the commonly used chemical methods of generating AgNPs (Figure 17).^{2b}

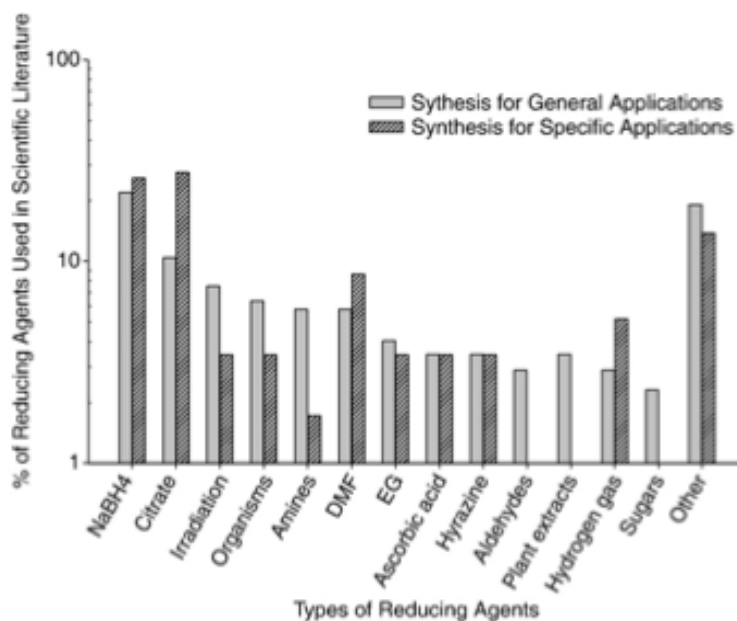


Figure 17: Analysis of reducing agents reported in studies of silver nanoparticle synthesis^{2b}

Lee-Meisel Method

In general citrate is a weaker reducing agent, hence the synthesis of AgNPs takes place under heating of the solution.⁴⁴ Due to the citrate's weaker Ag⁺-ion reducing capability, the size of the synthesised nanoparticles is relatively large but the nanoparticles are stabilized by the citrate

layer which coat the surfaces of AgNPs. The biggest drawback of this method is that the AgNPs generated are polydispersed in size.^{2e}

Creighton Method

An advantage of using NaBH₄ is its relatively high reactivity compared to citrate and other reductants.^{2a-e} In addition sodium borohydride has moderate toxicity compared to hydrazine and hydroxylamines. Furthermore, NaBH₄ has greater lab safety when compared to hydrogen gas and other physical methods.^{2e} However, the AgNPs generated in the presence of NaBH₄ are relatively small (1-15 nm) and unstable, therefore different stabilizers are used during the synthesis process.^{2b} Previous studies by Creighton and coworkers showed that the generation of AgNPs in larger sizes was difficult to control when NaBH₄ was used as the Ag⁺-ion reducing agent.⁴⁵

In most cases the generation of AgNPs in different sizes has been successfully achieved by using ascorbic acid which is a weaker Ag⁺-ion reducing agent than NaBH₄ but is a stronger reducing agent than citrate.^{2b}

The synthesis of silver nanoparticle by the bottom up approach can be arbitrarily divided into two main categories which are the photochemical and chemical generation methods.

1.2.2.1 Photochemical Method of Generating AgNPs

An important challenge in the synthesis of AgNPs is to control nanoparticle size and shape while maintaining a high overall yield of product. Photochemical method was the first reliable and high yielding method for making solution phase triangular Ag nanoprisms.⁴⁶ Moreover, photochemical methods of generating AgNPs can offer advantages such as fast reduction of Ag⁺-ions at ambient temperature. In addition, the reduction can be initiated homogeneously thereby avoiding local concentration gradients when reactants are mixed. The use of a stabilizing agent is crucial to prevent the aggregation of the generated nanoparticles. Pal et al. introduced ascorbic acid which is a photoactive molecule in the photochemical method of generating AgNPs.⁴⁶ They reported that their method of using an ordinary hand-held 15 W germicidal lamp as the source of light, was reproducible, simple and rapid (AgNP formation was complete in less than 5 minutes). TEM studies show that the individual particles are polydisperse and are in the size range of 15 - 60 nm

(Figure 18). Furthermore, the generated nanoparticles form assemblies of approximately 300 nm in size.

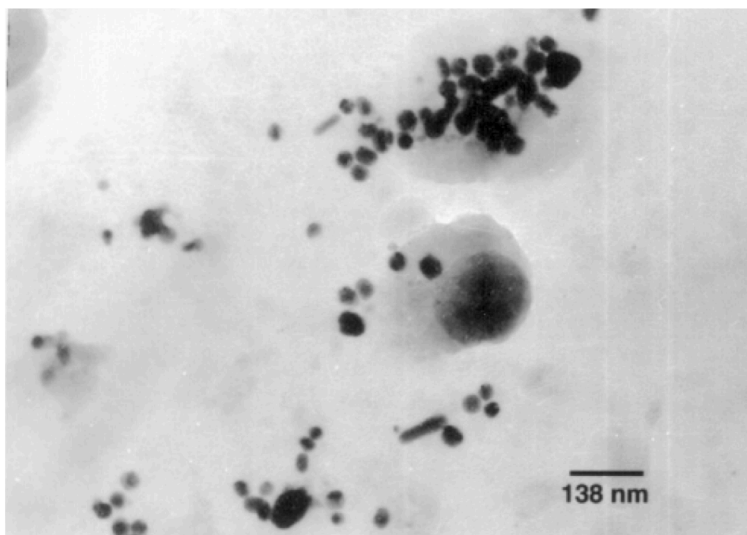


Figure 18: TEM images of the AgNPs generated by the photochemical method⁴⁶

In 2001 Mirkin et al. reported the first high yield synthetic method for triangular shaped Ag-nanoprisms by use of visible light.⁴⁷ The conversion of the nanoparticles to nanoprisms could be turned on and off simply by turning on or off the light source. Visible light was irradiated onto a solution containing trisodium citrate, bis(p-sulfonatophenyl)phenylphosphine dipotassium salt (BSPP) and AgNP seeds of diameter 6 to 8 nm. In this system, the citrate was the photoactive agent whereas BSPP stabilized the generated AgNPs. Spherical AgNPs were almost completely converted by visible light into thin triangular prisms with edge lengths of 100 ± 15 nanometers (Figure 19).

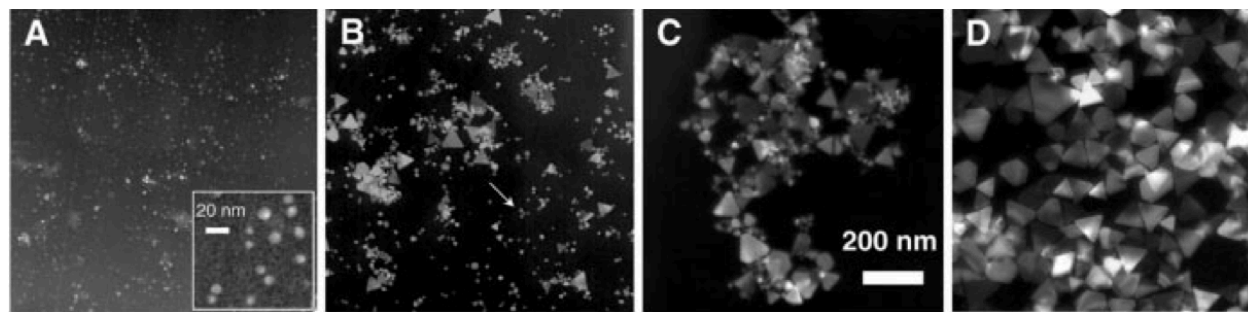


Figure 19: TEM images (A) before irradiation and after (B) 40, (C) 55, and (D) 70 hours of irradiation. Except for the inset in (A), the scale bar is 200 nm for all three images⁴⁷

Following Mirkin et al.'s initial report of triangular Ag nanoprism synthesis, other researchers have confirmed the results and significantly expanded upon their scope. For example, Brus et al. observed morphological changes of spherical AgNPs to nanoprisms when the spherical AgNPs were exposed to various wavelengths of visible light.⁴⁸ Irradiation of a solution of Ag⁺-ions, AgNP seeds and citrate with a 457 nm laser led to the generation of Ag-nanoprisms which increased in size from 14 to 50 nm after 5 and 90 minutes of irradiation respectively (Figure 20). Citrate served as a photoactive Ag⁺-ion reducing agent as well as a stabilizing ligand for the AgNPs. When this reaction was monitored over time using TEM, Brus et al. observed increasing numbers of Ag nanoprisms with increasing irradiation time.⁴⁸ Furthermore the authors reported that the irradiation time and the concentration of Ag⁺-ions in solution control the final size of the particles whereas the shape strongly depended on the excitation wavelength.

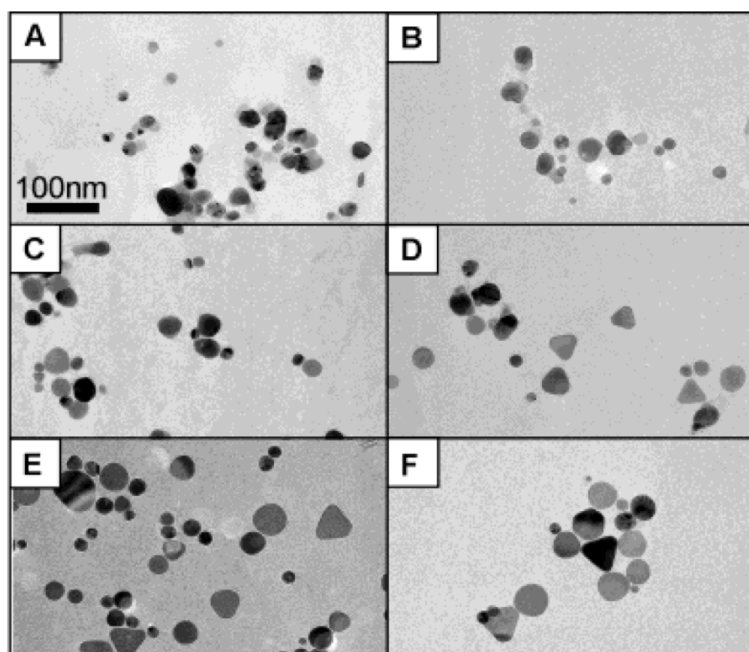


Figure 20: TEM pictures of AgNPs synthesized after 5 (A), 10 (B), 15 (C), 20 (D), 50 (E) and 90 (F) minutes of irradiation with a 457 nm laser⁴⁸

Brus et al. proposed that the excitation of a specific plasmon determines the growth direction of AgNPs.⁴⁸ Due to the shape dependence of the Ag⁰ plasmon resonance, the aspect ratio of nanoparticles is controlled by the irradiation wavelength. Therefore, an increase in the irradiation wavelength leads to an increase in the aspect ratio of nanoparticles. Brus et al. supported their hypothesis by using a 457 nm laser to irradiate Ag-nanoprisms (generated in the presence of a

457 nm laser) together with a solution of AgNO_3 and citrate.⁴⁸ The resulted nanoprticle size increased but their aspect ratio remained constant. However, irradiation with a laser of longer wavelength 514 nm resulted in the formation of Ag nanoprisms of a larger aspect ratio.

Despite the great effort which has been done to prepare AgNPs, the generation of AgNPs in defined shape variety and size remain a big and important challenge. Photo induced methods of AgNP synthesis have been used to generate defined Ag nanoprisms, however quite often the processes need several hours to prepare these nanoparticles in defined shape. Also, most light sources which are used for the generation of AgNPs of defined sizes and shapes are expensive.

1.2.2.2 Chemical Reduction Method of Generating AgNPs

The chemical reduction method is the most frequently applied method for the preparation of silver nanoparticles due to its easy accessibility. Along with that, the chemical method is generally cheaper in the costs involved in the generation of AgNPs. In addition this approach offers possibility of generating a variety of AgNPs of defined size and shape.⁴⁹ When Ag^+ -ions are reduced they form Ag^0 atoms which eventually agglomerate into oligomeric clusters and finally lead to AgNPs.^{49a} Due to the large positive reduction potential of Ag^0 , AgNP oxidation is thermodynamically unfavorable resulting in quite stable aqueous and alcoholic suspensions without the aid of capping ligands. The thick electrical double layers that form around metal nanoparticles in low-ionic-strength suspensions can inhibit aggregation. For high ionic strengths or organic-phase suspensions capping agents such as surfactants or polymers can be employed to protect the particles from aggregation.⁵⁰ Typical surfactants used for AgNPs include sodium dodecyl sulfate, oleic acid, alkyl phosphines and hexadecylmine. Common polymers which are used comprise of poly(vinyl pyrrolidine) (PVP) and polyethylene glycol (PEG). If the synthesis is carried out in the presence of capping agents, however, anisotropic particles may result due to the differing affinities of the ligands to the exposed crystal faces. For example Xia synthesised monodisperse Ag nanocubes in large quantities by reducing AgNO_3 with ethylene glycol in the presence of poly(vinyl pyrrolidone) (PVP) (Figure 21).⁵¹ The authors reported that the selective adsorption of PVP on various crystallographic planes of AgNPs played the major role in determining the product morphology.

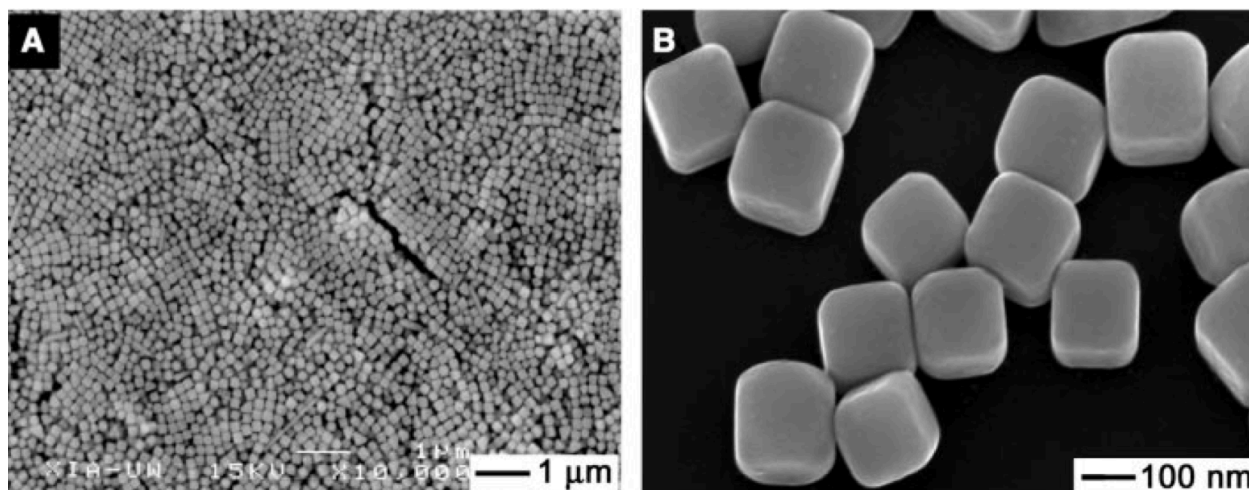


Figure 21: (A) Low- and (B) high-magnification SEM images of slightly truncated silver nanocubes synthesized in the presence of PVP and ethylene glycol as the reducing agent of Ag^+ -ions. The image shown in (B) was taken at a tilting angle of 20° ⁵¹

Previous studies by Pileni et al. have also shown that judicious use of stabilizing agents generates AgNPs of a variety of shapes.⁵² Sodium di(2-ethyl-hexyl)sulfosuccinate (Na(AOT)) was used to stabilize AgNPs whereas hydrazine was the Ag^+ -ion reducing agent. After the synthesis, single-crystal Ag nanoprisms in equilibrium with spheres were produced. The amount of reducing agent tuned the nanodisc size (between 30 and 100 nm by the relative amount of reducing agent) but did not affect the aspect ratios of the nanodiscs, hence the shape remained the same (Figure 22).

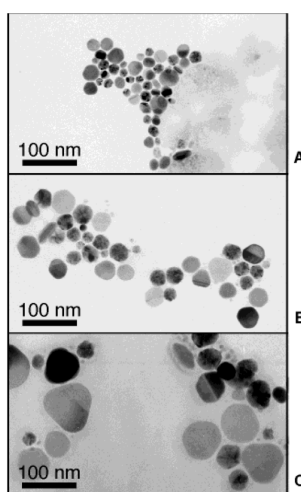


Figure 22: Ag nanoprisms as observed by TEM at $[(\text{hydrazine})/[\text{AOT}]$ of 5.35 (A), 6.6 (B), 8.2 (C)⁵²

Regardless of their good performance in controlling the size and shape, additives like surfactants or polymers very frequently make part of the AgNP compositions hence impact the physical, chemical and biological properties of such nanoparticles.^{2a-c} Depending on the intended area of application, in many cases these additives limit the application of AgNPs generated in their presence. As an example, the toxicity of these additives make them non-compatible with biomedical applications. To avoid this major drawback, recently peptides bearing functional groups that coordinate to Ag⁺ ions have become popular as additives.^{2a,d}

Moreover peptides display self assembly and recognition properties which make them useful as building blocks for binding and promoting the nucleation and growth of AgNPs.^{2a,d} Other advantages of using peptides besides their ability to control the structure and size of AgNPs, are their potential to improve nanoparticle dispensability and chemical stability.

Biosynthesis of AgNPs

Biosynthesis is one of the chemical methods of synthesising AgNPs.^{2a} Due to a growing need to develop environmentally friendly methods in nanoparticle synthesis, the biosynthesis has received increasing attention in AgNP generation.⁵³ Klaus and coworkers reported for the first time the intracellular biosynthesis of AgNPs which was performed using a bacterial strain *Pseudomonas stutzeri* AG259. The growth of cells in the presence of Ag⁺ was accompanied by the formation of AgNPs in diameters of up to 200 nm in the periplasmic space of cells (Figure 23).^{54,55}

Since the mechanism of AgNP formation under these conditions is still unclear, proteins with affinity for silver and containing fragments capable of acting as the nucleation sites were assumed to play a key role in the formation of AgNPs. It was speculated that the reduction of Ag⁺-ions proceeded by an extracellular mechanism by proteins from the cell wall structure of the fungus.⁵⁴⁻⁵⁵

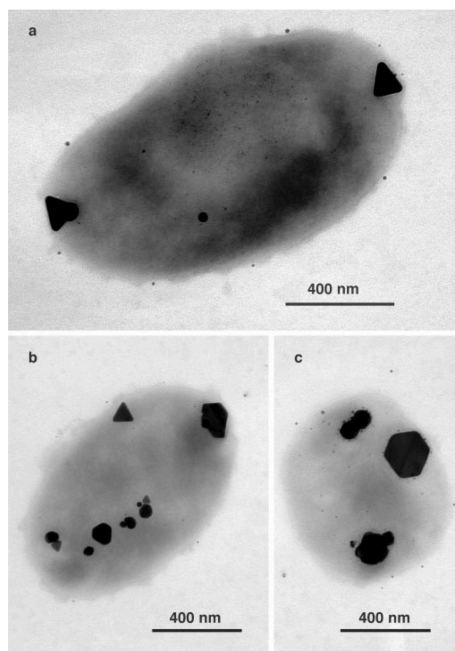


Figure 23: Different morphologies and sizes of AgNPs generated by *P. stutzeri* AG259. (a) TEM image of bacteria cell showing triangular Ag nanoprisms at both poles and an accumulation of smaller AgNPs all over the cell. (b and c) TEM images of triangular, hexagonal and spheroidal AgNPs accumulated at different cellular binding sites⁵⁴

Sastry et al. also showed that the fungus *Fusarium oxysporum* is capable of extracellular reduction of Ag⁺-ions to afford AgNPs with diameter of 5 to 15 nm (Figure 24).⁵⁶

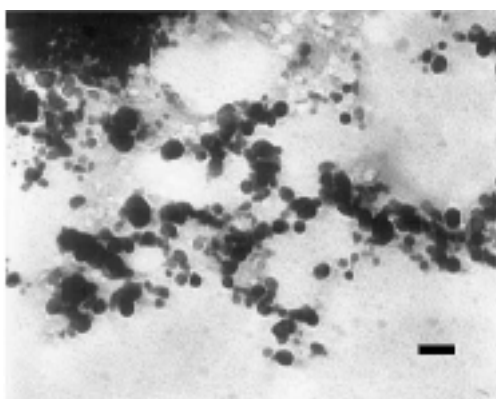


Figure 24: TEM micrograph recorded from a drop-coated film of an aqueous solution incubated with *Fusarium oxysporum* and reacted with Ag⁺-ions for 72 h. The scale bar corresponds to 100 nm

In order to understand the biosynthesis of AgNPs, Esposito et al. published the mechanism of Ag⁺-ion reduction by different strains of *Fusarium oxysporum*.⁵⁷ The authors reported that the scanning electron microscopy (SEM) data showed well-isolated AgNPs in the range of 20 to 50 nm in dimensions Figure 25.

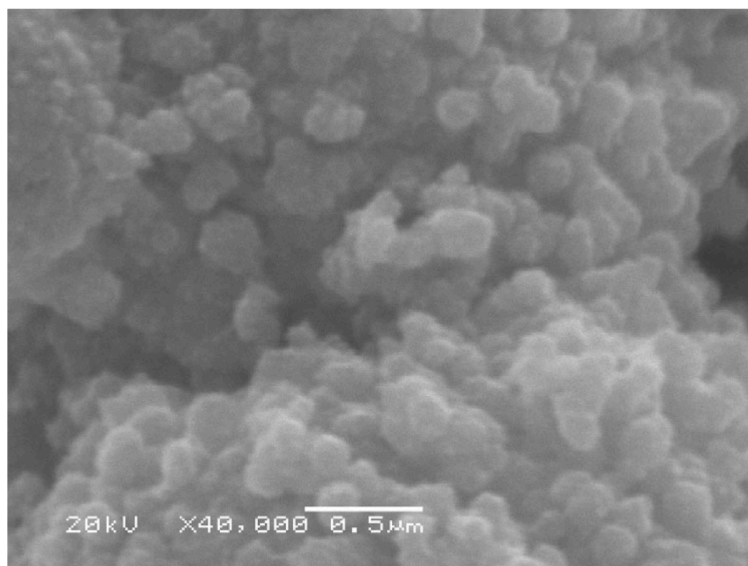


Figure 25: SEM micrograph from *F. oxysporum* showing silver nanoparticles recorded at X40 000 magnification⁵⁷

Fluorescence and visible absorption spectra of the solutions of AgNPs revealed that the stabilizing proteins contained tryptophan and tyrosine and were in their native form. However, the spectroscopic studies also showed the presence of 2-acetyl-3,8-dihydroxy-6-methoxy anthraquinone or its isomer 2-acetyl-2,8-dihydroxy-6-methoxy anthraquinone as well as the presence of NADP-dependent nitrate reductase.⁵⁷ Previously Kolter et al. had reported that the isomers which were observed act as extracellular electron carriers.⁵⁸ Hence Esposito et al. postulated that the mechanism of Ag⁺-ion reduction could include the conjugated oxidation-reduction reactions of electron carriers in which NADP- dependent nitrate reductase is involved (Figure 26).⁵⁷

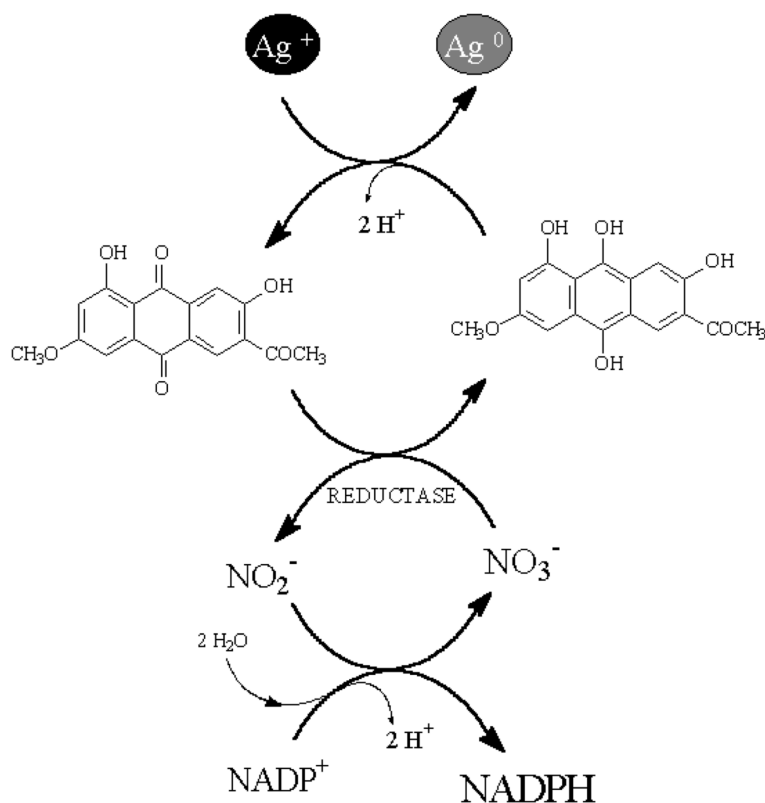


Figure 26: Hypothetical mechanisms of extracellular reduction of Ag⁺-ions by a strain of fungus *Fusarium oxysporum*⁵⁷

Even though the biosynthesis of AgNPs does not apply a stabilizing agent since the organic matrix of the bacteria is involved in stabilizing the nanoparticles and is a green process,⁵⁴ it is rather a slow process that can even take several days.⁵⁹ Only a few fast methods have been reported where bacteria is used to generate AgNPs.⁵⁹ The general understanding of the generation and growth of AgNPs through the bio-inspired synthesis are poorly understood, other approaches like the biomimetic synthesis have already been explored as possible solutions.^{2d}

A rational prediction of a diversity of peptides capable of inducing the formation of AgNPs of different sizes and shapes is difficult.^{2d} In order to address this problem combinatorial library approaches such as phage display libraries have been applied.^{60,61}

1.2.2.2.1 Phage Display Libraries and Biomimetic Synthesis of AgNPs

Naik et al. undertook the first studies aimed at identifying peptides that bind to and are able to induce the formation of AgNPs^{60,61} They used a phage display peptide library to identify the active peptides in generating AgNPs (Figure 27).

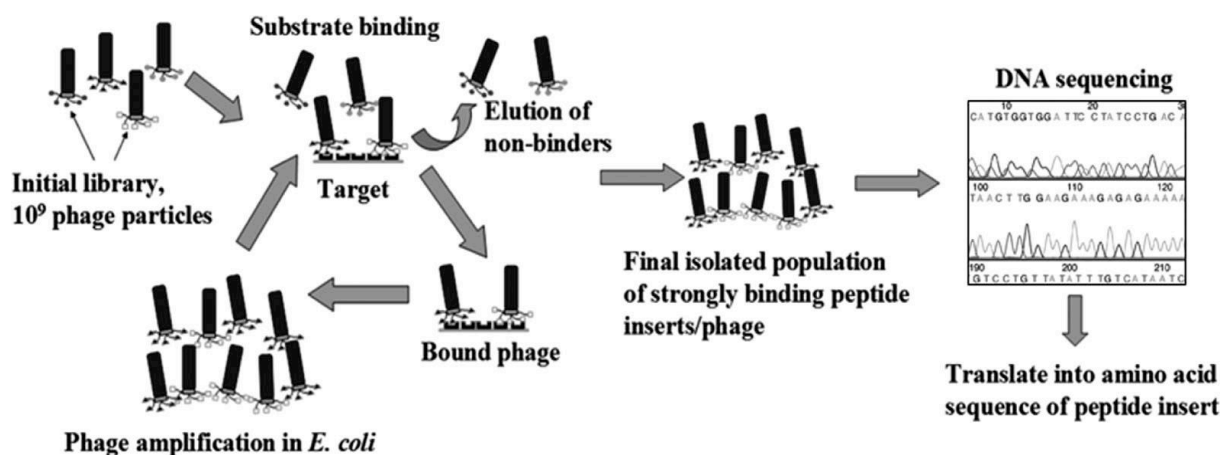


Figure 27: Procedure for the isolation of peptides possessing a high affinity for silver substrate from a phage-displayed library. Several (3-5) rounds of stringent washing and elution are used to remove weakly binding peptides from the final screened phage population. The amino acid sequence of the displayed peptide is determined through the DNA sequencing of the final phage clones^{1d}

Screening of a phage display library involves many steps.⁶¹ The phage library in a buffer solution is incubated with a Ag-salt resulting in a heterogeneous mixture of phages in contact with the silver substrate. Several washing cycles of the phages eliminate non-binders by disrupting weak interactions with the silver substrate. Bound phages are next eluted from the surfaces and amplified by reinfecting the host thereby completing the first round of biopanning. Generally, three to five cycles of biopanning are repeated using increased concentrations of the buffer in order to enrich for tight binders. Finally, individual clones are sequenced to obtain the amino acid sequence of the peptides binding to the silver substrate.⁶²

Through phage display screening, Naik et al. identified peptides AYSSGAPPMPPF and NPSSLFRYLPSD that proved capable of reducing silver ions and directing the formation of AgNPs.⁶¹ The identified silver-binding peptides indicated a preferential enrichment of proline and

hydroxyl-containing amino acid residues. Peptide NPSSLFRYLPSD was found to direct the formation of hexagonal, spherical, and triangular shaped AgNPs of 60 - 150 nm in size (Figure 28). This peptide is reported to bind specifically to the Ag(111) surface and thus enables the synthesis of polyhedral Ag crystals with face-centered-cubic lattice structures.

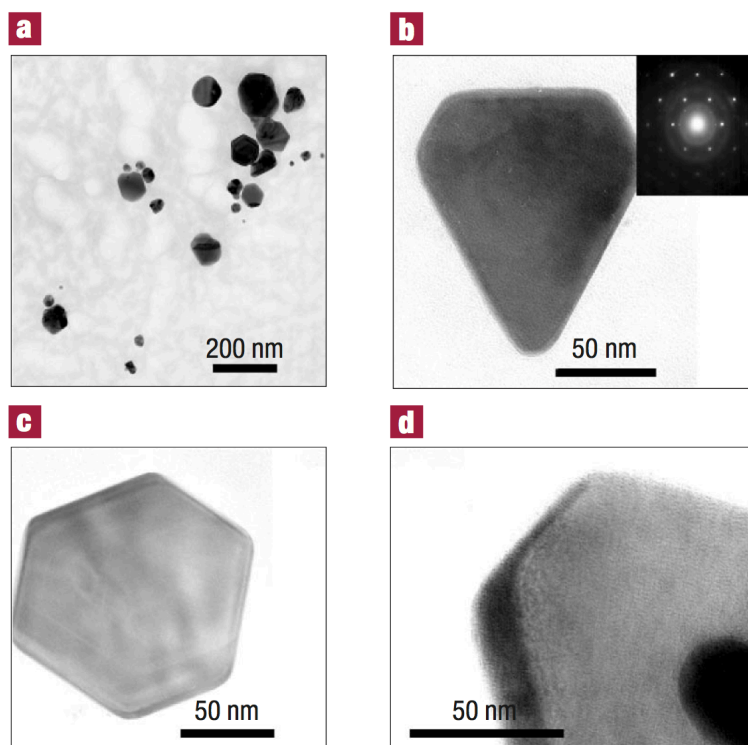


Figure 28: TEM image showing a variety of crystal morphologies of AgNPs obtained using peptide NPSSLFRYLPSD (a-d), electron diffraction pattern obtained from a AgNP (b) and edge of the truncated triangle showing the thickness of the plate (d)⁶⁰

In another study Naik et al. introduced polymerase chain reaction (PCR)-driven peptide screening method to isolate peptides that induce the formation of AgNPs.⁶¹ PCR was introduced as a versatile technique that could identify peptide sequences which possessed high affinity to silver that these sequences resisted elution and identification by standard biopanning procedures.⁶¹ Figure 29 depicts the general scheme for the PCR screening procedure.

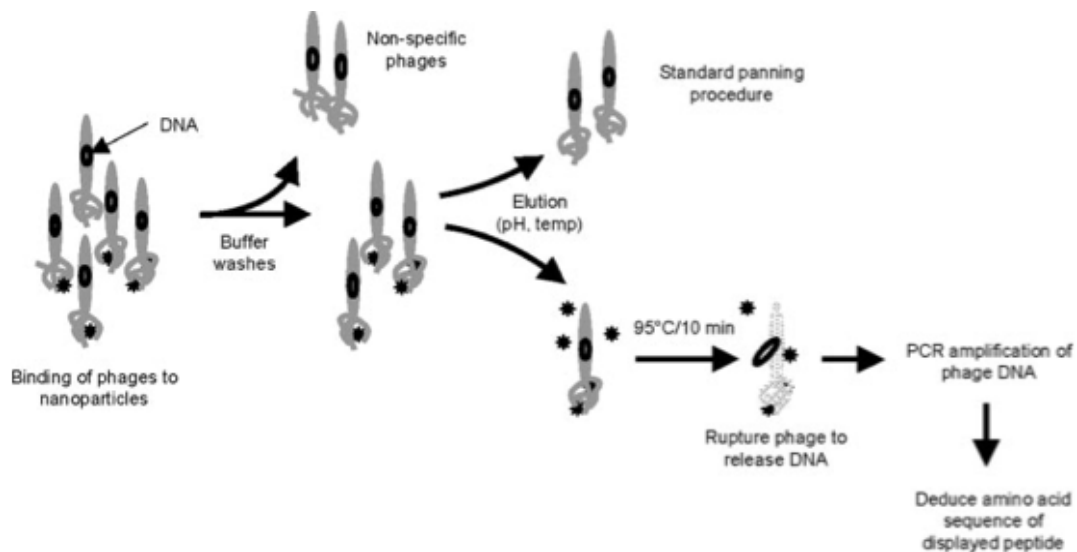


Figure 29: Schematic illustration of general PCR driven phage panning for peptides that bind to inorganic nanoparticles⁶¹

Several peptides were identified to be able to induce the formation of AgNPs (Table 1). Among the peptides identified peptides WSWRSPTPHVVT induced the formation of spherical nanoparticles of 52 ± 13.2 nm in size (Figure 30). Results from these reported phage display screening studies show that different peptides can induce different sizes of AgNPs.

KFLQFVCLGVGP	AVLMQKYHQLGP	IRPAIHIIPISH
NVIRASPPDTSY	LAMPNTQADAPF	QQNVPASGTCSI
NAMPGMVAWLCR	HNTSPSPIILTP	ASQTL LLPVPPL
YNKDRYEMQAPP	TLLLLAFVHTRH	PWATAVSGCFAP
SPLLYATTSNQS	WSWRSPTPHVVT	

Table 1: Silver-binding peptides identified by PCR screening technique⁶¹

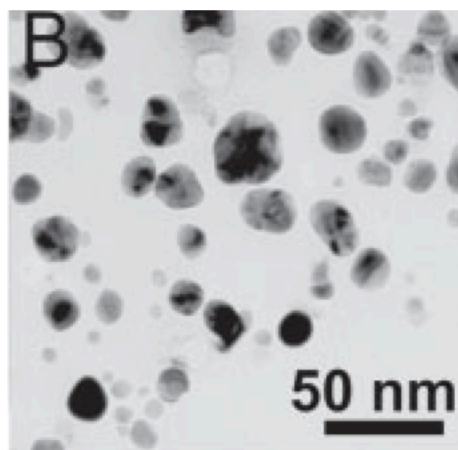


Figure 30: TEM image of AgNPs generated in the presence of peptide WSWRSPTPHVVT

Furthermore the importance of peptides was demonstrated as studies which were done by Naik and coworkers on single amino acid solutions of lysine, proline, serine, and arginine showed incapability in generating AgNPs. Moreover, tryptophan and aspartate that were used by Sastry et al to reduce Au^{+3} -ion in the synthesis of gold nanoparticles did not show the ability to reduce Ag^+ -ions.⁶³ Conformation, overall charge, and functional groups of peptides could all be contributing to the reduction of Ag^+ -ions and the subsequent formation of AgNPs.

Following Naik et al.'s breakthrough in using the phage display libraries in identifying peptides that are able to generate AgNPs, Bassindale and coworkers have also undertaken the screening of phage-displayed peptide libraries to identified silver-binding peptides.⁶⁴ From the peptides identified, two peptide sequences TVPPKAPRSSDL and LTRPNHGNTVDT were reported to generate distinct morphologies of AgNPs.⁶⁴

Xie et al. employed proteins extracted from the green algae *C. Vulgaris* and generated Ag nanoplates of size 44 nm in average diameter and in one-pot synthesis process (Figure 31).⁶⁵ Following chemical modifications of the algae protein they found that tyrosine residues were the source of bio-reduction of Ag^+ and the carboxyl groups in Asp and/or Glu were primarily responsible for the anisotropic growth of the Ag nanoplates.⁶⁵ Rational designed tripeptides also demonstrated that tyrosine residues in a peptide could reduce Ag^+ -ions.⁶⁵ Furthermore they published that the acidic residues comprising Asp and Glu are involved in directing the anisotropic growth of AgNPs.⁶⁵

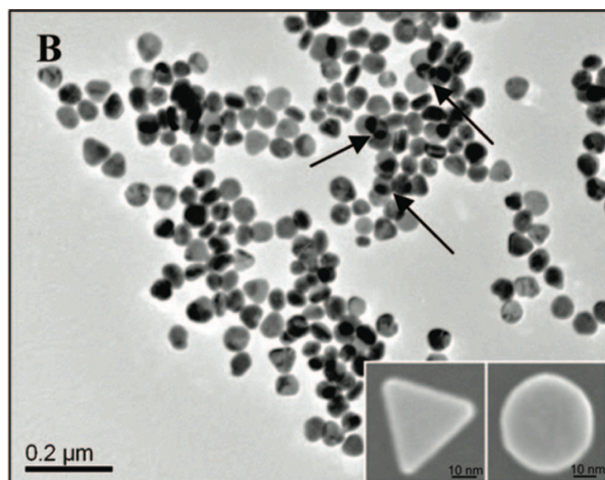


Figure 31: TEM image of the AgNPs synthesised by the green algae *C. Vulgaris*. The arrows point to locations where several flat particles had overlapped

In another study Wright et al. isolated peptide AHHAHHAAD from the histidine-rich protein of *Plasmodium falciparum* and used it in the formation of AgNPs of 7 nm in average size.⁶⁶

To date many scientists have invested much effort to understand the relationships between peptide sequences and their influence in the generation of nanoparticles. For example Xie et al. used rationally designed simple tripeptides as a proof of concept for the biomimetic synthesis of Ag nanoplates and to further test the nanoparticle formation mechanism (Table 2).⁶⁵ Furthermore, they investigated the Tyr Ag⁺-ion reducing power in the presence of different amino acids in a peptide. Peptide Gly-Tyr-Tyr, was the fastest in reducing Ag⁺-ions. Since peptide Gly-Gly-Gly does not contain a tyrosine residue, it showed no apparent formation of AgNPs.

Gly-Gly-Gly	His-His-Tyr
Gly-Gly-Tyr	Lys-Lys-Tyr
Gly-Tyr-Tyr	Asp-Asp-Tyr
Cys-Cys-Tyr	Ser-Ser-Tyr

Table 2: Silver-binding peptides identified by PCR screening technique⁶⁵

Intriguingly, the presence of peptides His-His-Tyr and Cys-Cys-Tyr resulted in no formation of AgNPs. For peptides Lys-Lys-Tyr and Asp-Asp-Tyr the binding of the Ag⁺-ions at the amine on Lys or carboxylic sites on Asp was found to be weaker than in the case of binding with the

imidazole on the His-His-Tyr or thiol on Cys-Cys-Tyr sites. Therefore, Ag⁺-ion reduction was found to be slower in the presence of peptides Lys-Lys-Tyr and Asp-Asp-Tyr than in the presence of peptides Gly-Gly-Tyr and Ser-Ser-Tyr. The ratio of carboxylic groups to Tyr per peptide molecule was found to be an important consideration in the high yield of Ag nanoplate formation.
65

In order to have more in depth knowledge on the influence of peptides in the formation of AgNPs, Mandal and coworkers used peptides NH₂-Leu-Aib-Trp-OMe and Boc-Leu-Aib-Trp-OH in the generation of AgNP and AuNPs.⁶⁷ Even though results on AgNP formation in the presence of both peptides was not fully reported, the influence of both peptides in the formation of AuNPs is well-outlined. Interestingly they found that peptide Boc-Leu-Aib-Trp-OH generated AuNPs of 7.33 ± 0.8 nm in size and better size distribution than peptide NH₂-Leu-Aib-Trp-OMe which generated bigger sizes of AuNPs in average diameter of 13.39 ± 2.7 nm (Figure 32). Due to the absence of free amino groups in peptide Boc-Leu-Aib-Trp-OH the stability of AuNPs which were generated in its presence was less than the stability of AuNPs prepared in the presence of peptide NH₂-Leu-Aib-Trp-OMe.⁶⁷

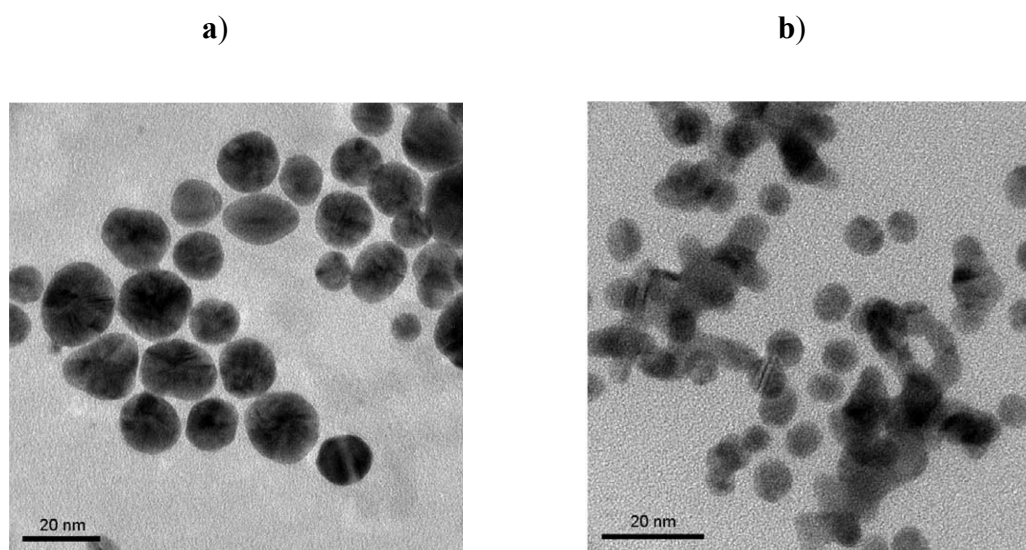


Figure 32: TEM images of AuNPs prepared in the presence of peptides NH₂-Leu-Aib-Trp-OMe (a) and Boc-Leu-Aib-Trp-OH (b)

The authors reported that peptide NH₂-Leu-Aib-Trp-OMe induced the formation of AgNPs of 13.66 ± 2.0 nm in size which is comparable to the average size of AuNPs synthesised in the presence of the same peptide (Figure 33).⁶⁷

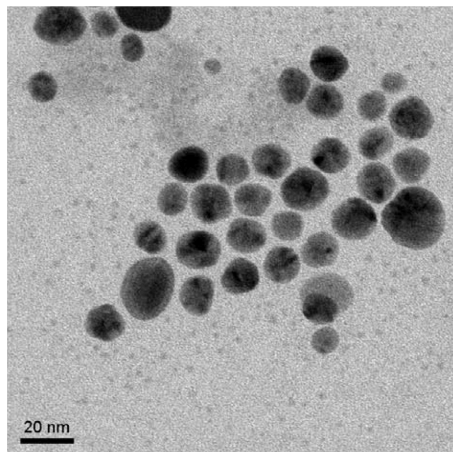


Figure 33: TEM image of AgNPs prepared in the presence of peptide NH₂-Leu-Aib-Trp-OMe

Banerjee et al. also published on the reduction of Ag⁺-ions by tyrosine residues which were incorporated into the gel forming tripeptides for the in situ generation of AgNPs (Figure 34).⁶⁸ The formation of AgNPs involved heating above 50 °C the methanol-water gel of tyrosine tripeptide and AgNO₃ until the appearance of a clear solution.

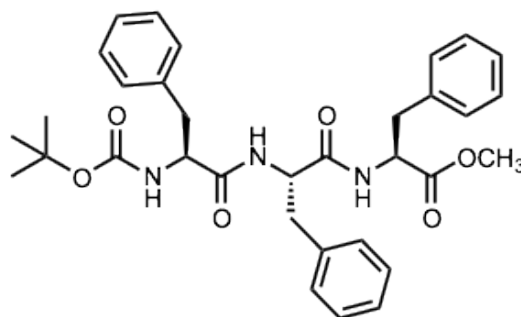


Figure 34: Gel forming tyrosine tripeptide used for AgNP formation within the gel-phase network.

Upon slow cooling the clear solution turned yellow indicating the formation of AgNPs through reduction of Ag⁺-ions by tyrosine residues within the tripeptide. The formation of AgNPs embedded in the tripeptide gel was rapid and took place immediately after the solution turned yellow.⁶⁸ Stabilization of AgNPs was achieved by the peptide's gel matrix.

Phage display library approach is a very powerful, successful and conventional panning method of identifying a variety of peptides which are able to induce the formation of AgNPs.¹ However the approach has its own shortcomings. For example the use of acid to release the phage from the silver substrate may selectively liberate predominantly basic peptides which could again be enhanced with each round of panning. In addition, the PCR method gives fragments of phage DNA so performing a second round of panning requires several time-consuming manipulations. Further analysis and studies of the properties of the peptide also require expensive individual syntheses. Moreover the peptides for the synthesis of AgNPs which are selected by screening of phage display libraries have varying compositions and structures making it difficult to understand peptide sequence-AgNPs size, shape and stability relationships. Furthermore, the peptides comprise of random and inactive amino acid sequences that also complicate the understanding of their influence in the formation of AgNPs.⁶¹

A different technique that does not only screen for peptides that bind to Ag⁰ but also for Ag⁺ could play an advantage. Such a technique could out-perform the phage display approach if it can be screened at milder conditions but still able to efficiently identify peptides that induce the formation of AgNPs in different sizes. Encoded split-and-mix library strategy could be techniques which can be used to address these drawbacks in the identification of peptides that induce the formation of AgNPs.

1.3 Combinatorial Chemistry

Combinatorial chemistry is an excellent tool where rational prediction reaches its limits. The principle of the approach is to synthesize a large number of different molecules ("library"), screen them simultaneously and select the active members. This can be viewed as the chemist's attempt to imitate nature's principles of random mutation and selection for the fittest.

The capacity to produce a large variety of molecules and the existence of effective screening methods to identify active members of the library are the two factors which determine the success of a combinatorial method.

In the last decades there has been rapid growth of interest in the application of combinatorial chemistry in many fields like drug discovery,⁶⁹ catalyst development⁷⁰⁻⁷¹ and material science.

⁷²⁻⁷³ Several strategies have been developed to generate molecular diversity.⁷⁴⁻⁷⁵ One-bead-one-compound library synthesis *via* split-and-mix strategy is one of the most elegant methods to create highly diversified pools of small molecules.⁷⁶⁻⁷⁷

1.3.1 One-Bead-One-Compound Synthesis

Lam and coworkers were the first to recognize the one-bead-one-compound strategy (OBOC). It is a concept that is based on the fact that one single compound is localized on one single bead that is prepared *via* a split-and-mix synthesis.⁷⁹ The principle for the generation of one-bead-one-compound libraries relies on successive cycles of splitting the solid phase resin into equal portions (step 1 of Figure 35). Subjecting each portion to a different reaction (step 2). The modified resin portions are combined and mixed (step 3) and are ready for splitting again into equal portions for the next synthesis cycle. This approach leads to an exponential increase of the diversity of products relative to the number of reactions performed. After x reaction cycles with n different reactions performed in each cycle the maximal number of compounds equals n^x . Since each bead has been subjected to only one reaction during each cycle, therefore each bead carries only one compound. This approach allows for the synthesis of a large number of compounds with relatively few reaction steps (Figure 35).

At the end of synthesis, depending on the resin loading, picomole quantity of compound is localized on each bead. This amount is sufficient to analyse *via* Edman degradation, however this method is restricted to linear peptides and do not allow the use of non-natural amino acids or totally different building blocks. Mass spectrometry⁸⁰⁻⁸² as well as ¹³C-NMR and ¹H-NMR⁸³⁻⁸⁴ (especially to large beads) are possible but the distinction of compounds with identical mass is rather difficult if not impossible by these methods. An alternative approach known as encoding technique was then introduced.⁸⁵

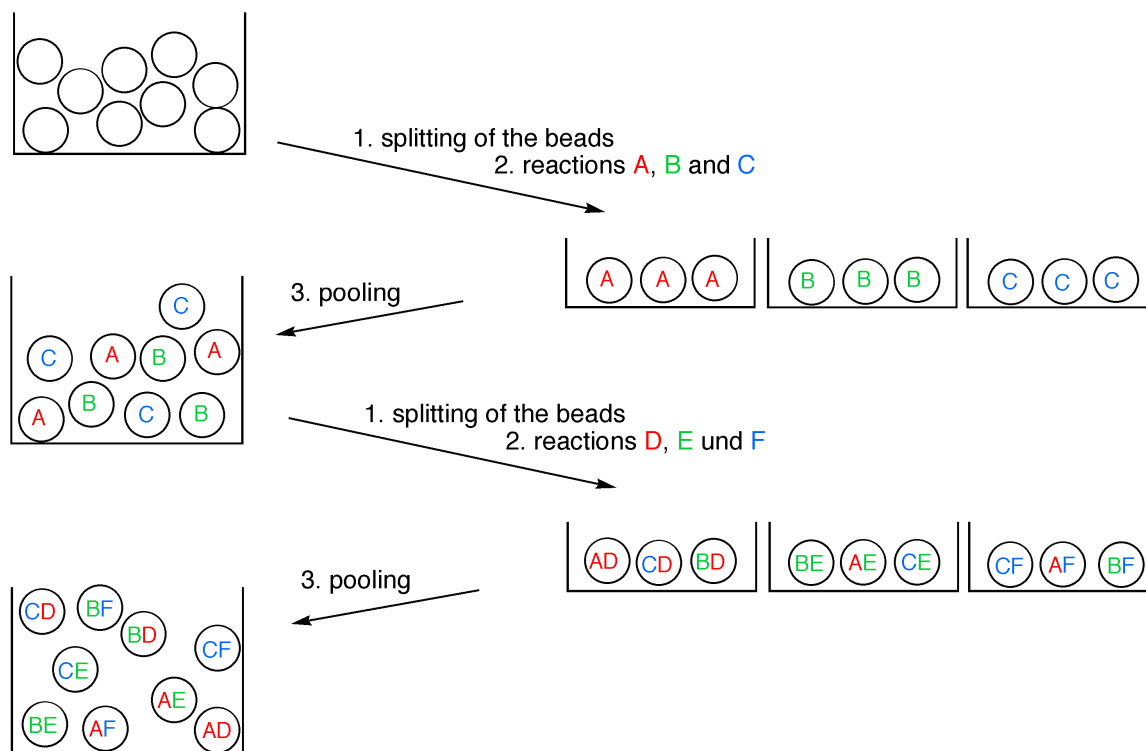


Figure 35: Split-and-mix synthesis

1.3.2 Encoded Split-and-Mix Synthesis

The principle of encoding relies on the attachment of molecular tags in each reaction vessel of each cycle to the resin beads that can be later cleaved off and analysed easily and unequivocally. Since each reaction step is encoded (Figure 38), the tags can report the synthetic history of the corresponding bead. The beauty about encoding is that the analysis can even be performed when the compound of interest has been modified during the screening.

The first molecular tags used were oligonucleotides⁸⁶ and oligopeptides.⁸⁷ However, their use had some disadvantages such as instability to numerous reaction conditions. Ideally, tag molecules should have the following properties:

- a) inert under various reaction conditions,
- b) easily detectable on a very small scale,
- c) easily attached and detached from the solid support.

The poly-halogenated aromatic alcohols shown in Figure 36 have been found to fulfill these requirements.⁸⁸⁻⁸⁹ They can be analysed on a 1 picomole scale by gas chromatography coupled to electron capture detection (EC-GC) since this detection method is very sensitive to halogenated compounds.

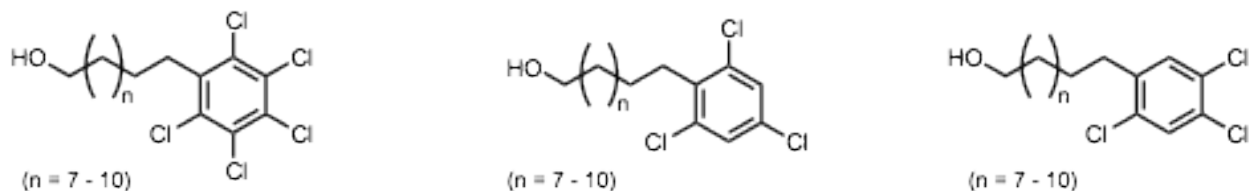


Figure 36: Tag alcohols used for library encoding

Variations of the halogen pattern as well as the hydrocarbon chain lengths result in different retention times in the EC-GC analysis. The tag alcohols are coupled either *via* a carbonate bond to 3-nitro-4-hydroxymethyl-benzoic acid⁸⁸ or *via* an ether bond to vanillic acid⁸⁹ which serve as linkers to the solid support (Figure 37). Irradiation with UV-light in case of the nitrobenzoic acid or oxidation with ceric ammonium nitrate (CAN) releases the tag alcohols for EC-GC detection.

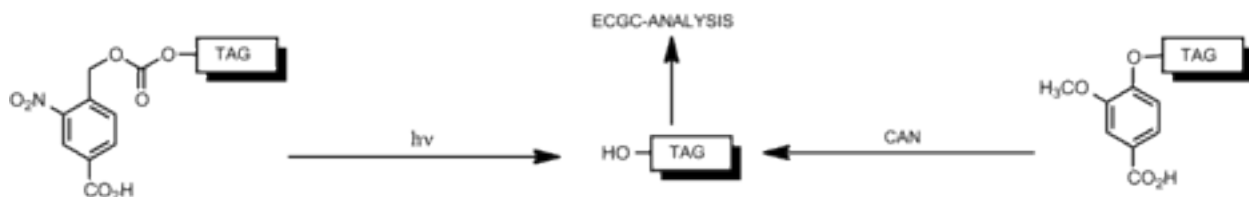


Figure 37: Linkers to attach the tags to the solid support

For encoding the reactions, a binary code is used whereby each reaction step is encoded by an array of tags rather than by one single tag and this allows for encoding of a large number of compounds.⁸⁸ As illustrated in Figure 35, given two tags (T_1 and T_2), T_1 encodes for reaction A and T_2 for reaction B while the combination of T_1 and T_2 can be used to encode for reaction C (rather than a third tag). Therefore, the binary encoding scheme allows the encoding of $2^N - 1$ reactions with N different tags.^{88,89}

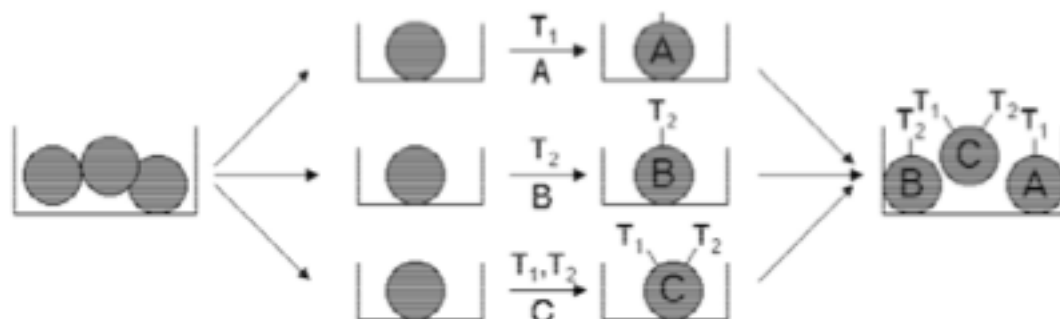


Figure 38: Encoded split synthesis

Since the detection sensitivity (1 pmol) of these tags is so high, only 1-2mol% of tags regarding the bead loading is sufficient for analysis. For peptide libraries, the tag molecules can be attached to the free *N*-terminus before the amino acid is coupled.

1.3.3 Screening Encoded Combinatorial Libraries

Combinatorial chemistry is a powerful tool that relies on the simultaneous screening of thousands of compounds in “on-bead screening” rather than testing each compound individually. In order, to visualize the selective binding of a receptor to a substrate, the receptor is marked with a dye or fluorescent molecule.⁹⁰ Such a dye-receptor conjugate system is then equilibrated with an on-bead library. The colour of the receptor concentrates on those beads carrying ligands with affinity for the receptor.

Visual inspection of the coloured beads is done through a low power microscope. A statistical representation of the coloured beads is then isolated, the tags cleaved from the beads and analysed by ECGC technique to reveal the structure of the active compounds (Figure 39).

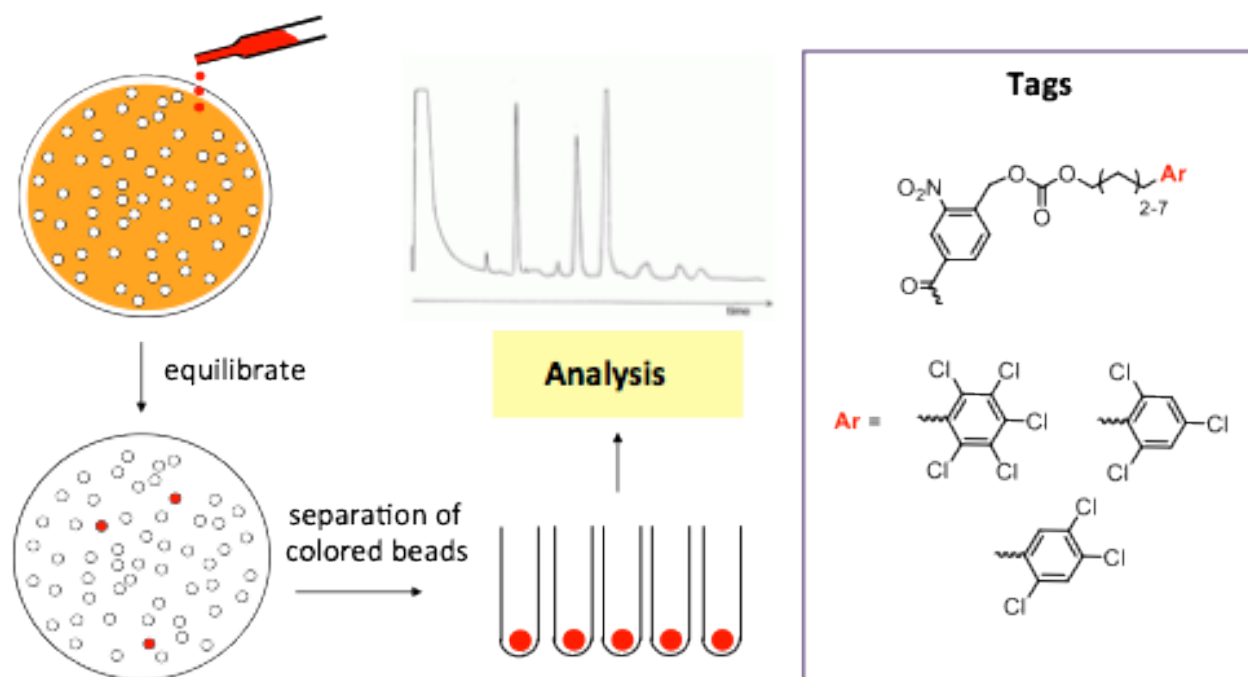


Figure 39: On bead screening of a dye marked receptor against an encoded library

II.

OBJECTIVE

Since a rational prediction might be difficult to identify a wide variety of peptides that induce AgNP formation, combinatorial approaches are attractive for the identification of suitable peptides.^{2a,d} Herein, we envisaged colorimetric on-bead screening of split-and-mix libraries to be powerful tools that could allow for the identification of peptides which can induce AgNP formation in different size.⁹¹⁻⁹² The typical size- and shape-dependent coloration of AgNPs^{2a-e} is anticipated to allow for a facile identification of active library members.

Therefore, the objective of this research was to identify, through combinatorial split-and-mix libraries, peptides that are able to induce the formation of AgNPs. The identified peptide hits were resynthesized and then evaluated as individual sequences for the formation of AgNPs on solid support. In subsequent studies, the ability of these peptides to induce the formation of AgNPs in solution and the possible formation kinetics were further explored to gain insight into the possible roles of peptides.

Since AgNPs are known to be antibacterial, studies were also carried out on the antibacterial activity of the AgNPs generated in the presence of different peptides.

III.

REFERENCES

1. R. P. Feynman. *Miniaturization*, **1961**, Reinhold, New York.
2. For reviews see: a) C.-L. Chen, N. L. Rosi, *Angew. Chem. Int. Ed.* **2010**, *49*, 2 – 21.; b) T. Tolaymat, A. El Badawy, A. Genaidy, K. Scheckel, T. Luxton, M. Suidan, *Sci. Tot. Environ.*, **2010**, *5*, 999 - 1006.; c) Y. Xia, Y. Xiong, B. Lim, S. E. Skrabalak, *Angew. Chem. Int. Ed.* **2009**, *48*, 60 – 103.; d) M. B. Dickerson, K. H. Sandhage, R. R. Naik, *Chem. Rev.*, **2008**, *108*, 4935 - 4978.; e) Y. A. Krutyakov, A. A. Kudrinskiy, A. Y. Olenin, G. V. Lisichkin, *Russian Chem. Rev.* **2008**, *77*, 233 - 257.
3. D. Kim, S. Park, J. H. Lee, Y. Y. Jeong, S. Jon, *J. Am. Chem. Soc.* **2007**, *129*, 7661.
4. P. C. Lee, D. J. Meisel, *Phy. Chem.* **1982**, *86*, 3391 - 3395.
5. H. Cong, C. F. Becker, S. J. Elliott, M. W. Grinstaff, J. A. Porco, *J. Am. Chem. Soc.*, **2010**, *132*, 7514–7518.
6. W. Yan, R. Wang, Z. Xua, J. Xu, L. Lin, Z. Shen, Y. Zhou, *J. Molecular Catalysis A: Chemical* **2006**, *255*, 81.
7. K. S. Shin, J. Y. Choi, C. S. Park, H. J. Jang, K. Kim, *Catal. Lett.*, 2009, *133*, 1–7.
8. J. Liu, A. Wang, Y. Chi, H. Lin, C. Mou, *J. Phys. Chem. B* **2005**, *109*, 40–3.
9. D. B. Hamal, K. J. Klabunde., *J. Colloid Interface Sci.*, **2007**, *311*, 514–22.
10. a) Zhao, Y. Tian, Y. Cui, W. Liu, W. Ma, X. Jiang, *J. Am. Chem. Soc.* **2010**, *132*, 12349–12356.; b) B. Hamad, *Nat. Rev. Drug Discovery* **2010**, *9*, 675.
11. a) V. K. Sharma, R. A. Yngard, Y. Lin, *Advances in Colloid and Interface Science* **2009**, *145*, 83.; b) L. S. Nair, C. T. Laurencin, *J. Biomed. Nanotechnol.* **2007**, *3*, 301.
12. J. S. Kim, E. Kuk, K. N. Yu, J.-H. Kim, S. J. Park, H. J. Lee, S. H. Kim, Y. K. Park, Y. H. Park, C.-Y. Hwang, Y.-K. Kim, Y.-S. Lee, D. H. Jeong, M.-H. Cho, *Nanomedicine: Nanotechnology, Biology, and Medicine* **2007**, *3*, 95–101.
13. http://en.wikipedia.org/wiki/Silver_Nano.

14. J. L. Elechiguerra, J. L. Burt, J. R. Morones, A. Camacho-Bragado, X. Gao, H. H. Lara, M. J. Yacaman, *J. Nanobiotechnol.*, **2005**, 3, 6.
15. R. Vaidyanathan, K. Kalishwaralal, S. Gopalram, S. Gurunathan, *Biotechnol. Adv.*, **2009**, 27, 924–937.
16. M. A. Franco-Molina, E. Mendoza-Gamboa, C. A. Sierra-Rivera, R. A Gómez-Flores, P. Zapata-Benavides, P. Castillo-Tello, J. M. Alcocer-González, D. F Miranda-Hernández, R. S. Tamez-Guerra, C. Rodríguez-Padilla, *J. Experimental & Clinical Cancer Research* **2010**, 29, 148.
17. National Cancer Institute: Breast Cancer Treatment. **2007**, <http://www.cancer.gov>.
18. D. W. Kim, G. H. Hong, H. H. Lee, S. H. Choi, B. G. Chun, C. K. Won, I. K. Hwang, M. H. Won, *Neuroscience* **2007**, 117, 387-400.
19. P. V. Asharani, M. P. Hande, S. Valiyaveetil, *BMC Cell Biology*, **2009**, 10, 65.
20. B. Y. Ahn, E. B. Duoss, M. J. Motala, X. Guo, S. Park, Y. Xiong, J. Yoon, R. G. Nuzzo, J. A. Rogers, J. A. Lewis, *Science* **2009**, 323, 1590.
21. S. M. Wang, C. W. Leung, P. K. L. Chan, *Appl. Phys. Lett.* **2010**, 97, 023511.
22. G. Gao, *Nanostructures and nanomaterials. Synthesis, Properties & Applications* **2004**, Imperial College Press, London.
23. R. Paul, R. N. Gayen, S. Hussain, V. Khanna, R. Bhar, A. K. Pal, *Eur. Phys. J. Appl. Phys.* **2009**, 47, 10502.
24. a) A. Fojtik, A. Henglein, *Ber. Buns. Gesellsch.-Phys. Chem.*, **1993**, 97, 252.; b) P. Smejkal, K. Siskova, B. Vlckova, J. Pflieger, I. Sloufova, M. Slouf, P. Mojzes, *Spectrochim Acta A Mol. Biomol. Spectrosc.* **2003**, 2321-9.
25. F. Mafune, J. Kohno, Y. Takeda, T. Kondow, H. Sawabe, *J. Phys. Chem. B* **2000**, 104, 9111.
26. F. Mafune, J. Kohno, Y. Takeda, T. Kondow, H. Sawabe, *J. Phys. Chem. B* **2000**, 104, 8333.
27. Y. H. Chen, C. S. Yeh, *Colloid and Surf. A* **2001**, 197, 133.
28. T. Tsuji, D. Thang, Y. Okazaki, M. Nakanishi, Y. Tsuboi, M. Tsuji, *Appl. Surface Sci.*, **2008**, 254, 5224.
29. J. M. Lehn. *Supramolecular Chemistry*, **1995**, VCH, Weinheim.
30. K. J. Lee, Y. Lee, I. Shim, B. H. Jun, J. H. Cho, J. Joung, *Sol. St. Phen.*, **2007**, 124–126,

1189–92.

31. a) D. Dorjnamjin, M. Ariunaa, Y. K. Shim, *Int J Mol Sci.*, **2000**, *9*, 807–20.; b) J. Yang, J. Y. Lee, H. Too, *J. Phys. Chem. B* **2005**, *109*, 19208–12.
32. A. Y. Olenin, Y. A. Krutyakov, A. A. Kudrinskii, G. V. Lisichkin, *J. Colloid*. **2008**, *70*, 71–6.
33. A. Roucoux, J. Schulz, H. Patin, *Chem. Rev.*, **2002**, *102*, 3757-3778.
34. R. J. Hunter, *Foundations of Colloid Science*, Oxford University Press, New York, **1987**, *1*, 316.
35. Y. Lin, R. G. Finke, *J. Am. Chem. Soc.* **1994**, *116*, 8335.
36. a) G. Schmid, B. Morun, J. O. Malm, *Angew. Chem., Int. Ed. Engl.*, **1989**, *28*, 778.; b) C. Amiens, D. De Caro, B. Chaudret, J. S. Bradley, R. Mazel, C. Roucau, *J. Am. Chem. Soc.*, **1993**, *115*, 11638.
37. L. Balan, J. Malval, R. Schneider, D. Burget, *Mater. Chem. Phys.*, **2007**, *104*, 417–421.
38. W. Wang, X. Chen, S. Efrima, *J. Phys. Chem. B* **1999**, *103*, 7238 - 7246.
39. L. Guo, J. Nie, B. Du, Z. Peng,, B. Tesche, K. Kleinermanns, *J. Colloid Interface Sci.*, **2008**, *319*, 175–181.
40. Z. Jiang, C. Liu, L. Sun, *J. Phys. Chem. B*, **2005**, *109*, 1730–5.
41. J. Turkevich, P. C. Stevenson, J. Hiller, *Discuss. Faraday Soc.* **1951**, *11*, 55.
42. H. Wang, X. Qiao, J. Chena, X. Wang, S. Ding, *Mater. Chem. Phys.*, **2005**, *94*, 449.
43. B. Wiley, Y. Sun, B. Mayers, Y. Xia, *Chem. Eur. J.*, **2005**, *11*, 454.
44. P. C. Lee, D. J. Meisel, *Phy Chem.* **1982**, *86*, 3391-3395.
45. J. A. Creighton, C. G. Blatchford, M. G. Albrecht, *J. Chem. Soc. Farad. Trans. II* **1979**, *75*, 790–798.
46. A. Pal, T. Pal, *J. Raman Spectrosc.*, **1999**, *30*, 199 - 204.
47. R. Jin, Y. Cao, C. A. Mirkin, K. L. Kelly, G. C. Schatz, J. G. Zheng, *Science* **2001**, *294*, 1901.
48. M. Maillard, P. Hung, L. Brus, *Nano Lett.*, **2003**, *3*, 1611.
49. a) V. K. Sharma, R. A. Yngard, Y. Lin, *Advances in Colloid and Interface Sci.*, **2009**, *145*, 83.; b) Y. J. Nam, J. R. Lead, *Sci. Tot. Env.* **2008**, *400*, 396–414.
50. Y. Xia, Y. Xiong, B. Lim, S. E. Skrabalak, *Angew. Chem. Int. Ed.* **2008**, *47*, 2 – 46.
51. Y. Sun, Y. Xia, *Science*, **2002**, *298*, 2176.
52. M. Maillard, S. Giorgio, M.-P. Pileni, *J. Phys. Chem. B* **2003**, *107*, 2466-2470.

53. H. H. Huang, X. P. Ni, G. L. Loy, C. H. Chew, K. L. Tan, F. C. Loh, J. F. Deng, G. Q. Xu, *Langmuir* **1996**, *12*, 909–912.
54. R. Klaus, R. Joerger, E. Olsson, C. G. Granqvist, *Proc. Natl. Acad. Sci. USA*, **1999**, *96* 13611.
55. T. Klaus-Joerger, R. Joerger, E. Olsson, C. G. Granqvist, *Trends Biotechnol.*, **2001**, *19*, 15.
56. A. Ahmad, P. Mukherjee, S. Senapati, D. Mandal, M. I. Khan, R. Kumar, M. Sastry, *Colloids Surf., B* **2003**, *28*, 313.
57. N. Dura'n, P. D. Marcato, O. L. Alves, G. I. H. De Souza, E. Esposito *J. Nanobiotechnol.*, **2005**, *3*, 81.
58. D. K. Newman, R. Kolter *Nature* **2000**, *405*, 94.
59. A.R. Shahverdi, S. Minaeian, H. R. Shahverdi, H. Jamalifar, A.-A. Nohi, *Pro. Biochem.*, **2007**, *42*, 919.
60. R. R. Naik, S. J. Stringer, G. Agarwal, S. E. Jones, M. O. Stone, *Nat. Mater.* **2002**, *1*, 169.
61. R. R. Naik, S. E. Jones, C. J. Murray, J. C. McAuliffe, R. A. Vaia, M. O. Stone, *Adv. Funct. Mater.* **2004**, *14*, 25.
62. C. F. Barbaras, D. R. Burton, J. K. Scott, G. J. Silverman, *Phage Display: A Laboratory Manual*, **2001**, Cold Spring Harbor Laboratory Press: Cold Spring Harbor, New York.
63. P. R. Selvakannan, A. Swami, D. Srisathiyarayanan, P. S. Shirude, R. Pasricha, A. B. Mandale, M. Sastry, *Langmuir* **2004**, *20*, 7825–7836.
64. A. R. Bassindale, A. Codina-Barrios, N. Frascione, P. G. Taylor, *Chem. Commun.*, **2007**, 2956.
65. J. Xie, J. Y. Lee, D. I. C. Wang, Y. P. Ting, *ACS Nano* **2007**, *1*, 429.
66. J. M. Slocik, J. T. Moore, D. W. Wright, *Nano Lett.*, **2002**, *2*, 169-173.
67. S. Si, T. K. Mandal, *Chem. Eur. J.*, **2007**, *13*, 3160 – 3168.
68. S. Ray, A. K. Das, A. Banerjee, *Chem. Commun.*, **2006**, 2816–2818.
69. G. Jung, ‘*Combinatorial Chemistry: Synthesis, Analysis, Screening*’, WILEY-VCH, **1999**.
70. M. T. Reetz, *Angew. Chem. Int. Ed.* **2001**, *40*, 284.
71. P. Krattiger, C. McCarthy, A. Pfaltz, H. Wennemers, *Angew. Int. Ed.* **2003**, *42*, 1722.
72. E. W. McFarland, W. H. Weinberg, *Trends in Biotechnology*, **1999**, *17*, 107.
73. H. M. Geysen, R.H. Meloen, S. J. Barteling, *Proc. Natl. Acad. Sci. USA* **1984**, *81*, 3398.
74. S. P. A. Fodor, J.L. Read, M. C. Pirrung, L. Stryer, A.T. Lu, D. Solas, *Science* **1991**, *251*, 767.

75. R. A. Houghten, C. Pinilla, S. E. Blondelle, J. R. Appel, C. T. Dooley, J. H. Cuervo, *Nature* **1991**, 352, 84.
76. A. Furka, F. Sebestyén, M. Asgedom, G. Dibo, *Int. J. Pept. Protein Res.* **1991**, 37, 487.
77. K. S. Lam, S. E. Salmon, E. M. Hersh, V. J. Hruby, W. M. Kazmierski, R. J. Knapp, *Nature* **1991**, 354, 82.
78. M. Lebl, V. Krchnak, N. F. Sepetov, B. Seligmann, P. Strop, S. Felder, K. S. Lam, *Biopolymers* **1995**, 7, 58.
79. K. S. Lam, M. Lebl, V. Krchnak, *Chem. Rev.* **1997**, 97, 411–448.
80. N. F. Sepetov, O. L. Issakova, M. Lebl, K. Swiderek, D.C. Stahl, T. D. Lee, *Rapid Comm. Mass Spectrom.* **1993**, 7, 58.
81. J. Metzger, S. Stevanovic, J. Brünjes, K.-H. Wiesmüller, *Methods* **1994**, 6, 425.
82. B. J. Egner, G. J. Langley, M. Bradley, *J. Org. Chem.* **1995**, 60, 2652.
83. R. C. Anderson, J. P. Stokes, M. J. Shapiro, *Tetrahedron Lett.* **1995**, 36, 5311.
84. J. K. Chen, S. L. Schreiber, *Angew. Chem. Int. Ed. Engl.* **1995**, 90, 953.
85. S. Brenner, R. A. Lerner, *Proc. Natl. Acad. Sci. USA* **1992**, 89, 5381.
86. M.C. Needles, D. G. Jones, E. H. Tate, G. L. Heinkel, L. M. Kocherberger, W. J. Dower, R. W. Barret, M. A. Gallop, *Proc. Natl. Acad. Sci. USA* **1993**, 90, 10700.
87. J. M. Kerr, S. C. Banville, R. N. Zuckermann, *J. Am. Chem. Soc.* **1993**, 115, 2529-2531.
88. M. H. J. Ohlmeyer, R. N. Swanson, L. W. Dillard, J. C. Reader, G. Asouline, R. Kobayashi, M. Wigler, W.C. Still, *Proc. Natl. Acad. Sci. USA* **1993**, 90, 10922.
89. H. P. Nestler, P. A. Bartlett, W.C. Still, *J. Org. Chem.* **1994**, 59, 4723.
90. J. K. Chen, W. S. Lane, A. W. Brauer, A. Tanaka, S. L. Schreiber, *J. Am. Chem. Soc.* **1993**, 115, 12591.
91. N. Srinivasan, J. D. Kilburn, *Curr. Opin. Chem. Biol.* **2004**, 8, 305 – 310.
92. J. D. Revell, H. Wennemers, *Curr. Opin. Chem. Biol.* **2007**, 11, 269 – 278.

IV.

RESULTS AND DISCUSSION

The aim of this thesis was to carry out solution phase studies and investigate how short peptides identified within split-and-mix-library **1** shown in Figure 40 (synthesized and screened by Dr. Kirsten Belser)^{1,2} could be used to induce the formation of different sized AgNPs. In this regard, the effect of pH, peptide/Ag⁺ ratio and the role of the linker between the amino acids were evaluated. Accompanying this account, are studies carried out using Isothermal Micro Calorimetric (IMC) technique on the antibacterial activity of the generated AgNPs.

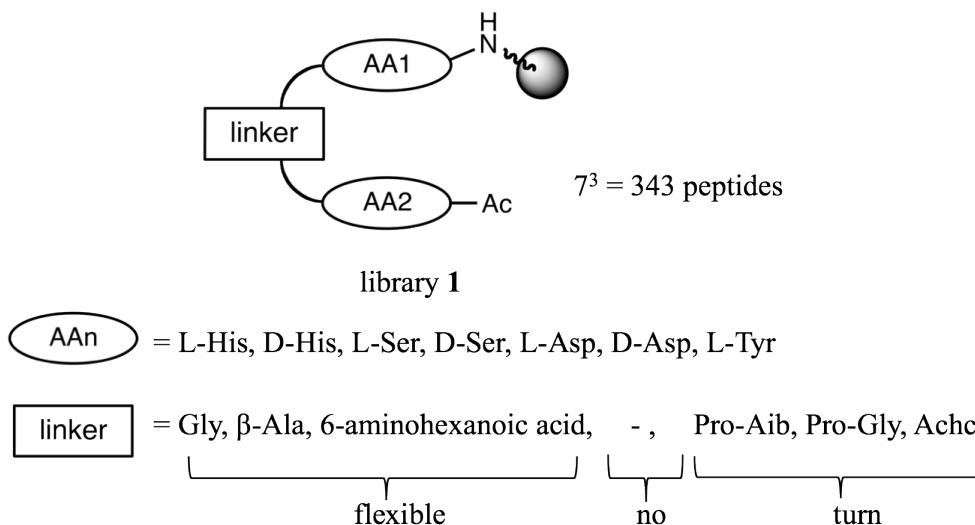
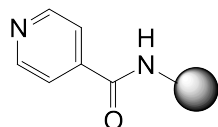


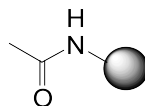
Figure 40: General structure of peptide library 1

4.1 Preliminary Experiments to the Generation of Silver Nanoparticles

Before the synthesis of library **1**, preliminary experiments were carried out (by Dr. Kirsten Belser)¹ to investigate the efficiency of calorimetric on bead (Tentagel resin) visualization of AgNPs. Tentagel resin was functionalized with isonicotinic acid, a well-known Ag-complex ligand.^{1,3} Acetylated Tentagel was used as control (Figure 41).



Isonicotinic acid coupled Tentagel



Ac-Tentagel

Figure 41: Scheme of the isonicotinic acid coupled Tentagel and acetylated Tentagel^{1,3}

Tentagel resin functionalized with isonicotinic acid and the acetylated form were treated with an aqueous solution of AgNO_3 (0.05 M). To guarantee a 100% uptake, the ratio of Ag^+ -ions to isonicotinic acid loading on the resin was approximately 10:1. The Ag^+ -ion treated Tentagel resin was then washed with nanopure water to remove the uncomplexed Ag^+ -ions, followed by the reduction of the complexed Ag^+ -ions with an aqueous solution of sodium ascorbate (0.05 M).

Analysis of the treated resin under a light microscope showed red coloured beads for the isonicotinic acid Tentagel beads whereas the acetylated Tentagel beads remained colourless (Figure 42).^{1,4} The formation of colour indicates the presence of AgNPs on the surface of isonicotinic acid Tentagel, which was confirmed by Scanning Electron Microscopy (SEM) studies (Figure 43). SEM studies revealed AgNPs of sizes up to 500 nm in diameter localized on the surface of isonicotinic acid Tentagel beads. Acetylated Tentagel beads, a control, did not show any evidence of AgNPs on the surface of beads.

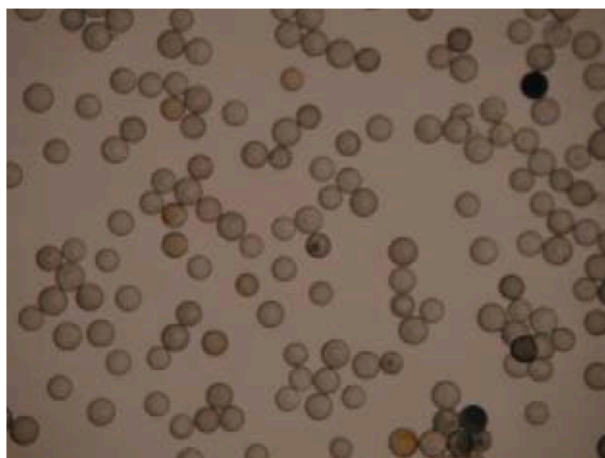


Figure 42: Light micrograph of AgNPs on isonicotinic acid functionalised Tentagel^{1,4}

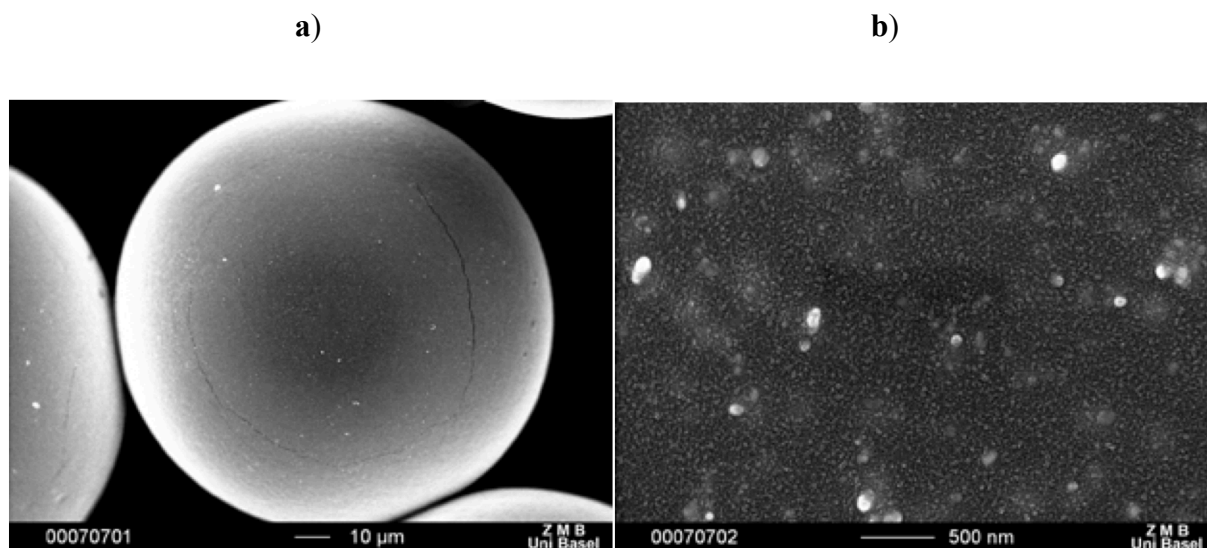


Figure 43: SEM images (a and b) of AgNPs on isonicotinic acid functionalised Tentagel^{1,4}

Thus, results shown on the image of beads from these experiments served as proof of concept of using the colourimetric on bead screening of AgNPs.

4.2 Split-and-Mix Synthesis of Encoded Library 1

Library 1 was used in our investigations to identify peptides which are able to induce the formation of AgNPs. The library was prepared by encoded photocleavable tags^{5,6} split-and-mix synthesis^{7,8} (see Chapter 1.3.2) on Tentagel resin by utilizing seven different linkers and seven different L- and D-amino acids in positions AA1 and AA2. In library 1, positions AA1 and AA2 consists of histidine (His), aspartic acid (Asp), serine (Ser), and tyrosine (Tyr), amino acids whose side groups contain N- and O- functional groups that were expected to coordinate to Ag⁺ (Figure 40). Since the Tyr moiety reduces Ag⁺-ions,^{9,10} its inclusion in the library was to allow the investigation of its influence in the formation of nanoparticles in solution. Amino acids in positions AA1 and AA2 were linked by linkers of varying flexibility and geometry to allow for diverse spatial arrangements of their side-chain functional groups. Aminoisobutyric acid (Aib), Pro-Aib, trans-2-Aminocyclohexanoic acid (Achc) and Pro-Gly were chosen as turn-inducing linkers whereas β-alanine, glycine (Gly) and 6-aminohexanoic acid (Ahx) as flexible linkers. At the end of the synthesis the library consisted maximally of $7^3 = 343$ different peptides (Figure 40), each localized on a single bead.

Amino acid couplings were performed by following the standard Fmoc/*t*Bu protocol for peptide synthesis using HCTU/*i*Pr₂NEt as the coupling reagent and piperidine for Fmoc deprotections (Fmoc = 9-fluorenylme-thyloxycarbonyl, HCTU = 2-(6-Chloro-1H-benzotriazole-1-yl)-1,1,3,3-tetramethylaminium hexafluorophosphate).

4.3 Combinatorial Screening of Encoded Split-and-Mix Library 1

Library 1 was then used to identify peptides which can induce the formation of AgNPs. Typically different sizes and shapes of AgNPs display different colours, a property utilized in the screening studies.¹¹ The screening involved the incubation of library 1 with an aqueous solution of AgNO₃ followed by several washing steps with nanopure water to remove the excess of silver ions. Sodium ascorbate was then used to reduce Ag⁺-ions which were complexed to the peptides on the beads. Within ten minutes several beads became coloured and the colour ranged from yellow and light orange to dark red (Figure 44). Different colours are indicative of AgNPs of different sizes.¹¹ Therefore, this result suggests that different peptides within the library induce the formation of AgNPs of different sizes upon chemical reduction of the Ag⁺-ions. This hypothesis was confirmed by SEM studies, which clearly demonstrate the formation of AgNPs on the coloured beads (Figure 44).⁴

Several coloured beads from each colour category of the assay were isolated. Following DMF washing of the beads, they were irradiated under high intensity UV light, liberating the tag alcohols contained on each bead. Subsequent EC-GC analyses of the sequences on the beads revealed Tentagel bound peptides bearing a histidine (His) residue in combination with either an aspartate (Asp), a serine (Ser) or a tyrosine (Tyr) residue give red or dark orange coloured beads whereas combinations between Tyr and Ser or Asp give yellow coloured beads (Table 3). Interestingly, linker type did not affect the colour, suggesting that the relative orientation of the two amino acids in a peptide is not crucial for their activity. Furthermore there was no pronounced selectivity for L- or D-configured amino acids which also indicates that the stereochemistry of the amino acids does not play a crucial role in the formation of AgNPs on the bead (Table 3).

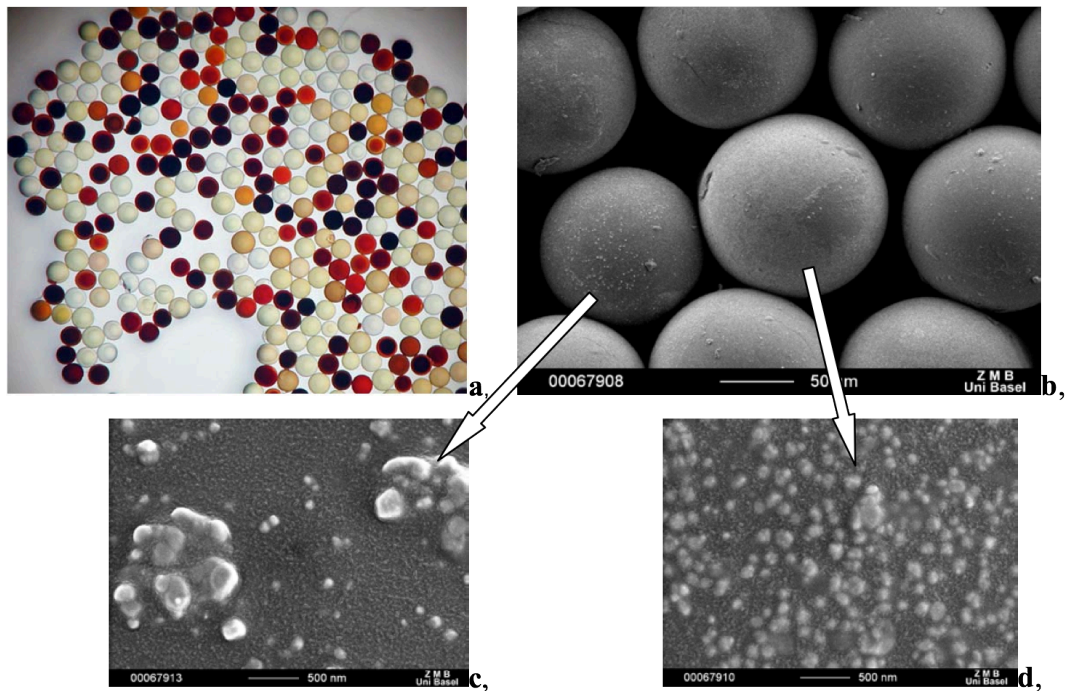


Figure 44: Library 1 after Ag^+ incubation and sodium ascorbate reduction of Ag^+ , light microscopic (a) and SEM images (b, c and d)⁴

Bead colour

Red/dark orange

Light orange/yellow

Active peptide

Ac-His-X-His-resin
 Ac-His-X-Asp-resin
 Ac-Asp-X-His-resin
 Ac-His-X-Tyr-resin
 Ac-Tyr-X-His-resin
 Ac-His-X-Ser-resin
 Ac-Ser-X-His-resin
 Ac-Asp-X-Asp-resin
 Ac-Ser-X-Tyr-resin
 Ac-Tyr-X-Ser-resin
 Ac-Asp-X-Ser-resin
 Ac-Ser-X-Asp-resin
 X = random linker

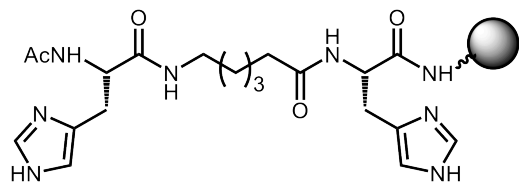
Table 3: Peptide consensus sequences on differently coloured beads

4.4 Ag-Nanoparticle Formation by Immobilised Peptides 2a-4b

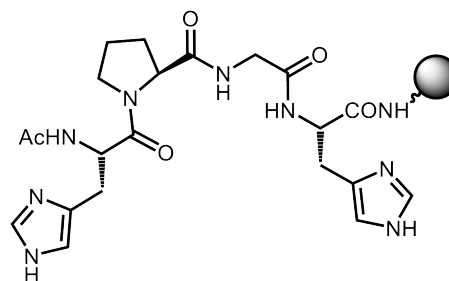
Based on the combinatorial screening results, we decided to look into further the ability of the active peptides to generate AgNPs as individual sequences as well as to validate the combinatorial screening results. Several representative samples of the identified peptides from each colour category were resynthesized on Tentagel resin. Peptides were resynthesized in order to evaluate the influence of the linker and the role of Tyr in the formation of AgNPs. Most importantly, the peptides chosen were expected to give better understanding of how the formation and size of AgNPs depend of the different peptides. Among several active peptide sequences resynthesized and evaluated for the AgNP formation, in this thesis peptides which showed higher frequencies from the combinatorial results are discussed.

Peptide sequences containing His with His (peptides **2a-b**) found on dark red coloured beads, His with Asp (peptides **3a-b**) found on light red coloured beads and Ser with Tyr found on yellow beads (**4a-b**) were resynthesised. To evaluate the effect of the nature of the linker, the sequences contain an aminohexanoic acid (Ahx) moiety as flexible linker (**2a**, **3a** and **4a**) or a proline-glycine (ProGly) as rigid linker (**2b**, **3b** and **4b**) (Figure 45). These linkers which we chose were all hits in the combinatorial screening experiments.

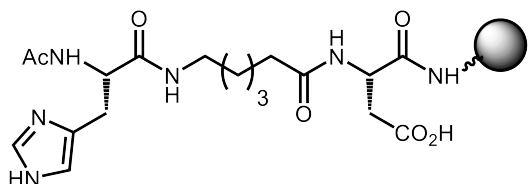
Scanning Electron Microscopy was used to characterize AgNP size and their distribution, and to understand the formation of the nanoparticles. For the determination of the loading of Ag⁺-ions on Tentagel beads localized with different peptides, we used Atomic Absorption Spectroscopy (AAS).



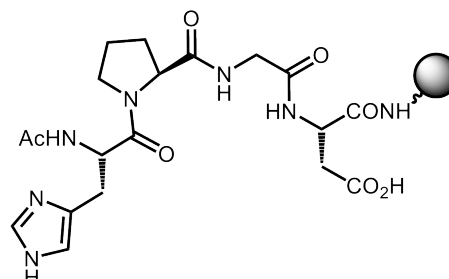
2a



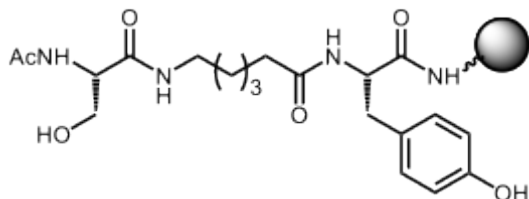
2b



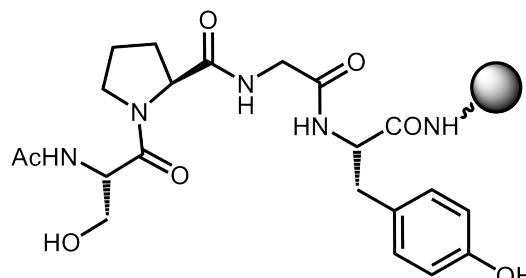
3a



3b



4a



4b

Figure 45: Structures of peptides **2-4** used for the AgNP formation on Tentagel solid support.

Peptides bound on Tentagel resin were treated under the same conditions as the tripeptide library during the generation of AgNPs. Thus, the beads were incubated with AgNO₃ solution, washed with nanopure water followed by incubation in a solution of sodium ascorbate. Visual inspection of the beads under a light microscope revealed that the beads bearing the His/His motive (**2a** and **2b**) had turned dark red, those with the His/Asp motive (**3a** and **3b**) were dark orange and the Ser/Tyr beads (**4a** and **4b**) were yellow, thereby confirming the combinatorial screening results (Figure 46). The nature of the linker did not affect the colouration in either bead bound peptide sequence, thus we reasoned that it plays no significant role in the formation of AgNPs.

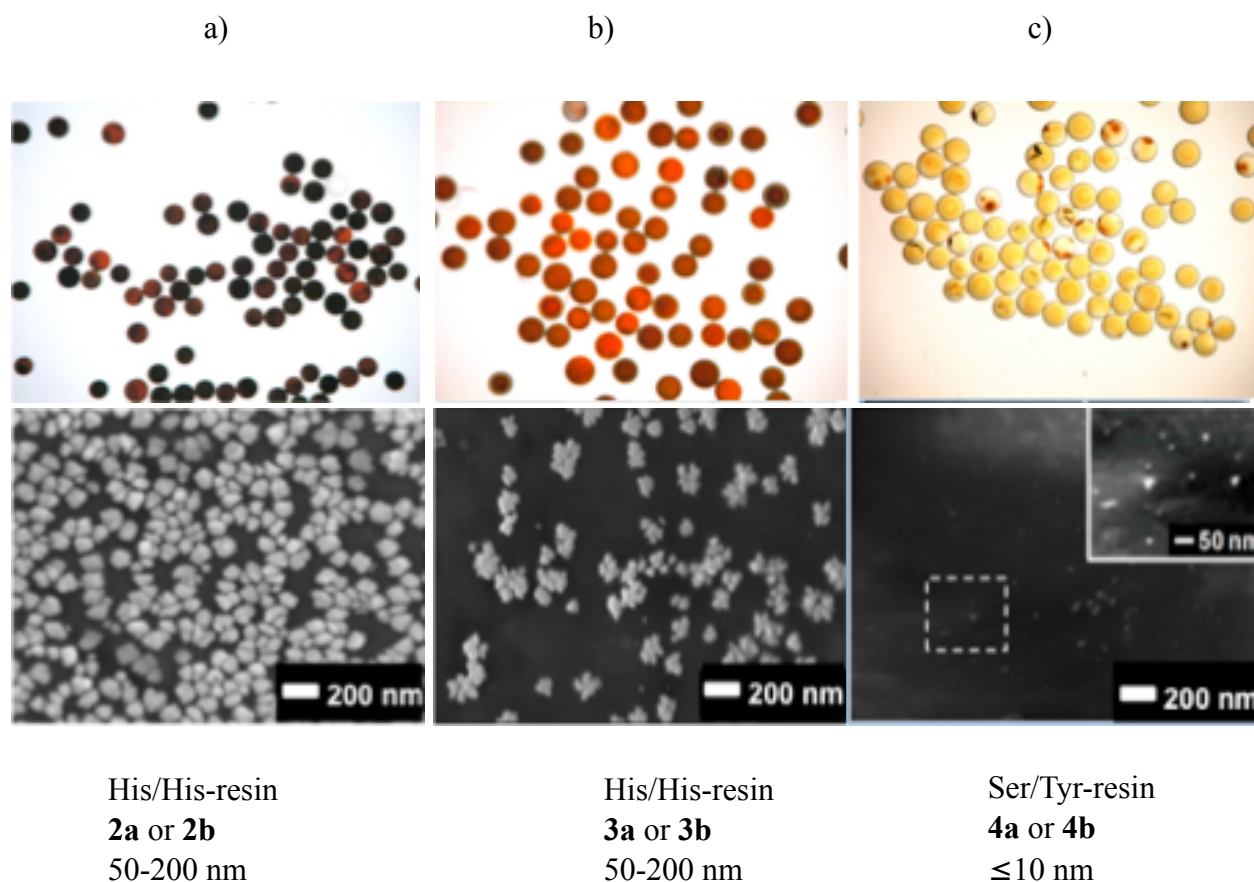


Figure 46: Light microscopic (top row) and SEM pictures (bottom row) for AgNPs generated by peptide sequences **2** (a), **3** (b) and **4** (c)

SEM analyses of the bead-bound AgNPs showed that the red or dark orange colour from the His/His or His/Asp peptides corresponds to NPs with an average diameter of approximately 50 nm that can agglomerate to larger assemblies of up to 200 nm (Figure 23). Contrastingly, the yellow coloured beads from the Ser/Tyr peptide reveal AgNPs which are significantly smaller, with an average diameter of approximately 10 nm (Figure 23). These results demonstrate that different peptides induce the selective formation of AgNPs of different sizes on bead.

Uptake of Ag⁺-ions by different peptides on beads was calculated by measuring the remaining Ag⁺-ion concentration after Ag⁺-ions are complexed by immobilized peptides (Table 4). Atomic Absorption Spectroscopy (AAS) was used in the Ag⁺-ion uptake studies. Such studies on the uptake of Ag⁺-ion can also give information on the Ag⁺-ion affinity of the different peptides with reference to earlier studies which were done by Conza with the Wennemers group.¹²

Peptide	Bead colour	AgNP size	mM Ag/mM peptide
2a	Dark red	50-200 nm	0.38
2b	Dark red	50-200 nm	0.64
3a	Dark orange	50-200 nm	0.55
3c	Dark orange	50-200 nm	0.47
4a	Yellow	≤10 nm	0.26
4b	Yellow	≤10 nm	0.19

Table 4: Ag⁺-ion uptake by peptides bound on Tentagel resin

Differences in the colour of beads correlate with the amount of Ag⁺-ions that are complexed by peptides **2a-4b**, as shown in Ag⁺-ion uptake studies. A more intense colorcolour of the AgNPs on the beads, indicates that the more Ag⁺ ions is are bound to the immobilized peptide (Table 4). The uptake measurements show a significant Ag⁺-ion affinity for the sequences containing His amino acid. Except **2a**, peptide sequences containing His/His moieties have the highest Ag⁺-ion affinity, followed by His/Asp sequence. Repeats of experiments on Ag⁺-ion uptake by peptide **2a** did not result in a significant change of the result. It is not clear why this peptide gives Ag⁺-ion uptake results which differ from other His/His peptides.

Lowest Ag⁺-ion affinities were recorded for Ser/Tyr peptide sequences. These results correlate with previous studies which showed peptides containing His moieties having higher Ag⁺ ion affinity among different amino acids in various peptides.¹ These findings are in close agreement with earlier studies which showed the general tendency of silver preferring coordination with N-donor group compared to O- groups.¹³

Studies were also done to investigate if the Tyr is was able to reduce Ag⁺-ions and form AgNPs without the addition of sodium ascorbate which is the reducing agent for Ag⁺-ions. After incubating beads bearing peptides **4a** and **4b** with AgNO₃, the beads remained colourless. Hence, under these conditions Tyr is unable to reduce Ag⁺-ions.

4.5 Do the Free N-termini on Immobilized Peptides 2c-4c Influence the Formation of AgNPs ?

During the design and synthesis of library **1**, the peptides were acetylated at their N-termini to avoid unselectively binding of Ag⁺-ions to all peptide library members since Ag⁺ is known to complex with N-donor groups.¹³ Furthermore Banerjee et al. reported the participation of peptides' free amine groups (-NH₂) in capping AgNPs and stabilized the nanoparticles to prevent them from aggregation.¹⁴ Similar findings were published earlier by Reimer et al. who reported the interaction between the lone pair of electrons of on the free amine group (-NH₂) with the vacant orbitals of Ag in their its neutral state.¹⁵ In this regard we wanted to investigate if the free N-termini on immobilized peptides could have an influence in the generation of AgNPs in solution. Peptides **2c** (His/His), **3c** (His/Asp) and **4c** (Ser/Tyr) were prepared for this investigation (Figure 47). Since the linker was found to play an insignificant role in the formation of AgNPs, only the flexible linker Ahx was chosen to connect the active amino acids in the peptides.

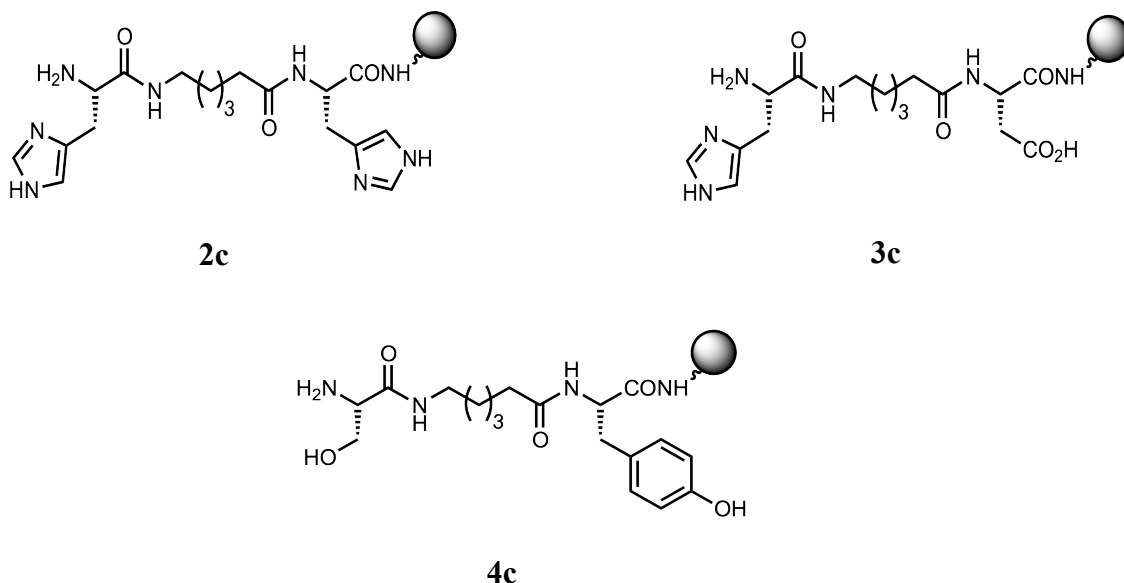


Figure 47: Structure of peptides **2c** (His/His), **3c** (His/Asp) and **4c** (Ser/Tyr) used for the AgNP formation on Tentagel solid support

In the generation of AgNPs, peptides **2c**, **3c** and **4c** were treated under the same conditions as the combinatorial screening library. Similarly, the colour of AgNPs on solid supported peptides was visualized under the light microscope (Figure 48 top). In all cases, the heterogeneity of the colour

of AgNPs on solid bound peptides shows that the $-NH_2$ group influences the generation of AgNPs. Efforts to address the inhomogeneity of the colour on beads were fruitless.

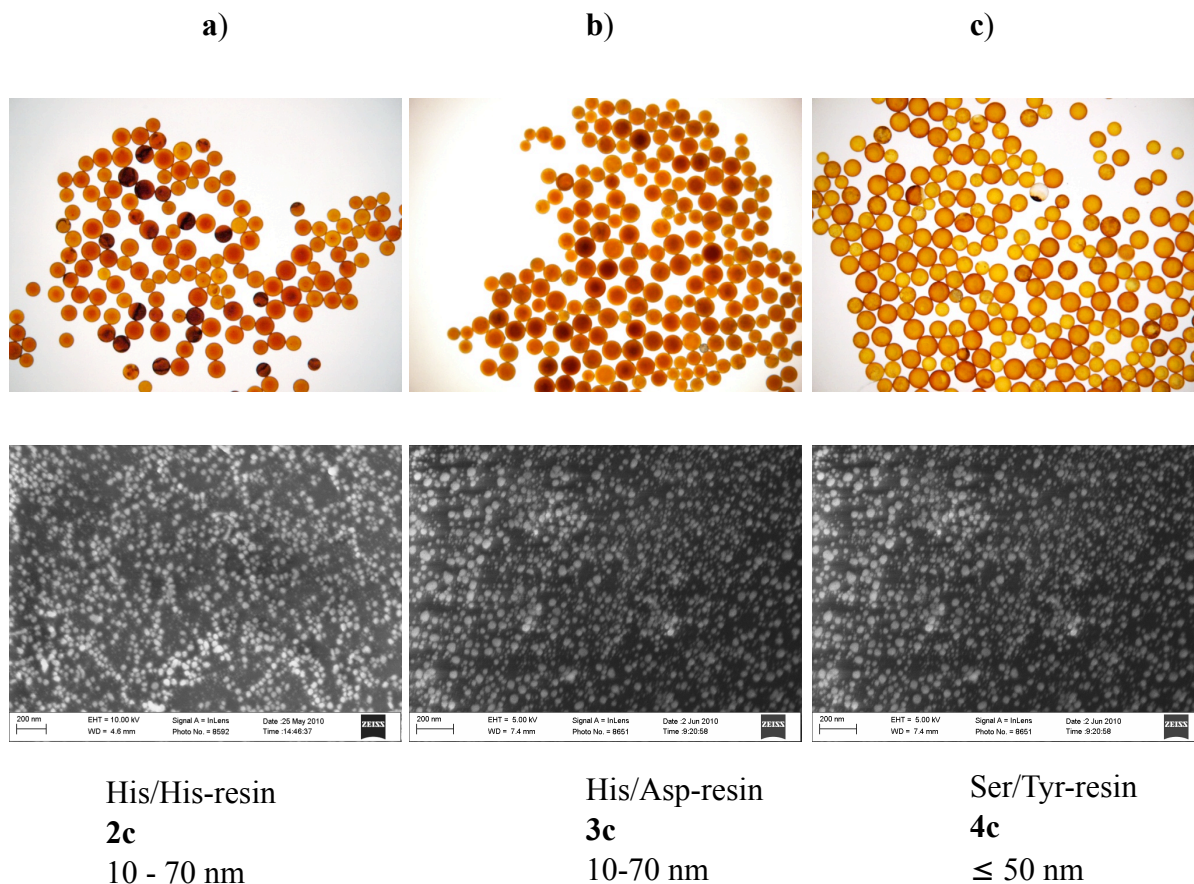


Figure 48: Light microscopic (top) and SEM pictures (bottom) for AgNPs generated in the presence of peptide sequences **2c** (a), **3c** (b) and **4c** (c)

SEM pictures reveal the highly polydisperse AgNPs on the surface of beads (Figure 48, bottom row). AgNPs generated in the presence of His/His **2c** and His/Asp **3c** were on average smaller than their acetylated counterparts, **2a** and **3a** respectively. The $-NH_2$ group on peptides **2c** and **3c** may have controlled the size of AgNPs and prevented aggregation of the nanoparticles to sizes of up to 200 nm as observed in the presence of the acetylated peptides **2a** and **3a**. However, the formation of the nanoparticles was poorly controlled by the $-NH_2$ group which is indicated by the highly polydisperse AgNPs.

Contrary to this, the Ser/Tyr **4c** peptide generates bigger nanoparticles as compared to the acetylated form, **4a**. The $-NH_2$ group could increase binding affinity of peptide **4c** to Ag^+ -ions leading to more and bigger AgNPs being generated after the reduction process.

Overall, SEM analyses of AgNPs on immobilized N-termini peptides also show the general trend in the sizes of AgNPs generated with different sequences (His/His or His/Asp > Ser/Tyr) regarding their acetylated counterparts on (Figure 46).

AgNPs formed on beads bearing resynthesized Ac- $-NH_2$ -peptides proved to be stable for several months without any change.

4.6 Ag-Nanoparticle Formation by Peptides 2d-4e in Solution Phase

Having successfully used different peptides to generate different sizes of AgNPs on solid support, we were also interested in finding out if the same trend could be achieved in solution. Moreover, many applications of AgNPs take place in solution, hence the need to investigate if our peptides could also induce the formation of AgNPs in solution which could later be tested for other applications like antibacterial action.

Peptide sequences **2d-4e** (which are similar to their solid supported counterparts), were prepared on Rink amide resin (Figure 49). The syntheses were accomplished following the general procedure for solid phase peptide synthesis (Experimental section).

Unlike the generation of AgNPs on solid support, solution phase experiments in the presence of peptides **2d-4e** proved to be more challenging since AgNPs were aggregating during their formation. However, through careful adjustment of experimental conditions like pH, ratios of peptide/ Ag^+ and Ag^+ /sodium ascorbate led to the generation of AgNPs with stabilities comparable to AgNPs on bead. For the first experiments, an excess of the peptides (10 equiv.) in comparison to silver nitrate was used for mimicking the excess found on bead. As for the generation of AgNPs on bead, sodium ascorbate was used as the reducing agent. The generation and the stability of the AgNPs were followed by UV-Visible spectroscopy, the aggregation of AgNPs being linked to the enlargement of the peaks with a decrease of their intensity over time. The size of the AgNPs was determined using TEM and in all cases the TEM pictures reported in this thesis are of scale bar 40 nm.

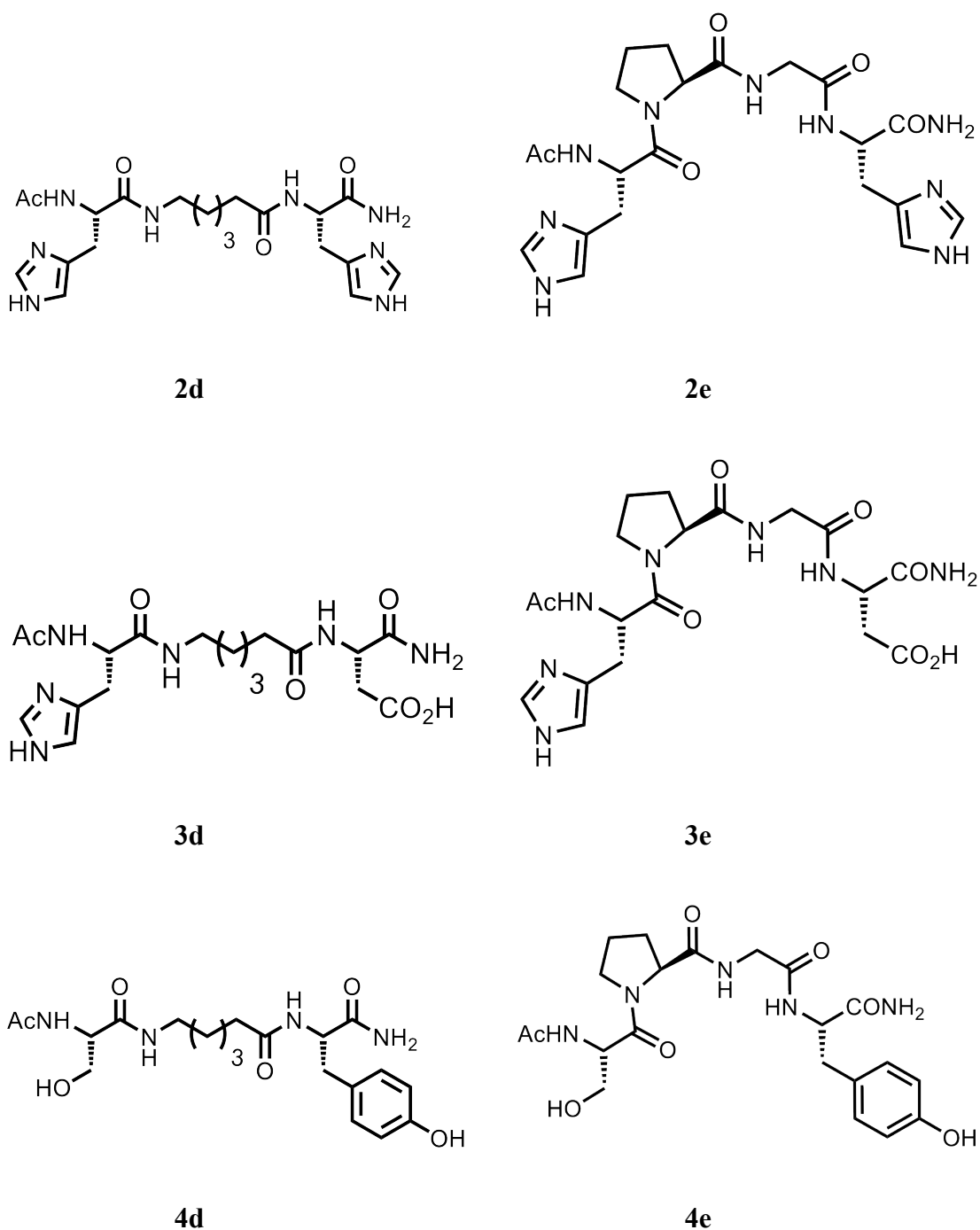


Figure 49: Structures of peptides **2d-4e** used for the AgNP formation in solution

The first experiments did not show any evidence of AgNP formation. Since PEG is predominant on Tentagel beads used as solid support for the immobilized peptides, we carried out experiments in the presence of varying amounts of PEG to act as an external stabilizer of AgNPs. The UV-spectra showed the broadening of the SPR peaks with a decrease of their intensity within a few

minutes, for example around 10 minutes. Transmission Electron Microscopy (TEM) analyses of the AgNP solutions showed aggregates of nano-and micro-particles.

Godet et al. reported sodium dodecyl sulfate (SDS) to be a capping agent for AgNPs to prevent them from aggregation during their formation.¹⁶ After the use of SDS in the presence of our peptides similar results when PEG was used were observed. SDS could not prevent the aggregation of AgNPs during their formation and this could be due to different reaction conditions from those reported.¹⁶ Godet et al. used SDS as a AgNP stabilizer but sodium citrate and hydrazine hydrate were used as reducing agents. Fortunately, after several trials, through careful adjustment of experimental conditions we found conditions that solved the challenge of AgNP instability and formation control. Herein, we demonstrate how careful adjustments of the experimental conditions allowed for the formation of highly stable AgNPs in solution.

4.6.1 Influence of pH on the Generation of AgNPs

Since the ionic state of each peptide is crucial for their properties, the generation of AgNPs was carried out in acidic and basic conditions (pH; 3, 10 and 12).¹⁷ As mentioned in section 4.6, the first experiments involved the use of an excess of the peptides (10 equiv.) compared to silver nitrate to mimick the excess found on-bead. In addition, sodium ascorbate (1.2 equiv. in all reported cases of AgNP synthesis) was used as the Ag⁺-ion reducing agent.

His/His Peptide Sequence 2d

In the presence of peptide **2d**, AgNPs did not form at any of the tested pHs. An explanation could be the strong binding affinity of His/His peptide residues to Ag⁺ as discussed in Chapter 4.4 and 4.6.3. To overcome this a stronger reducing agent like NaBH₄ could reduce Ag⁺-ions to form AgNPs. The use of NaBH₄ to reduce Ag⁺-ions in the presence of a His rich peptide Ala-His-His-Ala-His-His-Ala-Ala-Asp, was reported by Wright et al.¹⁸

His/Asp Peptide Sequence 3d

At pH 3, a slight formation of AgNPs was found in the presence of peptide **3d** with the apparition of a broad peak after 2 h (Figure 50). TEM analyses revealed the formation of large and heterogeneous aggregates of up to 500 nm in diameter. The modest formation of AgNPs that

aggregate at pH 3 might have been due to poor coordination of the peptide on the AgNPs. At this acidic pH, the amino acids His/Asp in peptide **3d** are in their protonated states (pK_a ; His_{imidazole} \approx 6 and Asp-COOH \approx 4). Therefore the imidazole as well as the carboxylic moieties bore by the peptide **3d** might not efficiently bind to AgNPs to enhance their stability.

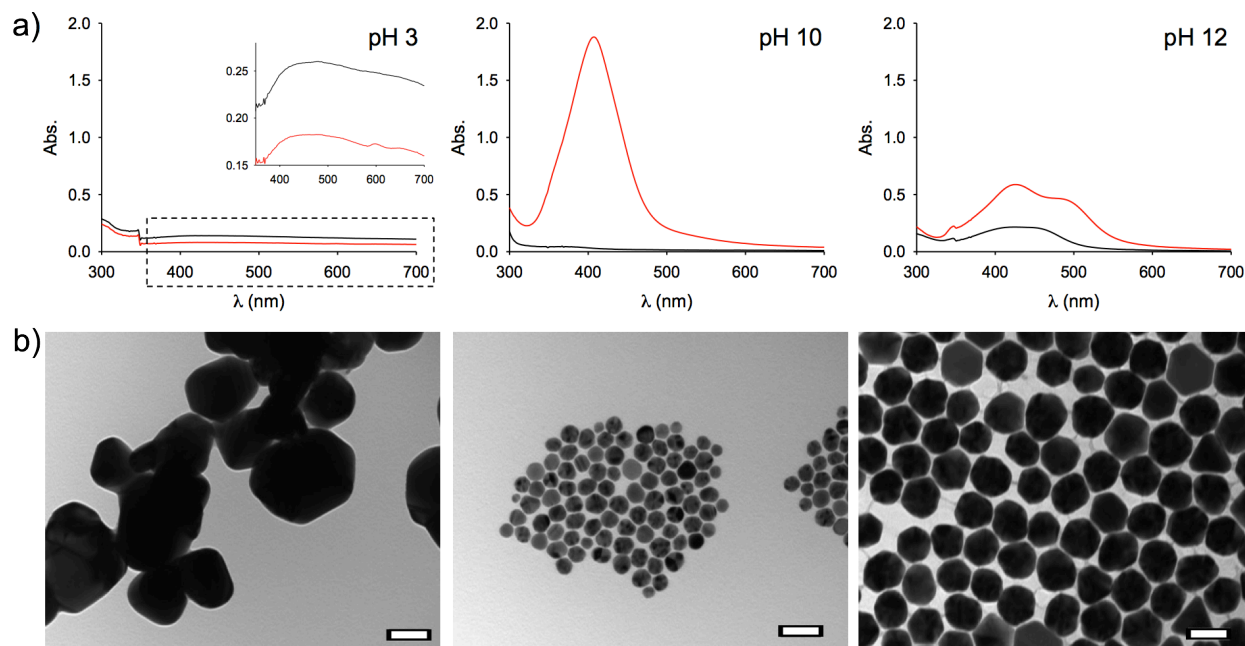


Figure 50: a) UV-Vis spectra after 10 min (black curve) and 2 hours (red curve) and b) TEM pictures (scale bar 40 nm) of the AgNPs solution generated in the presence of Ac-His-Ahx-Asp-NH₂ **3d** (10 equiv.)

Peptide **3d** at pH 10 gives AgNPs with a sharp and intense plasmon resonance band after 2 h with a maximum at a wavelength around 405 nm (Figure 27a). At pH 10 peptide **3d** generates AgNPs in defined size with an average diameter of 20 nm (Figure 50b). Peptide **3d** contains free carboxylate and imidazole groups which could influence the generation of defined size of AgNPs and stabilise the nanoparticles against aggregation at pH 10. Studies by Wright et al. reported that the carboxylate and imidazole groups of peptide Ala-His-His-Ala-His-His-Ala-Ala-Asp interacted with Ag⁰ which led to the formation of stable AgNPs at pH 8.6.¹⁸ Recently, Wang et al. also reported that a polypeptide containing aspartate and imidazole groups led to the formation of stabilised AgNPs.¹⁹ We therefore infer that the presence of negatively charged carboxylate groups and neutral imidazole on peptide **3d** has a higher affinity for coordination to AgNPs resulting in their controlled growth and stability.

AgNPs generated in the presence of peptide **3d** at pH 12, are associated with a less intense double SPR peak which both Mirkin et al.²⁰ and Xie et al.⁹ attributed this to AgNPs not having a spherical shape (Figure 50). Interestingly, the size and the shape of the AgNPs synthesized in the presence of peptide **3d** are significantly different at pH 10 and pH 12. Compared with the small uniform nanoparticles produced at pH 10, larger nanoparticles with an average size of 40 nm with different shapes, such as triangles or hexagons, were produced at pH 12 (Figure 50). These results suggest that at pH 12 the Ag⁺ ions are bound tighter to the peptide in comparison to pH 10. This tighter binding at pH 12 could mean that less Ag⁺-ions are available at the initiation of the reduction, hence fewer nuclei are formed, resulting in bigger AgNPs.

Our findings regarding the smaller size of AgNPs generated at pH 10 and bigger size of nanoparticles generated at pH 12, could be compared to the data by Sharma et al.²¹ The authors synthesised AgNPs by the tollens method in the presence of sugars (glucose, galactose, maltose or lactose). They found that an increase in pH (11.5 to 13.0) led to a relative increase in the size of AgNPs during their generation. Sharma et al reported that an increase in pH resulted in a decrease in free Ag⁺-ions in solution and following reduction of these ions, Ag nuclei were formed which grew to larger AgNPs.²¹

Therefore, our AgNP results achieved in the presence of peptide **3d** could indicate that the peptide is acting as a reservoir of Ag⁺ ions, releasing them slowly into the media for the growth process and this explains the slow growth of AgNPs at pH 12 in comparison to pH 10 (Figure 50). On the another hand, the binding of peptide **3d** to the AgNPs could allow a preferential addition of Ag⁰ atoms onto the AgNPs controlling their shape, giving triangles and hexagons at pH 12.

Our results could also be explained by the findings of Wright et al. when they used peptide Ala-His-His-Ala-His-His-Ala-Ala-Asp in the generation of AgNPs.¹⁸ After carrying out infrared analysis of the purified AgNPs, they found that the pattern of vibrational stretching frequencies revealed AgNP-carboxylate interactions. Furthermore, the histidine analogues on their peptide were found to display a loss of N-H bands implying the imidazole binding to AgNPs. From their results Wright et al. concluded that the peptide ligand interacts with Ag⁺-ions to form a ligand-stabilized precursor complex. Upon addition of reductant, small nuclei were reported to form

rapidly. The peptide would then adhere to growing Ag nuclei which results in lower surface energy on the bound faces leading to biased deposition of Ag nuclei on the unbound faces.¹⁸ The biased addition of Ag nuclei onto the nanoparticle could then explain the different shapes of AgNPs we obtained.

Ser/Tyr Peptide Sequence 4d

In a fashion similar to that observed with peptide **3d** at pH 3, TEM analyses revealed the formation of large heterogeneous aggregates of up to 500 nm in diameter (Figure 51). These aggregates of AgNPs formed at pH 3 could be a result of poor coordination of the peptide **4d** on the AgNPs, a requirement for AgNP stability. At pH 3 amino acids Ser/Tyr in peptide **4d** are in their neutral states, consequently the tyrosine residue, in its phenol form, is not able to bind tightly to the AgNPs. However, even at pH 10 peptide **4d** does not induce the formation of individual silver nanoparticles, instead aggregates are formed like at pH 3 indicated by a broad peak in the UV-Vis spectrum. This was confirmed by TEM analyses (Figure 51). The AgNP aggregates could reveal that there is still less stabilization of the growing nanoparticles since the Tyr residue in peptide **4d** is only partially deprotonated whereas the Ser is neutral at pH 10.

Interestingly, at pH 12 in the presence of peptide **4d**, nanoparticles which are formed are small and disjointed (15 nm average size) highlighted by a sharp and intense plasmon resonance band (maximum at 410 nm) in UV-Vis spectroscopy and confirmed by TEM (Figure 51). Above pH 11, the Tyr residues of peptide **4d** are deprotonated ($pK_a \approx 10$) and are available for forming peptide-AgNPs interactions as evidenced by the formation of individual AgNPs. The reduction and the AgNPs growth processes are faster than the ones observed for peptide **3d** which could be a result of the combined effect of Ag^+ ions reduction by Tyr^{9,10} along with sodium ascorbate activity. Furthermore, AgNPs generated in the presence of peptide **4d** show a larger size distribution perhaps due to the peptide being a weaker binder of Ag^+ than peptide **3d**. This lower affinity would result in both nucleation and the growth processes taking place simultaneously and this could then explain the slightly polydispersed **4d**-AgNPs.

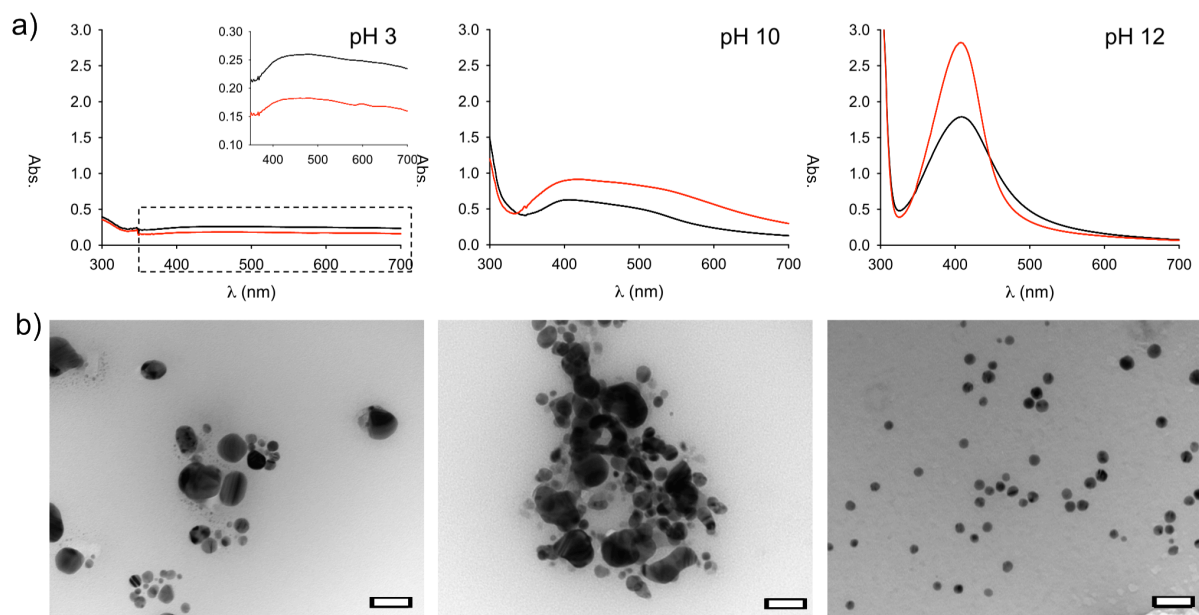


Figure 51: a) UV-Vis spectra after 10 min (black curve) and 2 hours (red curve) and b) TEM pictures (scale bar = 40 nm) of the AgNPs solution generated in the presence of Ac-Ser-Ahx-Tyr-NH₂ **4d** (20 equiv.)

Investigation of Ag₂O by Xray Photoemission Spectroscopy

Xray Photoemission Spectroscopy (XPS) analysis did not show any evidence of silver oxide formation during the generation of AgNPs. Silver oxide can affect the shape of the nanoparticles that the peptides induce. This could result in the formation of poorly defined shapes of AgNPs. Therefore XPS analysis of AgNPs was carried out to learn more about the behaviour of silver on the surface and during the reduction process. This measurement reveals the chemical environment and the oxidation state of silver in different reduced and non-reduced samples. Figure 52 shows the XPS spectrum of the Ag 3d region for **3d**- and **4d**-AgNPs. Two silver bands centred at binding energies of 367.6 and 373.6 eV, are typical for Ag⁰ and can be assigned to the 3d_{5/2} and 3d_{3/2} Ag peaks respectively.²² Anantharaman and coworkers reported the binding energy of silver oxide to be around 366 eV.²²

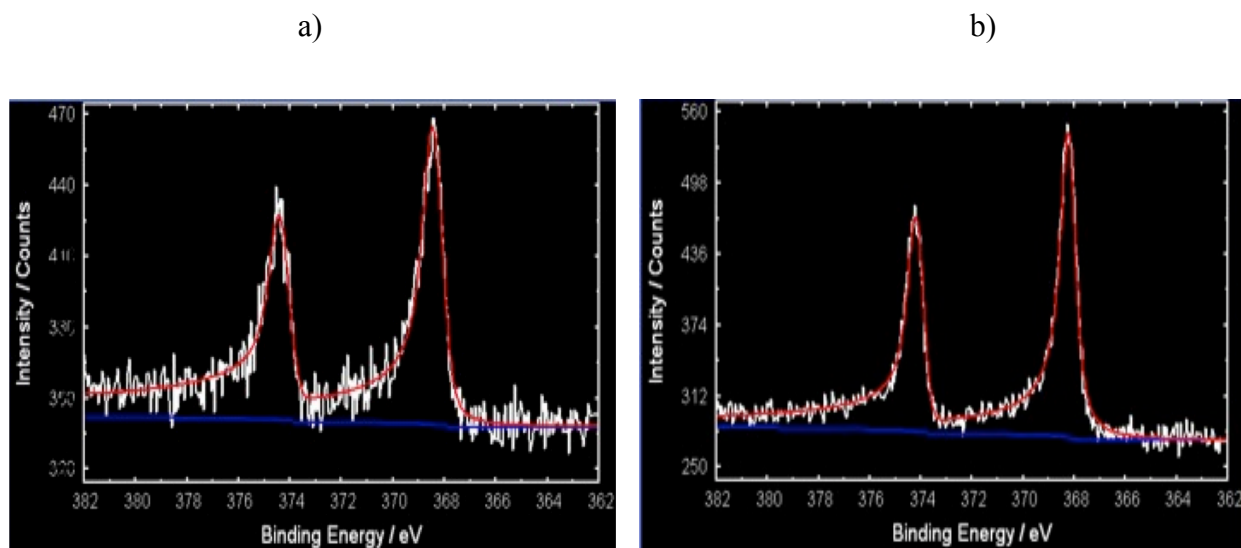


Figure 52: XPS spectra for **3d**-AgNPs (a) and **4d**-AgNPs (b) generated at pH 12.

4.6.2 Influence of Peptide Concentration on the Generation of AgNPs

After determining the optimum pH for the generation of AgNPs for each peptide, several experiments with different ratios of peptide to Ag^+ were carried out to investigate the influence of the peptide on the stability of AgNPs. We chose to use both pH 10 and 12 for the experiment with peptide **3d** since two different sizes of AgNPs were found earlier. Generations of AgNPs with different quantities of peptide **4d** were performed at the optimized pH 12. The effect of concentration of the peptide in the formation of AgNPs was monitored by measuring the UV-Vis spectra of the AgNP solution media at different time intervals. Size characterisation of AgNPs was determined by TEM analyses of the nanoparticle solution dried on carbon-coated copper grids.

His/Asp Peptide Sequence 3d

The growth rate of AgNPs at pH 10 and pH 12 was followed over a period of one hour when the growth of AgNPs terminated for peptide/ Ag^+ ratio of 1 in the presence of peptide **3d** (Figure 53 and 54). The nature of the normalised absorbance curves calculated from the UV-Vis absorbance spectra of AgNPs as a function of time indicates that the rate of AgNP formation decreases with an increase of the peptide/ Ag^+ ratio from 1:1 to 20:1 at pH 10 and pH 12 (Figures 53 and 54).

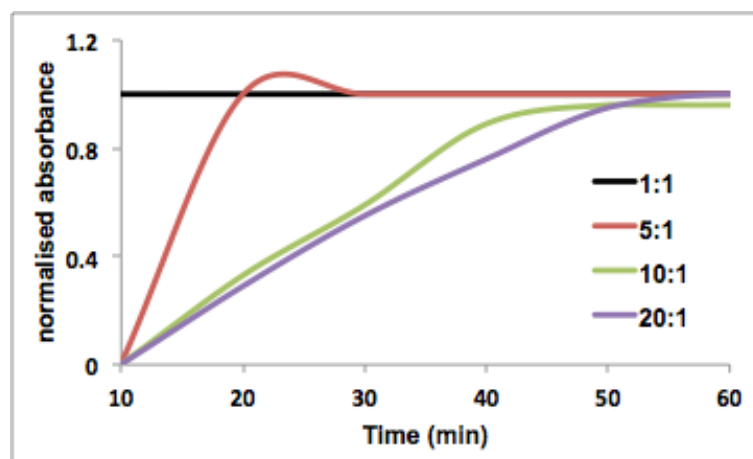


Figure 53: Normalised absorbance curves of AgNPs generated in the presence of **3d**/ Ag^+ ratios of 1:1 (at $\lambda = 402$ nm), 5:1 (at $\lambda = 404$ nm), 10:1 (at $\lambda = 406$ nm) and 20:1 (at $\lambda = 418$ nm) at pH 10

We reported (Chapter 4.6.1) that peptide **3d** could be acting as a reservoir of Ag^+ ions, releasing them slowly into the media for the growth of AgNPs. Therefore, we speculate that an increase of peptide/ Ag^+ ratio (from 1:1 to 5:1, 10:1 and 20:1) leads to more Ag^+ ions being complexed on the peptide resulting in a lower concentration of free Ag^+ -ions in solution to be reduced to form AgNPs. This slows the growth rate of AgNPs as observed in Figure 53 and 54. Furthermore, the decrease in the rate of AgNP formation with an increase of the peptide/ Ag^+ ratio (from 1:1 to 5:1, 10:1 and 20:1) could indicate that peptide **3d**'s major impact is on AgNP growth. Moreover, it has been observed by Vaia et al. that an increase in the concentration of peptide leads to a decrease in the rate of nanoparticle growth.²³ Such a role of peptide on AgNP formation takes place if the peptide's major impact is on the nanoparticle growth due to the passivation of the surface of nanoparticles.²³

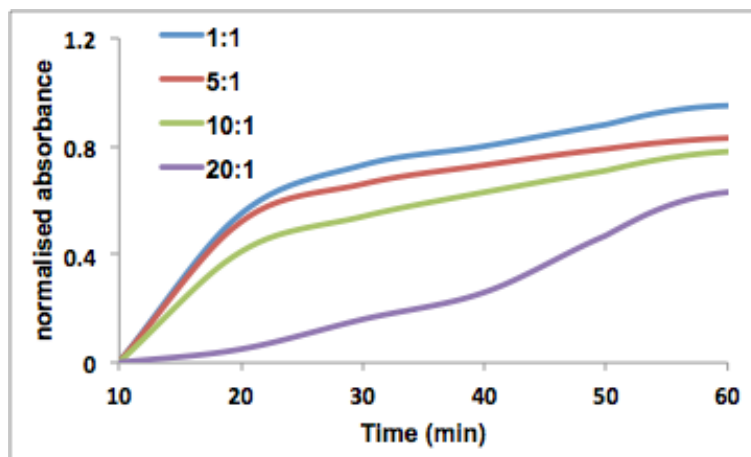


Figure 54: Normalised absorbance curves of AgNPs generated in the presence of **3d**/ Ag^+ ratios of 1:1 (at $\lambda = 409$ nm), 5:1 (at $\lambda = 428$ nm), 10:1 (at $\lambda = 432$ nm) and 20:1 (at $\lambda = 445$ nm) at pH 12

At pH 10 non-aggregated AgNPs were formed in the presence of peptide **3d** when the peptide/ Ag^+ ratio was greater than 1 (Figure 55). An increase in the size of AgNPs is correlated with an increase in the **3d**/ Ag^+ ratio from 1:1 to 20:1. Highly stable (for at least 3 months) and uniform size AgNPs were achieved when the ratio of **3d**/ Ag^+ was between 5:1 and 10:1. At lower peptide **3d**/ Ag^+ ratios (ratio = 1:1), the nanoparticles exist in form of aggregates at pH 10 revealing that there is inadequate peptide in solution to stabilise the AgNPs (Figure 55). A further increase in the **3d**/ Ag^+ ratio to 20:1 resulted in the aggregation of AgNPs over time (3 months) which can be confirmed by UV-Vis spectra (Figure 55). The aggregation of AgNPs was also confirmed by TEM analysis (Figure 55). In addition, the nanoparticles which were generated at a **3d**/ Ag^+ ratio of 20:1 are on average larger than the nanoparticles which are generated at lower **3d**/ Ag^+ ratios.

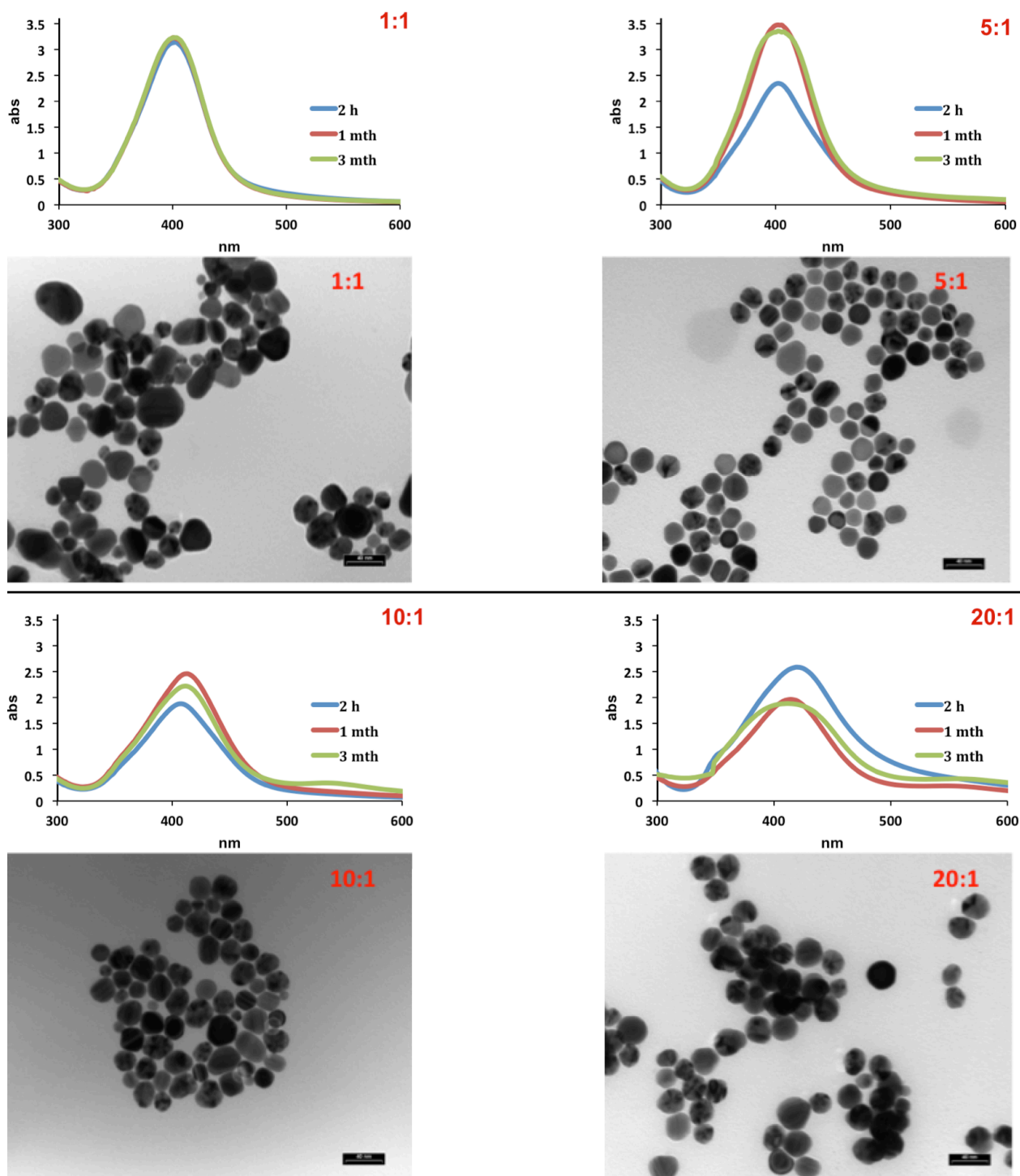


Figure 55: UV-Vis spectra and TEM pictures (scale bar = 40 nm) of **3d**-AgNPs generated in the presence of different peptide/Ag⁺ ratios at pH 10 (results presented were taken at 3 months)

Similarly, at pH 12 the average size of the AgNPs increases with an increase in the **3d**/Ag⁺ ratio (from 1:1 to 5:1, 10:1 and 20:1) as shown in Figure 56.

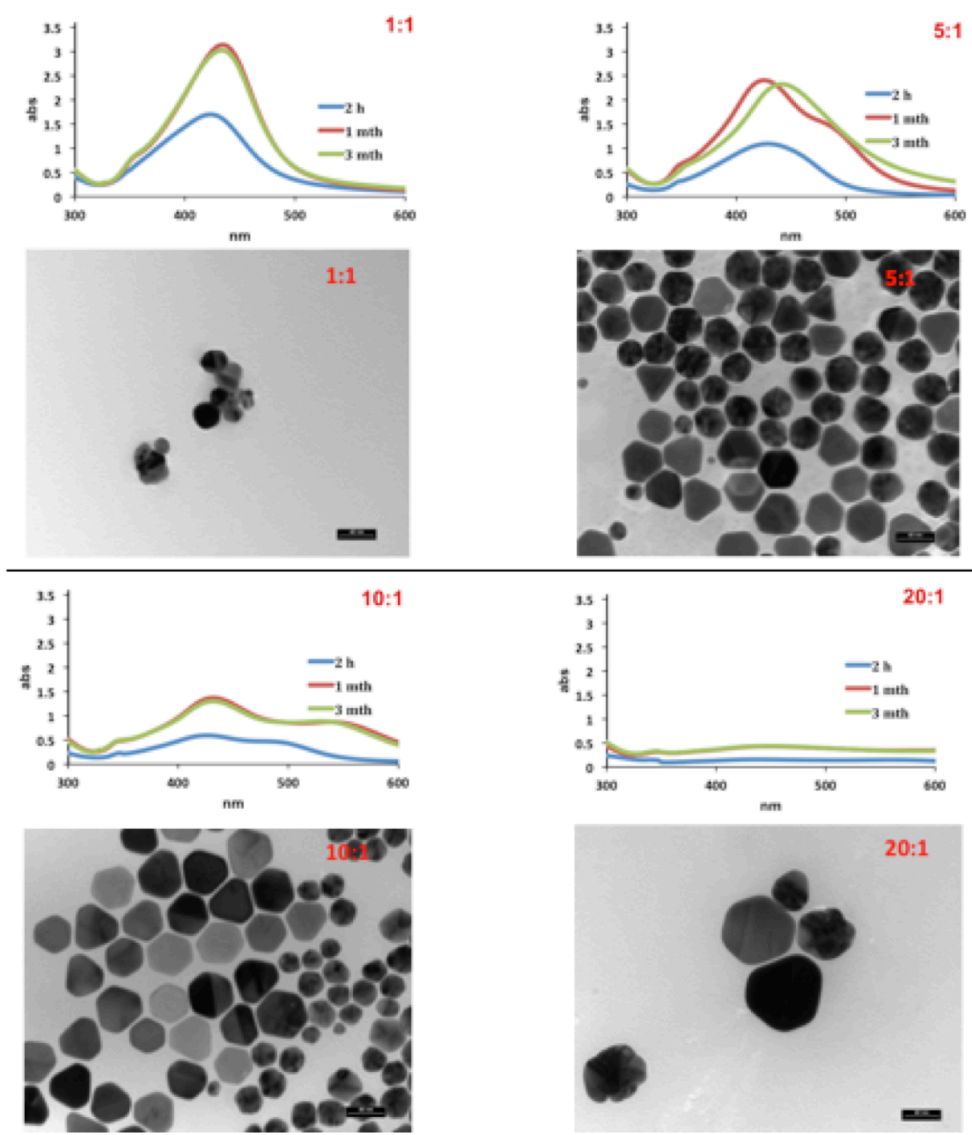


Figure 56: UV-Vis spectra and TEM pictures (scale bar = 40 nm) of **3d**-AgNPs generated in the presence of different peptide/ Ag^+ ratios at pH 12 (results presented are taken at 3 months)

An increase in the concentration of peptide **3d** could lead to more peptide- Ag^+ -ions adsorbing on the surface of growing nanoparticles resulting in the corresponding increase in nanoparticle size. Furthermore, an increase in the **3d**/ Ag^+ ratio (from 1:1 to 5:1, 10:1 and 20:1) could enhance preferential binding of the peptide on certain faces of nanoparticles. The surface energy of the faces of AgNPs where the peptides bind are lowered thereby biasing the addition of Ag-atoms on unbound faces, which could explain the formation of different shapes of AgNPs such as triangles or hexagons at pH 12. Overall AgNPs synthesised at different peptide/ Ag^+ ratios were also stable for at least three months (Figure 56).

Ser/Tyr Peptide Sequence 4d

Unlike the results achieved in the presence of peptide **3d**, an increase of peptide/Ag⁺ ratio (from 1:1 to 5:1, 10:1 and 20:1) leads to an increase in the growth rate of AgNPs in the presence of peptide **4d** (Figure 57). These results could indicate that unlike peptide **3d** whose major influence could be on the growth of AgNPs, the major impact of peptide **4d** could be in the nucleation process. Vaia and coworkers reported similar findings.²³ The pronounced decrease in the absorbance of AgNPs generated in the presence of **4d**/Ag⁺ ratios of 1:1 and 5:1 could be due to the change of nanoparticle size in the solution over time (Figure 58).

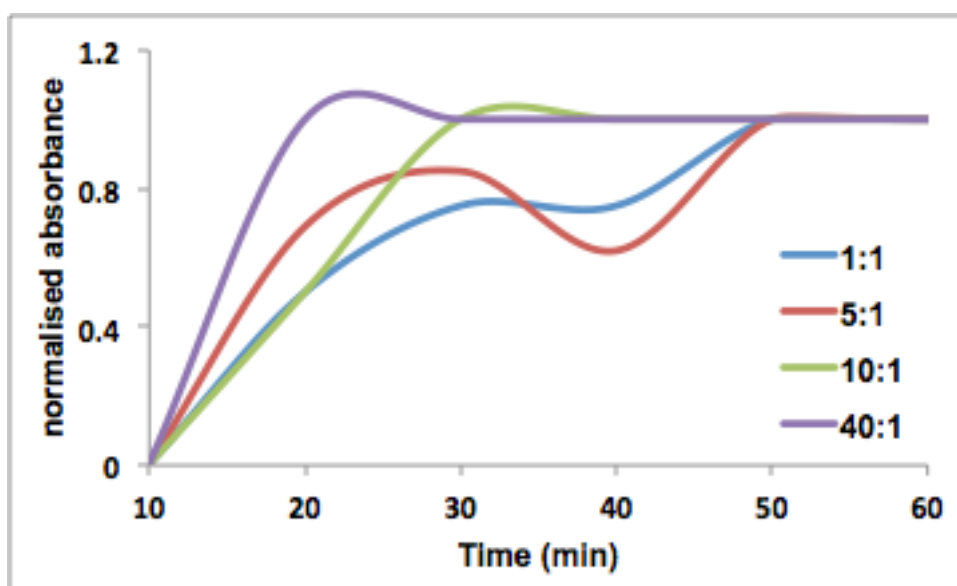


Figure 57: Normalised absorbances (at $\lambda = 409$ nm) of AgNPs generated at pH 12 in the presence of **4d**/Ag⁺ ratios of 1:1, 5:1, 10:1 and 40:1. Growth rate results of AgNPs which are presented were taken over a period of an hour when the growth of AgNPs terminated

In the presence of peptide **4d**, AgNPs aggregate at a ratio of peptide/Ag⁺ of 1:1 (Figure 58) at pH 12. Figure 58 shows that the UV-Vis spectra become sharper as the **4d**/Ag⁺ ratio increases from 1:1 to 40:1 favouring the generation of smaller (≤ 15 nm) and nearly monodisperse nanoparticles (Figure 58).

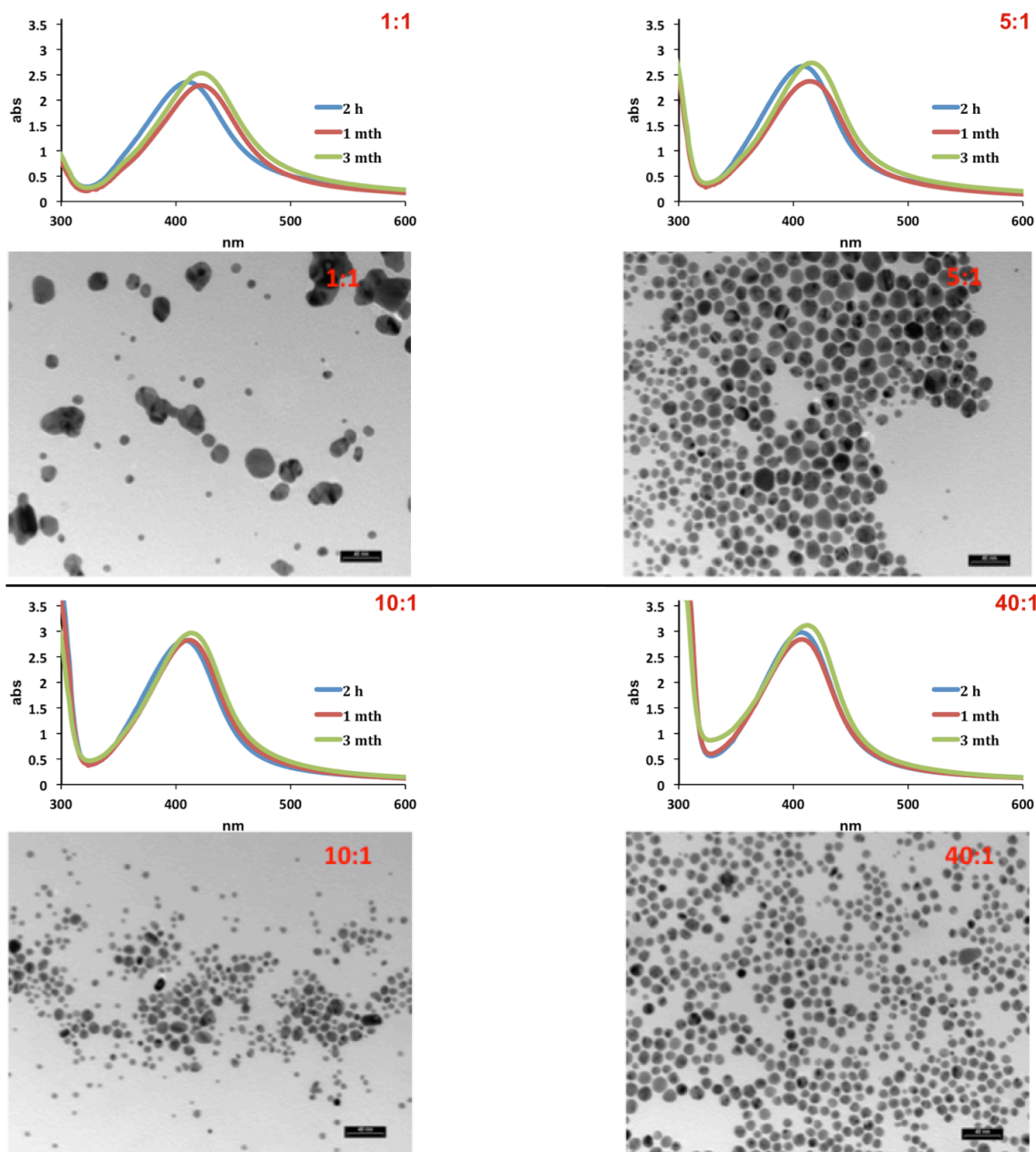


Figure 58: UV-Vis spectra and TEM pictures (scale bar = 40 nm) of **4d**-AgNPs generated in the presence of different peptide/Ag⁺ ratios at pH 12 (results presented were taken at 3 months)

4.6.3 The Role of the Linker in AgNP Formation

The combinatorial screening studies have shown that the relative orientations of the two amino acids in a given peptide might not be crucial for the affinity of the peptides to Ag⁺/AgNPs whereas the nature of the amino acids is responsible for the different size of the AgNPs.² In order to support this finding, we carried out further studies on the formation of AgNPs in solution.

The morphology of the AgNPs obtained in the presence of peptides **3e** and **4e**, which both bear a rigid linker are similar to their respective counterparts with a flexible linker, at the optimized conditions (Figure 55). These results further support the finding that the linker does not play a crucial role in the formation of AgNPs, but only the different active amino acids in a peptide (Figure 59).

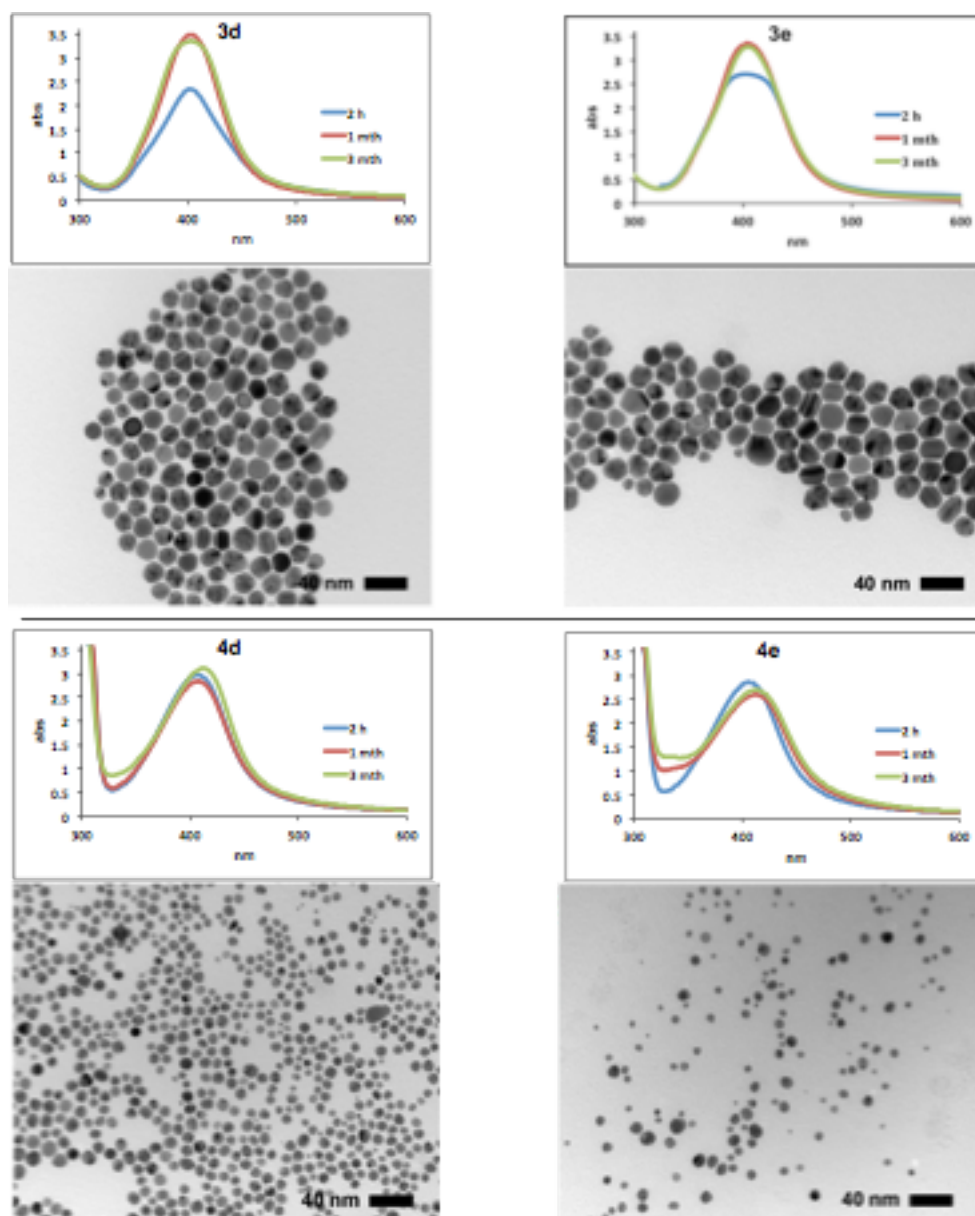


Figure 59: UV-Vis spectra and TEM pictures (scale bar = 40 nm) of AgNPs generated in the presence of different linkers of peptides **3d-e** and **4d-e** at pH 10 and pH 12 respectively (results presented were taken at 3 months)

Peptide-Ag⁺ Binding Affinity Studies by Isothermal Titration Calorimetry

Isothermal titration calorimetry (ITC) is a powerful and highly sensitive technique that is capable of measuring the change in the enthalpy upon intermolecular/intramolecular interaction of species in solution.²⁴ We have investigated the non-covalent interaction of peptides during titration against aqueous AgNO₃ to rationalize the observed different behaviour of the different peptides during the formation of AgNPs.

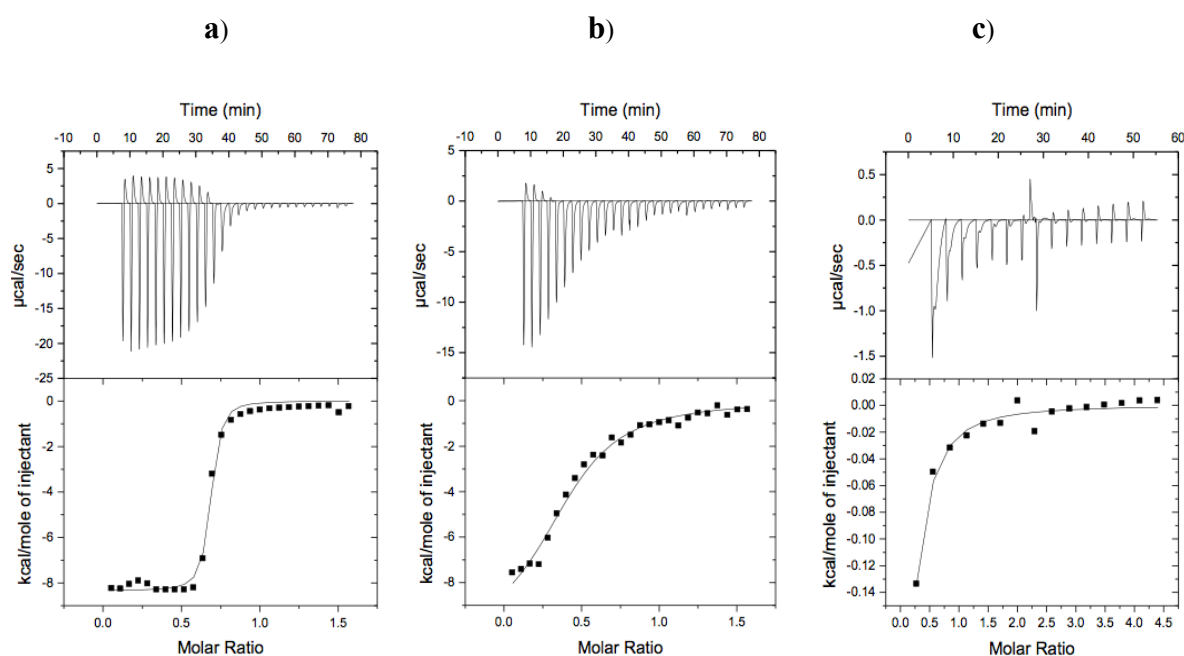


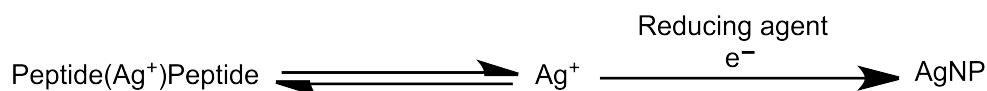
Figure 60: ITC titration data describing the interaction of peptide **2d** (a), **3d** (b) and **4d** (c) with Ag⁺-ions at pH 7.5

The experiment revealed that peptide **2d** bearing two His residues binds Ag⁺ at pH 7.5 with a binding $\Delta G = -8.5 \pm 0.06$ kcalmol⁻¹ and is the strongest ligand among the peptides tested (Figure 60 and Table 5). This could explain the observation that when using ascorbate as a reducing agent no AgNP were formed in the presence of this peptide. Ag⁺-ions are probably bound tightly to the imidazole moieties of this peptide. Xie and coworkers reported that Ag⁺ complexation lowers the reducibility of Ag⁺-ions.⁹ Therefore, the reducibility of the peptide(Ag⁺)peptide complex is expected to decrease with an increase in the binding strength. In case of Ac-His-Ahx-His-NH₂ **2d**, the equilibrium lies heavily to the peptide(Ag⁺)peptide complex resulting in no Ag⁺-ions in available solution to be reduced to form AgNPs (Scheme 4).

Peptide	ΔG (kcalmol ⁻¹)
Ac-His-Ahx-His-NH ₂ 2d	-8.5 ± 0.06
Ac-His-Ahx-Asp-NH ₂ 3d	-5.5 ± 0.12
Ac-Ser-Ahx-Tyr-NH ₂ 4d	-4.2 ± 0.34

Table 5: Binding affinities of peptides **2d**, **3d** and **4d** to Ag⁺-ions

In addition, the ITC measurements indicate stronger binding of peptide **3d** ($\Delta G = -5.5 \pm 0.12$ kcalmol⁻¹) with Ag⁺-ions whereas the interaction is weaker for peptide **4d** ($\Delta G = -4.2 \pm 0.34$ kcalmol⁻¹) under identical conditions. For peptide **2d** the observed binding affinity is a result of the combined non-covalent interactions of the two imidazole residues (pKa His (imidazole) ≈ 6) with Ag⁺-ions. At pH 7.5 the imidazole and the aspartic acid (pKa Asp (-COOH) ≈ 4) residues in peptide **3d** could be both contributing to non-covalent interactions with Ag⁺-ions. For peptide **4d** containing amino acids tyrosine (pKa ≈ 10) and serine (pKa ≈ 13), at pH 7.5 the observed binding affinity ($\Delta G = -4.2 \pm 0.34$ kcalmol⁻¹) could be mainly from the Ag⁺-ions interacting with tyrosine's π -electron system.



Scheme 4: General outline of a peptide-Ag⁺ complex

4.6.4 Could the free N-termini on Peptides Influence the Formation of AgNPs in Solution?

Similarly, studies were carried out to investigate the influence of the terminal NH₂-group of peptides **2f**, **3f** and **4f** on the formation of AgNPs (Figure 61).

Peptides **2f** (NH₂-His-Ahx-His-NH₂), **3f** (NH₂-His-Ahx-Asp-NH₂) and **4f** (NH₂-Ser-Ahx-Tyr-NH₂) were used as additives under identical conditions to those used with their acetylated forms during the generation of AgNPs. For comparison, only pH 10 was considered and used for peptide **2f** and **3f** while pH 12 was used for peptide **4f**.

After mixing peptide **2f** with AgNO_3 and subsequent addition of sodium ascorbate, the mixture remained colourless. The extra $-\text{NH}_2$ group did not improve the problems on the formation of AgNPs in the presence of the peptide $\text{NH}_2\text{-His-Ahx-His-NH}_2$ **2f**.

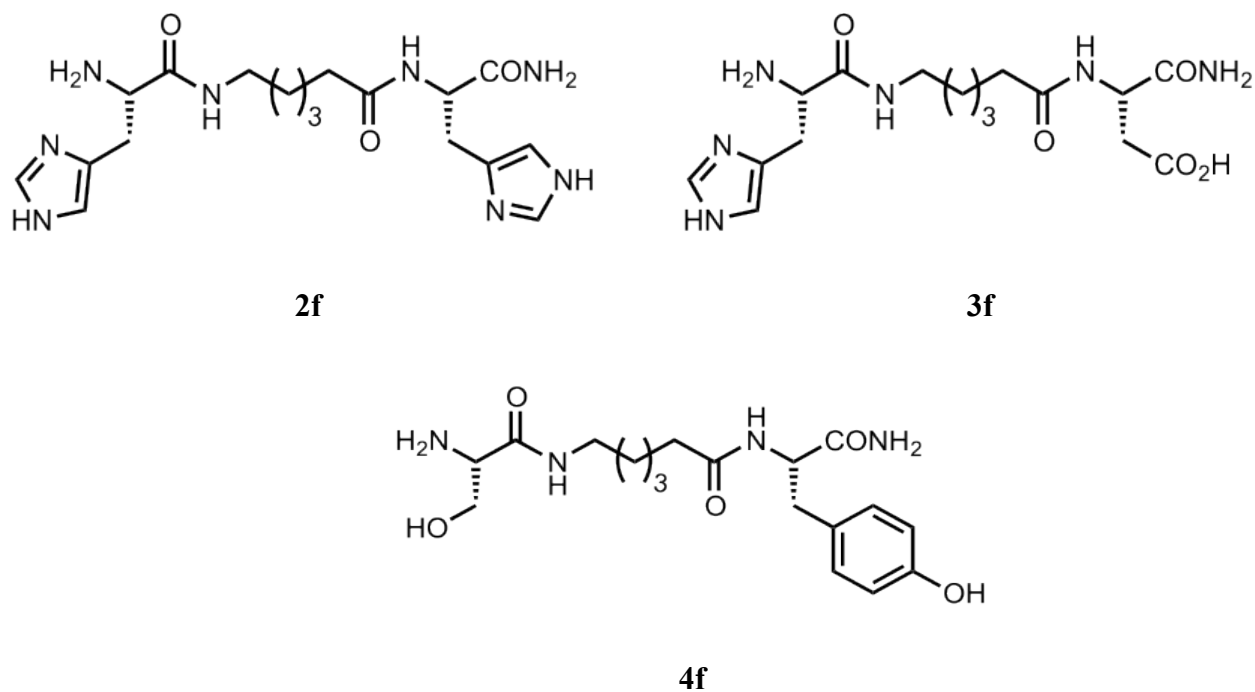


Figure 61: Structures of peptides **2f**, **3f** and **4f** which were used in AgNP formation

Interestingly, in the presence of the His and Asp residue bearing peptide **3f** highly stable (for at least 3 months) AgNPs were generated. Comparing the 2 h UV spectra (Figure 62a-b) of **3f**- and **3d**-AgNPs, the $-\text{NH}_2$ group led to lower SPR absorbance of AgNPs. This was expected since the $-\text{NH}_2$ group is an extra binder of silver that could result a reduction in number of unbound Ag^+ ions in solution compared with peptide **3d** whose N-terminus is acetylated. In addition, the $-\text{NH}_2$ group could be repelling the nanoparticles from each other resulting in their enhanced stability over time.

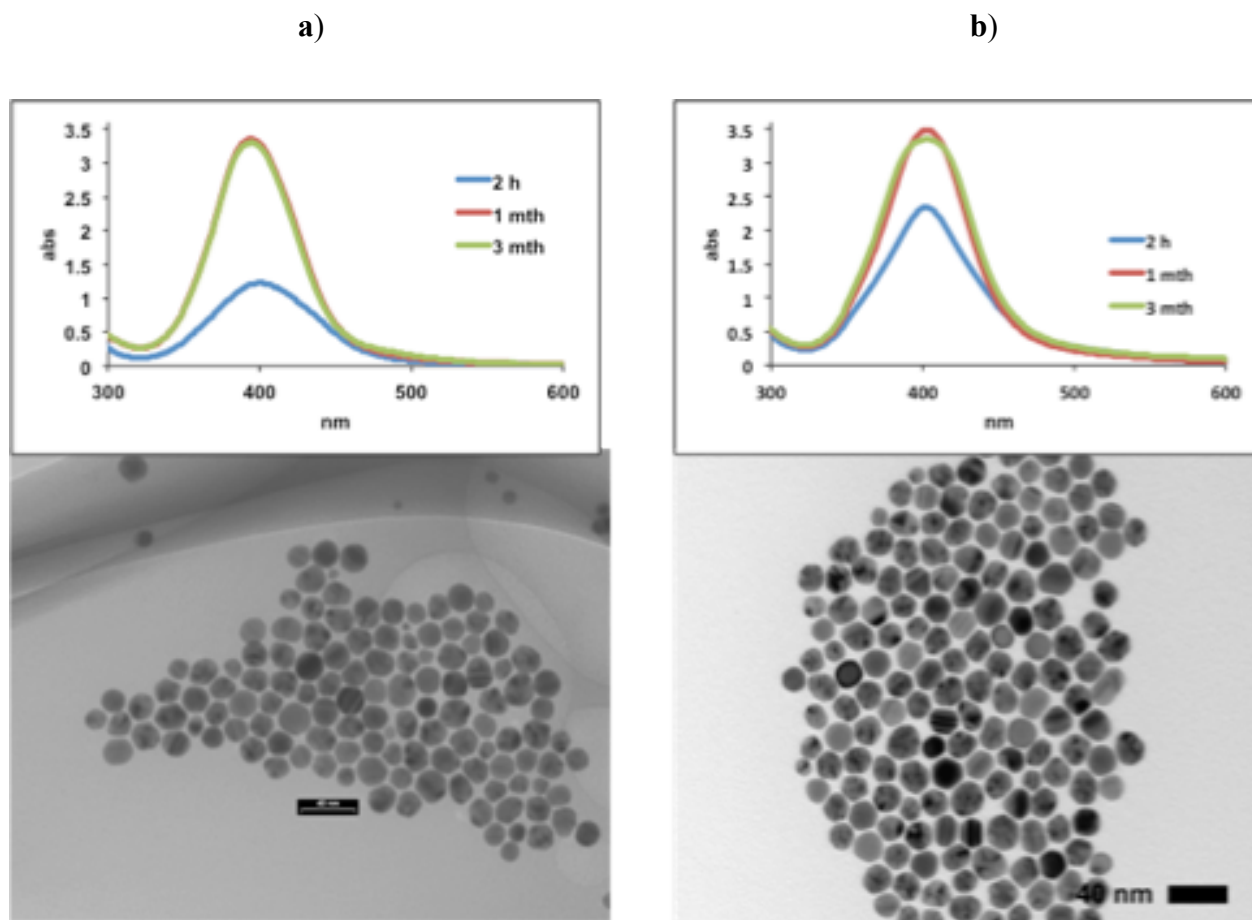


Figure 62: UV-Vis spectra and TEM pictures (scale bar = 40 nm) for **3f**-AgNPs (a) and **3d**-AgNPs (b) generated at pH 10, (results presented were taken at 3 months)

The broad UV spectra (Figure 63a) as well as the TEM results indicate that peptide NH₂-Ser-Ahx-Tyr-NH₂ **4f** generates highly polydispersed and aggregates of AgNPs. The TEM images implies that the use of peptide NH₂-Ser-Ahx-Tyr-NH₂ **4f** as an additive generates bigger size of AgNPs than the nanoparticles synthesised in the presence of peptide Ac-Ser-Ahx-Tyr-NH₂ **4d** (Figure 63b). The bigger size of AgNPs which are generated could mean that peptide **4f** is a stronger binder (from the -NH₂ group) of silver than its acetylated form Ac-Ser-Ahx-Tyr-NH₂ **4d** that generates smaller AgNPs.

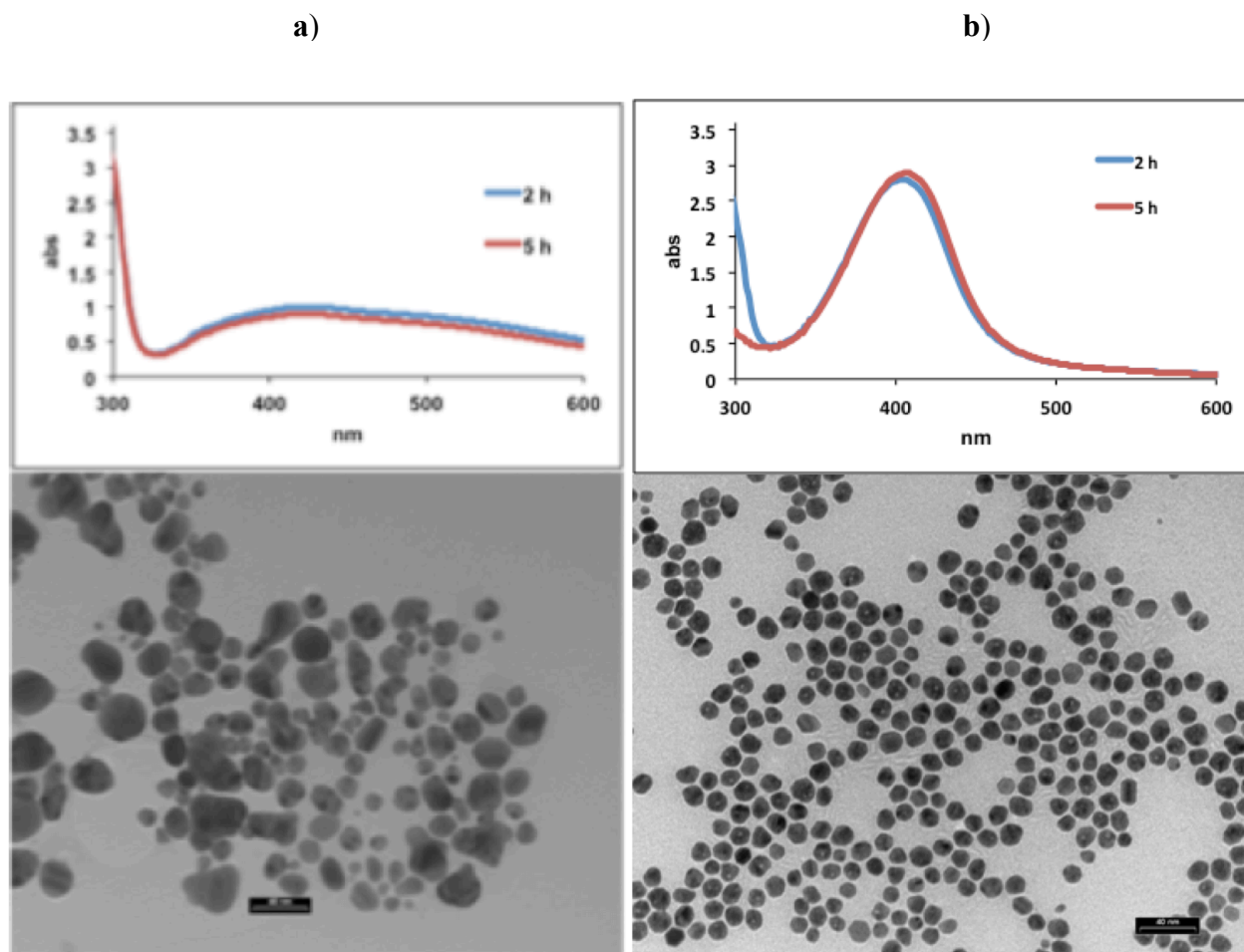


Figure 63: UV-Vis spectra and TEM pictures (scale bar = 40 nm) for **4f**-AgNPs (a) and **4d**-AgNPs (b) at pH 12 (results presented were taken at 5 h)

4.6.5 The Generation of AgNPs Without Sodium Ascorbate

Studies were carried out investigating the formation of AgNPs in the presence of our peptides but without inclusion of the reducing agent, sodium ascorbate. The aim was to explore a new method of utilising peptides **3d** and **4d** in reducing Ag^+ -ions to Ag^0 that could lead to the formation of defined size and shape of AgNPs. A few publications have reported that peptides bearing non Ag^+ reducing amino acid residues like tyrosine or tryptophane are able to reduce Ag^+ to Ag^0 leading to the formation of AgNPs.^{9,10} Most of the reported findings emphasise the need for carboxyl groups like aspartate or glutamate which supply electrons to reduce Ag^+ to Ag^0 .^{25,26} Belcher et al. used hexaglutamic acid and hexaaspartic acid in the synthesis of AgNPs at room temperature without a reducing agent.²⁵ They found that silver ions bound to carboxyl groups were easily reduced even

at ambient light.²⁵ In another study Aroca et al. generated AgNPs in the presence of amino acids glycine, cysteine and lysine as in situ reducing agents for Ag⁺ to Ag⁰ under boiling conditions.²⁶

Despite extensive research, the control of size and shape of AgNPs is still a great challenge in the generation of AgNPs using peptides as Ag⁺-ion reducing agents. Therefore, we speculated that the generation of AgNPs in the presence of peptide **3d** or **4d** could lead to better control of nanoparticle size and shape than existing techniques. We carried out studies on generating AgNPs without a reducing agent using our optimised reaction conditions. Silver nanoparticle formation in the presence of peptide **3d** was followed at pH 10 and pH 12 whereas nanoparticle formation in the presence peptide **4d** were done at pH 12. In all cases a peptide/Ag⁺ ratio of 5:1 was used.

The Generation of AgNPs in the Presence of Peptide 3d

Figure 64 show a comparison of the UV-Vis surface plasmon absorption spectra and TEM images for AgNPs prepared in the presence and absence of sodium ascorbate which is the Ag⁺-ion reducing agent. Without sodium ascorbate peptide **3d** cannot reduce Ag⁺-ions to induce the generation of AgNPs and only aggregates of micro-molecules which could be AgNO₃ are observed at pH 10.

An increase of pH to 12 led to the formation of AgNPs in the presence of peptide **3d** without sodium ascorbate as additive (Figure 65). Therefore peptide **3d** is able to reduce an Ag⁺-ion to Ag⁰ leading to the generation of AgNPs at pH 12. TEM images in Figure 65 show AgNPs in similar shapes and average sizes of 40 nm. However, the UV-Vis spectra for AgNPs synthesized without sodium ascorbate are typical for nanoparticles with a non-spherical shape.^{9,20} The aspartate group on peptide **3d** could be responsible for the reduction of Ag⁺ which led to the formation of AgNPs. Recently, Khan and coworkers reported evidence of the aspartate group being responsible for providing electrons to the reduction of Ag⁺-ions at pH 11.5. Their evidence was derived from spectrophotometric, kinetic, and TEM data that showed the dependence of the reduction process on the concentrations of NaOH and aspartate.²⁷

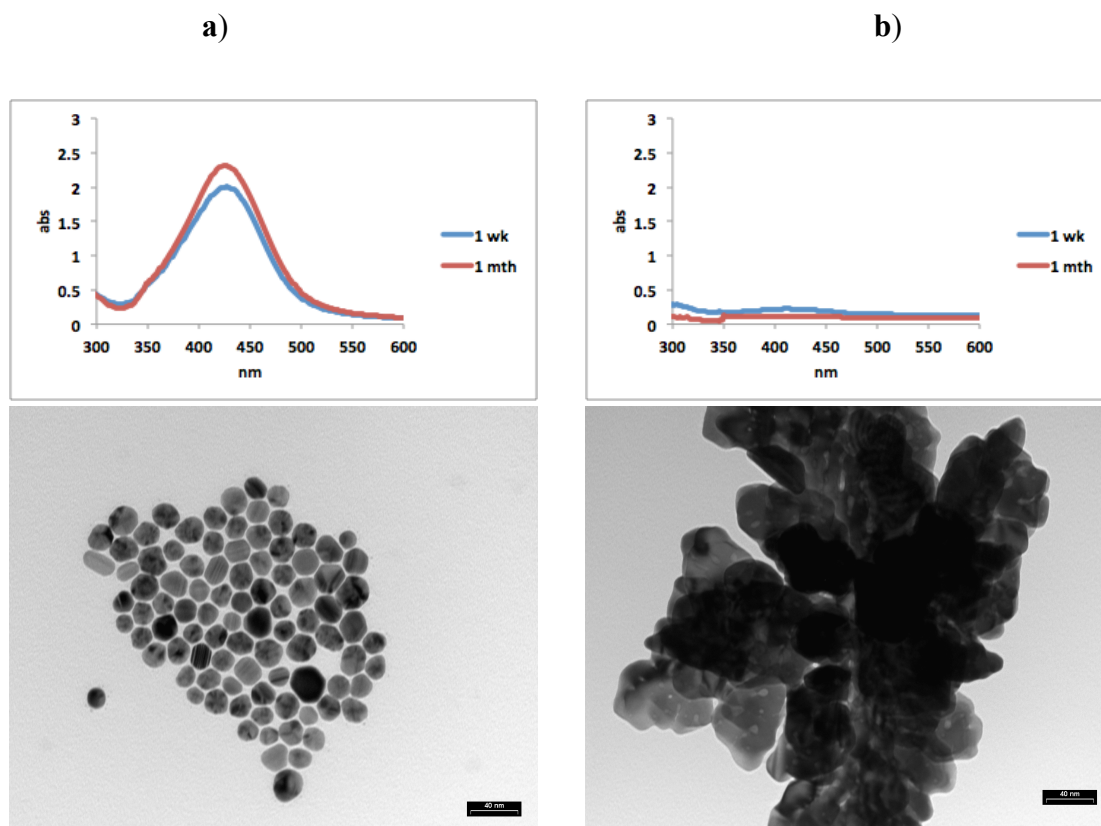


Figure 64: UV-Vis spectra and TEM pictures (scale bar = 40 nm) for **3d**-AgNPs generated in the presence of sodium ascorbate (a) and without sodium ascorbate (b) at pH 10, (results presented were taken after 1 month)

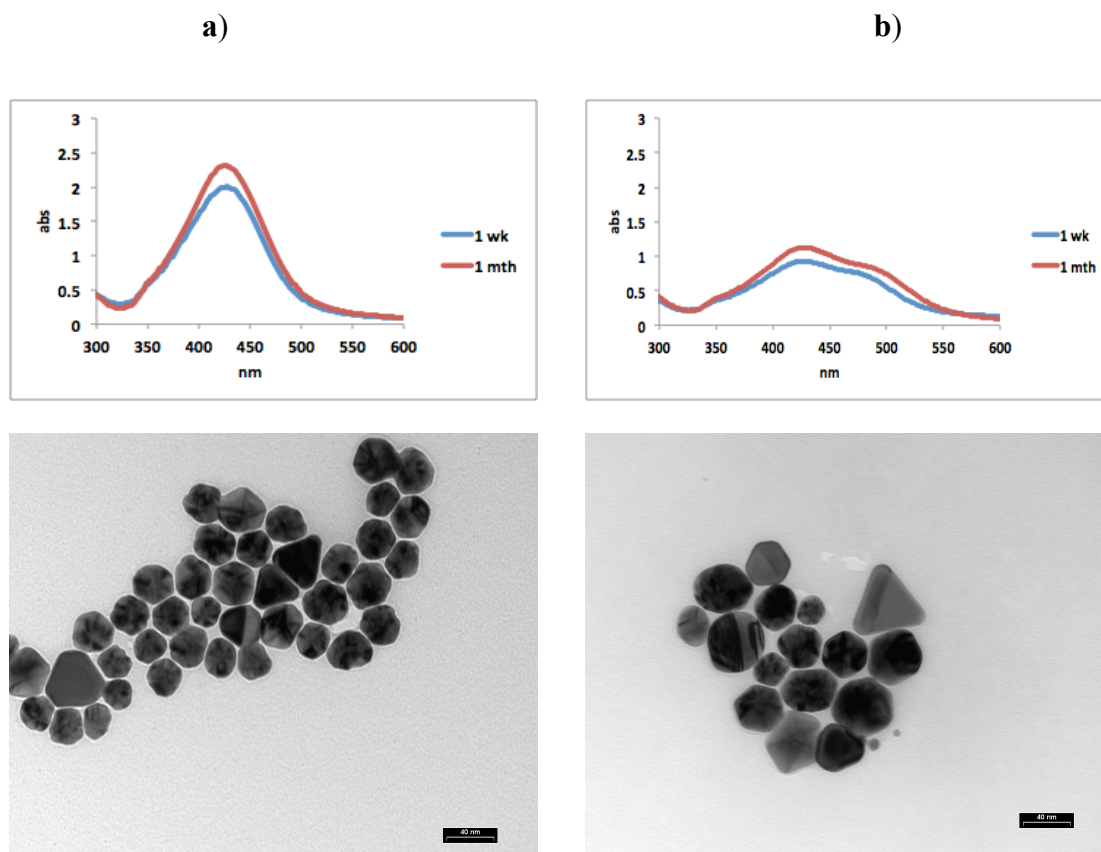


Figure 65: UV-Vis spectra and TEM pictures (scale bar = 40 nm) for **3d**-AgNPs generated in the presence of sodium ascorbate (a) and without sodium ascorbate (b) at pH 12

The Generation of AgNPs in the Presence of Peptide 4d

Peptide **4d** as an additive led to the formation of AgNPs in the presence or without sodium ascorbate as an additive (Figure 66). Peptide **4d** bears a tyrosine residue which is able to reduce Ag^+ to Ag^0 at pH 12.¹⁰ TEM images in Figure 66b show that larger (≤ 40 nm) AgNPs were generated without sodium ascorbate whereas smaller size (≤ 15 nm) AgNPs were generated in the presence of sodium ascorbate as an additive (Figure 66a). Sodium ascorbate could be required to promote the formation of smaller size of AgNPs in the presence of peptide **4d** as an additive.

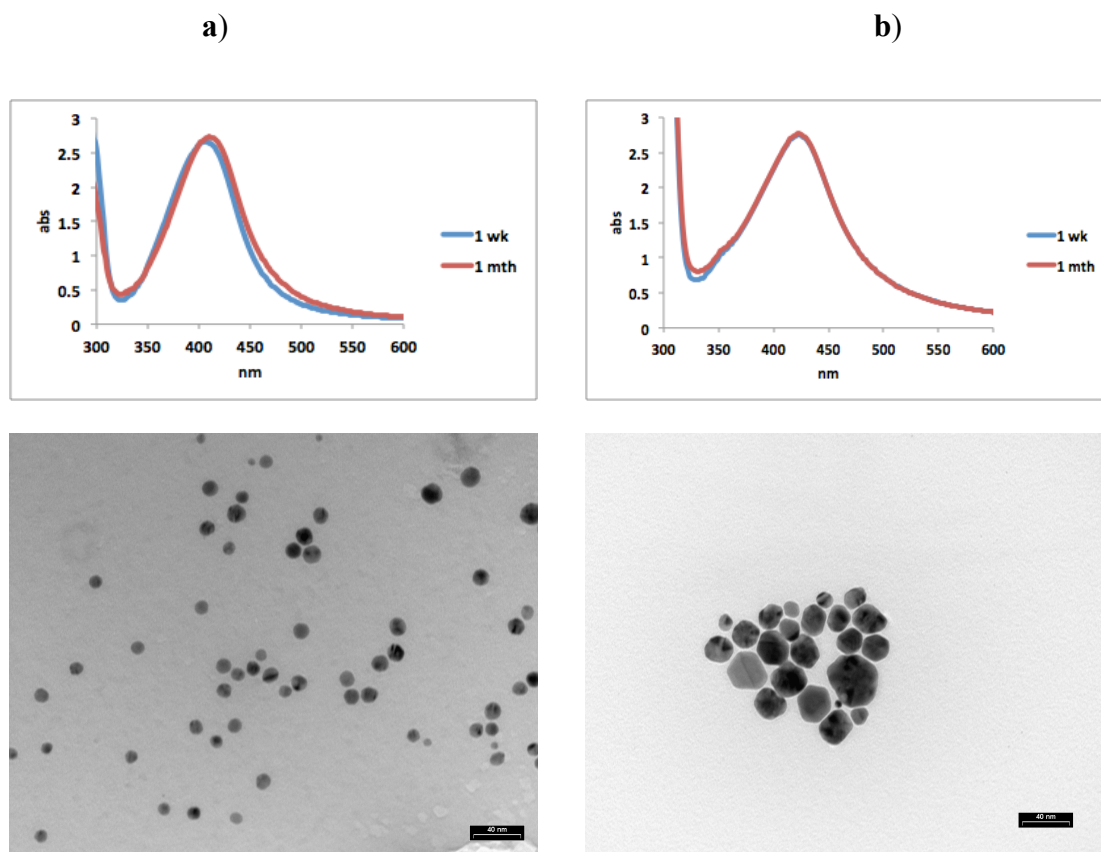


Figure 66: UV-Vis spectra and TEM pictures (scale bar = 40 nm) for **4d**-AgNPs generated in the presence of sodium ascorbate (a) and without sodium ascorbate (b) at pH 12 (results presented were taken at 1 month)

4.6.6 Investigation of the Influence of Dehydroascorbate on the Generation of AgNPs

Efforts to purify our AgNPs through centrifugation or size exclusion chromatography using sephadex have not been successful. AgNPs aggregated after the centrifugation process and size exclusion chromatography led to the AgNPs sticking on the column resulting in no elution of nanoparticles. Studies were then carried out to investigate the influence of dehydroascorbate, the oxidised form of sodium ascorbate which is present in the AgNP solution during and after their synthesis.

In our investigations, dehydroascorbate/sodium ascorbate ratios of 0:3, 1:2, 2:1 and 3:0 were explored in the formation of AgNPs in the presence of peptide **3d** or **4d**. The optimised conditions were used for the generation of AgNPs, which were pH 10 and pH 12 for peptide **3d** and pH 12 for peptide **4d**. The ratio of peptide/Ag⁺ used in these studies was 5:1.

The Generation of AgNPs in the presence of peptide 3d

The UV-Vis spectra and TEM images show that at pH 10 dehydroascorbate by itself facilitates the formation of AgNPs (Figure 67 and 68d). Without the reducing agent, sodium ascorbate, the source of electrons to reduce Ag^+ to Ag^0 is unknown and yet to be explored.

In addition, an increase of the ratio of dehydroascorbate/sodium ascorbate ratio from 0:3 to 1:2, 2:1 and 3:0 resulted in a general decrease of the size of the AgNPs that were generated (Figure 67). Furthermore, an increase in the ratio of dehydroascorbate/sodium ascorbate from 0:3 to 1:2, 2:1 and 3:0 resulted in the generation of polydispersed AgNPs which increased in relation to an increase in the concentration of dehydroascorbate. The decrease in the nanoparticle size as well as the increase in nanoparticle dispersity relative to an increase in the concentration of dehydroascorbate could indicate that dehydroascorbate determines the number of critical nuclei during the formation of AgNPs. In this system it could be that the processes of nucleation and growth of AgNPs are taking place simultaneously. Efrima et al. reported that the processes of nucleation and growth are critical in the formation of AgNPs.²⁸ Therefore, polydisperse nanoparticles are produced if these two processes take place simultaneously.²⁹ In Figure 64, peptide **3d** at pH 10 could not induce the formation of AgNPs without sodium ascorbate. Therefore the TEM results shown in Figure 68d indicate that dehydroascorbate plays a role in the reduction of Ag^+ -ion to Ag^0 in the formation of nanoparticles.

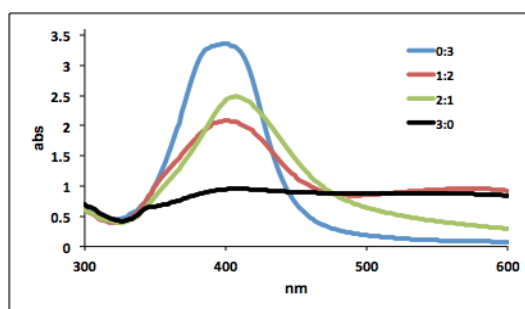


Figure 67: UV-Vis spectra of **3d**-AgNPs generated in the presence of dehydroascorbate /ascorbate ratio of 0:3, 1:2, 2:1 and 3:0 at pH 10 (results presented were taken at 24 h)

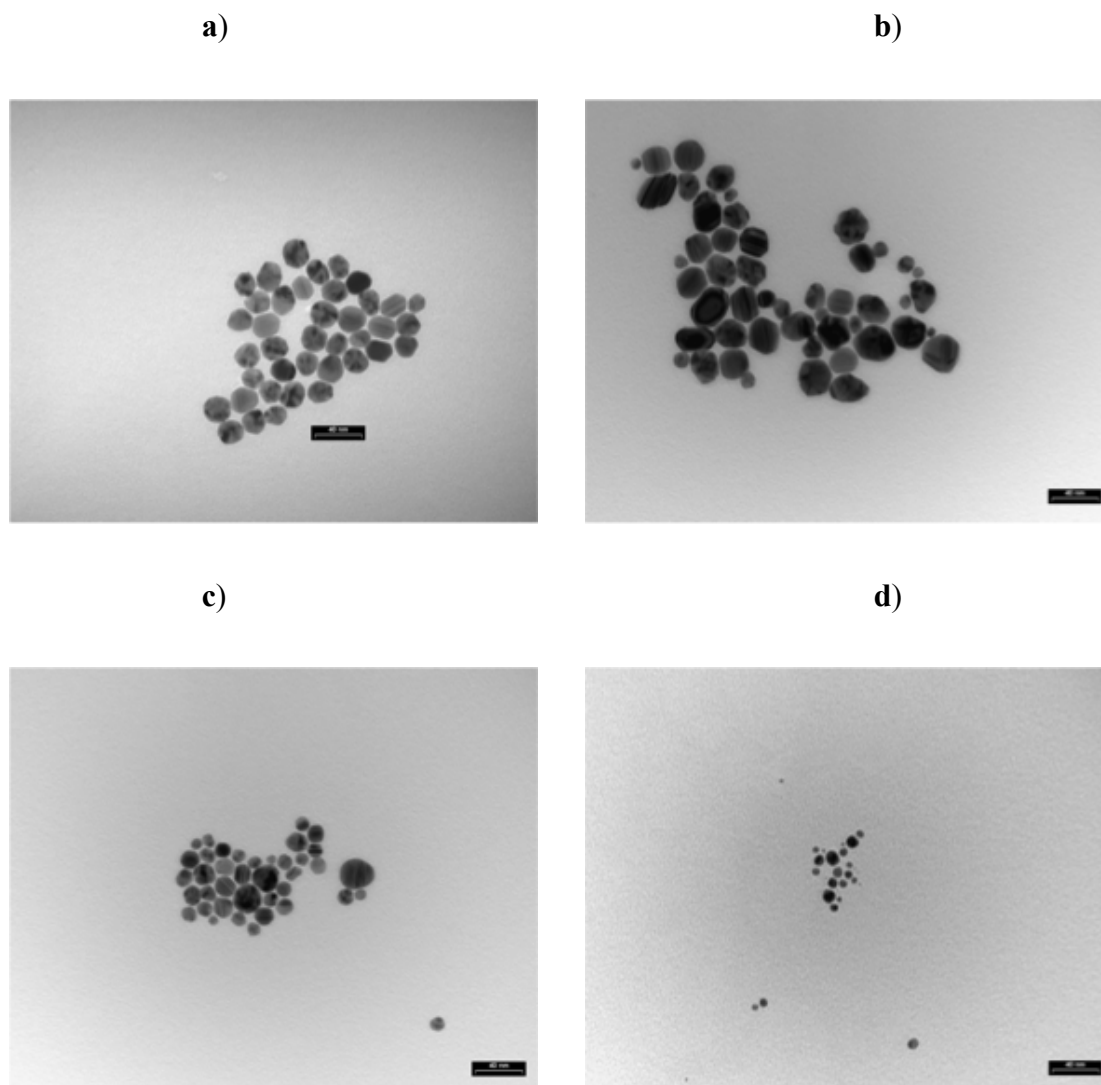


Figure 68: TEM pictures (scale bar = 40 nm) of **3d**-AgNPs generated in the presence of dehydroascorbate /ascorbate ratios of 0:3 (b), 1:2 (c), 2:1 (d) and 3:0 (e) at pH 10 (results presented were taken at 24 h)

Likewise, the UV-Vis spectra and TEM images show that at pH 12 dehydroascorbate by itself leads to the formation of AgNPs (Figure 69 and 70). Previously in Figure 65, peptide **3d** without a reducing agent has been shown to induce the formation of AgNPs at pH 12. Therefore, the results achieved at pH 12 could be a contribution of peptide **3d** and dehydroascorbate. Unlike the results at pH 10, the UV-Vis results of AgNPs generated at pH 12 show a clear red shift in the spectra relating to an increase in the ratio of dehydroascorbate/sodium ascorbate from 0:3 to 1:2, 2:1 and 3:0.

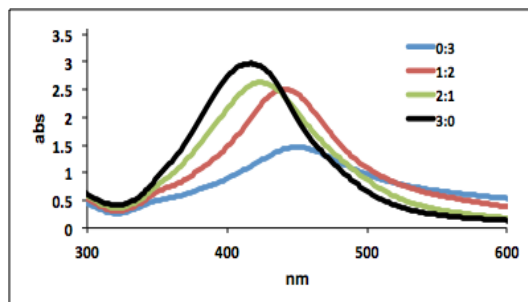


Figure 69: UV-Vis spectra of **3d**-AgNPs generated in the presence of dehydroascorbate /ascorbate ratio of 0:3, 1:2, 2:1 and 3:0 at pH 12 (results presented were taken at 24 h)

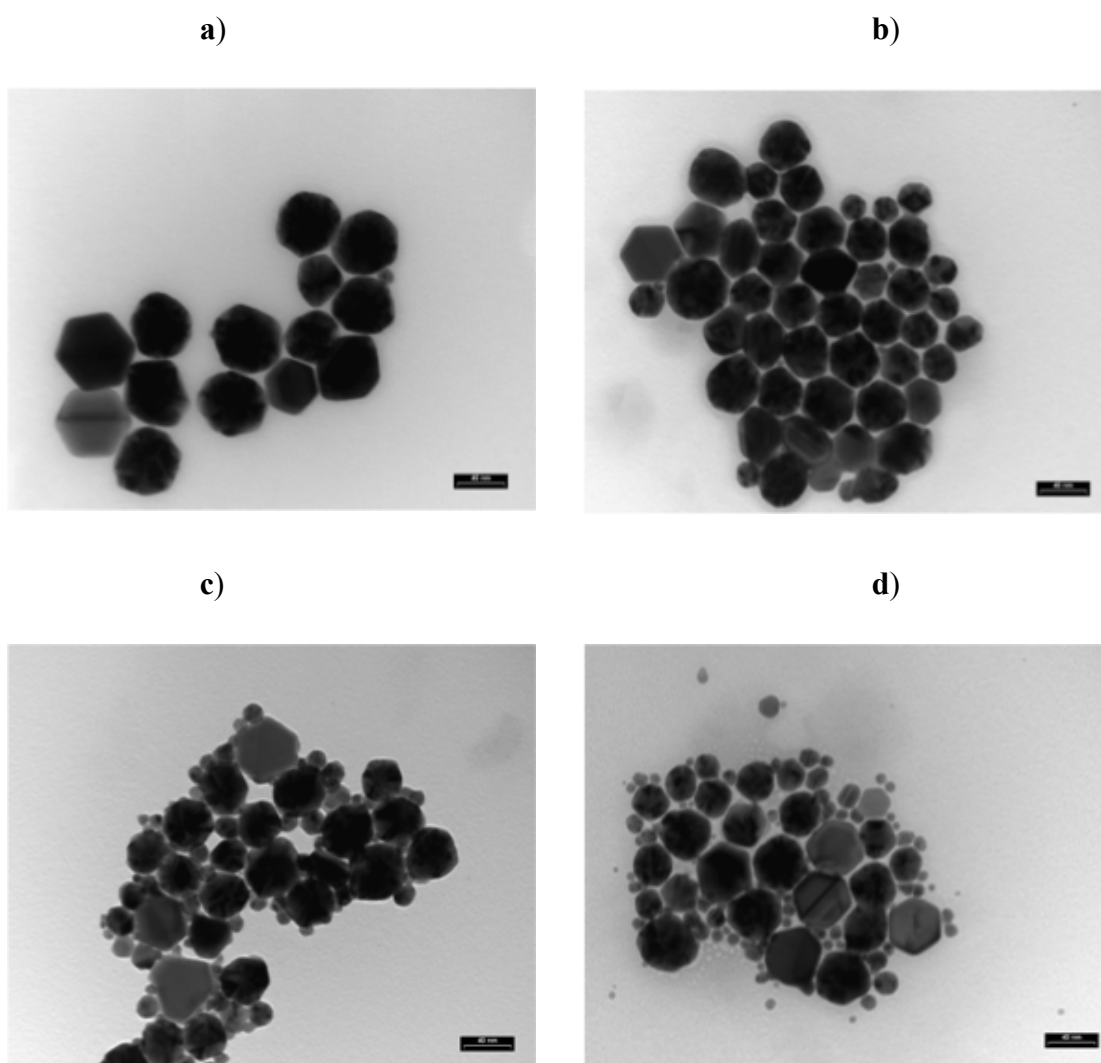


Figure 70: TEM pictures (scale bar = 40 nm) of **3d**-AgNPs generated in the presence of dehydroascorbate /ascorbate ratios of 0:3 (b), 1:2 (c), 2:1 (d) and 3:0 (e) at pH 12 (results presented were taken at 24 h)

In a fashion similar to that observed with peptide **3d** at pH 10, UV-Vis and TEM analyses revealed that an increase in the ratio of dehydroascorbate/sodium ascorbate from 0:3 to 1:2, 2:1 and 3:0 resulted in the generation of polydisperse AgNPs at pH 12 (Figure 69 and 70). Furthermore the polydispersity of AgNPs increased with respect to an increase in the ratio of dehydroascorbate/sodium ascorbate from 0:3 to 1:2, 2:1 and 3:0. The decrease in the nanoparticle size as well as the increase in nanoparticle dispersity relative to an increase in the concentration of dehydroascorbate could also indicate that dehydroascorbate determines the number of critical nuclei during the formation of AgNPs. In this system at pH 12 the processes of nucleation and growth of AgNPs could be taking place simultaneously.

Overall, these studies have shown that dehydroascorbate influences the size dispersity of AgNPs during their generation especially at pH 12, this could explain the wide size variation of AgNPs generated at pH 12 in Figure 56.

The Generation of AgNPs in the presence of peptide 4d

The UV-Vis spectra shown in Figure 71 also indicate that there is AgNP formation in the presence of dehydroascorbate at pH 12. In this system the influence of dehydroascorbate is unclear, given that without a reducing agent such as sodium ascorbate, the tyrosine moiety in peptide **4d** is able to reduce Ag^+ to Ag^0 to form AgNPs at pH 12 (Figure 72).

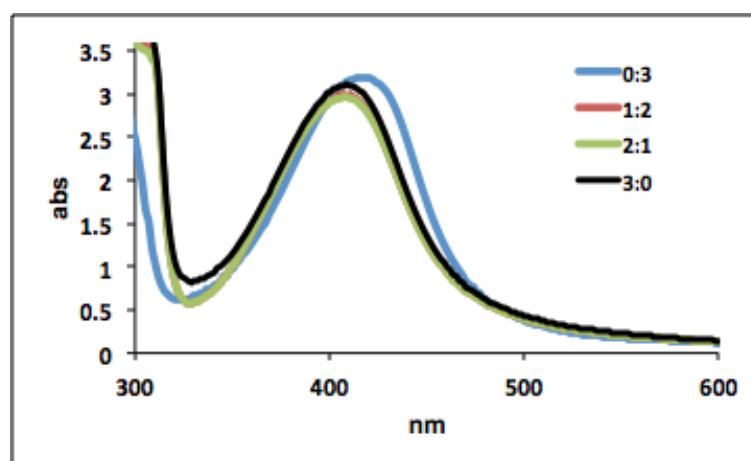


Figure 71: UV-Vis spectra of **4d**-AgNPs generated in the presence of dehydroascorbate /ascorbate ratios of 0:3, 1:2, 2:1 and 3:0 at pH 12 (results presented were taken at 24 h)

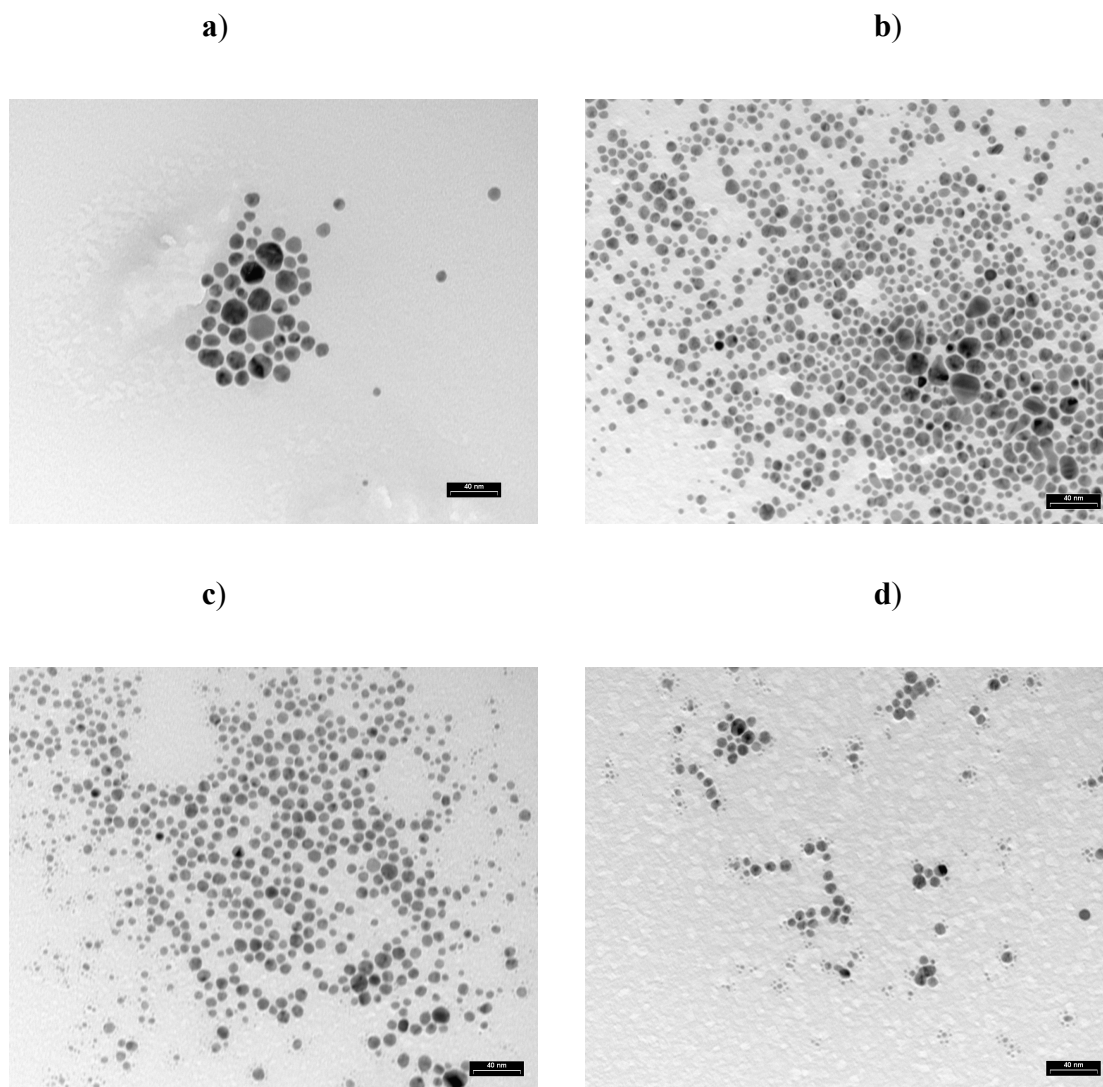


Figure 72: TEM pictures (scale bar = 40 nm) of **4d**-AgNPs generated in the presence of dehydroascorbate /ascorbate ratio of 0:3 (b), 1:2 (c), 2:1 (d) and 3:0 (e) at pH 12 (results presented were taken at 24 h)

An increase of the ratio of dehydroascorbate/sodium ascorbate ratio from 0:3 to 1:2 also favours the formation of smaller size of AgNPs (Figure 72). Unlike the studies which were carried out in the presence of peptide **3d**, increments of dehydroascorbate/sodium ascorbate ratio to 2:1 and 3:0 did not lead to a significant change in the size of the resulting AgNPs in the presence of peptide **4d**. These results imply that peptides **3d** and **4d** interact differently with AgNPs in the presence of dehydroascorbate and sodium ascorbate leading to the observed variation in nanoparticle size.

4.6.7 The Generation of AgNPs in the Presence of Inorganic Salts

We could successfully generate AgNPs in different sizes in the presence of different peptides, however the generation of homogeneously defined shapes of AgNPs is yet to be achieved. Kitaev and coworkers have discovered that addition of inorganic salts like chlorides and bromides could control the shape of AgNPs by the coordination of these halides to the active facets of the nanoparticles during their formation.³⁰ Halides are presumed to help in coordinating to silver nuclei, thereby stabilizing them against aggregation.³¹ Stabilization against aggregation could result in the generation of defined shapes of AgNPs.³⁰

Bearing these results in mind, we explored the use of peptides **3d** and **4d** in the generation of AgNPs in the presence of potassium chloride (KCl), potassium bromide (KBr), sodium chloride (NaCl) and sodium bromide (NaBr). With the generation of AgNPs carried out at the optimized conditions, that is at pH 10 and pH 12 for peptide **3d** whereas the pH was 12 for **4d**. Ratios of halide/Ag⁺ of 0.24 and 1 will be illustrated to show the influence of halides in the formation of AgNPs in the presence of peptides **3d** and **4d** as additives at pH 12.

Generation of AgNPs in the Presence of Peptide 3d and Halides

AgNPs which were generated in the presence of peptide **3d** and KCl show a typical SPR band which is centered at 405 nm (Figure 51). The TEM image on Figure 51a shows monodisperse AgNPs of average size of 20 nm.

It was surprising to observe a few nanorods of average length of 30 nm. When the ratio of KCl/Ag⁺ was increase to 1, the nanorods were found to increase in length to about 60 nm as well as increase in quantity (Figure 73). Beyond the KCl/Ag⁺ ratio of 1, the nanoparticle solution turned faint white accompanied by a slow formation of AgNPs. The white colouration could be the formation of AgCl. The decrease in the ratio of KCl/Ag⁺ from 0.24 resulted in no significant effect to the generation of AgNPs. These results show that KCl contributes to the formation of Ag-nanorods since experiments in absence of KCl did not reveal the formation of nanorods.

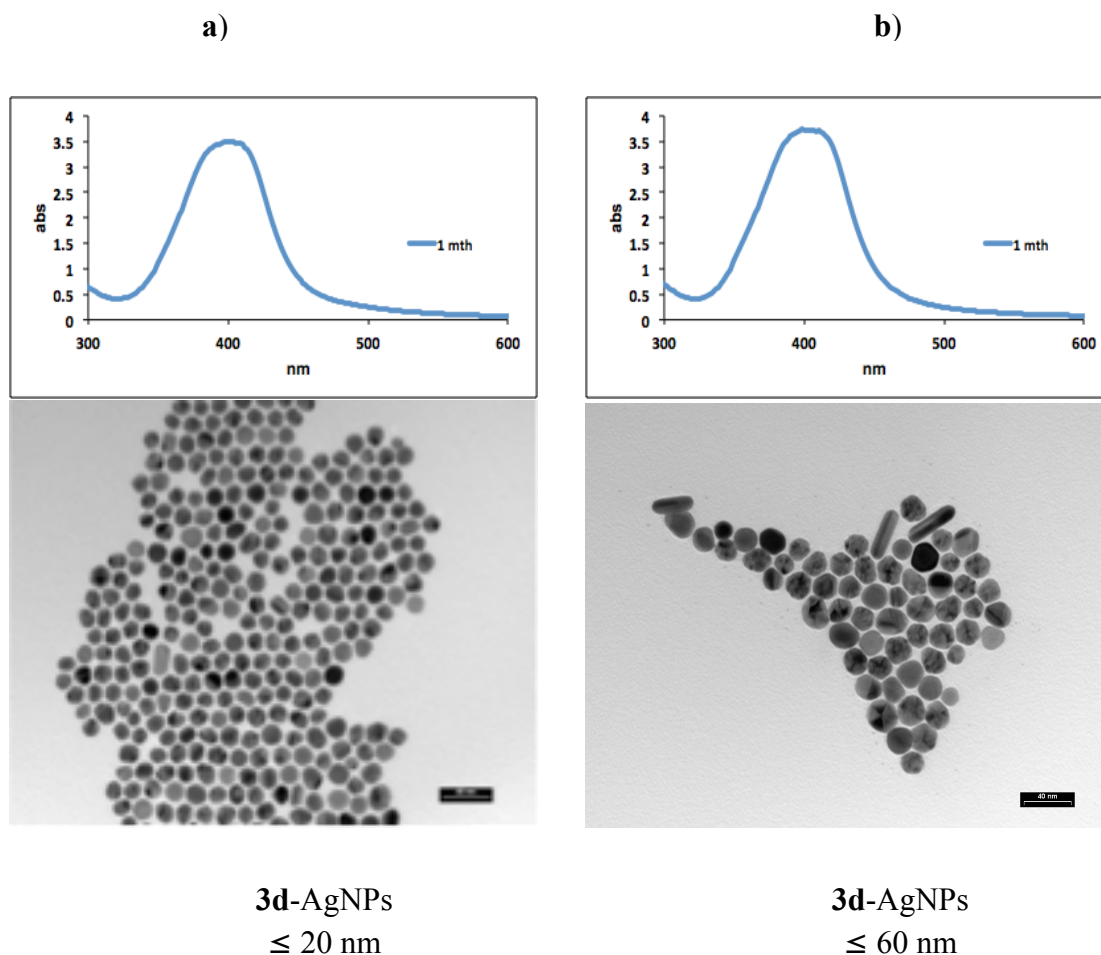


Figure 73: UV-Vis spectra and TEM pictures (scale bar = 40 nm) of **3d**-AgNPs generated in the presence of KCl/Ag⁺ ratio of 0.24 (a) and KCl/Ag⁺ ratio of 1 (b) at pH 10

In order to evaluate the influence of other halides in the generation of AgNPs, experiments were carried out in the presence of KBr, NaBr and NaCl in a ratio of halide/Ag⁺ of 0.24. Figure 74 showed no significant influence of these halides in the formation of AgNPs in the presence of peptide **3d** at pH 10. The observed differences in the UV-Vis spectra as well as nanoparticle size in Figure 52a-c could be a result of the influence of the cation (Na⁺- or K⁺-ion) in the formation of AgNPs.

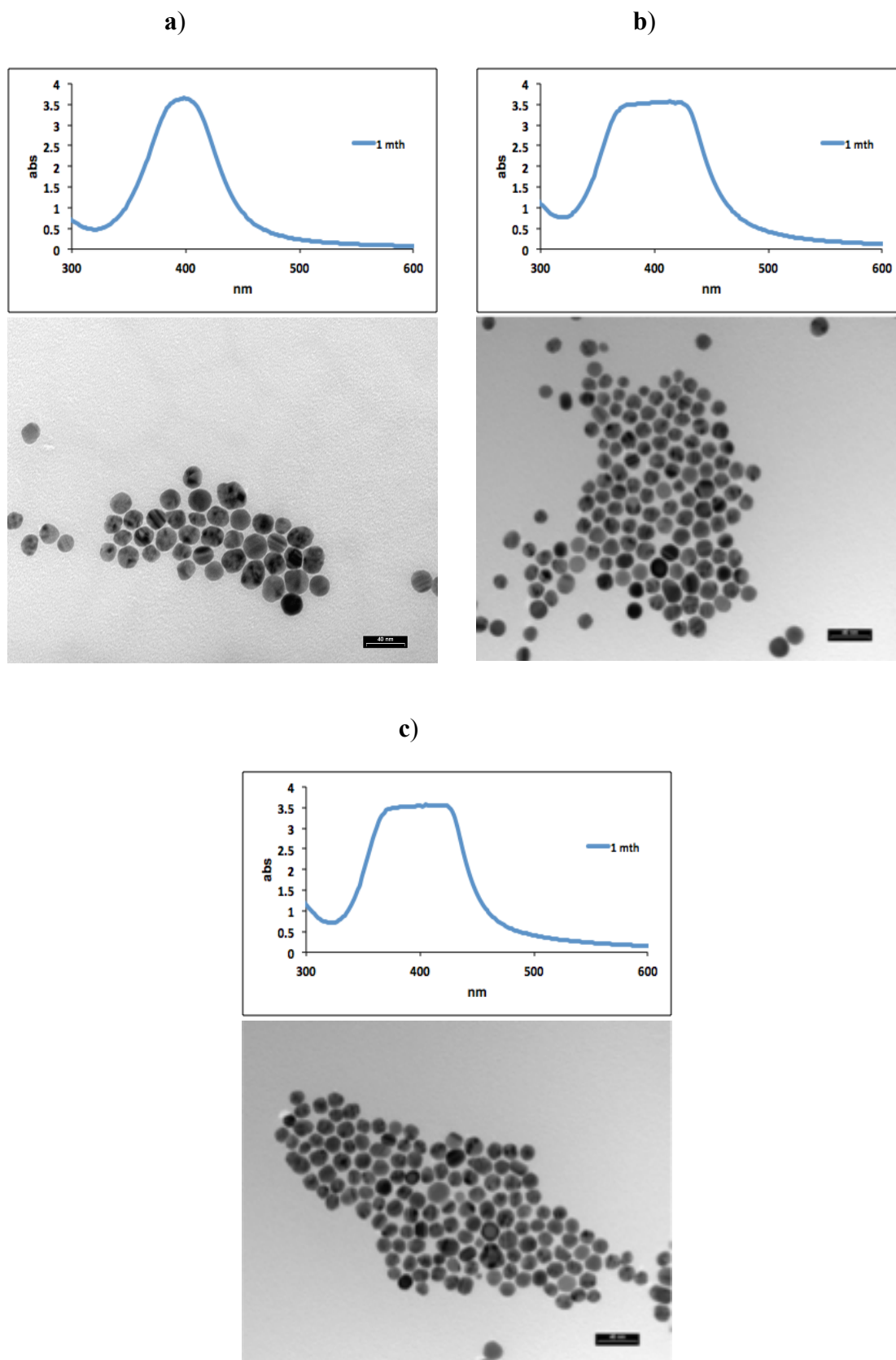


Figure 74: UV-Vis spectra and TEM pictures (scale bar = 40 nm) of **3d**-AgNPs generated in the presence of KBr (a), NaBr (b) and NaCl (c) in a ratio of halide/ Ag^+ of 0.24 at pH 10

Figure 75 also shows that peptide **3d** can induce the formation of AgNPs at pH 12 in the presence of KCl. TEM studies confirm the formation of AgNPs which also look like nanorods.

Future studies using a high resolution TEM that has a tiltable specimen stage could reveal the actual shapes of AgNPs.

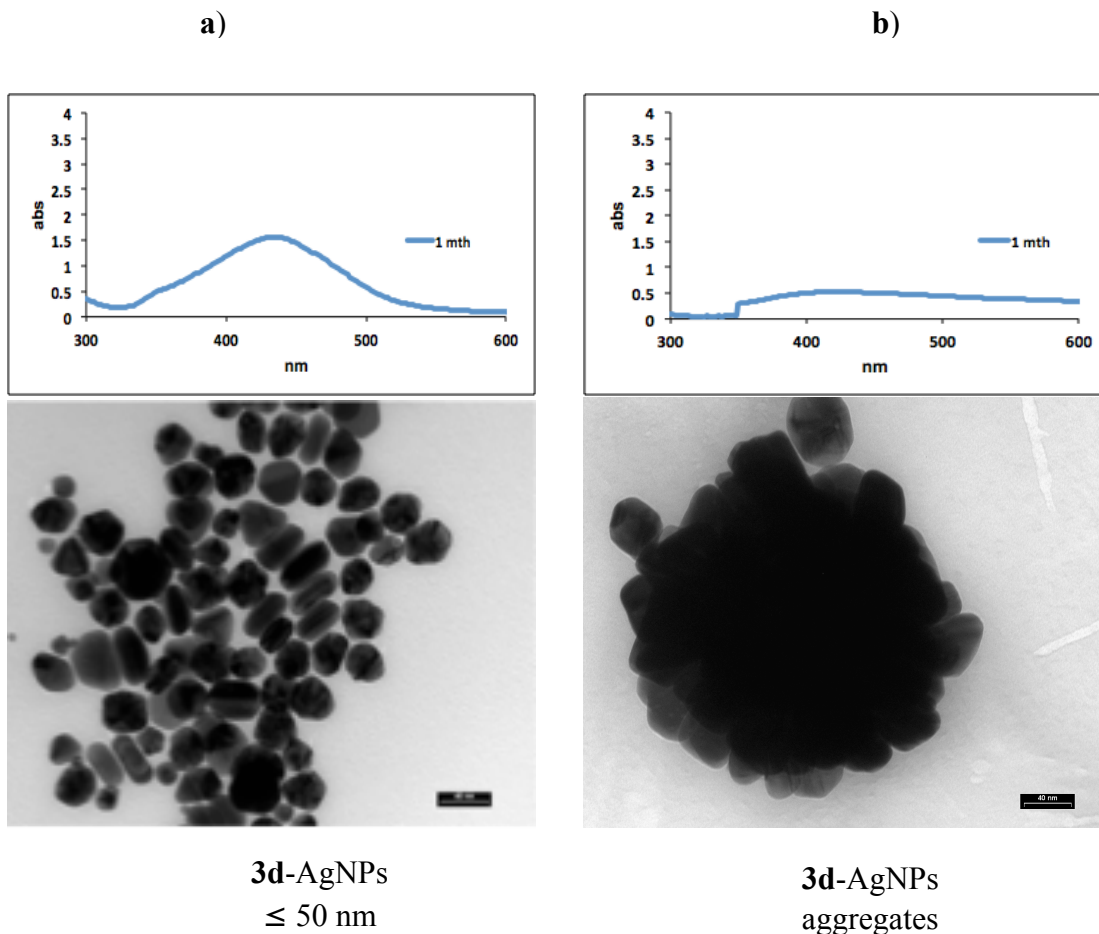


Figure 75: UV-Vis spectra and TEM pictures (scale bar = 40 nm) of **3d**-AgNPs generated in the presence of KCl/Ag⁺ ratio of (a) 0.24 and (b) 1 at pH 12

Unlike the observations at pH 10, when the ratio of KCl/Ag⁺ was increased to 1, the nanoparticle solution turned faint white accompanied by aggregation of AgNPs (Figure 75b). Similarly, a decrease in the ratio of KCl/Ag⁺ from 0.24 resulted in no significant effect to the generation of AgNPs. AgNPs which were generated in the presence of peptide **3d** and KCl show a SPR band which is centered at 450 nm (Figure 75).

Overall the generation of AgNPs at pH 12 in the presence of **3d** and halides such as KBr, NaBr

and NaCl in a ratio of halide/ Ag^+ of 0.24 led to formation of AgNP aggregates (Figure 76).

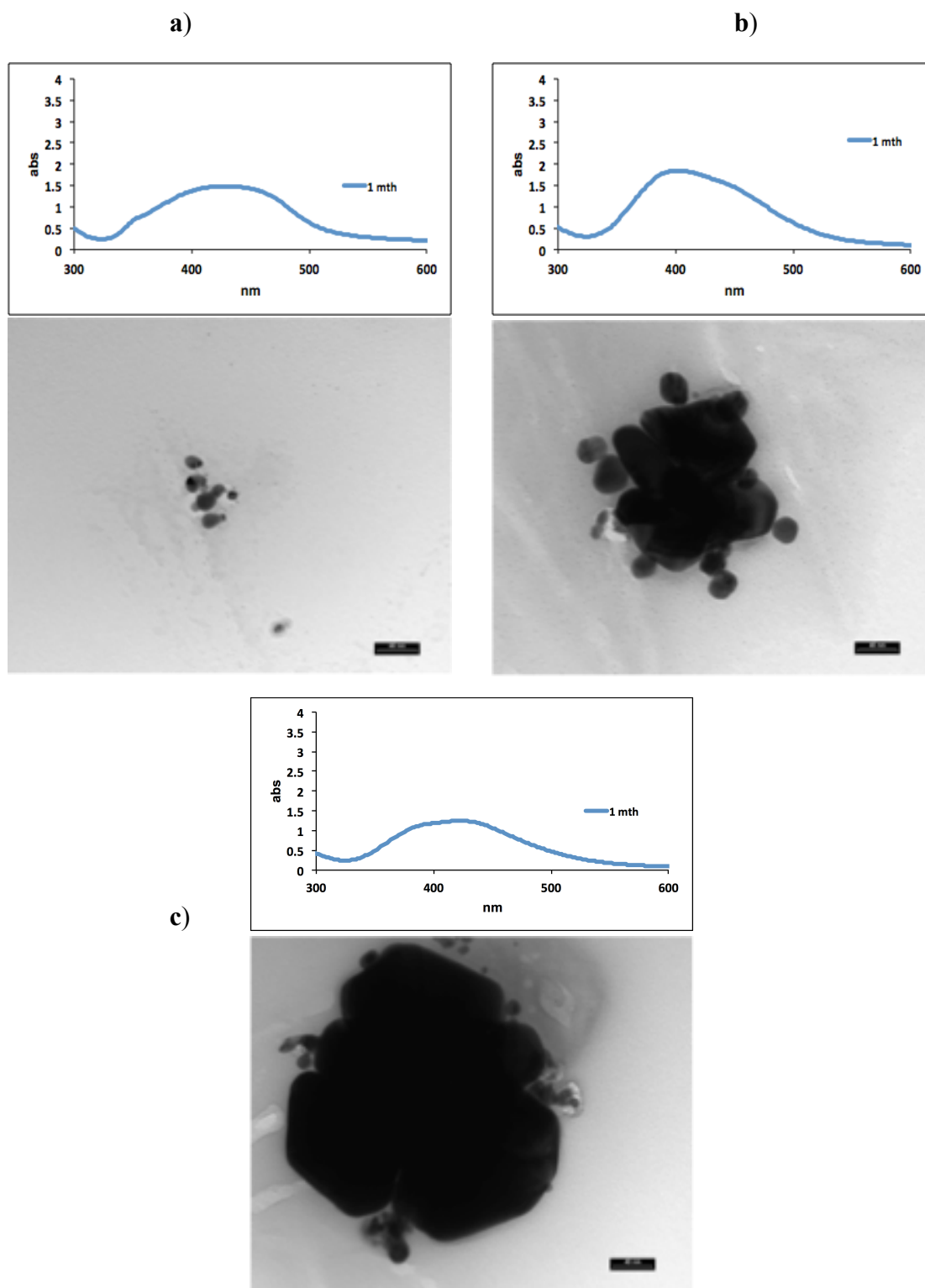


Figure 76: UV-Vis spectra and TEM pictures (scale bar = 40 nm) of **3d**-AgNPs generated in the presence of KBr (a), NaBr (b) and NaCl (c) in a ratio of halide/ Ag^+ of 0.24 at pH 12

The UV and TEM studies of AgNP formation in the presence of peptide **4d** and halide KCl, KBr, NaCl or NaBr indicate that halides do not play a significant influence in the synthesis of AgNPs (Figure 77 and 78). Even after the increase or decrease of the halide/Ag⁺ ratio, the observations did not change. This was a surprising result since one would expect to observe similar effects to those observed for peptide **3d**, especially on increasing the halide/Ag⁺ ratio from 0.24 and above. Above this ratio of 0.24, the nanoparticle solution could show the formation of AgCl or AgBr, a white precipitate. One explanation could be that the combination of peptide **3d** and **4d** with halide leads to different interactions with crystallographic facets of AgNPs.³² These different interactions can lead to the anisotropic growth of AgNPs which result in the observed nanorods for **3d** or no effect regarding peptide **4d**.

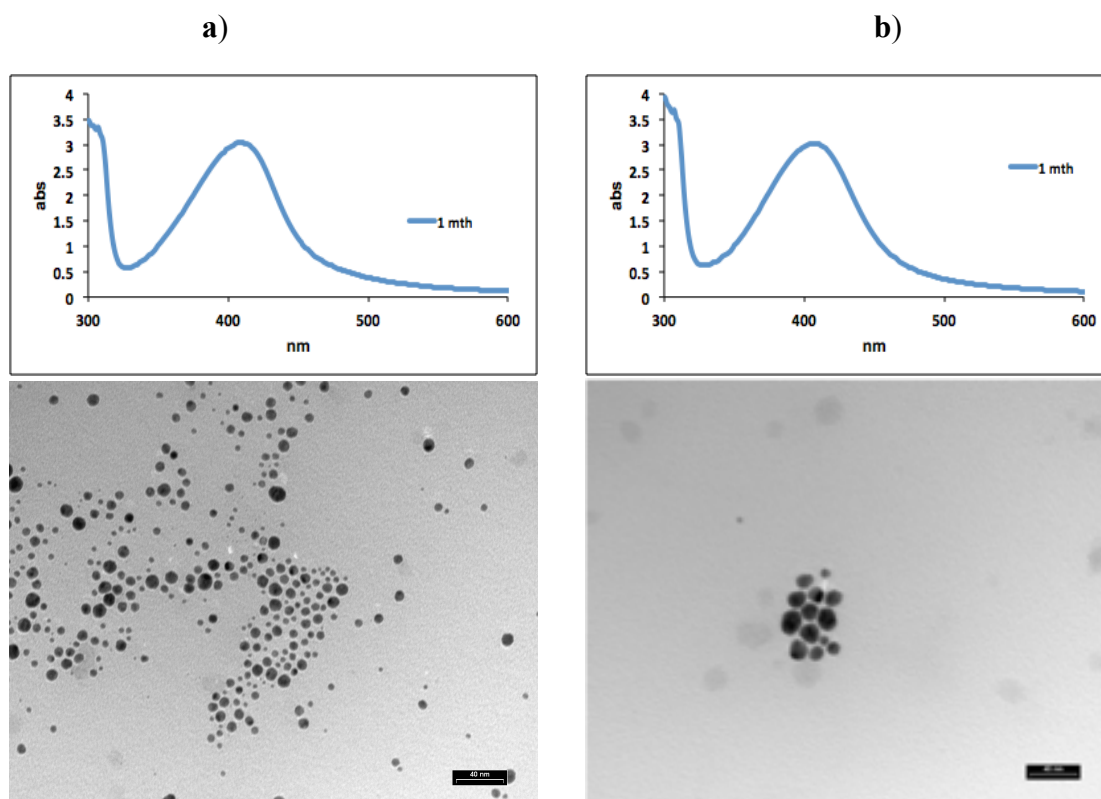


Figure 77: UV-Vis spectra and TEM pictures (scale bar = 40 nm) of **4d**-AgNPs generated in the presence of KCl (a), KBr (b) in a ratio of halide/Ag⁺ of 0.24 at pH 12

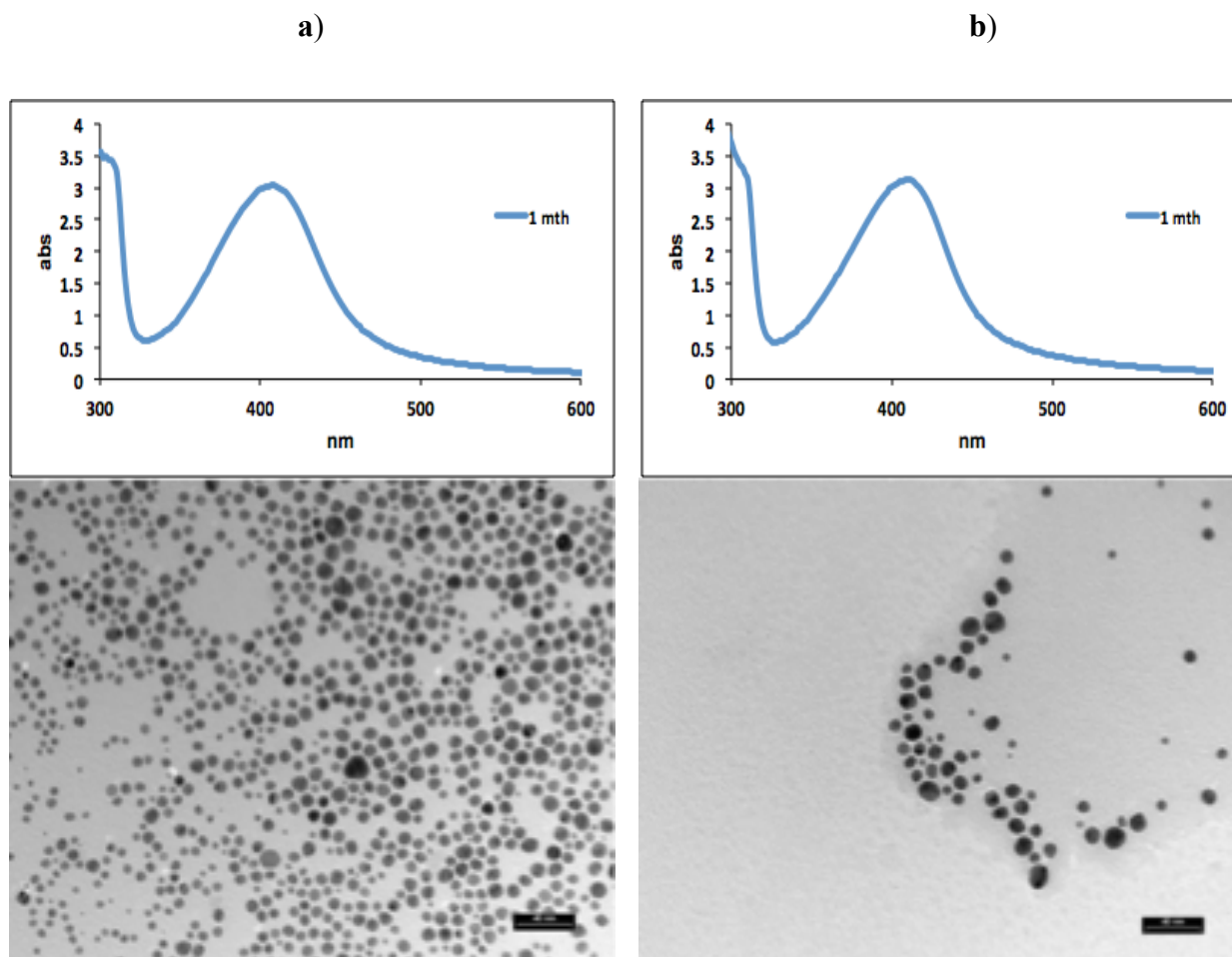


Figure 78: UV-Vis spectra and TEM pictures (scale bar = 40 nm) of **4d**-AgNPs generated in the presence of NaCl (a), NaBr (b) in a ratio of halide/ Ag^+ of 0.24 at pH 12

Figure 79 illustrates the general mechanism for the formation of different shapes of AgNPs from Ag-nuclei.³³ Tsuji et al. proposed that different shapes of AgNPs evolved from various face centred cubic Ag nanoprecursors (Table 6 and Figure 79).

Initial shape of AgNP	Final shape of AgNP
small multiple-twinned sphere	nanosphere
decahedron	nanorod or nanowire
cubo-octahedron	cube
triangular and hexagonal nanoplate	triangular bi-pyramid and 1-D nanoplate

Table 6: Inital and final shapes of AgNPs as proposed by Tsuji et al³³

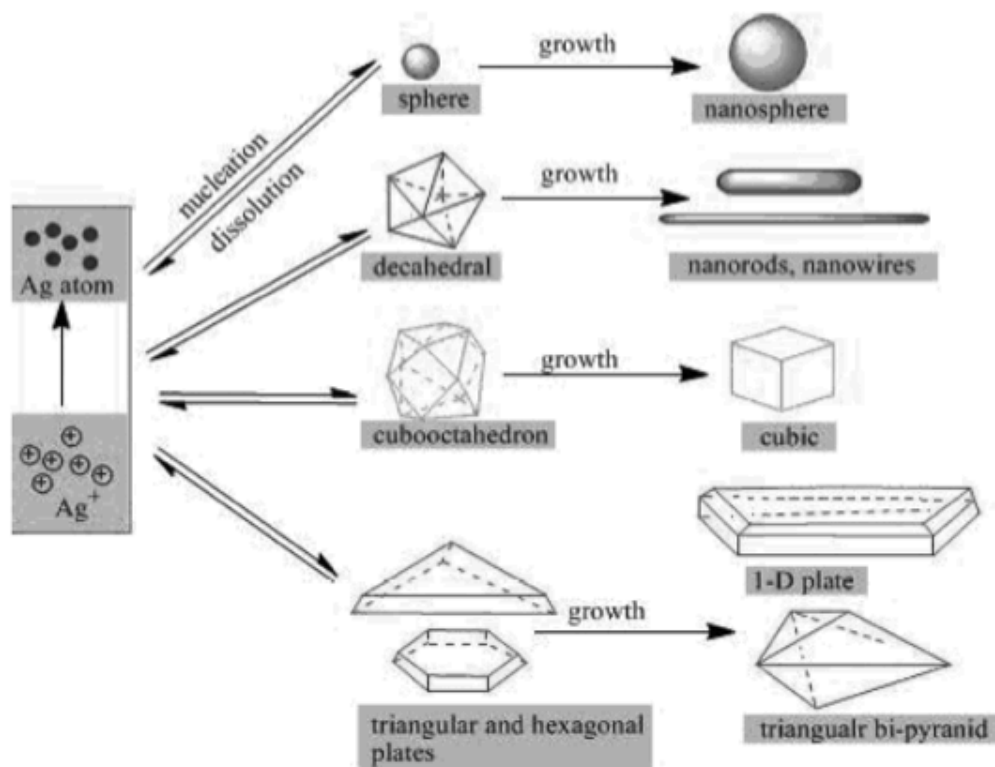


Figure 79: Mechanism of shape selective oxidative etching and crystal growth of Ag-nanostructures³³

Moreover, for biological applications, AgNPs should display high stability in high ionic strength environments. Studies that were done on the formation of AgNPs on the presence of especially KCl show that **3d**- and **4d**-AgNPs are highly stable under a wide concentration range of KCl in comparison to the condition in a biological system. Such results represent exciting opportunities of using these **peptide**-AgNPs in some biological applications like in antibacterial studies (see Chapter V) where the media could have high ionic strength.

4.6.8 Generation of AgNPs in Solution in the Presence of Other Peptides Identified Within the Combinatorial Screening of Library 1

As evidence to show that other peptides identified from the combinatorial screening are also able to control the formation of AgNPs of different sizes, results from solution phase studies are given below for the Ac-His-ProAib-Ser-NH₂ **5** and Ac-Asp-Ahx-Ser-NH₂ **6** peptides (Figure 80). The linkers used to connect the active amino acids were chosen at random among the linkers which

were hits from the combinatorial screening results. For Ac-His-ProAib-Ser-NH₂ **5** the linker chosen was Pro-Aib whereas Ahx was chosen to connect Asp with Ser in **6** (Figure 80)

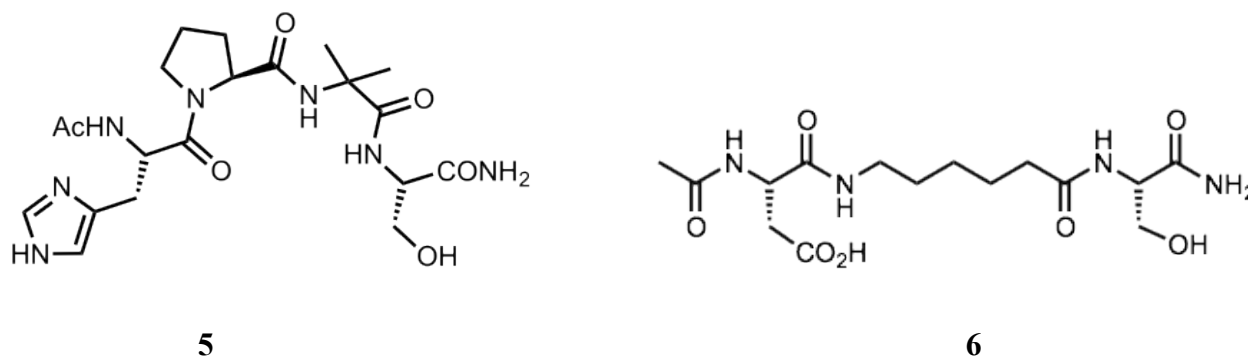


Figure 80: Structures of peptides Ac-His-ProAib-Ser-NH₂ **5** and Ac-Asp-Ahx-Ser-NH₂ **6** which were used in AgNP formation

From the combinatorial screening, peptides bearing His and Ser residues gave red or dark orange colored beads whereas combinations between Asp and Ser gave yellow colored beads. Hence one would expect bigger sizes of AgNPs to be generated by peptide Ac-His-ProAib-Ser-NH₂ **5** and smaller sizes to be formed in the presence of peptide Ac-Asp-Ahx-Ser-NH₂ **6**. The optimised conditions were used for the generation of AgNPs in the presence of peptides **5** and **6**, that is at pH 12 and peptide/Ag⁺ ratio of 5.

Figure 81 show the UV spectra as well as the TEM results of the AgNPs which were generated in the presence of peptides **5** and **6**. Different morphologies of AgNPs such as triangles or hexagons were generated in the presence of the Ac-His-ProAib-Ser-NH₂ **5** (Figure 81). These morphologies are similar to those formed in the presence of the sequence Ac-His-Ahx-Asp-NH₂ **3d**, also the average size of 40 nm AgNPs was comparable under similar conditions (Figure 56). This should not be surprising since the binding affinities of these peptides to Ag⁺-ions are similar (experimental section), hence they are expected to control the growth of AgNPs in a similar manner which results in comparable sizes of AgNPs.

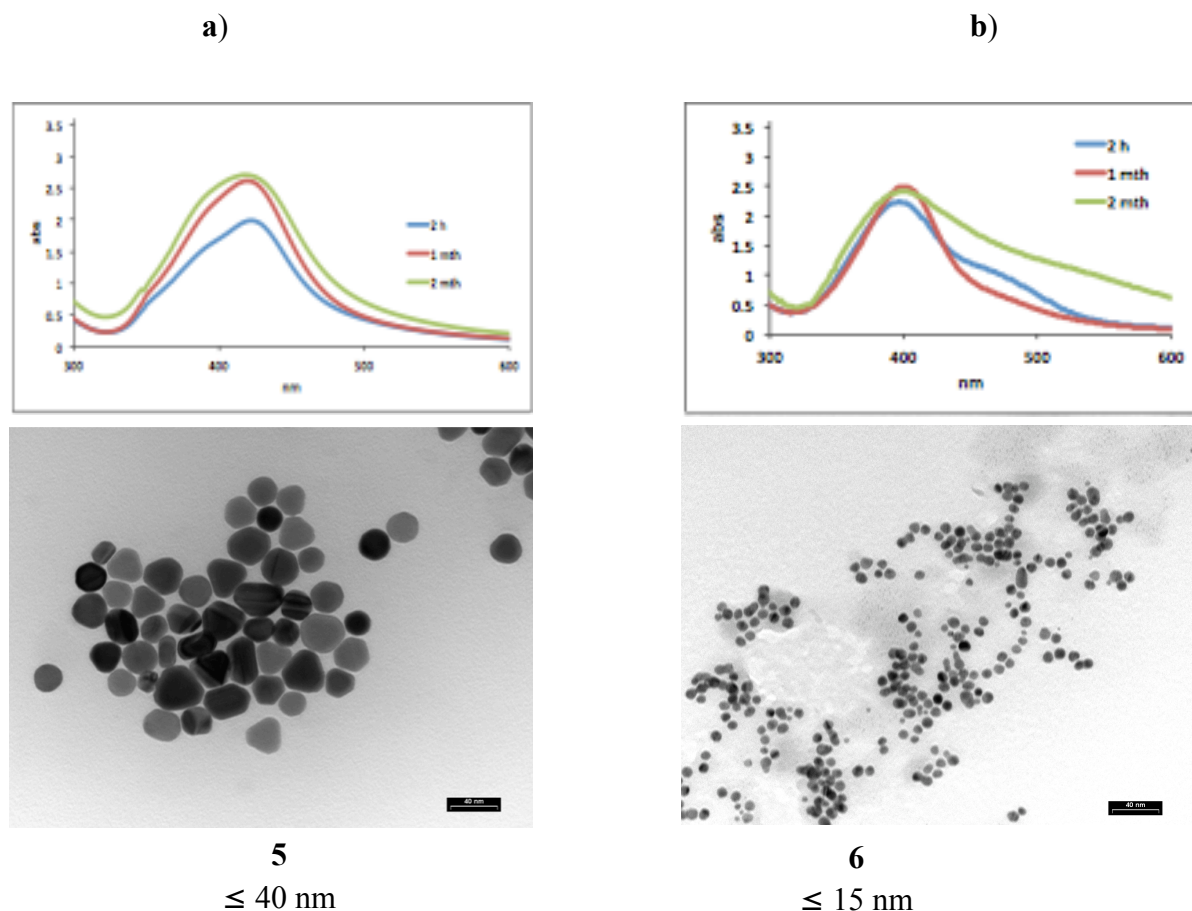


Figure 81: UV-Vis spectra and TEM pictures (scale bar = 40 nm) of **5**-AgNPs (a) and **6**-AgNPs (b) generated at pH 12 (results presented were taken at 3 month)

The sizes of AgNPs (≤ 15 nm) which were formed in the presence Ac-Asp-Ahx-Ser-NH₂ **6** are also similar to the sizes of AgNPs which were generated using the Ac-Ser-Ahx-Tyr-NH₂ **4d** peptide. Surprisingly, the binding affinity of Ac-Ser-Ahx-Tyr-NH₂ **4d** (-4.2 ± 0.34 kcalmol⁻¹) differ from that of Ac-Asp-Ahx-Ser-NH₂ **6** (-7.0 ± 0.87 kcalmol⁻¹).

4.7 Attachment of AgNPs on Glass Support

Infections on implant devices are an increasing concern.³⁴ Since silver nanoparticles are antibacterial,^{11e} attachment of these nanoparticles on the surface of implant devices could serve as a versatile tool in addressing this problem. Peptides are known to be biocompatible¹¹ therefore they could be good additives for the generation of AgNPs for antibacterial applications. Furthermore, peptides could improve nanoparticle dispensability and chemical stability during the application of these nanoparticles in different fields.

We explored the efficiency of incorporating our AgNPs on surfaces to use them in antibacterial studies. Mirkin et al. reported a procedure of attaching AgNPs on activated glass surface,³⁵ hence we used glass microscope slides as a reaction model (Figure 82). Our investigation involved activating the glass slides followed by attachment of our already prepared AgNPs which were generated in the presence of peptide **3d** at pH 10 and pH 12 (Figure 55 and 56). For peptide **4d** the AgNPs which were used in this evaluation were generated at pH 12 (Figure 58).

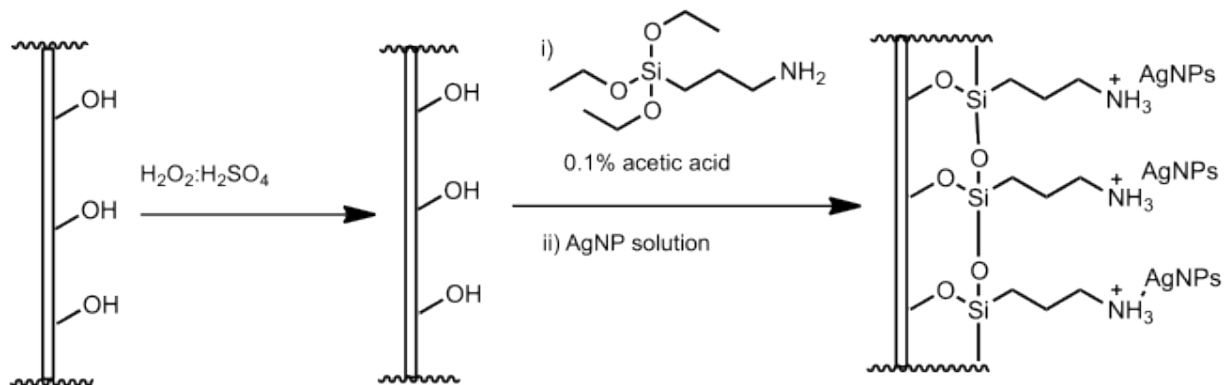


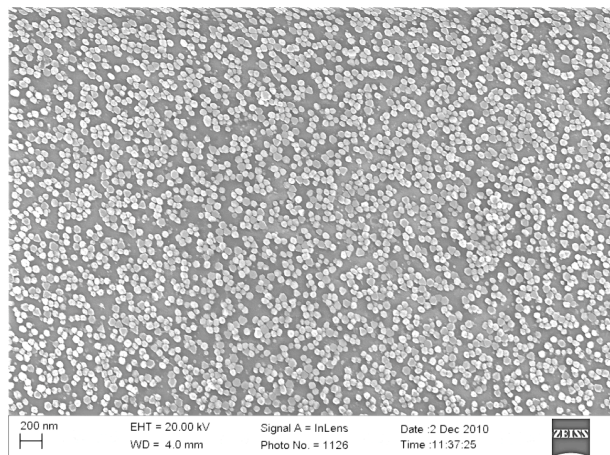
Figure 82: General scheme for functionalising glass surface and attachment of AgNPs³⁵

We pretreated the glass slide with a solution of H₂SO₄ and HNO₃ for cleaning and activation of the glass surface and then, under acidic conditions introduced reactive primary amine functionalities using 3-aminopropyltrimethoxysilane (Figure 82).³⁵ The modified glass substrates were rinsed thoroughly with nanopure water before use.

The silanised glass slides were then immersed for 24 hours in a solution of previously synthesized AgNPs. Following washing with nanopure water, the characterization of the nanoparticles was carried out by SEM analysis (Figure 83).

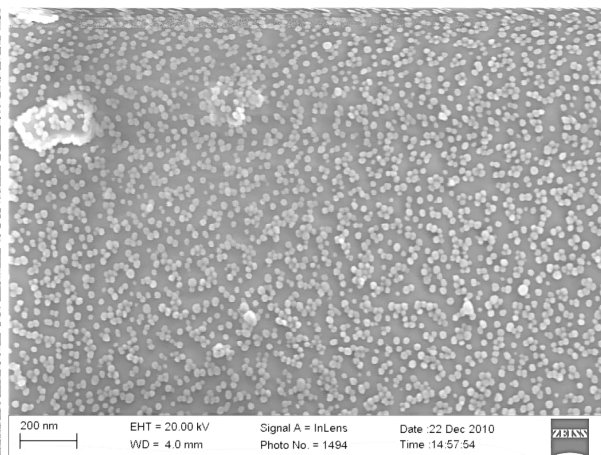
In all cases, the SEM images show a monolayer of AgNPs which are attached to the glass surface. Overall, the sizes of the AgNPs are within similar ranges to the size before attachment onto the glass surface. Like other studies,³⁵ there is no significant tendency observed for the nanoparticles to stack in a face-to-face manner. Such tendency could be overcome by the electrostatic interactions between the amine-coated glass slide and probably the peptide which is protecting the AgNPs.

a)



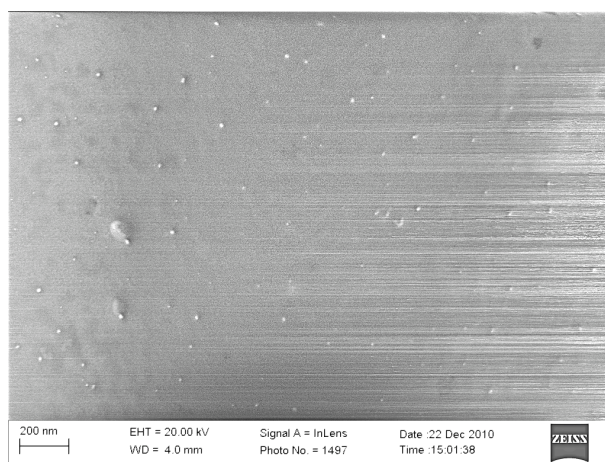
3d-AgNPs (pH 12)
 ≤ 50 nm

b)



3d-AgNPs (pH 10)
 ≤ 20 nm

c)



4d-AgNPs (pH 12)
 ≤ 15 nm

Figure 83: SEM images of AgNPs on activated glass slide surface generated in the presence of peptide **3d** at pH 12 (a) and pH 10 (b) whereas (c) shows SEM image of **4d**-AgNPs generated at pH 12

V.

ANTIBACTERIAL STUDIES

Silver nanoparticles have been known for a long time to be antibacterial.^{21,36} Since then there has been a wide range of healthcare products where AgNPs are incorporated and examples include medical devices, burn dressings and water purification systems.³⁷

For antibacterial activity, the dimensions of AgNPs play a major role and studies showed smaller nanoparticles to have greater antimicrobial effect than larger ones.^{21,36} Hence, different methods have been reported to prepare AgNPs for potential applications as antibacterials. Apart from the size, the shape of AgNPs has also been reported to play a significant role in their antimicrobial effect.³⁸ Pal et al. found that triangular AgNPs had greater antibacterial action than either rod or spherical nanoparticles.³⁹ The enhanced antibacterial effect of triangular AgNPs was assumed to be due to a higher fraction of active faces present in these shapes. This proposition was supported by X-ray diffraction studies where the diffraction patterns of triangular nanoparticles were found to have more high-atom-density facets than other shapes, favouring the reactivity of silver.

In the generation of AgNPs, the control of the shape and size for enhanced antibacterial applications still poses a great challenge. We envisioned the use of our highly stable **peptide-AgNPs** as antibacterials to be effective approach to address this challenge. Two different sizes of AgNPs derived from peptides were used, **3d-AgNPs** (20 nm) and **4d-AgNPs** (≤ 15 nm).

Staphylococcus epidermidis was used as bacteria model to investigate the antimicrobial activity of silver nanoparticles. This strain of *Staphylococcus* produces large quantities of biofilm and post operative infections of the implants which complicate treatments.⁴⁰

Isothermal Micro Calorimetric (IMC) technique was used to probe bacterial growth at varying amounts of AgNPs. The versatility of IMC is its ability to detect changes in heat production rate as low as 22 nJ/s equivalent to a change of only $\sim 10^4$ in the number of active bacteria present.⁴¹ It

is thus a non-invasive method for detecting and quantifying growth kinetics of bacteria in a liquid culture.

To compare the antibacterial activity of AgNPs generated by non-peptide ligands, citrate stabilized AgNPs (≤ 15 nm in diameter) were also prepared (Figure 84).⁴²

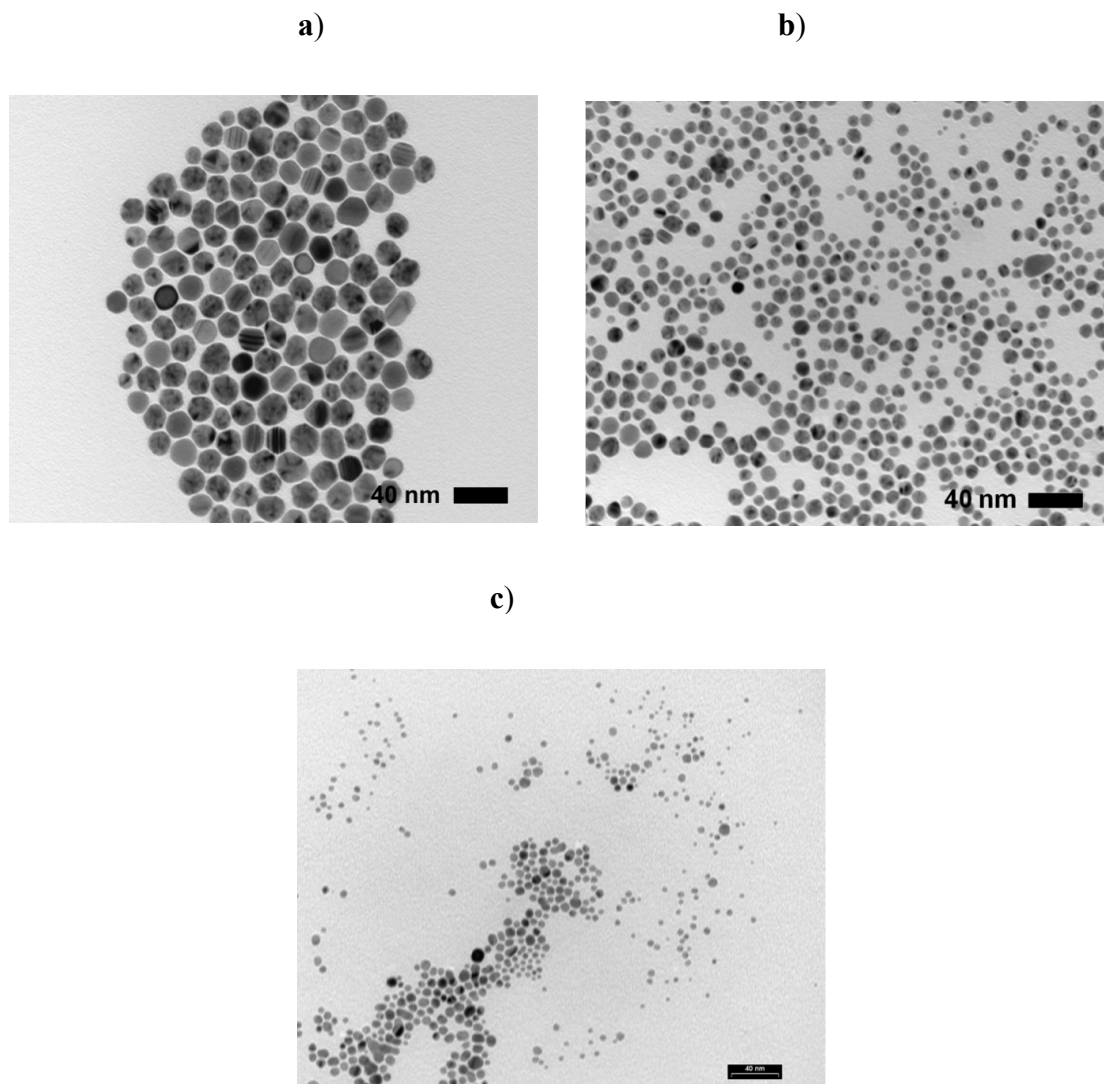


Figure 84: TEM pictures (scale bar = 40 nm) of **3d**-AgNPs (a), **4d**-AgNPs (b) and **citrate**-AgNPs (c) applied in antibacterial studies

The **citrate**-AgNPs have a considerably lower stability (≤ 24 h) than AgNPs induced in the presence of peptides **3d** and **4d** which are stable for several months. Problems associated with polydispersity as well as stability of **citrate**-AgNPs are well known.⁴²

All medium solutions, micro-calorimetric vials, and caps were sterilized by autoclaving at 121°C. Approximately 10^5 bacteria population and Brain Heart Infusion (BHI) medium were mixed in 3 mL ampoules together with AgNPs of different concentrations (2, 5, 10, and 20 $\mu\text{g/mL}$). Controls including peptides, vitamin C, citrate and NaBH_4 were also prepared and treated under identical conditions. The ampoules were sealed with caps prior to loading them into the Isothermal Micro Calorimeter.

The growth inhibition of AgNPs at 37°C was followed as power-time curve recordings on the computer (Figure 85). The generated power-time curves were integrated using the R-programme to obtain the heat over time curve.^{43a-b} As these curves are considered as proxy for the growth curves,⁴⁴ they were fitted using the Richards equations by applying the grofit package for R.^{43a,b} This allowed calculating the maximum growth rate (μ) and the lag phase duration (λ) both of which are affected by the AgNP.

Interestingly Figure 85a shows a change in the pattern of the heat flow curves. In this case with increase in the concentration of **3d**-AgNPs results in a decrease of the maximum heat flow indicating a lower metabolic activity. The nature of these curves indicates the unique behavior of **3d**-AgNPs which are both bactericidal (kill bacteria) and bacteriostatic (slow the growth of the surviving bacteria).

Furthermore, **3d**-AgNPs reveal a concentration dependent antibacterial effect. This is supported by the increase in the lag phase (λ) as well as the relative gradual decrease of the growth rate constant (μ) of the *Staphylococcus epidermidis* with an increase in the concentration of nanoparticles (Figure 86a). **3d**-AgNPs are relatively larger than the pores on the cell membrane of bacteria.⁴⁵ Larger size of AgNPs have smaller surface area to interact with bacterial cell functions to cause physiological damage. Permeability of these bulkier nanoparticles into the bacteria's cell is limited.

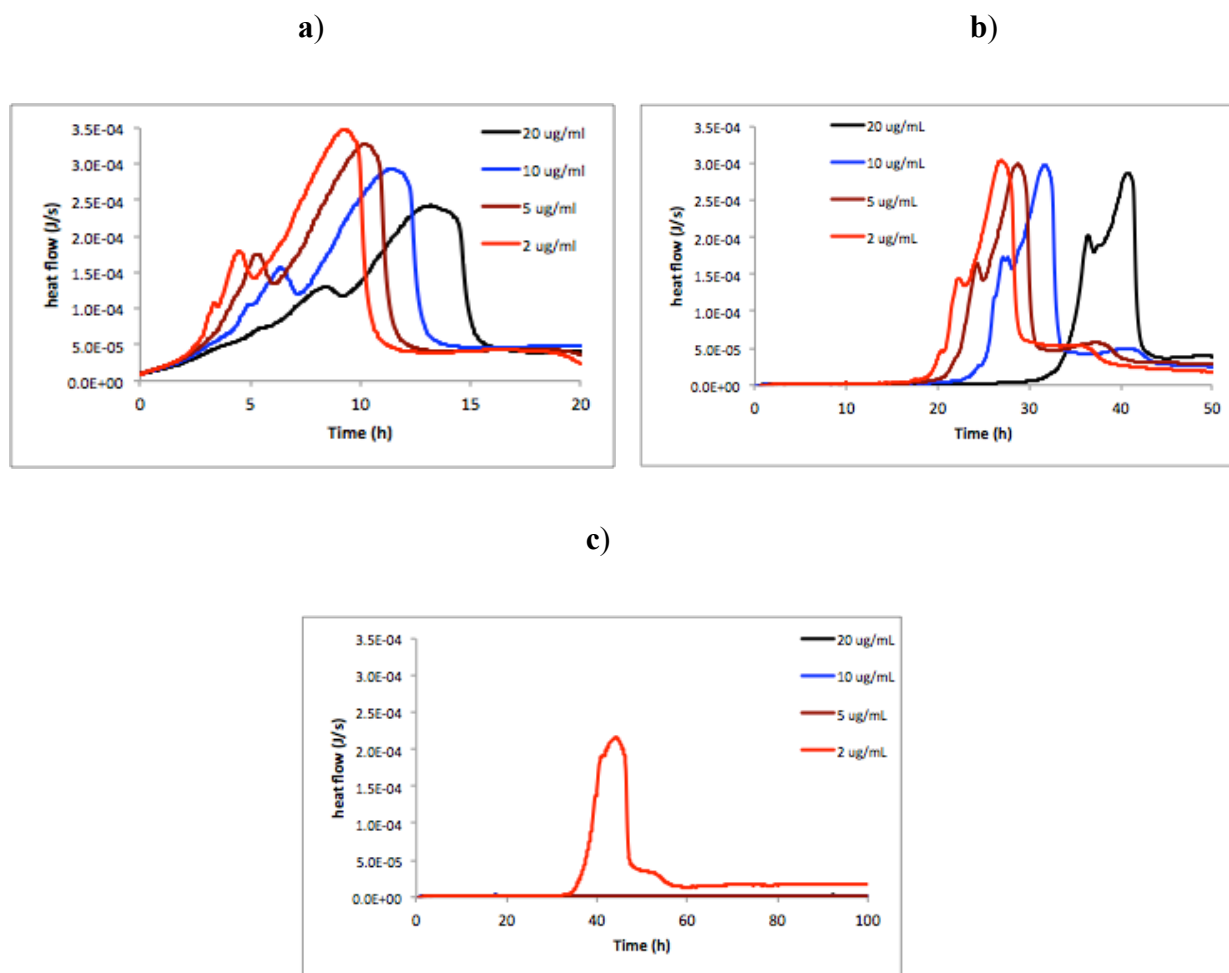


Figure 85: Effect of AgNPs on bacterial growth in the presence of **3d**-AgNPs (a), **4d**-AgNPs (b) and **citrate**-AgNPs (c)

On the contrary, the smaller sizes (≤ 15 nm) **4d**-AgNPs are only bactericidal since there is no significant decrease in the gradient of the heat flow curves with an increase in the concentration of the nanoparticles (Figure 85b). In addition, Figure 86b shows that **4d**-AgNPs kill bacteria more efficiently than **3d**-AgNPs which is supported by considerably higher increase in the lag phase (λ) of bacterial growth when the concentration of the nanoparticles was increased.

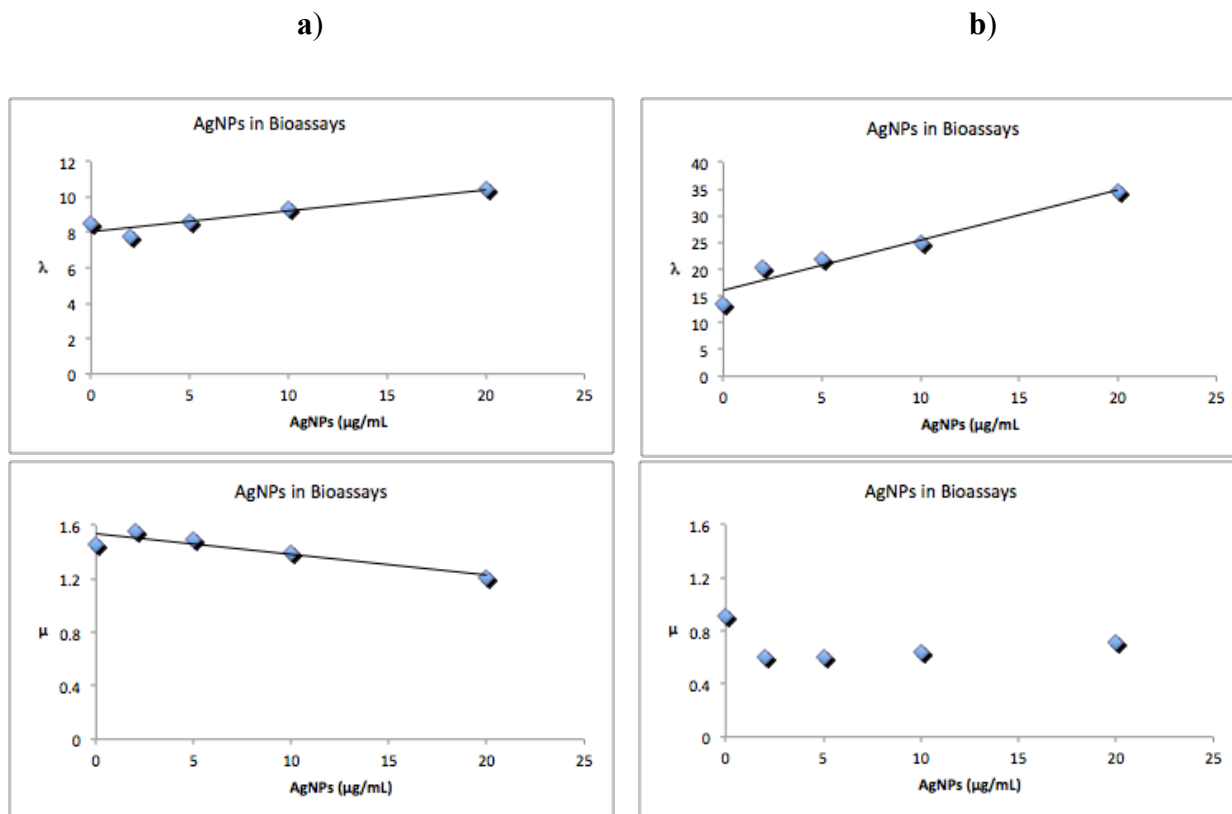


Figure 86: Effect of AgNPs on bacterial growth in the presence of **3d**-AgNPs (a), **4d**-AgNPs (b)

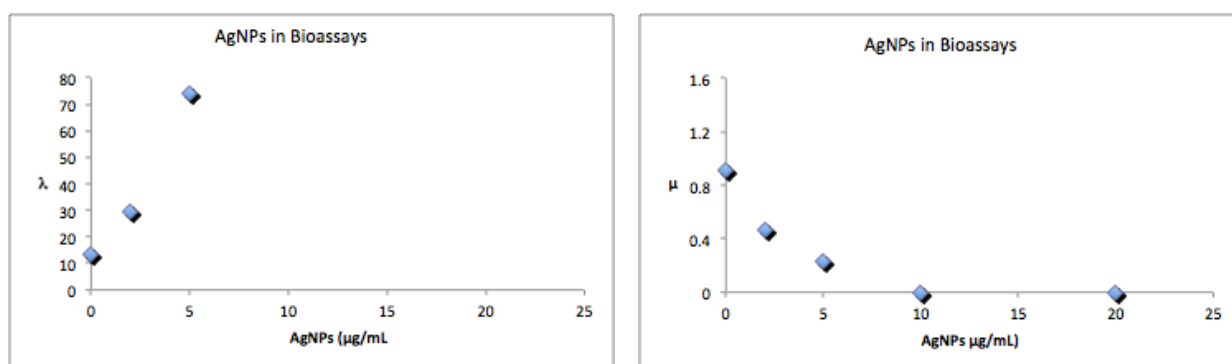


Figure 87: Effect of AgNPs on bacterial growth in the presence of **citrate**-AgNPs

Surprisingly, **4d**-AgNPs show a decrease followed by a gradual increase in the maximum growth rate (μ) of the *Staphylococcus epidermidis* with respect to an increase in the concentration of nanoparticles (Figure 86b). More bacteria than in the presence of **3d**-AgNPs are killed soon after inoculation with **4d**-AgNPs. However, the selection pressure applied by AgNPs might result in

favouring growth AgNP resistant mutants. These mutants would in turn have a slightly higher growth rate in the presence of AgNP, thus explaining the unexpected increase in the maximum growth rate (μ) with an increase in concentration of **4d**-AgNPs (Figure 86b). In this context it must be noted that this increase does not compensate the initial drop of the maximum growth rate (μ). Because **4d**-AgNPs are in the size range of bacteria's cell membrane pores, their permeability into bacteria cell is easier and faster than **3d**-AgNPs.⁴⁵ Furthermore, the difference in the antibacterial action between **3d**- and **4d**-AgNPs could be due to the difference in the shape of AgNPs since shape could also be a decisive factor in the antibacterial effect.³⁸ Unfortunately the exact shapes of our generated AgNPs have not been determined since efforts to access a high resolution TEM machine coupled with a diffractometer have not been successful.

Citrate-AgNPs have the highest antibacterial activity compared to both **3d**- and **4d**-AgNPs. (Figure 85 and 87). Since smaller AgNPs are known to be more antibacterial than bigger AgNPs, the antibacterial activity trend **3d** < **4d** < **citrate**-AgNPs is as expected (Figure 85). Due to their size, **citrate**-AgNPs can pass easily into bacterial cell to cause the most physiological damage. Furthermore **citrate**-AgNPs have the largest surface area available for interaction with bacteria cell functionalities thereby expressing more antibacterial activity than either **3d**- or **4d**-AgNPs.⁴⁶

Even though **citrate**-AgNPs displayed the highest antibacterial activity, the stability (< 24 h) of these AgNPs limit their applicability as compared to **3d**- or **4d**-AgNPs (at least 3 months). Overall, these results show that for the enhancement of antibacterial activity future **peptide**-AgNPs should be designed in the size range of the **citrate**-AgNPs or lower.

Intriguingly, the Isothermal Micro Calorimetry approach can easily follow and clearly display antibacterial activity of smaller (≥ 15 nm) AgNPs at very low concentration (2 $\mu\text{g/mL}$) of AgNPs.

In our experimental conditions, the controls including peptides, vitamin C, citrate and NaBH_4 showed no antibacterial activity against *Staphylococcus epidermidis*. These results indicate that AgNPs were the contributing agents for the observed antibacterial activity.

VI.

SUMMARY AND OUTLOOK

6.0 Summary

Different peptides induce AgNPs in different sizes on solid support and these nanoparticles have very high stabilities (several months). This study has shown that there is no significant effect of the linker and the stereochemistry of the amino acid in the formation of AgNPs.

Notably, this report has shown that short peptides bearing imidazole, carboxyl and hydroxyl functional groups can generate AgNPs with high stabilities of at least 3 months in solution without use of an additional stabilizer. The reduction of Ag^+ and the formation of AgNPs of a given size depend not only on the ratio of peptide/ Ag^+ but also to a large extent on the combination of different amino acids in the peptide sequence. In this regard, AgNPs that were generated in the presence of the His/Asp peptide were found to be larger on average than those produced under identical conditions using the Ser/Tyr peptide. These results also demonstrate that the synergistic effect of amino acids in peptide sequences and the reaction conditions (for example pH of the reaction medium) can easily modulate the affinity of short peptides for Ag^+ ions and AgNPs resulting in different size and shape. Alteration of these parameters has shown to result in the production of AgNPs of diverse shapes (spherical, quasi-spherical, triangular and hexagonal nanoplates) and sizes ranging from around 5 to 60 nm and stabilities of up to 3 months.

Additionally, this study is anticipated to promote easy understanding of the roles which amino acids in short peptides play in the formation of AgNPs of different sizes. Expansion of this powerful knowledge could allow for the large assembly of AgNPs in different size and shape by using different peptides and reaction conditions.

Most importantly, these findings demonstrate an easy approach of generating AgNPs of different sizes for antimicrobial studies. Isothermal Micro Calorimetry is a versatile sensitive technique to investigate the activity of bacteria at different concentrations of AgNPs. This report provides a basis for the measurement of size-dependent antibacterial activity of AgNPs. Bigger nanoparticles (≤ 20 nm), **3d**-AgNPs have the ability to slow the growth rate and also kill bacteria at the same time. As expected, the antibacterial activity of AgNPs was found to be size and concentration-dependent and in the observed trend **3d** < **4d**-AgNPs. Therefore the size and concentration of AgNPs are very important considerations in the application of AgNPs as antibacterial agents. However, the mechanism through which AgNPs manifest antibacterial properties still remain to be explored.

6.1 Outlook

Further AgNP characterization using other techniques like TEM coupled with an electron diffractometer can help to understand the crystalline nature of the AgNPs. In addition the use of a high resolution TEM could identify the actual shapes of AgNPs. In particular, the AgNPs that are of sizes of less than 30 nm could not be clearly imaged by the readily available normal TEM to reveal the shapes.

So far the purification of AgNPs has not been successful. Future studies can be done using dialysis tubes. Thermogravimetric analysis (TGA) on the purified AgNPs could give information on the presence of peptides anchoring on the surface of nanoparticles. This information helps in understanding the role of peptides in the formation of AgNPs.

Furthermore TGA analysis can also reveal the number of peptides which are available per nanoparticle. For biological applications like the targeting of organs, it is achieved by conjugating to nanoparticles, a biomolecule that selectively binds a receptor over-expressed on the target.⁴⁷⁻⁴⁸ The knowledge of the number of peptides per given nanoparticle helps in the design of the nanoparticle-biomolecule model.

Expanding this research into medical devices that are frequently colonized by *Staphylococcus epidermidis* and the coating of the surface of such devices with **peptide**-AgNPs could address this big challenge. Since attachment of AgNPs on activated glass slides has been successful,

future studies can be extended to antibacterial studies of AgNPs which are attached to the surface of glass. To overcome problems that could be associated with inefficient access of AgNPs on the flat glass slides to antibacterial activity, the use of spherical glass beads can be considered.

To understand how our AgNPs kill bacteria, bacteria cells from bioassays can be sliced and then imaged by high resolution TEM to check if AgNPs also enter the bacterial cell. Evidence of AgNPs inside the cells could furthermore support the hypothesis that the AgNPs cause physiological damage by interacting with cell functionalities like DNA.

either flexible or turn inducing rigid motives to allow for large structural peptide diversities (Figure 88).

Moreover, the new library **2** is designed with possibility for the peptide library members to have their N-termini either free or acetylated. This allows for easy screening in the identification of N-termini free or acetylated peptides which are able to induce the formation of AgNPs.

7.1 Combinatorial Screening of Ac-Library 2 Without a Reducing Agent

Library **2** was screened under the same screening conditions as for library **1**. Interestingly, after 10 min of treating the acetylated form (Ac-library **2**) with an aqueous solution of AgNO_3 some beads turned orange-to-yellow colour before the addition of sodium ascorbate, or any other Ag^+ -ion reducing agent (Figure 89). This was surprising since such a result was not observed during the screening of library **1**.

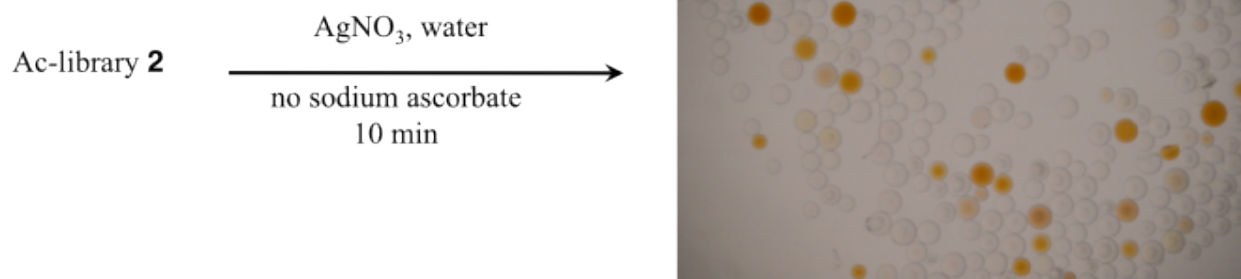


Figure 89: Light micrograph of Ac-library **2** after incubation with AgNO_3 without a reducing agent

Isolation of several of the coloured beads from the assay and analysis of the peptides on them, revealed the main consensus sequences listed in Table 7. Surprisingly, the peptide consensus sequences had a Lys moiety connected to any amino acid without any selectivity for either Tyr or Trp which are known to reduce Ag^+ to Ag .^{9,49} We would have expected most of the sequences to comprise of Tyr or Trp connected to a basic amino acid like Lys or Arg. Like the findings to library **1**, the linker and the stereochemistry of the amino acids were found to be random.

AA2	Linker	AA1
D-Lys	D-Leu	Trp
D-Lys	Val	Ala
D-Lys	Pro-Gly	Glu
D-Lys	Pro	Trp
D-Lys	-	Ala
D-Lys	-	D-His
Val	Val	Lys
Asp	Ala	Lys
His	Ala	Lys
D-Ala	D-Leu	Lys
Tyr	D-Val	Lys
D-Ala	Pro-Gly	D-Tyr

Table 7: Peptide sequences found on coloured beads after treating Ac-library **2** with AgNO₃ without a reducing agent

Similar findings of Lys being able to reduce Ag⁺ to Ag⁰ were reported by Aroca et al.^{9,10} Encouraged by these results, we resynthesized some of the active peptides to check if they are also able to induce the formation of AgNPs as individual sequences without sodium ascorbate as additive.

7.2 Ag-Nanoparticle Formation by Peptides Immobilized on Solid Support

Among the sequences we investigated, as examples we chose peptide Ac-Lys-Pro-Trp-resin **7a** which contain a Ag⁺ reducing agent Trp (Table 8). Moreover we chose peptide Ac-Asp-Ala-Lys-resin **8a** which contain an acid to check if the formation of AgNPs can take place in the presence of an acidic group without sodium ascorbate as an additive.

Ac-D-Lys-Pro-Trp-resin	7a
Ac-Asp-Ala-Lys-resin	8a

Table 8: Peptide **7a** and **8a** used in AgNP formation

In the formation of AgNPs, we treated peptides **7a** and **8a** under the same conditions as to the library screening. As in the combinatorial assay, after 10 minutes of incubating the peptides with an aqueous solution AgNO_3 , the beads became orange coloured (Figure 90 and 91) thereby confirming the combinatorial screening results. SEM analysis also confirmed the presence of AgNPs on the surface of beads (Figure 90 and 91). On average peptide **7a** induces AgNPs of sizes of approximately 20 nm that can form assemblies of 200 nm (Figure 90). Similar morphologies of the AgNPs are observed for peptide **8a** (Figure 91). The source of electrons in the Lys reduction of Ag^+ is yet to be fully investigated.

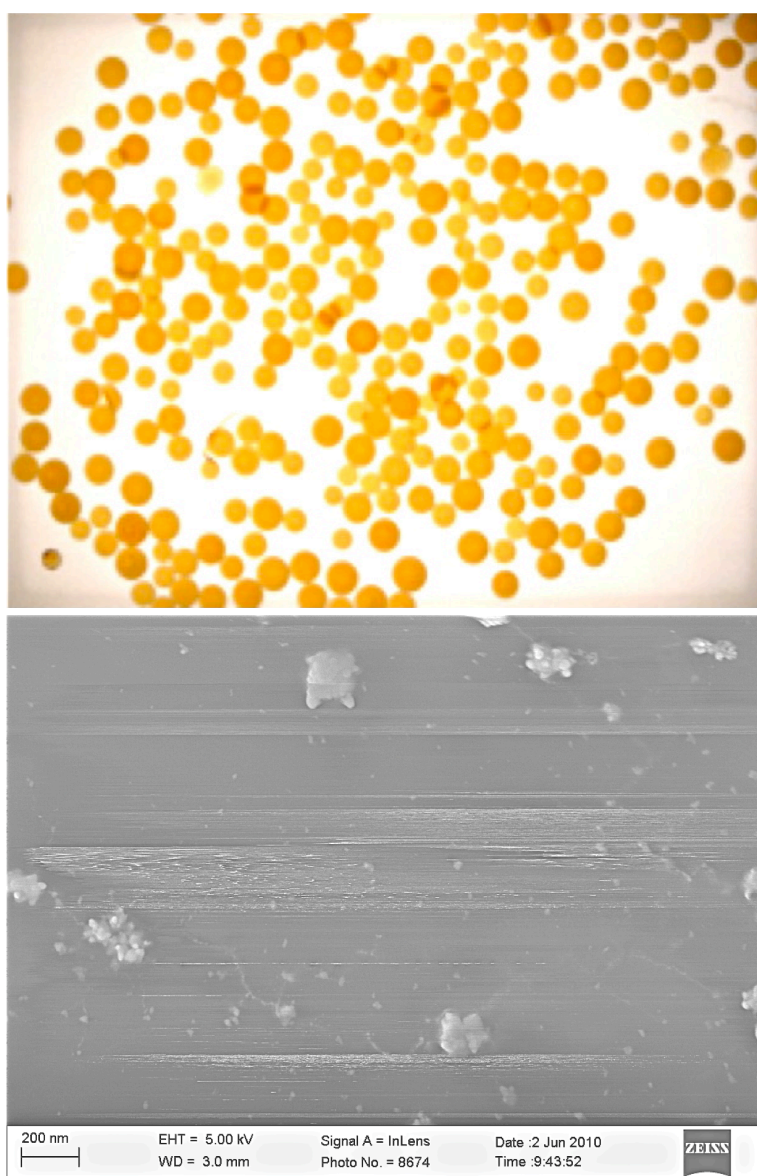


Figure 90: Light micrograph and SEM pictures of Ac-D-Lys-Pro-Trp-resin **7a**-AgNPs

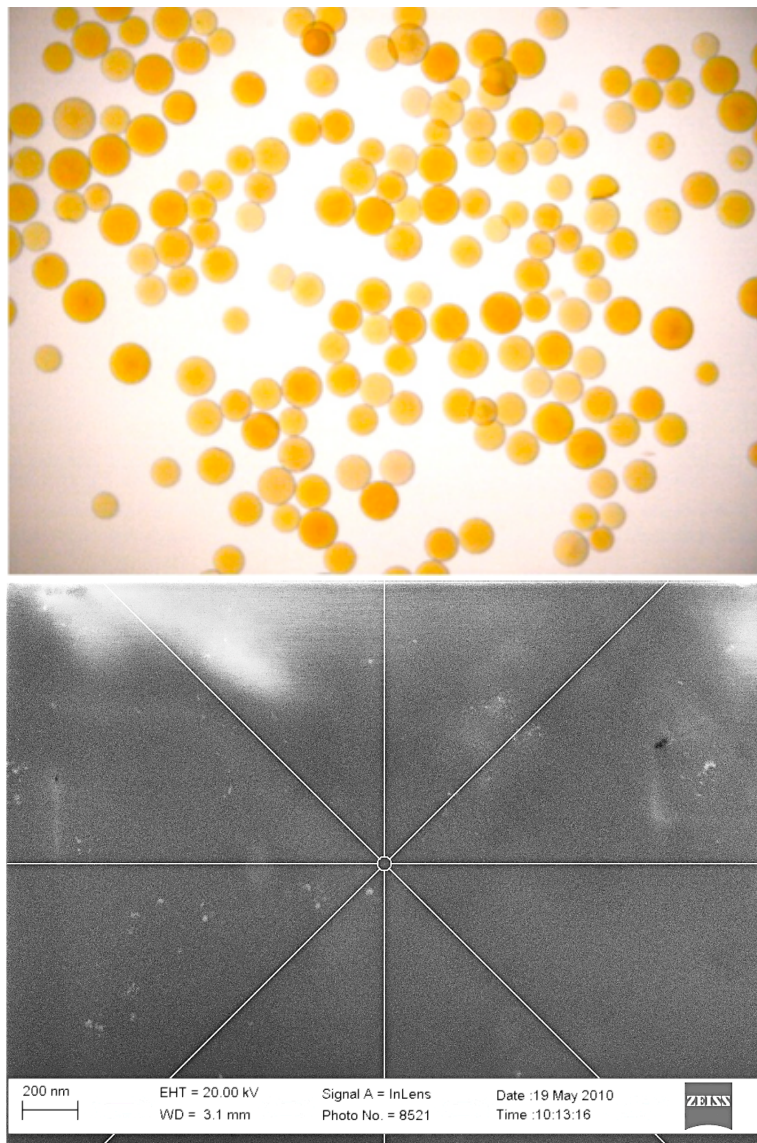


Figure 91: Light micrograph and SEM pictures of Ac-Asp-Ala-Lys-resin **8a**-AgNPs

7.3 Combinatorial Screening of Ac-Library **2** in the Presence of a Reducing Agent (Sodium Ascorbate)

To gain more insight into the ability of Ac-library **2** to identify peptides that are able to induce the formation of AgNPs we treated the library with AgNO_3 followed by sodium ascorbate. Visualization of the assay under the Light microscope showed beads with a diversity of colours (Figure 92).

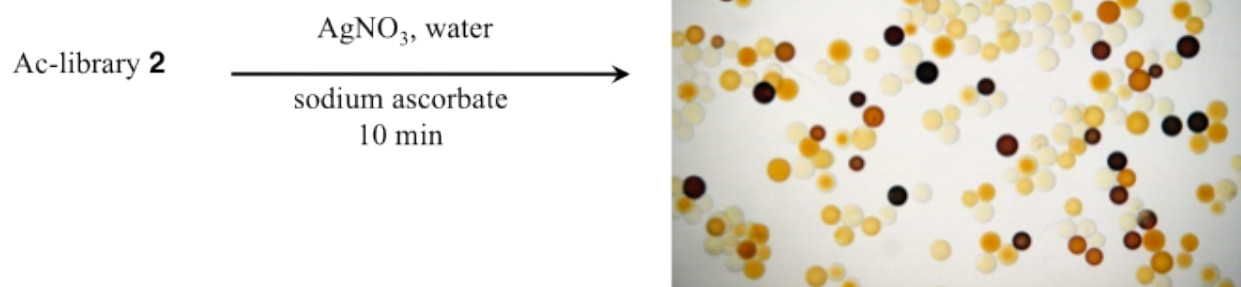


Figure 92: Light micrograph of Ac-library 2 after incubation with AgNO_3 followed by sodium ascorbate

Isolation of several of the coloured beads from the assay and analysis of the peptides on them, revealed the main consensus sequences listed in Table 9. It was encouraging to find that some of the peptide sequences in Table 9 are similar to the sequences we have already found after screening library 1 (Table 3). Like library 1, the results show that the linker and the stereochemistry of the amino acid are random, hence play an insignificant role in the formation of AgNPs.

AA2	Linker	AA1	Bead colour
Ser	Pro-Gly	D-His	red
D-Ala	D-Leu	D-His	red
D-Lys	Ala	D-Asp	red
D-Trp	Pro-Aib	D-Asp	red
Thr	D-Leu	Asp	red
D-Glu	D-Phe	Glu	red
Ala	Phe	D-Glu	red
Val	Pro-Aib	Thr	red
Ser	–	D-Ser	red
His	Phe	D-Tyr	orange
His	Pro	Thr	orange

His	–	Ala	orange
Asp	D-Leu	D-Arg	orange
Tyr	Leu	D-Arg	orange
D-Glu	Pro-Gly	D-Tyr	orange
D-Lys	Pro	Trp	orange
Ser	Gly	Lys	orange
D-Pro	Pro	Pro	orange
D -Trp	D-Phe	D-Ser	yellow
D-Trp	Pro-Gly	Ala	yellow
D-Trp	Pro-Aib	Thr	yellow
D-Trp	Pro-Aib	Trp	yellow
D -Pro	Gly	Trp	yellow
D-Phe	(1S,2S)-Achc	Trp	yellow
D-Pro	Leu	Phe	yellow
D-Ala	Pro-Gly	D-Asn	yellow
Ser	D-Phe	D-Asn	yellow

Table 9: Peptide sequences found on coloured beads after treating Ac-library **2** with AgNO₃ and sodium ascorbate.

7.4 Ag-Nanoparticle Formation by Peptides Immobilized on Solid Support

Based on the combinatorial screening results, we then investigated the ability of the peptides to generate AgNPs as individual sequences as well as to validate the combinatorial screening results. We chose peptide sequences which were expected to allow for easy comparison to the results that were achieved in the investigations with sequences identified after screening library **1**. As examples, **9a** containing Ser with His residue found on red colored beads, **7a** containing Lys with Trp residue found on orange colored beads and **10a** containing Trp with Ser found on yellow coloured beads (Table 9). The linkers and the stereochemistry of the amino acid were chosen as they appear as hits from the combinatorial screening studies.

Ac-Ser-Pro-Gly-D-His-resin	9a
Ac-D-Lys-Pro-Trp-resin	7a
Ac-D-Trp-D-Phe-D-Ser- resin	10a

Table 9: Peptides chosen from the combinatorial screening results to investigate the formation of AgNPs on solid support

Peptides bound on Tentagel resin were treated under the same conditions as previously discussed during the generation of AgNPs. Visual inspection of the treated beads under a light microscope revealed that the beads bearing the Ac-Ser-ProGly-D-His **9a** had turned red, those with the Ac-Lys-Pro-Trp **7a** were dark orange and the Ac-D-Trp-D-Phe-D-Ser **10a** were yellow thereby confirming the combinatorial screening results (Figure 93 and 94).

SEM analyses of the bead-bound AgNPs showed that the dark orange color from the Ac-Ser-ProGly-D-His **9a** corresponds to silver nanoparticles with an average diameter of approximately 70 nm (Figure 93b). AgNPs induced by the Ac-Lys-Pro-Trp sequence are of approximately 20 nm in diameter whereas the yellow colour on the Ac-D-Trp-D-Phe-D-Ser beads are due to smaller sizes of AgNPs of about 15 nm in average size (Figure 94). These results further confirm that different peptides induce selective formation of AgNPs in different sizes on bead.

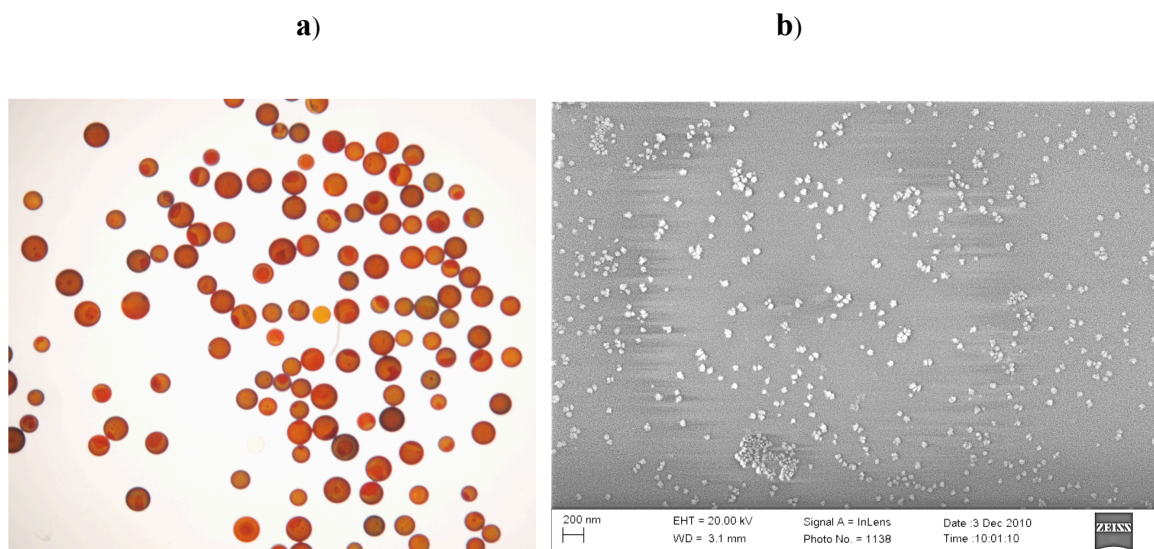


Figure 93: Light microscopic (a) and SEM (b) pictures for AgNPs generated in the presence of peptide Ac-Ser-ProGly-D-His **9a**

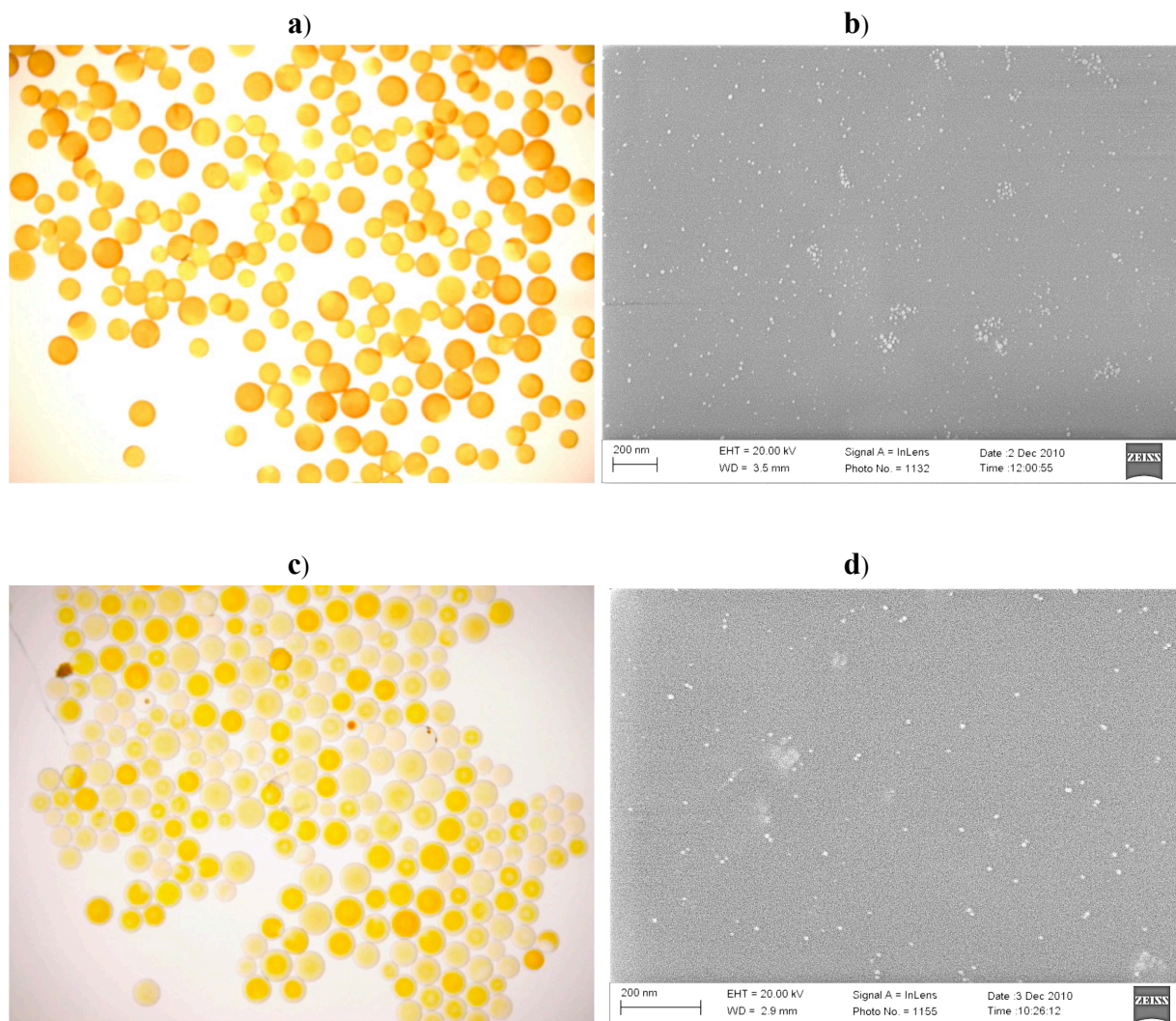


Figure 94: Light microscopic (a and c) and SEM (b and d) pictures for AgNPs generated by peptide sequences **7a** (left) and **10a** (right)

7.5 Ag-Nanoparticle Formation by Peptides in Solution Phase

We also investigated if peptides **9b**, **7b** and **10b** are able to generate AgNPs in solution as they did on solid support. Preliminary studies in the generation of AgNPs have been done at the optimized conditions as discussed for peptide sequences identified in library **1**, that is at pH 12 and peptide/ Ag^+ ratio of 5.

The UV-visible spectra show the development of a weak surface plasmon resonance (SPR) band at around 422 nm which is noticeable after a week for the AgNP formation in the presence of the Ac-Ser-Pro-Gly-D-His-NH₂ **9b** (Figure 95a). TEM analysis reveal AgNPs of about 40 nm in

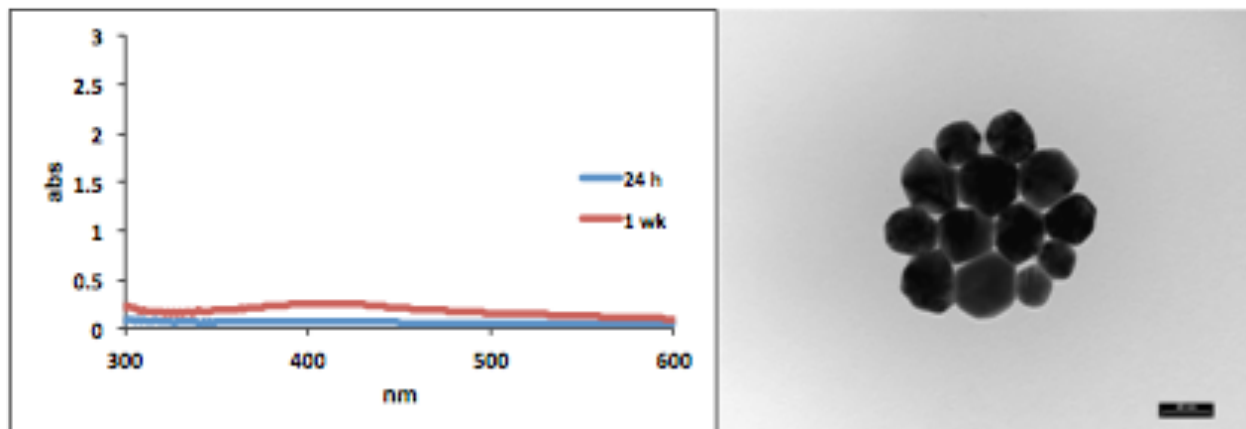
average diameter which corresponds to the observed weak SPR. The size of the AgNPs is comparable to the size obtained when a similar peptide Ac-His-Pro-Aib-Ser-NH₂ **5** was used in the generation of AgNPs under the same conditions (Figure 81).

The generation of AgNPs in the presence of the Ac-D-Lys-Pro-Trp-NH₂ **7b** is faster in comparison to the use of Ac-Ser-Pro-Gly-D-His-NH₂ **9b** peptide (Figure 95a). Since previous studies have shown that the His amino acid is a strong binder of Ag⁺, this could explain the observed differences in the AgNP formation between the stronger Ag⁺ binding peptide Ac-Ser-Pro-Gly-D-His-NH₂ and the Ac-D-Lys-Pro-Trp-NH₂ peptide could be a weaker binder (Figure 95b). ITC studies in the presence of these peptides is expected to give more information about the binding strength of the peptides to Ag⁺-ions as well as to AgNPs. TEM results show that Ac-D-Lys-Pro-Trp-NH₂ **7b** induce the formation of smaller size of nanoparticles of 20 nm in average diameter. These nanoparticles corresponds to the SPR band centered at 418 nm (Figure 95b).

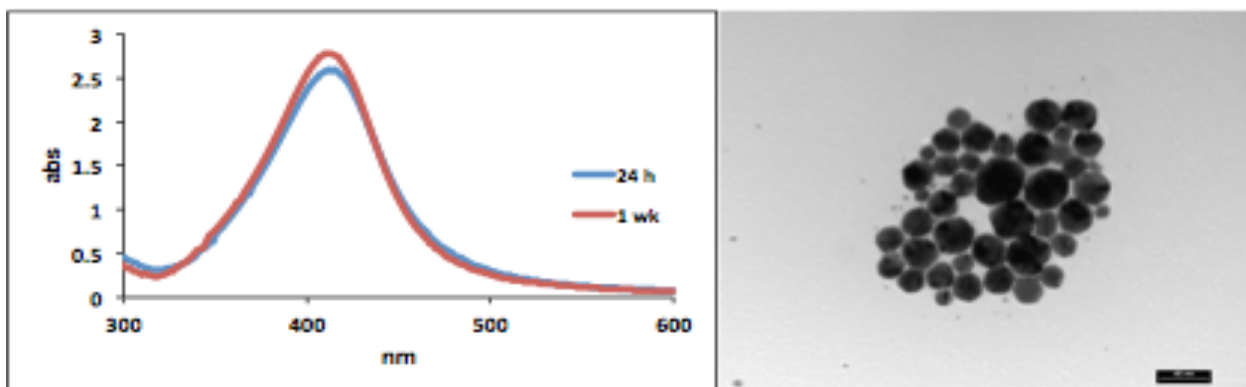
As expected Ac-D-Trp-D-Phe-D-Ser-NH₂ **10** induces the formation of smaller sizes of AgNPs of approximately 15 nm in size. The UV-spectra show an absorption band around 418 which is due to the presence of these small sizes of AgNPs (Figure 95c).

These studies have shown that peptides identified from the combinatorial screening of Ac-library **2** are also able to generate different sizes of AgNPs in solution. AgNPs which are generated in the presence of Ac-D-Lys-Pro-Trp-NH₂ and Ac-D-Trp-D-Phe-D-Ser-NH₂ in solution or on solid support are of the same size, 20 nm and 15 nm respectively.

a)



b)



c)

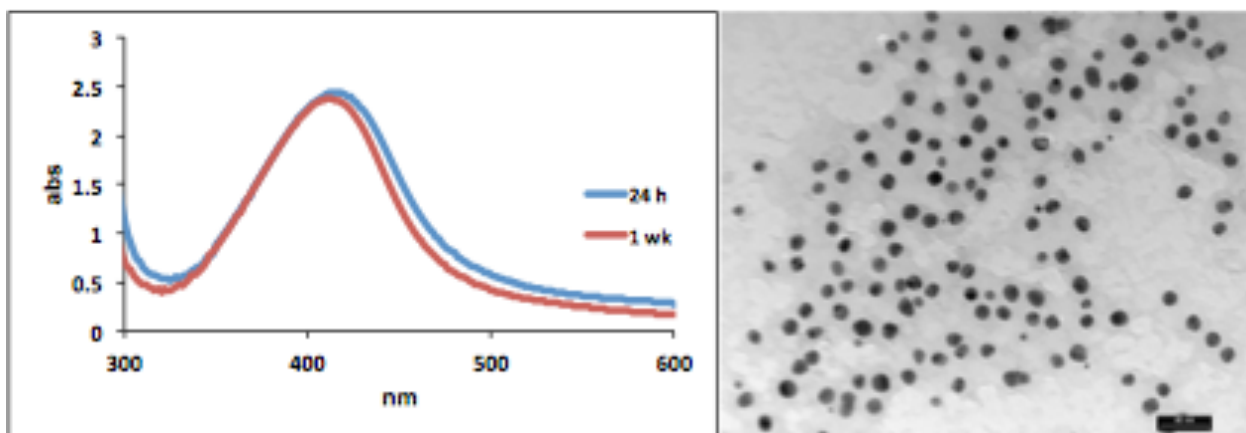


Figure 95: UV-Vis spectra and TEM pictures (scale bar = 40 nm) for AgNPs generated by peptide sequences **9b** (a), **7b** (b) and **10b** (c) (results presented were taken at 1 week).

7.6 Combinatorial Screening of NH₂-Library 2 Without a Reducing Agent

Studies that were carried out on the active peptides identified after the combinatorial screening of library **1** could not clearly demonstrate if the N-termini on peptides could influence the generation of AgNPs. For that reason, the easy flexibility of library **2** to have its peptides N-termini free was taken advantage to screen for peptides which can induce the formation of AgNPs.

After treating library **2** (N-termini free) with AgNO₃ followed by incubation for ten minutes without adding a reducing agent, some beads turned orange/yellow in colour (Figure 96).

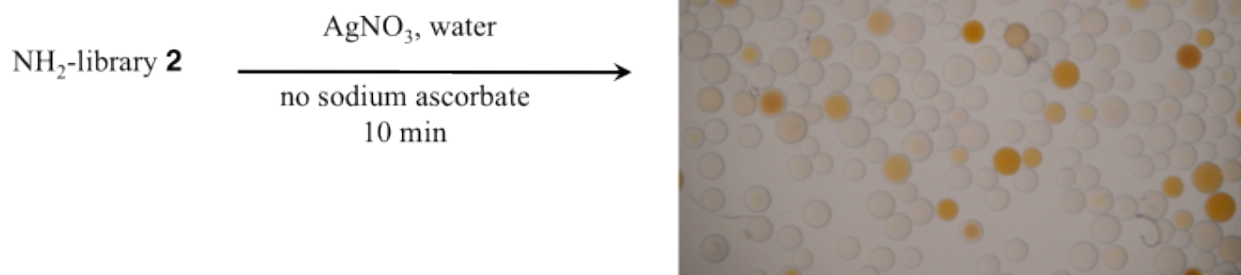


Figure 96: Light micrograph of NH₂-library **2** after incubation with AgNO₃ followed, no addition of sodium ascorbate.

Like the results from the screening of the Ac-library **2**, most of the peptides identified had a Lys connected to any amino acid as previously found after the screening of Ac-library **2** (Table 10). On the few peptide sequences identified where the His moiety is connected to Trp, this could result in the increase of pH which then raises the reducing power of Trp for Ag⁺-ions to form AgNPs.

AA2	Linker	AA1
D-Trp	-	D-His
D-Trp	Ahx	D-His
D-Trp	(1S,2S)-Achc	Lys
Tyr	Ahx	Lys
Glu	D-Le	Lys
D-Phe	-	Lys
D-Lys	Pro	Phe
D-Lys	-	D-Asp
D-Lys	Ahx	Arg
Arg	(1R,2R)-Achc	D-His

Table 10: Peptide sequences found on coloured beads after treating NH₂-library **2** with AgNO₃, no addition of sodium ascorbate.

Further investigations in the generation of AgNPs in the presence of peptides bound on solid support could give more insight into the source of electrons during the reduction process. This could involve protecting the -NH₂ side group and investigate if the reduction of Ag⁺ still takes place without an external reducing agent.

7.7 Combinatorial Screening of NH₂-Library **2** in the Presence of Sodium Ascorbate

NH₂-library **2** was also treated with AgNO₃ and then sodium ascorbate in order to investigate if different peptides will be obtained compared to the results obtained after the screening of the Ac-library **2**. Another aim of screening NH₂-library **2** was to identify peptides which are able to induce the formation of AgNPs when their N-termini are free.

Differently coloured beads were obtained upon treatment of NH₂-library **2** with AgNO₃ and sodium ascorbate (Figure 97).

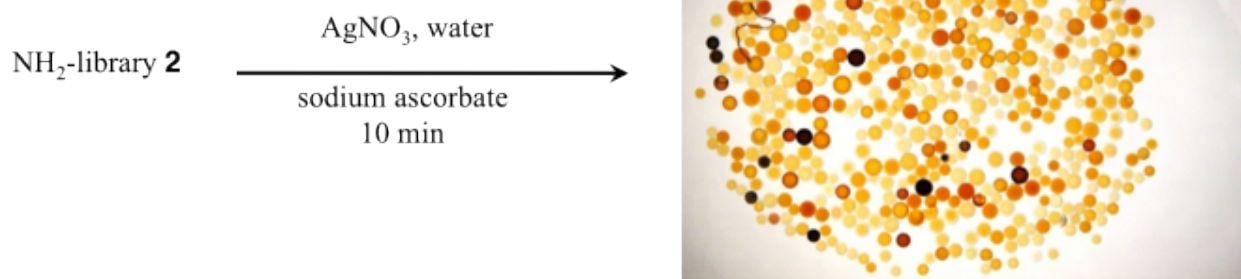


Figure 97: Light micrograph of NH₂-library **2** after incubation with AgNO₃ followed by sodium ascorbate

Several coloured beads from each colour category of the assay were isolated. Following DMF washing of the beads, they were irradiated under high intensity UV light, liberating the tag alcohols contained on each bead. Subsequent EC-GC analyses of the sequences on the beads revealed that most of the red coloured beads consists of His connected to Glu or Asp (Table 11). This confirms that this combination of amino acids is crucial for the generation of AgNPs of a large size. The Phe and Tyr moieties are the most predominant amino acids in the category of the yellow coloured beads. In all cases the linker and the stereochemistry of the amino acid do not play a significant role.

AA2	Linker	AA1	Bead Colour
His	D-Phe	Glu	red X 2
His	Phe	Glu	red
His	D-Val	Glu	red X 2
His	D-Leu	Glu	red
His	Phe	D-Asp	red
His	Val	D-Asp	red
His	Ala	D-Asp	red
His	(1S,2S)-Ache	D-Asp	red
D-Phe	Val	D-His	red
D-Lys	D-Leu	Lys	red
D-Trp	Val	Glu	red
Asp	Pro-Gly	D-Asp	red

AA2	Linker	AA1	Bead Colour
D-Thr	(1R,2R)-Achc	D-Asp	orange
Val	Ala	D-Asp	orange
D -Gln	D-Phe	D-Asp	orange X 2
D-Thr	Phe	Glu	orange
D-Ala	–	Glu	orange
D-Pro	Val	D-His	orange
D-Ala	Ahx	His	orange
His	D-Val	D-Arg	orange
D-Trp	Ahx	D-Arg	orange
Arg	(1R,2R)-Achc	Pro	orange
Arg	D-Val	Pro	orange
Val	–	Trp	orange
D-Phe	Ahx	Lys	orange
L Tyr	Pro-Gly	D Tyr	yellow
L Tyr	Phe	D Tyr	yellow
D Pro	Phe	D Tyr	yellow
D Phe	Pro	Thr	yellow
D Ala	Val	Phe	yellow
D Glu	(1R,2R)-Achc	Phe	yellow
D Thr	D-Phe	Phe	yellow
L Val	D-Val	Phe	yellow
D Ala	D-Phe	D-Ser	yellow
L Val	Phe	Glu	yellow
L Val	D-Leu	Thr	yellow
D Lys	D-Val	Glu	yellow

Table 11: Peptide sequences found on coloured beads after treating NH₂-library **2** with AgNO₃ and sodium ascorbate

Future studies involve re-synthesis of the active peptides as well as AgNP formation on solid support and in solution get more information on the generation of AgNPs.

VIII.

REFERENCES

1. K. Belser, PhD dissertation: *Peptid-Metall Wechselwirkungen-Anwendung selektiver Bindung zur Esterhydrolyse und Bildung von Silber-Nanopartikeln*, **2008**, University of Basel.
2. K. Belser, T. V. Slenters, C. Pfumbidzai, G. Upert, L. Mirolo, K. M. Fromm, H. Wennemers, *Angew. Chem. Int. Ed.* **2009**, *48*, 3661–3664.
3. A. Robin; *Doctoral thesis, Structural diversity of Cu(I), Ag(I) and Cu(II) coordination polymers with the ligand ethanediyl bis(isonicotinate)*, **2005**, University of Basel.
4. Tünde Vig Slenters, PhD dissertation: *Novel silver containing antimicrobial coatings for implant materials: new applications of Ag(I) coordination networks*, **2009**, University of Basel.
5. M. H. J. Ohlmeyer, R. N. Swanson, L. W. Dillard, J. C. Reader, G. Asouline, R. Kobayashi, M. H. Wigler, W. C. Still, *Proc. Natl. Acad. Sci. USA* **1993**, *90*, 10922 – 10926.
6. H. P. Nestler, P. Bartlett, W. C. Still, *J. Org. Chem.* **1994**, *59*, 4723 – 4724.
7. À. Furka, F. Sebestyén, M. Asgedom, G. Dibô, *Int. J. Pept. Protein Res.* **1991**, *37*, 487 – 493.
8. K. S. Lam, S. E. Salmon, E. M. Hersh, V. J. Hruby, W. M. Kazmierski, R. J. Knapp, *Nature* **1991**, *354*, 82 – 84.
9. J. Xie, J. Y. Lee, D. I. C. Wang, Y. P. Ting, *ACS Nano*, **2007**, *1*, 429–439.
10. M. Sjodin, S. Styring, B. Akermark, L. Sun, L. Hammarstrom, *J. Am. Chem. Soc.* **2000**, *122*, 3932–3936.
11. For reviews see: a) C.-L. Chen, N. L. Rosi, *Angew. Chem. Int. Ed.* **2010**, *49*, 2 – 21.; b) T. Tolaymat, A. El Badawy, A. Genaidy, K. Scheckel, T. Luxton, M. Suidan, *Sci. Tot. Environ.*, **2010**, *5*, 999 - 1006.; c) Y. Xia, Y. Xiong, B. Lim, S. E. Skrabalak, *Angew. Chem. Int. Ed.* **2009**, *48*, 60 – 103.; d) M. B. Dickerson, K. H. Sandhage, R. R. Naik, *Chem. Rev.*, **2008**, *108*,

- 4935 - 4978.; e) Y. A. Krutyakov, A. A. Kudrinskiy, A. Y. Olenin, G. V. Lisichkin, *Russian Chem. Rev.* **2008**, *77*, 233 - 257.
12. M. Conza, H. Wennemers, *Chem. Commun.* **2003**, 866 – 867.
13. K. Nomiya, S. Takahashi, R. Noguchi, S. Nemoto, T. Takayama, M. Oda, *Inorganic Chemistry*, **2000**, *39*, 3301.
14. P. P. Bose, M. G. B. Drew, A. Banerjee, *Org. Lett.*, **2007**, *9*, 2489-2492.
15. A. A. Lambropoulos, J. R. Reimer, *J. Chem. Phys.*, **2002**, *116*, 10277-10285.
16. M. G. Guzmán, J. Dille, S. Godet, *Int. J. Chem. Biomol. Eng.* **2009**, *3*, 104.
17. M. Sigh, I. Sinha, R. K. Mandal, *Mater. Lett.* **2009**, *63*, 425–427.; b) R. A. Alvarez-Puebla, E. Arceo, P. J. G. Goulet, J. J. Garrido, R. F. Aroca, *J. Phys. Chem. B* **2005**, *109*, 3787–3792.; c) R. F. Aroca, R. A. Alvarez-Puebla, N. Pieczonka, S. Sanchez-Cortez, J. V. Garcia-Ramos, *Adv. Colloid Interface Sci.* **2005**, *116*, 45–61.
18. J. M. Slocik, D. W. Wright, *Biomacromolecules* **2003**, *4*, 1135 - 1141.
19. Y. Liu, X. Liu, X. Wang, *Nanoscale Res. Lett.* **2011**, *6*, 22.
20. R. Jin, Y. C. Cao, E. Hao, G. S. Metraux, G. C. Schatz, C. A. Mirkin, *Nature* **2003**, *425*, 487–490.
21. A. Panacek, L. Kvitek, R. Prucek, M. Kolar, R. Vecerova, N. Pizurova, V. K. Sharma, T. Nevecná, R. Zboril, *J. Phys. Chem. B* **2006**, *110*, 16248-16253.
22. S. Thomas, K. Nair, E. M. A. Jamal, S. H. Al-Harhi, M. R. Varma, M. R. Anantharaman, *Nanotechnology* **2008**, *19*, 075710.
23. S. Diamanti, A. Elsen, R. Naik, R. Vaia, *J. Phys. Chem. C* **2009**, *113*, 9993–9997.
24. H. Joshi, P. S. Shirude, V. Bansal, K. N. Ganesh, M. Sastry, *J. Phys. Chem. B* **2004**, *108*, 11535-11540.
25. K. T. Nam, Y. J. Lee, E. M. Krauland, S. T. Kottmann, A. M. Belcher, *ACS Nano*, **2008**, *2*, 1480–1486.
26. R. A. Alvarez-Puebla and R. F. Aroca, *Anal. Chem.* **2009**, *81*, 2280–2285.
27. A. Rafey, K. B. L. Shrivastava, S. A. Iqbal, Z. Khan, *J. Colloid and Interface Science* **2011**, *354*, 190–195.
28. X. Zhai, S. Efrima, *J. Phys. Chem.* **1996**, *100*, 1779-1785.

29. Y. A Krutyakov, A. A. Kudrinskiy, A. Y. Olenin, G. V. Lisichkin, *Russian Chemical Reviews* **2008**, *77*, 233 - 257.
30. N. Cathcart, A. J. Frank, V. Kitaev, *Chem. Commun.*, **2009**, 7170–7172.
31. D. L. V-Hyning, C. F. Zukoski, *Langmuir* **1998**, *14*, 7034.; b) H. S. Shin, H. J. Yang, S. B. Kim, M. S. Lee, *J. Colloid Interface Sci.* **2004**, *274*, 89.
32. R. Christopher Doty, T. Robert Tshikhudo, Mathias Brust, David G. Fernig, *Chem. Mater.* **2005**, *17*, 4630-4635.
33. M. Tsuji, K. Matsumoto, P. Jiang, R. Matsuo, X.-L. Tang, K. S. N. Kamarudin, *Colloids and Surfaces A: Physicochem. Eng. Aspects* **2008**, *316*, 266–277.; b) Zhang *et al.* *Rev. Adv. Mater. Sci.* **2010**, *24*, 10-25.
34. Y. Zhao, Y. Tian, Y. Cui, W. Liu, W. Ma, X. Jiang, *J. Am. Chem. Soc.* **2010**, *132*, 12349–12356.; b) S. B. Levy, B. Marshall, *Nat. Med.* **2004**, *10*, S122–S129.
35. a) C. Xue, Z. Li, C. A. Mirkin, *small* **2005**, *1*, 513 –516.; b) J. Song, J. Chen, C. M. Klapperich, V. Enga, C. R. Bertozzi, *J. Mater. Chem.*, **2004**, *14*, 2643–2648.
36. L. S. Nair, C. T. Laurencin, *J. Biomed. Nanotechnol.* **2007**, *3*, 301.
37. a) V. Thomas, M. M. Yallapu, B. Sreedhar, S. K. Bajpai, *J. Colloid Interface Sci.*, **2007**, *315*, 389 – 395.; b) S. Kim, H. J. Kim, *Int. Biodeterioration Biodegradation*, **2006**, *57*, 155–162.
38. D. R. Monteiroa, L. F. Gorupb, Al. S. Takamiyaa, A. C. Ruvollo-Filhob, E. R. Camargob, D. B. Barbosa, *Int. J. Antimicrobial Agents* **2009**, *34*, 103–110.
39. S. Pal, Y. K. Tak, J. M. Song, *Appl Environ Microbiol.* **2007**, *73*, 1712–20.
40. G. Hedin, *Scan. J. Infect. Disea.*, **1993**.
41. U. Ah, D. Wirz, A. Daniels, *BMC Microbiology* **2009**, *9*, 106.
42. X. Dong, X. Ji, H. Wu, L. Zhao, J. Li, and W. Yang, *J. Phys. Chem. C* **2009**, *113*, 6573-6576.
43. a) M. Kahm, G. Hasenbrink, H. L. Fraté, J. Ludwig, M. Kschischo, *J. Stat. Soft.*, **2010**, *33*, 1-21.; b) M. H. Zwietering, I. Jongenburger, F. M. Rombouts, K. V. Riet, *Appl. Environ. Microbiol.*, **1990**, *56*, 1875-1881.
44. D. Bravo, O. Braissant, A. Solokhina, M. Clerc, A. U. Daniels, E. Verrecchia P. Junier, *FEMS Microbiol. Ecol.*, **2011**, 1–9.
45. L. Kvitek, A. Panacek, J. Soukupova, M. Kolar, R. Vecerova, R. Prucek, *J. Phys. Chem. C* **2008**, *112*, 5825.

46. a) R. Morones, J. L. Elechiguerra, A. Camacho, K. Holt, J. Kouri, J. T. Ramirez, M. J. Yacaman *Nanotechnology*, **2005**, *16*, 2346.; b) I. Sondi, B. Salopek-Sondi, *J . Colloid Interface Sci.* **2004**, *275*, 177-182.
47. W. Cai, T. Gao, H. Hong, J. Sun, *Nanotech., Sci. Appl.* **2008**, *1*, 17-32.
48. S. Bhattacharyya, R. A. Kudgus, R. Bhattacharya, P. Mukherjee *Pharm Res.* **2011**, *28*, 237-259.
49. S. Si, T. K. Mandal, *Chem. Eur. J.* **2007**, *13*, 3160 – 3168.

IX.

PLATINUM NANOPARTICLES

9.0 Platinum Nanoparticles (PtNPs)

Over the past decade, platinum nanoparticles have been extensively explored due to their unique properties for new applications and improving current applications.¹ Recently the potential application of PtNPs in cancer radiation treatment has been reported.² Studies have shown that the size and shape of PtNPs play crucial roles in their applications.³⁻⁷ Due to their synthetic challenge, to date the generation of PtNPs is often done at high temperature.⁸⁻⁹ Quite often the resulting nanoparticle products have drawbacks in different applications due to insolubility in water. Although there have been some reports on the synthesis of water-soluble PtNPs some of which include the use of peptides, the control of size and size distributions still poses a great challenge.^{1,8-10}

Since we had synthesised library **2** which is decorated with functional groups that could coordinate to Pt⁺². We decided to test this library for peptides that are able to generate PtNPs. For the first experiments, we started by screening the Ac-library **2**.

9.1 Combinatorial Screening of Encoded Split-and-Mix Library **2**

Following the incubation of approximately 10 mg resin of Ac-library **2** with an aqueous solution of K₂PtCl₄, the resin was treated with an aqueous solution of NaBH₄. The screening was evaluated using a light microscope.

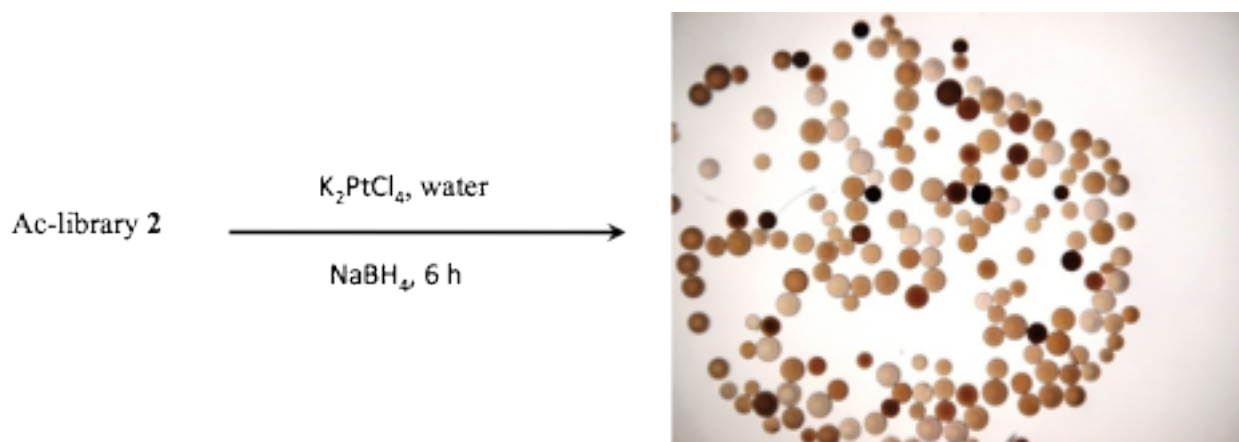


Figure 97: Light micrograph of Ac-library 2 after incubation with K_2PtCl_4 followed by NaBH_4

Figure 97 show the light microscopic image of differently coloured beads after the treatment with K_2PtCl_4 followed by NaBH_4 . Following isolation and EC.GC analysis of the sequences on the beads revealed that the brown coloured beads had predominantly the Ala connected to an Ala motive. For the red coloured beads there is high selectivity for peptides which contain at least an Arg moiety. This could be due to the high basicity of Arg which increases the binding of Pt^{+2} to the peptide resulting in the reduction of Pt^{+2} to generate PtNPs. Some of the peptides contain a His or Lys that shows that the red coloured beads consist of PtNPs that are generated by peptides whose ligand groups are basic.

Under the yellow coloured bead category, it is difficult to generalize the amino acid combinations which induce the formation of PtNPs. Picking more yellow coloured beads from library 2 combinatorial assay and analyse them could help to confirm these results.

In all of the colours generated, the rigid linker has higher occurrence on peptides identified by GC analysis (Table 12). Since the attachment of Pt^{2+} and its reduction, is expected to take place near each other, hence the most pronounced occurrence of the rigid linker show that the spatial arrangement of the active peptides is important for PtNP formation.

AA2	Linker	AA1	Bead colour
D-Ala	Ala	Ala	brown X 7
D-Ala	(1S,2S)-Achc	Ala	brown X 4
D-Ala	D-Phe	Ala	brown X 2
D-Phe	D-Phe	Ala	brown
Ser	(1S,2S)-Achc	Ala	brown
Arg	(1S,2S)-Achc	Trp	brown
Arg	–	Trp	brown
D-Ala	(1S,2S)-Achc	D-Arg	red X 2
D-Ala	(1R,2R)-Achc	D-Arg	red
D-Ala	D-Phe	D-Arg	red
D-Ala	Ahx	D-Arg	red
Ser	(1R,2R)-Achc	D-Arg	red
Ser	(1S,2S)-Achc	D-Arg	red
D-Glu	Pro	D-Arg	red X 2
D-Trp	Pro	D-Arg	red
D-Thr	Pro-Gly	D-Arg	red
D-Ala	(1S,2S)-Achc	Glu	yellow
D-Ala	Gly	D-Arg	yellow
Ser	–	D-His	yellow
D-Trp	Ahx	D-His	yellow
Arg	Leu	D-His	yellow
His	Ahx	Thr	yellow
D-Lys	(1R,2R)-Achc	D-Asn	yellow
D-Thr	D-Val	Lys	yellow
Val	Pro-Aib	D-Ser	yellow
D-Pro	Ahx	D-Ser	yellow

Table 12: Most often found peptide sequences on coloured beads after EC-GC analysis

To confirm the presence of PtNPs on the surface of the coloured beads, resynthesis of the active peptides could be done and then generate PtNPs using the procedure similar to the combinatorial screening. SEM studies could then be done on the surface of beads to confirm the presence of PtNPs. Due to the limited time such studies have not yet been done.

Conclusion

Ac-library **2** could be a suitable tool to identify peptides which are able to form PtNPs. Differently coloured beads were generated after treating the library with K_2PtCl_4 salt followed by $NaBH_4$. Differently coloured beads could denote different sizes of PtNPs on bead. Further studies using SEM could give the relationships of sizes among the identified active peptides.

X.

REFERENCES

1. Y. Li, G. P. Whyburn, Y. Huang, *J. Am. Chem. Soc.* **2009**, *131*, 15998–15999.
2. E. Porcell, S. Liehn, H. Remita, N. Usami, K. Kobayashi, Y. Furusawa, C. L. Sech, S. Lacombe, *Nanotechnology* **2010**, *21*, 085103.
3. H. Lee, S. E. Habas, S. Kveskin, D. Butcher, G. A. Somorjai, P. D. Yang, *Angew. Chem., Int. Ed.* **2006**, *45*, 7824–7828.
4. R. Narayanan, M. A. El-Sayed, *J. Phys. Chem. B* **2003**, *107*, 12416–12424.
5. C. Wang, H. Daimon, Y. Lee, J. Kim, S. Sun, *J. Am. Chem. Soc.* **2007**, *129*, 6974–6975.
6. N. Tian, Z. Y. Zhou, S. G. Sun, Y. Ding, Z. L. Wang, *Science* **2007**, *316*, 732–735.
7. C. K. Tsung, J. N. Kuhn, W. Y. Huang, C. Aliaga, L. I. Hung, G. A. Somorjai, P. D. Yang, *J. Am. Chem. Soc.* **2009**, *131*, 5816–5822.
8. J. C. Huang, C. B. He, X. M. Liu, Y. Xiao, K. Y. Mya, J. W. Chai, *Langmuir* **2004**, *20*, 5145–5148.
9. D. G. Duff, P. P. Edwards, B. F. G. Johnson, *J. Phys. Chem.* **1995**, *99*, 15934–15944.
10. T. Teranishi, M. Hosoe, T. Tanaka, M. Miyake, *J. Phys. Chem. B* **1999**, *103*, 3818–3827.
11. P. Tsiveriotis, N. Hadjiliadis, *Coordination Chemistry Reviews*, **1999**, 190–192171–184.
12. L. Yu, I. A. Banerjee, H. Matsui, *J. Mater. Chem.*, **2004**, *14*, 739–743.

XI.

EXPERIMENTAL

11.0 General Aspects

Materials and reagents were of the highest commercially available grade and used without further purification. The reagents and solvents used in this work were obtained from Aldrich, Fischer, Fluka, Cambridge Isotope Laboratories and Acros chemical supplies. Amino acids were purchased from Bachem and IRIS Biotech. Resins for solid phase synthesis were obtained from Novabiochem (Merck Biosciences) or Rapp Polymere AG.

For all the solution and the washing steps only nanopure/ultrapure water was used. Sodium ascorbate, AgNO₃ and NaBH₄ solutions were prepared fresh. CH₂Cl₂ (follow abbreviations in section XII) was dried by distillation from calcium hydride under nitrogen. Reactions were monitored by thin layer chromatography using aluminium-backed Merck silica gel 60 F254 plates. Compounds were visualized by UV, KMnO₄, ninhydrin or FeCl₃ solutions. Yields given are based upon chromatographically and spectroscopically (¹H and ¹³C NMR) pure materials.

11.1 Analytical Equipments

¹H, ¹³C and ¹⁹F NMR

The spectra were recorded on a Bruker DPX500 or DPX400 spectrometer. Chemical shifts (δ) are reported in ppm using Tetramethylsilane (TMS) or the residual solvent peak as a reference. All spectra of 1D and 2D experiments were assigned by COSY, HMQC and HMBC analysis and the coupling constants (J) are given in Hertz (Hz). The signals are indicated as s = singlet, d = doublet, t = triplet, q = quartet, quin = quintet or m = multiplet.

Mass spectroscopy

Electrospray (ESI) mass spectra were recorded on a Finnigan MAT LCQ spectrometer. Analytical grade methanol was used as the carrier solvent, with samples prepared to a final concentration of approximately 1 mg/mL. The values are given in atom mass per charge (m/z).

Light microscopy (LM)

Combinatorial assays were analyzed with an Olympus SZX12 light microscope.

Electron capture gas-chromatography (EC-GC)

EC-GC measurements were performed on a Hewlett Packard HP 6890 from Agilent. Tag alcohol solutions were silylated *in situ* by addition of BSA (1 μ L) and analysed by EC-GC detector (temperature gradient: 200-320 $^{\circ}$ C in 11 min).

Atomic absorption spectroscopy (AAS)¹

The measurements were performed on Shimadzu AA-6300. Standard solutions of concentration 1, 2, 4, 6 and 8 ppm were used. HNO₃ (10 %) was added to all the solutions to keep the Ag⁺-ions in solution. Blank solutions were also measured.

Scanning electron microscopy (SEM)

Some of the measurements were carried out using Philips ESEM XL 30 FEG or Hitachi S- 4800 at the Zentrum für Mikroskopie in Pharmazentrum with the University of Basel by Gianni Morson, Marcel Düggelin, Daniel Mathys or Eva Bieler. Other measurements were carried out in the Department of Physics in the University of Basel by Jon Agustsson or Dr. Claire Barrett.

X-ray photoemission spectroscopy (XPS)

XPS measurements were performed by Dr. Laurent Marot in the Department of Physics in the University of Basel. A Leybold EA 10N spectrometer equipped with a twin anode (Mg_{K α} 1253.6 eV and Al_{K α} line) and an X-ray source providing monochromatic Al_{K α} light for excitation of the photoelectrons was used. AgNPs were deposited on a silicon wafer followed by drying at room temperature. The complete surface of the sample was excited and the analyzed area was defined

by the settings of the analyzer which was 0.8 cm². Mathematical analysis of the XPS data was made using the software UNIFIT.

UV/Vis spectroscopy

The UV-Vis spectra were recorded in quartz SUPRASIL[®] (Hellma, Typ 114-QS, d = 10 mm) cuvettes or Acryl cuvettes from Semadeni (d = 10mm) with an optical path length of 1 cm on a Varian Carry 300 incl. Thermostat.

Transmission electron microscopy (TEM)

TEM images were taken on a Philips EM 400 microscope operated at 80 kV. The microscope is located at the Zentrum für Mikroskopie in Pharmazentrum in the University of Basel. Samples were deposited on carbon-coated copper grids and directly imaged after drying in air. At times samples were diluted with ultrapure water before imaging to allow for better imaging conditions.

Isothermal titration calorimetry (ITC)

Isothermal calorimetric (ITC) measurements were carried out to characterize the interaction between Ag⁺-ions with peptides using a Micro Cal VP-ITC instrument operated at 25 °C. The titrations were carried out by stepwise injection of solution from a syringe into the sample cell at intervals of 150 s. The syringe was tailor-made such that the tip acts as a blade-type stirrer to ensure continuous mixing efficiency at 300 rpm. Using the interactive software, an injection schedule was automatically carried out by setting the number of injections, volume of each injection, and time between each injection. The reference cell was filled with ultrapure water (1.50 mL) and aqueous peptide solution (1.20 mL) was filled in the titration cell. AgNO₃ solution (0.30 mL) in ultrapure water was added from the syringe into the titration cell in small steps of 8 μL. The heat evolved during the interaction of the different species was measured. Control experiments were carried out by taking distilled water into the cell and titrated with an aqueous solution of AgNO₃ from the syringe. In addition an aqueous solution of peptide in the cell was titrated with ultrapure water from the syringe.

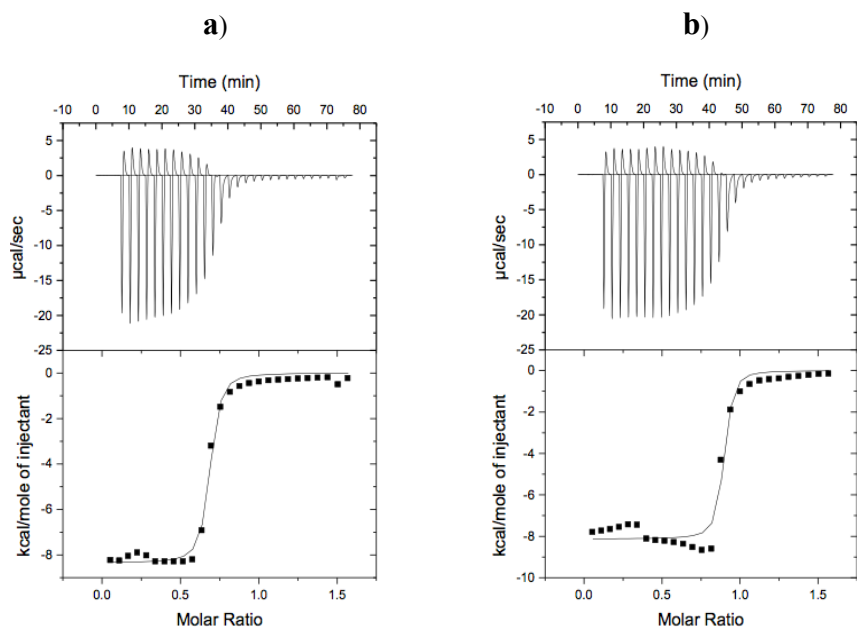


Figure 98: ITC titration data describing the interaction of peptide Ac-His-Ahx-His-NH₂ **2d** (a) and Ac-His-ProGly-His-NH₂ **2e** (b) with Ag⁺ at pH 7.5. The results were obtained after titrating (each injection 8 μL) of an aqueous solution of AgNO₃ (5 mM) into the calorimetric cell containing 1.2 mL of an aqueous solution of peptide (0.5 mM)

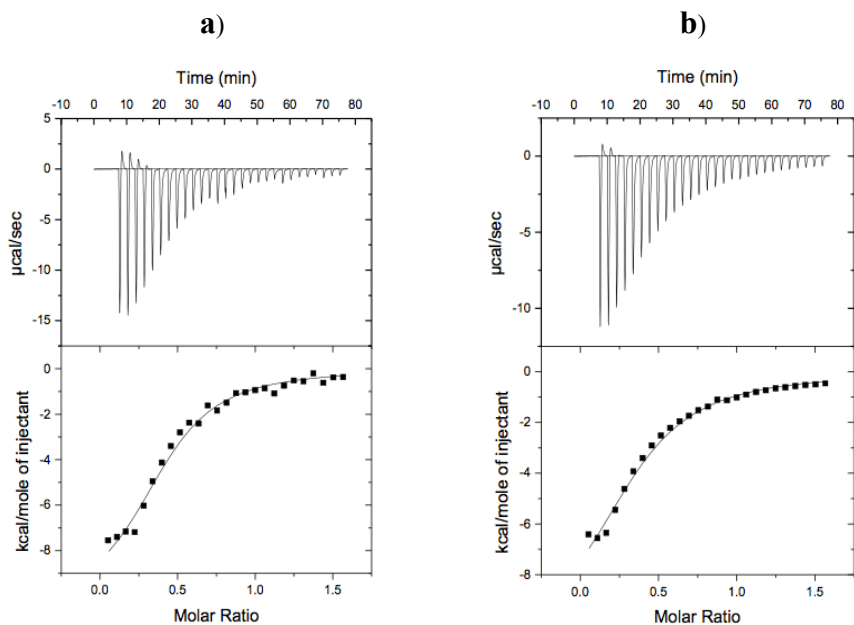


Figure 99: ITC titration data describing the interaction of peptide Ac-His-Ahx-Asp-NH₂ **3d** (a) and Ac-His-ProGly-Asp-NH₂ **3e** (b) with Ag⁺ at pH 7.5. The results were obtained after titrating (each injection 8 μL) of an aqueous solution of AgNO₃ (2 mM) into the calorimetric cell containing 1.2 mL of an aqueous solution of peptide (0.5 mM)

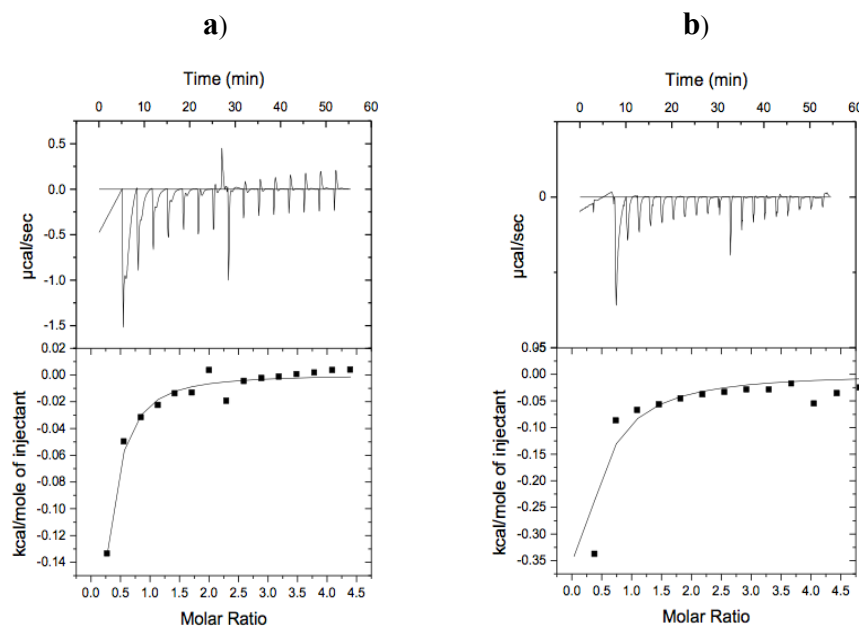


Figure 100: ITC titration data describing the interaction of peptide Ac-Ser-Ahx-Tyr-NH₂ **4d** (a) and Ac-Ser-ProGly-Tyr-NH₂ **4e** (b) with Ag⁺ at pH 7.5. The results were obtained after titrating (each injection 8 μL) an aqueous solution of AgNO₃ (100 mM) into the calorimetric cell containing 1.2 mL of an aqueous solution of peptide (2 mM)

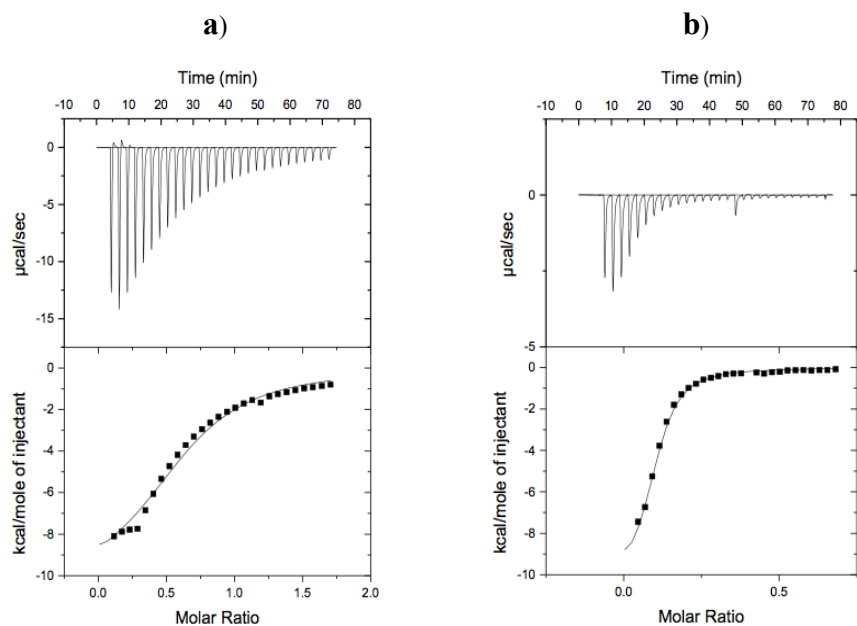


Figure 101: ITC titration data describing the interaction of peptide Ac-His-ProAib-Ser-NH₂ **5** (a) and Ac-Asp-Ahx-Ser-NH₂ **6** (b) with Ag⁺ at pH 7.5. The results were obtained after titrating (each injection 8 µL) an aqueous solution of AgNO₃ (5 mM) into the calorimetric cell containing 1.2 mL of an aqueous solution of peptide (0.5 mM)

	Peptide	ΔG (kcalmol ⁻¹)
2d	Ac-His-Ahx-His-NH ₂	-8.5 ± 0.06
2e	Ac-His-ProGly-His-NH ₂	-8.6 ± 0.04
3d	Ac-His-Ahx-Asp-NH ₂	-5.5 ± 0.12
3e	Ac-His-ProGly-Asp-NH ₂	-5.8 ± 0.94
4d	Ac-Ser-Ahx-Tyr-NH ₂	-4.2 ± 0.34
4e	Ac-Ser-ProGly-Tyr-NH ₂	-4.5 ± 0.69
5	Ac-His-ProAib-Ser-NH ₂	-5.6 ± 0.02
6	Ac-Asp-Ahx-Ser-NH ₂	-7.0 ± 0.87

Table 13: Binding affinities of peptides to Ag⁺-ions

11.2 Preparation of Amine-Terminated Glass Slides

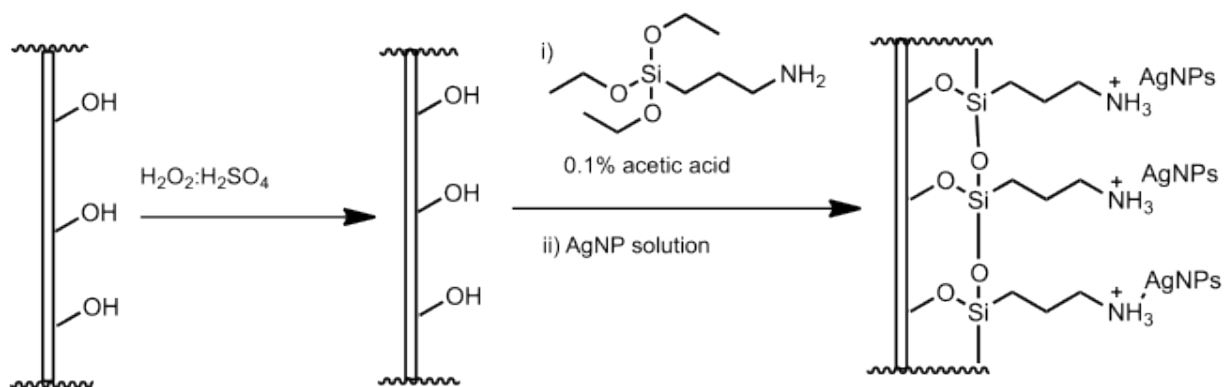


Figure 102: General scheme for functionalising glass surface and attachment of AgNPs²

Glass microscope slides were pretreated with Piranha solution (H₂O₂: H₂SO₄ 1:3, v/v) for half an hour and after removal from the cleaning solution they were rinsed with nanopure water. Following drying the glass slides in a stream of nitrogen they were immersed in a 2-propanol solution of 1% 3-aminopropyltrimethoxysilane in the presence of 0.1 % acetic acid for 5 h. The modified glass slides were rinsed with nanopure water to remove silane molecules that were not covalently bonded to the glass. Finally the cleaned glass slides were dried in a stream of nitrogen.

2

11.3 AgNPs on the Surface of Tentagel Beads or Glass Slides

Samples were either sputtered with 5 nm Au and measured or measured directly without pre-coating with Au.

In order to attach AgNPs on glass slides, dried and modified glass slides are immersed in a solution of prepared AgNPs and left for 24 hours. Ultrapure water was used to wash-off AgNPs which were not bound electrostatically to the glass slides. This followed drying of the glass slides without exposure to light at room temperature. SEM measurements were carried out by Dr. Claire Barrett in the Department of Physics at the University of Basel.

11.4 Biological Assays

Antibacterial studies of AgNPs were performed in the Laboratory of Biomechanics & Biocalorimetry at the University of Basel in collaboration with Prof. Dr. Alma U. Daniels and his coworker Dr. Olivier Braissant. The bioassays were investigated using isothermal micro calorimetry (IMC).

All medium solutions, microcalorimetric vials, and caps were sterilized by autoclaving at 121°C. Approximately 10^5 of the bacteria population and Brain Heart Infusion (BHI) medium were mixed in 3 mL ampoules together with AgNPs of the corresponding concentration (from 0-20 $\mu\text{g}/\text{mL}$). Controls were also prepared and treated under similar conditions. The ampoules were sealed with caps prior to loading them into the Isothermal Micro Calorimeter.

The growth inhibition of AgNPs at 37°C was followed as power-time curve recordings on computer. The generated power-time curves were integrated using the R-programme to obtain the heat over time curve. As these curves are considered as proxy for the growth curves,³ they were fitted using the Richards equations using the grofit package for R.⁴ This allowed calculating the maximum growth rate (μ) and the lag phase duration (λ) both of which are affected by the AgNP.

11.5 General Protocols for Solid-Phase Peptide Synthesis

Peptides were prepared on solid-phase polymeric supports following the general protocols for manual or automated Fmoc/*t*Bu peptide synthesis.⁵ Prior to manual peptide synthesis, reaction vessels were silylated to reduce the tendency of the resin beads to stick to the glass surfaces. This was achieved through overnight agitation of reaction vessels containing a solution of 10 % (v/v) TMSCl in anhydrous toluene. Before use, reaction vessels were washed with CH_2Cl_2 (5x) and dried at 110 °C overnight.

11.5.1 Functionalisation of Rink Amide AM resin

Rink amide resin was deprotected prior to the first amino acid functionalisation. The deprotection process involved addition of 20 % (v/v) piperidine in DMF to the resin (pre-swollen in DMF and drained) followed by agitation for 10 min, draining and rinsing with neat DMF solvent. Deprotection was repeated for a further 10 min after which the resin was washed alternatively

with DMF and CH₂Cl₂ (5x each). The coupling of the first amino acid occurred under the same conditions as described for general solid phase synthesis using the HCTU/*i*-Pr₂NEt (Protocol A).

Protocol A: Manual peptide synthesis using HCTU/*i*-Pr₂NEt

i-Pr₂NEt (9 eq as a 3 M solution in NMP) was added to a solution of the Fmoc-amino acid (3.3 eq) and HCTU (3 eq) in DMF. The coupling mixture was agitated for 2 minutes and then added directly to the amino-functionalised resin (pre-swollen in DMF and drained). The reaction mixture was agitated for 45 - 60 min before washing alternatively with DMF (5x) and CH₂Cl₂ (5x). A few beads were then sampled and checked for complete coupling using standard tests according to the functionalisation of the *N*-terminus (Chloranil,⁶ TNBS⁷ or Kaiser⁸ test). In the case of incomplete functionalisation of the resin, the entire coupling procedure was repeated. In the case of complete coupling, the Fmoc deprotection was performed as detailed in the previous section.

Protocol B: Manual peptide synthesis using DIC/HOBt

A solution of the Fmoc-amino acid (2 eq) and HOBt (2 eq) dissolved in the minimum amount of DMF necessary was added to the suspension of the amino-functionalised resin (pre-swollen in CH₂Cl₂ and drained). The mixture was agitated for 2 min before addition of DIC (2 eq) and then agitated for a further 45-60 min. The suspension was washed alternatively with DMF (5x) and CH₂Cl₂ (5x). The completeness of each coupling was monitored using standard tests according to the functionalisation of the *N*-terminus (Chloranil,⁶ TNBS⁷ or Kaiser⁸ test). In the case of incomplete functionalisation of the resin, the entire coupling procedure was repeated. In the case of complete coupling, the Fmoc deprotection was performed as detailed in the previous section.

Protocol C: Automated peptide synthesis

For automated peptide synthesis, a Syro Peptide Synthesizer (MultiSynTech GmbH, Witten, Germany) was employed.

i-Pr₂NEt (12 eq as a 3 M solution in *N*-methylpyrrolidone) was added to a solution of Fmoc-amino acid (4 eq) and HCTU (4 eq) in DMF. The activated amino acid was added to the amino-functionalized resin, swollen in DMF (100 mM concentration) and the mixture was agitated for

1.5 h before washing with DMF (5x). The Fmoc deprotection was performed by the addition of 40 % (v/v) piperidine in DMF to the resin (preswollen in DMF). The reaction mixture was agitated for 3 min, drained and the piperidine treatment repeated for 10 min. Finally the resin was washed with DMF (7x). The entire protocol was then repeated for the next cycle. The final Fmoc deprotection was omitted when the corresponding Boc-amino acid was employed for the last coupling.

Protocol D: General procedure for N-terminal acetylation

NEt₃ (20 eq) followed by Ac₂O (20 eq) were added to the amine-functionalised resin (pre-swollen in CH₂Cl₂) to a final concentration of ≈ 100 mM in CH₂Cl₂. The mixture was agitated for 1 h and then thoroughly washed alternatively with DMF (5x) and CH₂Cl₂ (5x). The completeness of acetylation was monitored using standard tests according to the preceding functionalisation of the N-terminus (Chloranil,⁶ TNBS⁷ or Kaiser⁸ test).

Protocol E: Cleavage from the solid support and isolation of peptides

The solid supported peptides were cleaved from the Rink Amide resin by agitation in a mixture of TFA/CH₂Cl₂ 1:1 v/v for 1 h and then repeated for a further 30 min. The acidic filtrates were combined and removal of all volatiles under reduced pressure followed by precipitation with Et₂O afforded the crude peptides as their trifluoroacetate salts. Peptide salts were then triturated with Et₂O (at least 3 times) and filtered over a fine glass frit (grade 3) or a syringe filter, dried under high vacuum and used without further purification unless specifically stated.

11.6 General Protocol for Ion Exchange of Peptides

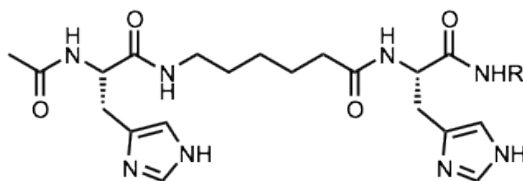
Ion exchange was performed using Dowex® resin (1x2-400) from Sigma-Aldrich or VariPure™ IPE tubes from Varian. Nanopure water was used as the eluting solvent and TLC spots were visualised with ninhydrin, KMnO₄ or FeCl₃. Peptide containing fractions were pooled and lyophilised thereby obtaining the desalted peptide as a white solid. The absence of TFA was confirmed by ¹⁹F NMR analysis.

11.7 Peptides Prepared by Solid-Phase Synthesis

Peptides on solid support were prepared either by automated or by manual synthesis (Fmoc/*t*Bu strategy)⁵ according to the general procedures and obtained as white solids and in yields of 70 % to 85 % unless otherwise stated.

Ac-His-Ahx-His-NHR (R=Tentagel (2a) and R=H (2b))

C₂₀H₃₀N₈O₄ 446.50 g/mol



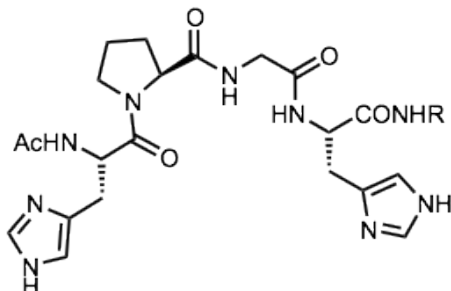
¹H-NMR (400.0 MHz, D₂O, 25°C): δ (ppm) = 8.81 (d, J = 4.6 Hz, 2H, *CH*mi), 7.33 (d, J = 6.6 Hz, 2H, *CH*mi), 4.73 (dd, J = 8.6 Hz, 5.6 Hz, 1H, *CH* α His), 4.66 (dd, J = 8.1 Hz, 5.8 Hz, 1H, *CH* α His), 3.23 (dd, J = 13.6 Hz, 5.3 Hz, 2H, *CH*2 β His), 3.16 (t, J = 7.1 Hz, 2H, *CH*2 β His), 3.07 (m, 2H, *NHCH*2 Ahx), 2.23 (m, 2H, *CH*2CO Ahx), 1.96 (s, 3H, *CH*3 Ac), 1.50 (m, 4H, *CH*2 Ahx), 1.21 (m, 2H, *CH*2 Ahx)

¹³C-NMR (100.6 MHz, D₂O, 25°C): δ (ppm) = 176.1, 174.8, 173.4, 172.1, 135.0, 134.7, 131.4, 131.4, 118.4, 118.3, 53.8, 53.1, 40.4, 36.6, 29.9, 28.2, 27.3, 26.3, 22.6, 22.6

ESI-MS: 447.1 [M+H]⁺ (calcd.: 446.5).

Ac-His-Pro-Gly-His-NHR (R=Tentagel (2c) and R=H (2d))

C₂₁H₂₉N₉O₅ 487.51 g/mol



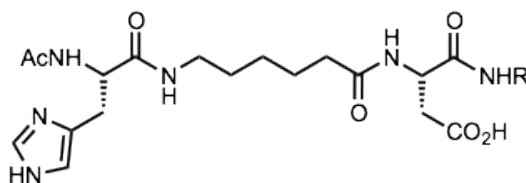
¹H-NMR (400.0 MHz, D₂O, 25°C): δ (ppm) = 8.80 (s, 1H, *CHI*mi), 7.40 (s, 1H, *CHI*mi), 4.89 (m, 1H, *CH*α Pro), 4.70 (dd, *J* = 9.1 Hz, 4.8 Hz, 1H, *CH*α His), 3.9 (d, *J* = 17.1 Hz, 1H, *CH*2 Gly), 3.78 (d, *J* = 17.1 Hz, 2H, *CH*2 Gly, *CH*2δ Pro), 3.60 (m, 1H, *CH*2δ Pro), 3.30-3.13 (m, 6H, *CH*2β His), 2.28 (m, 1H, *CH*2β Pro), 2.09 (m, 1H, *CH*2β Pro), 1.97 (m, 2H, *CH*2γ Pro), 1.94 (s, 3H, *CH*3 Ac);

¹³C-NMR (100.6 MHz, D₂O, 25°C): δ (ppm) = 175.5, 174.5, 173.6, 172.1, 171.7, 170.9, 135.14, 135.12, 131.3, 131.1, 118.6, 118.5, 62.6, 53.6, 53.3, 43.8, 30.5, 28.0, 27.4, 26.3, 26.1, 22.5.

ESI-MS: 488.1 [M+H]⁺ (calcd.: 487.5).

Ac-His-Ahx-Asp-NHR (R=Tentagel (3a) and R=H (3b))

C₁₈H₂₈N₆O₆ 424.21 g/mol



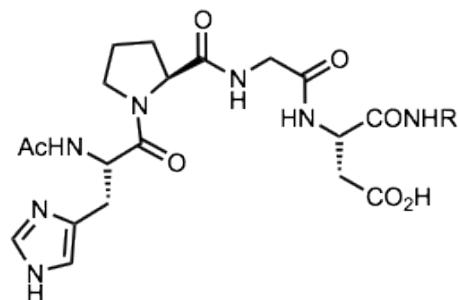
¹H-NMR (400 MHz, D₂O, 25 °C): δ (ppm) = 8.49 (s, 1H, *CHI*mi), 7.16 (s, 1H, *CHI*mi), 4.45 (m, 2H, *CH*α His, *CH*α Asp), 3.04 (m, 4H, *CH*2β His, *NHCH*2 Ahx), 2.58 (dd, *J* = 5.01 Hz, 15.98 Hz, 2H, *CH*2β Asp, *CH*2β Asp), 2.46 (dd, *J* = 8.76 Hz, 15.98 Hz, 2H, *NHCH*2 Ahx), 2.15 (t, *J* = 7.18 Hz, 14.18 Hz, 2H, *CH*2CO Ahx), 1.86 (s, 3H, *CH*3 Ac), 1.43 (m, 2H, *CH*2 Ahx) 1.29 (m, 2H, *CH*2 Ahx), 1.07 (m, 2H, *CH*2 Ahx)

¹³C-NMR (100.6 MHz, D₂O, 25°C): δ (ppm) = 177.3, 176.7, 174.4, 171.9, 133.9, 129.0, 117.5, 53.3, 51.6, 39.5, 39.0, 35.6, 28.2, 26.9, 25.6, 25.0, 22.0

ESI-MS: 425.1 [M+H]⁺ (calcd.: 424.2).

Ac-His-Pro-Gly-Asp-NHR (R=Tentagel (3e) and R=H (3d))

C₁₉H₂₇N₇O₇ 465.46 g/mol



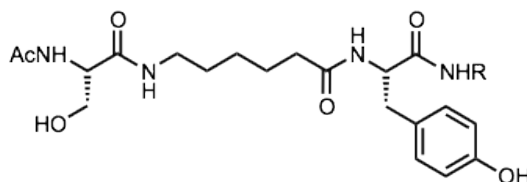
¹H-NMR (400.0 MHz, D₂O, 25°C): δ (ppm) = 8.79 (s, 1H, *CH*Imi), 7.43 (s, 1H, *CH*Imi), 4.97 (t, $J = 6.8$ Hz, 1H, *CH* α His), 4.80 (dd, $J = 8.3$ Hz, 5.6 Hz, 1H, *CH* α Asp), 4.35 (t, $J = 7.1$ Hz, 1H, *CH* α Pro), 4.05 (d, $J = 16.6$ Hz, 1H, *CH*2 Gly), 3.83 (m, 1H, *CH*2 δ Pro), 3.77 (d, $J = 16.6$ Hz, 1H, *CH*2 Gly), 3.50 (m, 1H, *CH*2 δ Pro), 3.20 (dd, $J = 15.1$ Hz, 6.8 Hz, 1H, *CH*2 β His), 3.07 (dd, $J = 15.1$ Hz, 6.8 Hz, 1H, *CH*2 β His), 2.94 (dd, $J = 16.9$ Hz, 5.3 Hz, 1H, *CH*2 β Asp), 2.83 (dd, $J = 16.7$ Hz, 8.3 Hz, 1H, *CH*2 β Asp), 2.25 (m, 1H, *CH*2 β Pro), 2.08 (m, 1H, *CH*2 β Pro), 1.97 (m, 5H, *CH*3 Ac, *CH*2 γ Pro);

¹³C-NMR (100.6 MHz, D₂O, 25°C): δ (ppm) = 175.7, 174.1, 173.1, 171.6, 170.9, 135.2, 130.4, 119.1, 62.4, 51.7, 51.1, 43.9, 36.7, 30.7, 27.6, 26.3, 25.0, 22.3

ESI-MS: 466.1 [M+H]⁺ (calcd.: 465.5).

Ac-Ser-Ahx-Tyr-NHR (R=Tentagel (4a) and R=H (4b))

C₂₀H₃₀N₄O₆ 422.48 g/mol



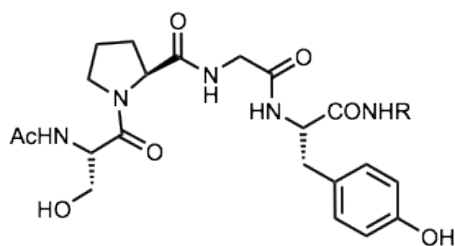
¹H-NMR (400.0 MHz, D₂O, 25 °C): δ (ppm) = 7.03 (d, $J = 8.44$ Hz, 2H, Tyr), 6.71 (d, $J = 8.48$ Hz, 2H, Tyr), 4.43 (m, 1H, *CH* α , Tyr), 4.20 (t, $J = 5.38$ Hz, 10.72 Hz, 1H, *CH* α Ser), 3.69 (d, $J = 5.38$ Hz, 2H, *CH*2 β Ser), 3.01 (m, 4H, COCH₂ Ahx), 2.70 (m, 2H, *CH*2 β Tyr), 2.04 (m, 2H, *CH*3 Ac), 1.24 (m, 4H, *CH*2 Ahx), 0.86 (m, 2H, *CH*2 Ahx)

¹³C-NMR (100.6 MHz, D₂O, 25°C): δ (ppm) = 177.3, 176.7, 174.8, 171.9, 154.7, 130.8, 128.9, 115.8, 61.5, 56.3, 54.9, 39.5, 36.6, 35.7, 28.3, 25.2, 22.1

ESI-MS: 423.2 [M+H]⁺ (calcd.: 422.5).

Ac-Ser-ProGly-Tyr-NHR (R=Tentagel (4e) and R=H (4e))

C₂₁H₂₉N₅O₇ 463.48 g/mol



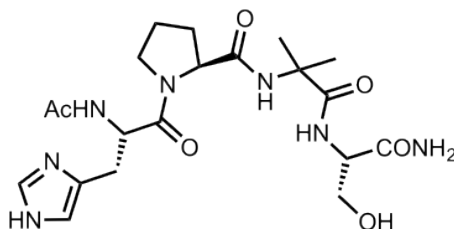
¹H-NMR (400.0 MHz, D₂O, 25°C): δ (ppm) = 7.01 (d, *J* = 8.34 Hz, 2H, Tyr), 6.71 (d, *J* = 8.36 Hz, 2H, Tyr), 4.60 (m, 1H, CH_α Tyr), 4.40 (dd, *J* = 6.22 Hz, 8.37 Hz, 1H, CH_α Ser), 4.30 (dd, *J* = 5.88 Hz, 8.32 Hz, 1H, CH_α Pro), 3.65 (m, 4H, CH₂ Gly, CH₂β Ser), 2.97 (dd, *J* = 6.10 Hz, 14.07 Hz, 1H, CH₂δ Pro), 2.82 (dd, *J* = 8.44 Hz, 14.13 Hz, 2H, CH₂β Tyr), 2.13 (m, 1H, CH₂β Pro), 1.88 (m, 4H, CH₃ Ac, CH₂γ Pro), 1.74 (m, 2H, CH₂γ Pro).

¹³C-NMR (100.6 MHz, D₂O, 25°C): δ (ppm) = 176.1, 175.1, 174.5, 171.4, 170.8, 154.8, 130.9, 128.6, 115.8, 61.3, 60.9, 55.1, 54.1, 48.4, 42.6, 36.5, 29.6, 25.0, 21.9.

ESI-MS: 464.1 [M+H]⁺ (calcd.: 463.5).

Ac-His-ProAib-Ser-NH₂ (5)

C₂₀H₃₁N₇O₆ 465.50 g/mol



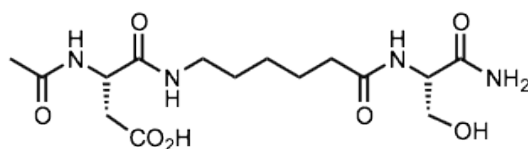
¹H-NMR (400.0 MHz, D₂O, 25°C): δ (ppm) = 8.80 (s, 1H, CH His), 7.39 (s, 1H, CH His), 4.67 (m, 2H, CH_α His), 4.28 (m, 2H, CH_α Pro, CH_α Ser), 3.83 (m, 2H, CH_{2β} Ser, CH_{2δ} Pro), 3.62 (m, 1H, CH_{2δ} Pro), 3.21 (dd, J = 15.1 Hz, 5.6 Hz, 1H, CH_{2β} His), 3.06 (dd, J = 15.4 Hz, 8.2 Hz, 1H, CH_{2β} His), 2.26 (m, 1H, CH_{2β} Pro), 2.10 (m, 1H, CH_{2β} Pro), 1.97 (m, 5H, CH₃ Ac, CH_{2γ} Pro), 1.48 (s, CH₃ Aib), 1.45 (s, CH₃ Aib).

¹³C-NMR (100.6 MHz, D₂O, 25°C): δ (ppm) = 175.6, 174.7, 174.6, 173.1, 170.9, 134.9, 131.1, 118.8, 62.9, 58.2, 57.9, 51.9, 36.4, 30.6, 27.8, 26.2, 25.6, 25.6, 25.4, 22.4.

ESI-MS: 466.3 [M+H]⁺ (calcd.: 465.5).

Ac-Asp-Ahx-Ser-NH₂ (6)

C₁₅H₂₆N₄O₇ 374.39 g/mol



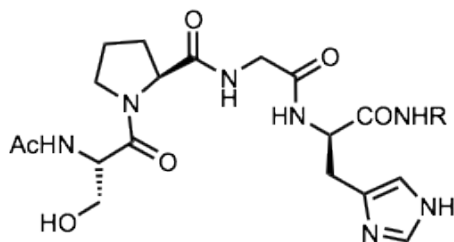
¹H-NMR (500.0 MHz, D₂O, 25°C): 4.58 (t, J = 6.5 Hz, 1H, CH_α Asp), 4.33 (t, J = 5.0 Hz, 1H, CH_α Ser), 3.68 (m, 2H, CH_{2β} Ser), 3.10 (t, J = 6.5 Hz, 1H, NHCH₂ Ahx), 2.70 (dd, J = 16.5 Hz, 7.5 Hz, 2H, CH_{2β} Asp, CH_{2β} Asp), 2.20 (m, 4H, NHCH₂ Ahx, CH₂CO Ahx), 1.90 (s, 3H, CH₃ Ac), 1.54 (m, 2H, CH₂ Ahx), 1.44 (m, 2H, CH₂ Ahx), 1.27 (m, 2H, CH₂ Ahx).

¹³C-NMR (100.6 MHz, D₂O, 25°C): δ (ppm) = 176.2, 176.1, 174.8, 173.6, 169.0, 63.1, 56.5, 51.5, 40.3, 37.0, 36.7, 29.9, 27.4, 26.3, 22.7.

ESI-MS: 375.2 [M+H]⁺ (calcd.: 374.4).

Ac-Ser-ProGly-D-His-NH (R=Tentagel (9a) and R=H (9b))

C₁₈H₂₇N₇O₆ 437.45 g/mol



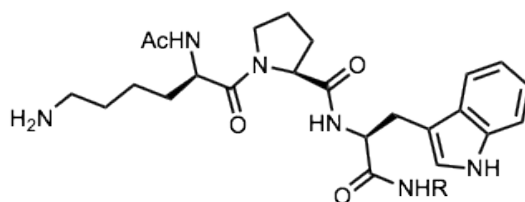
¹H-NMR (400.0 MHz, D₂O, 25°C): δ (ppm) = 7.67 (s, 1H, *CH*Imi), 6.95 (s, 1H, *CH*Imi), 4.73 (t, J = 6.80 Hz, 2H, *CH*_α His), 4.54 (m, 1H, *CH*_α Ser), 4.40 (t, J = 7.0 Hz, 1H, *CH*_α Pro), 3.83 (m, 1H, *CH*₂δ Pro, *CH*₂ Gly), 3.78 (m, 4H, *CH*₂ Gly, *CH*₂β Ser), 3.74 (m, 2H, *CH*₂δ Pro), 3.12 (dd, J = 14.5 Hz, 5.5 Hz, 1H, *CH*₂β His), 3.07 (dd, J = 15.0 Hz, 9.5 Hz, 1H, *CH*₂β His), 2.27 (m, 1H, *CH*₂β Pro), 2.01 (m, 1H, *CH*₂β Pro), 1.95 (s, 3H, *CH*₃ Ac), 1.88 (m, 2H, *CH*₂γ Pro).

¹³C-NMR (100.6 MHz, D₂O, 25°C): δ (ppm) = 175.6, 174.9, 174.1, 171.2, 170.5, 136.0, 61.0, 60.4, 53.7, 53.5, 53.0, 48.0, 42.4, 31.5, 28.6, 24.6, 21.4.

ESI-MS: 438.3 [M+H]⁺ (calcd.: 437.5).

Ac-D-Lys-Pro-Trp-NHR (R=Tentagel (7a) and R=H (7b))

C₂₄H₃₄N₆O₄ 470.56 g/mol



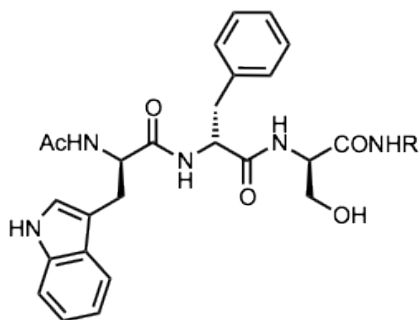
¹H-NMR (400.0 MHz, D₂O, 25°C): δ (ppm) = 7.65 (d, J = 7.5 Hz, 1H, *CH* Trp), 7.40 (d, J = 7.5 Hz, 1H, *CH* Trp), 7.26 (s, 1H, *CH* Trp), 7.08 (m, 2H, Trp), 4.65 (m, 1H, *CH*_α Trp), 4.16 (m, 2H, *CH*_α Lys, *CH*_α Pro), 3.40 (m, 4H, *CH*₂δ Pro, *CH*₂β Trp), 2.66 (t, J = 7.5 Hz, 2H, *CH*₂ Lys), 2.26 (m, 1H, *CH*₂δ Pro), 1.96 (m, 4H, *CH*₂β Pro, *CH*₃ Ac), 1.83 (m, 2H, *CH*₂γ Pro), 1.24 (m, 5H, *CH*₂ Lys).

¹³C-NMR (100.6 MHz, D₂O, 25°C): δ (ppm) = 176.1, 174.1, 173.8, 173.7, 173.3, 136.1, 126.9, 121.8, 119.2, 118.2, 111.72, 109.7, 61.1, 55.2, 53.8, 52.3, 47.7, 39.7, 39.5, 29.5, 29.3, 28.6, 26.3, 23.5, 22.0, 21.4, 21.2.

ESI-MS: 471.3 [M+H]⁺ (calcd.: 470.6).

Ac-D-Trp-D-Phe-D-Ser-NHR (R=Tentagel (10a) and R=H (10b))

C₂₅H₂₉N₅O₅ 479.53 g/mol



¹H-NMR (400.0 MHz, CD₃OD, 25°C): δ (ppm) = 7.55 (d, J = 9.0 Hz, 1H, CH Trp), 7.40 (d, J = 8.5 Hz, 1H, CH Trp), 7.14 (t, J = 7.5 Hz, 2H, CH Trp, CH Phe), 4.59 (m, 4H, CH_α Trp, CH_α Phe), 4.34 (m, 1H, CH_α Ser), 3.90 (t, J = 6.5 Hz, 2H, CH_{2β} Ser), 3.03 (m, 4H, CH_{2β} Phe, Trp), 1.89 (m, 3H, CH₃ Ac).

¹³C-NMR (100.6 MHz, CD₃OD, 25°C): δ (ppm) = 176.1, 174.1, 173.8, 173.7, 173.3, 136.1, 138.3, 138.1, 129.6, 128.8, 127.9, 122.5, 119.9, 119.3, 112.3, 110.8, 63.0, 56.8, 56.0, 38.1, 28.5, 22.5.

ESI-MS: 480.3 [M+H]⁺ (calcd.: 479.5).

11.8 Ag-Nanoparticle Formation by Solid Supported Peptides

In the formation of AgNPs, peptides bound on Tentagel resin were treated under the same conditions as for the screening of the libraries. Images were taken using a light microscope and the formation of AgNPs on bead was confirmed by SEM studies.

11.9 Ag⁺ Uptake Studies of Solid Supported Peptides

Sample preparation: 10.0 mg of dry resin (exact weight) were suspended in a solution of AgNO₃ (0.05 M, 660 μL) solution and sonicated for 15 min. Then, 500 μL of the solution was removed and diluted to 50 mL. 5 mL of the solution obtained was diluted again to 100 mL after addition of 2 mL of 10% HNO₃. Then the Ag concentration of this solution was measured by atom

absorption spectroscopy (AAS) measurements and compared with the concentration of the reference solution prepared from the starting AgNO₃ solution (0.05 M) diluted in the same way.

Peptide	Bead colour	AgNP size	mM Ag/mM peptide
2a	Dark red	50-200 nm	0.38
2b	Dark red	50-200 nm	0.64
3a	Dark orange	50-200 nm	0.55
3c	Dark orange	50-200 nm	0.47
4a	Yellow	≤10 nm	0.26
4b	Yellow	≤10 nm	0.19

Table 14: Ag⁺-ion uptake by peptides bound on Tentagel resin

11.10 Solution Phase Experiments of AgNP Formation in the Presence of Peptides

An aqueous solution of AgNO₃ was added to an aqueous solution of peptide (already adjusted to the required pH by using either NaOH (2 M) or HNO₃ (2 M)) followed by incubating the reaction mixture for 15 minutes. Vitamin C was then added to reduce Ag⁺ to Ag⁰. UV-Vis spectroscopy was used as an initial confirmation for the formation of AgNPs whose sizes were then determined by TEM analyses.

11.11 Synthesis of Library 1

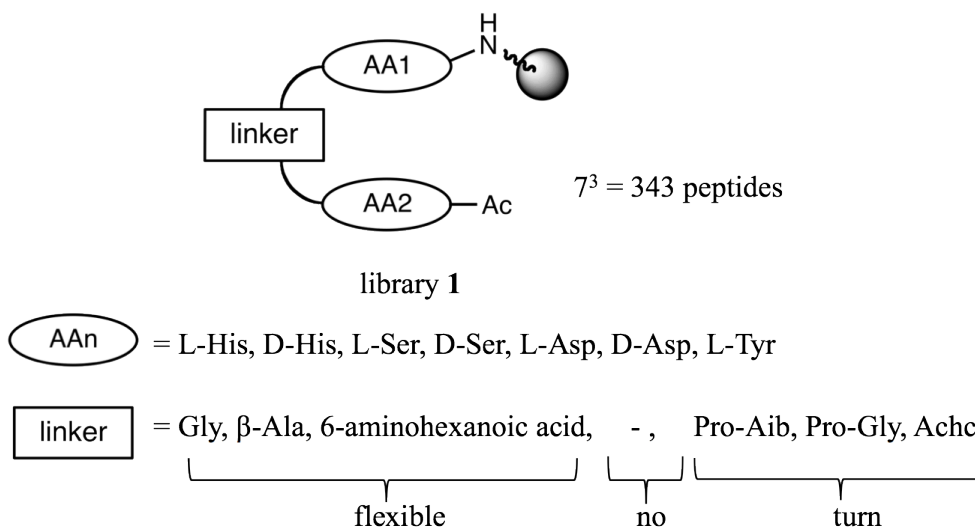


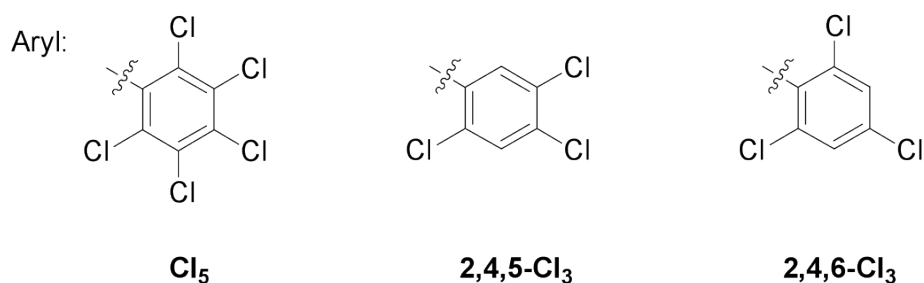
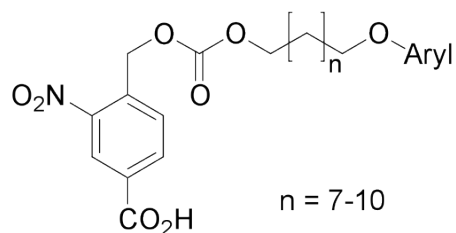
Figure 103: General structure of peptide library 1⁸

Prior to library synthesis, reaction vessels were silylated using TMSCl (10% (v/v)) in anhydrous toluene to reduce the tendency of the resin beads to stick to the glass surfaces. This was achieved through overnight agitation of reaction vessels containing the silylating mixture. Before use, the reaction vessels were washed with CH₂Cl₂ (5x) and dried at 110 °C overnight.

Splitting and encoding: Prior to the coupling of Fmoc amino acids, poly halo tags encoding each amino acid residue are coupled, allowing each peptide immobilised on an individual bead to be unequivocally identified after library screening. Amino-functionalized Tentagel resin (2.1 g, 0.92 mmol, loading 0.44 mmol/g) was split into seven equal portions of 300 mg (0.13 mmol) each and placed into fifteen 25 mL Merrifield shaking vessels. Each portion was then suspended in dry CH₂Cl₂ (5 mL). The relevant tags (2 mol% total resin loading) encoding each amino acid in the library and HOBt (1.0 eq) were dissolved in the smallest amount of DMF possible and added to the resin in the reaction vessels. The mixtures were shaken for at least 5 min to ensure an equal distribution of the tags. This was followed by the addition of DIC (20 µL, 0.20 mmol, 1.5 eq. per tag) to each reaction vessel and the mixture was shaken immediately and allowed to continue shaking overnight (nominally 12 hours). The fifteen portions of resin were then washed with DMF (3x) and with CH₂Cl₂ (3x).

Decoding of tags: In order to check the efficiency of each coupling, 5 beads from each reaction vessel were isolated and analysed. Sampled beads were transferred to microscope slides and swollen in GC quality DMF. Single beads were chosen at random and each transferred by Eppendorf (10 µL micro tips) to the open mouth of a 20 µL capillary tube (previously flame-melted at one end and cut to a length of 4.5 cm). Capillaries were centrifuged (10,000 rpm for 30 seconds) to move the bead to the closed end of the capillary, and were subsequently washed with GC quality DMF (5x) with an analytical syringe (10 µL) to remove debris or traces of coupling reagents from the bead. A final quantity of GC quality DMF (2.5 µL) was added to each capillary in preparation for tag cleavage. Capillaries were then closed at the open end and irradiated for 2 h under high intensity UV light thereby liberating the tag alcohols contained on each bead into the supernatant DMF. Tag alcohol solutions were silylated *in situ* by addition of BSA (1 µL) and analysed by GC-ECD (temperature gradient: 200-320 °C in 11 min). In cases where insufficient trace intensity was produced, the tag coupling protocol was repeated.

Coupling of the Amino Acids: Amino acid couplings and the Fmoc-deprotections were performed as described in the general protocol. After tag coupling was confirmed to be successful, the processes of splitting, encoding of the resin and coupling of each amino acid cycles were repeated using the protocols described above until the tripeptides were assembled (Figure 104 and Table 14). Finally, the *N*-termini were acetylated following the general protocol for acetylation.



Step 1:	(CH ₂) ₁₀ -Cl ₅ (646.74 g/mol, 2.64 μmol, 8.5 mg) = tag Nr. 1 (T₁)
	(CH ₂) ₁₁ -Cl ₅ (660.77 g/mol, 2.64 μmol, 8.7 mg) = tag Nr. 2 (T₂)
	(CH ₂) ₁₂ -Cl ₅ (674.80 g/mol, 2.64 μmol, 9.0 mg) = tag Nr. 3 (T₃)
Step 2:	(CH ₂) ₁₂ -2,4,6-Cl ₃ (604.90 g/mol, 2.64 μmol, 8.0 mg) = tag Nr. 1 (T₄)
	(CH ₂) ₁₂ -2,4,5-Cl ₃ (604.90 g/mol, 2.64 μmol, 8.0 mg) = tag Nr. 2 (T₅)
	(CH ₂) ₉ -Cl ₅ (632.72 g/mol, 2.64 μmol, 8.4 mg) = tag Nr. 3 (T₆)
Step 3:	(CH ₂) ₁₀ -2,4,5-Cl ₃ (576.85 g/mol, 2.64 μmol, 7.6 mg) = tag Nr. 1 (T₇)
	(CH ₂) ₁₁ -2,4,6-Cl ₃ (590.88 g/mol, 2.64 μmol, 7.8 mg) = tag Nr. 2 (T₈)
	(CH ₂) ₁₁ -2,4,5-Cl ₃ (590.88 g/mol, 2.64 μmol, 7.8 mg) = tag Nr. 3 (T₉)

Figure 104: Tags and amount used for each encoding step

Step 1	M [g mol ⁻¹]	m [mg]	Tag	Code		
				T ₁	T ₂	T ₃
Fmoc-L-Asp(O ^t Bu)-OH	411.45	163	T ₃	0	0	1
Fmoc-D-Asp(O ^t Bu)-OH	411.45	163	T ₂	0	1	0
Fmoc-L-Ser(O ^t Bu)-OH	383.44	152	T ₂ + T ₃	0	1	1
Fmoc-D-Ser(O ^t Bu)-OH	383.44	152	T ₁	1	0	0
Fmoc-L-His(Trt)-OH	619.72	245	T ₁ + T ₃	1	0	1
Fmoc-D-His(Trt)-OH	619.72	245	T ₁ + T ₂	1	1	0
Fmoc-L-Tyr(O ^t Bu)-OH	459.54	182	T ₁ + T ₂ + T ₃	1	1	1
Step 2	M [g mol ⁻¹]	m [mg]	Tag	Code		
				T ₄	T ₅	T ₆
1) Fmoc-Aib-OH (Pro-Aib)	325.36	129	T ₆	0	0	1
2) Fmoc-L-Pro-OH (Pro-Aib)	337.37	134				
Fmoc-ε-Ahx-OH	353.40	140	T ₅	0	1	0
Fmoc-Cl (no motif)	258.70	102	T ₅ + T ₆	0	1	1
Fmoc-Gly-OH	297.31	118	T ₄	1	0	0
1) Fmoc-Gly-OH	297.31	118	T ₄ + T ₆	1	0	1
2) Fmoc-L-Pro-OH	337.37	134				
Fmoc-β-Alanin-OH	311.30	123	T ₄ + T ₅	1	1	0
Fmoc-rac-Achc-OH	365.00	145	T ₄ + T ₅ + T ₆	1	1	1
Step 3	M [g mol ⁻¹]	m [mg]	Tag	Code		
				T ₇	T ₈	T ₉
Fmoc-L-Asp(O ^t Bu)-OH	411.45	163	T ₉	0	0	1
Fmoc-D-Asp(O ^t Bu)-OH	411.45	163	T ₈	0	1	0
Fmoc-L-Ser(O ^t Bu)-OH	383.44	152	T ₈ + T ₉	0	1	1
Fmoc-D-Ser(O ^t Bu)-OH	383.44	152	T ₇	1	0	0
Fmoc-L-His(Trt)-OH	619.72	245	T ₇ + T ₉	1	0	1
Fmoc-D-His(Trt)-OH	619.72	245	T ₇ + T ₈	1	1	0
Fmoc-L-Tyr(O ^t Bu)-OH	459.54	182	T ₇ + T ₈ + T ₉	1	1	1

Table 14: Scheme of encoding library 1

Step 1	M (g/mol)	m (mg)	Tag	Code			
				T ₁	T ₂	T ₃	T ₄
Fmoc-L-Pro-OH	337.38	223	T ₁	1	0	0	0
Fmoc-D-Arg(Pbf)-OH	648.78	428	T ₂	0	1	0	0
Fmoc-L-Lys(Boc)-OH	468.55	309	T ₃	0	0	1	0
Fmoc-D-His(Trt)-OH	619.72	409	T ₄	0	0	0	1
Fmoc-L-Trp(Boc)-OH	526.59	348	T ₁ + T ₂	1	1	0	0
Fmoc-D-Asp(O ^t Bu)-OH	411.46	272	T ₁ + T ₃	1	0	1	0
Fmoc-L-Glu(O ^t Bu)-OH	443.50	293	T ₁ + T ₄	1	0	0	1
Fmoc-D-Asn(Trt)-OH	596.68	394	T ₂ + T ₃	0	1	1	0
Fmoc-L-Gln(Trt)-OH	610.71	403	T ₂ + T ₄	0	1	0	1
Fmoc-D-Ser(^t Bu)-OH	383.44	253	T ₃ + T ₄	0	0	1	1
Fmoc-L-Thr(^t Bu)-OH	397.47	262	T ₁ + T ₂ + T ₃	1	1	1	0
Fmoc-D-Tyr(^t Bu)-OH	459.54	303	T ₁ + T ₂ + T ₄	1	1	0	1
Fmoc-L-Phe-OH	387.44	256	T ₁ + T ₃ + T ₄	1	0	1	1
Fmoc-D-Val-OH	339.39	224	T ₂ + T ₃ + T ₄	0	1	1	1
Fmoc-L-Ala-OH.H ₂ O	329.35	217	T ₁ + T ₂ + T ₃ + T ₄	1	1	1	1

Step 2	M (g/mol)	m (mg)	Tag	Code			
				T ₁	T ₂	T ₃	T ₄
Fmoc-L-Pro-OH	337.38	222	T ₅	1	0	0	0
1) Fmoc-Aib-OH (Pro-Aib)	325.36	215	T ₆	0	1	0	0
2) Fmoc-L-Pro-OH	337.38	223					
Fmoc-Ahx	353.42	234	T ₇	0	0	1	0
1) Fmoc-Gly-OH (Pro-Gly)	297.31	196	T ₈	0	0	0	1
2) Fmoc-L-Pro-OH	337.36	222					
(1R,2R)-Fmoc-Achc-OH	365.43	241	T ₅ + T ₆	1	1	0	0
(1S,2S)-Fmoc-Achc-OH	365.43	241	T ₅ + T ₇	1	0	1	0
Fmoc-Cl (no motif)	258.7	171	T ₅ + T ₈	1	0	0	1
Fmoc-Gly-OH	297.31	196	T ₆ + T ₇	0	1	1	0
Fmoc-L-Leu-OH	353.42	233	T ₆ + T ₈	0	1	0	1
Fmoc-D-Leu-OH	353.42	233	T ₇ + T ₈	0	0	1	1
Fmoc-D-Phe-OH	387.44	256	T ₅ + T ₆ + T ₇	1	1	1	0
Fmoc-L-Phe-OH	387.44	256	T ₅ + T ₆ + T ₈	1	1	0	1

Fmoc-D-Val-OH	339.39	224	T ₅ + T ₇ + T ₈	1 0 1 1
Fmoc-L-Val-OH	339.39	224	T ₆ + T ₇ + T ₈	0 1 1 1
Fmoc-L-Ala-OH.H ₂ O	329.35	217	T ₅ + T ₆ + T ₇ + T ₈	1 1 1 1
Step 3	M (g/mol)	m (mg)	Tag	Code
				T₁ T₂ T₃ T₄
Fmoc-D-Pro-OH	337.38	223	T ₉	1 0 0 0
Fmoc-L-Arg(Pbf)-OH	648.78	428	T ₁₀	0 1 0 0
Fmoc-D-Lys(Boc)-OH	468.55	309	T ₁₁	0 0 1 0
Fmoc-L-His(Trt)-OH	619.72	409	T ₁₂	0 0 0 1
Fmoc-D-Trp(Boc)-OH	526.59	347	T ₉ + T ₁₀	1 1 0 0
Fmoc-L-Asp(O ^t Bu)-OH	411.46	272	T ₉ + T ₁₁	1 0 1 0
Fmoc-D-Glu(O ^t Bu)-OH	425.48	281	T ₉ + T ₁₂	1 0 0 1
Fmoc-L-Asn(Trt)-OH	596.68	394	T ₁₀ + T ₁₁	0 1 1 0
Fmoc-D-Gln(Trt)-OH	610.71	403	T ₁₀ + T ₁₂	0 1 0 1
Fmoc-L-Ser(^t Bu)-OH	383.44	253	T ₁₁ + T ₁₂	0 0 1 1
Fmoc-D-Thr(^t Bu)-OH	397.47	262	T ₉ + T ₁₀ + T ₁₁	1 1 1 0
Fmoc-L-Tyr(^t Bu)-OH	459.54	303	T ₉ + T ₁₀ + T ₁₂	1 1 0 1
Fmoc-D-Phe-OH	387.44	256	T ₉ + T ₁₁ + T ₁₂	1 0 1 1
Fmoc-L-Val-OH	339.39	224	T ₁₀ + T ₁₁ + T ₁₂	0 1 1 1
Fmoc-D-Ala-OH.H ₂ O	329.35	217	T ₉ + T ₁₀ + T ₁₁ + T ₁₂	1 1 1 1

Table 15: Scheme of encoding library 2

11.13 Combinatorial Screening Experiments (AgNPs)

Approximately 10 mg of the library were suspended in a solution of AgNO₃ (0.05 M, 660 μL), sonicated for 5 min and allowed to incubate for another 10 min. After washing with nanopure water (10 x 1 mL), the beads were incubated with a solution of sodium ascorbate (0.05 M, 660 μL, ~6 eq.) for 10 min before washing with nanopure water (10 x 1 mL).

Color	AA2	Linker	AA1	No. of analyzed beads bearing this sequence
Dark orange Red	D His	Pro-Aib	D Asp	1
	D His	Pro-Aib	L Asp	2
	L His	-	L Asp	1
	L His	Achc	D Asp	1
	D Asp	Ahx	D His	1
	D Asp	Achc	D His	1
	D Asp	-	L His	1
	D Asp	Pro-Gly	L His	1
	L Asp	Pro-Aib	L His	1
	L Asp	Achc	L His	1
	L Asp	Ahx	D His	1
	D His	-	D Ser	1
	L His	Achc	L Ser	1
	L Ser	Gly	L His	1
	L Ser	Ahx	D His	1
	L Ser	Achc	L His	1
	D Ser	Ahx	D His	1
	L His	Ahx	L Tyr	1
	L His	Achc	L Tyr	1
	L Tyr	Achc	D His	1
	L Tyr	Gly	D His	1
	L Tyr	Ahx	L His	1
	L Tyr	Achc	L Tyr	1
	D His	Pro-Gly	D His	1
	L His	-	D His	1
	D His	β -Ala	L His	1
	D His	Gly	L His	1
	D His	Pro-Aib	L His	1
	L His	Gly	D His	1
	L His	Gly	D His	1
L His	Achc	D His	1	
Light orange Yellow	L-Tyr	Achc	D-Ser	1
	L-Tyr	Ahx	D-Ser	1
	D Asp	Pro-Aib	D Asp	1
	D Asp	Pro-Gly	L Asp	1
	L Asp	β -Ala	D Asp	1
	L Asp	Pro-Gly	L Asp	1
	L Asp	β -Ala	L Asp	1
	L Asp	Gly	L Asp	1
	D Asp	Pro-Gly	L Ser	1
	L Asp	Ahx	D Ser	1
	D Ser	Pro-Aib	D Asp	1
	D Asp	Pro-Gly	D His	1
	D Asp	-	D His	1
	D His	Ahx	D Asp	1
	D Ser	-	D His	1
	D Ser	-	L His	1
	D His	-	L His	1
	L Tyr	-	D His	1

Table 16: Consensus peptide sequences of library 1 on differently coloured beads

The combinatorial screening assays were evaluated using a light microscope, a sample of beads from each colour category were isolated and the peptide sequences analyzed by EC-GC.

11.14 Combinatorial Screening Experiments (PtNPs)

Approximately 10 mg of library-beads were suspended in an aqueous solution of K_2PtCl_4 (0.05 M, 660 μ L), sonicated and allowed to incubate for 15 min. After washing with deionized water (10 x 1 mL), the beads were incubated with a solution of sodium borohydride (0.4 M, 660 μ L) for 6 h before washing with deionized water (10 x 1 mL). The combinatorial screening assay was evaluated using a light microscope, a sample of beads from each colour category were isolated and the peptide sequences analyzed by EC-GC.

XII.

ABBREVIATIONS

AcOH	Acetic acid
Ag	Silver
Ahx	6-Aminohexanoic acid
Aib	Aminoisobutyric acid
Alloc	Allyloxycarbonyl
Boc	<i>tert</i> -Butyloxycarbonyl
BSA	<i>N,O</i> -Bistrimethylsilylacetamide
CDCl₃	Deuterated Chloroform
CH₂Cl₂	Dichloromethane
d	Doublet
δ	Chemical shift (ppm)
DCC	<i>N,N'</i> -Dicyclohexylcarbodiimide
DIC	<i>N,N'</i> -Diisopropylcarbodiimide
DMF	<i>N,N</i> -Dimethylformamide
DMSO	Dimethylsulfoxide
ESIMS	Electrospray Ionisation Mass Spectrometry
eq	Equivalents
Et₃N	Triethylamine
Et₂O	Diethyl Ether
Fmoc	9-Fluorenylmethoxycarbonyl
GC	Gas Chromatography
HCTU	2-(6-Chloro-1-H-benzotriazole-1-yl)-1,1,3,3-tetramethyluronium hexafluorophosphate
HOBt	1-Hydroxybenzotriazole

<i>i</i>-Pr₂NEt	<i>N,N</i> -Diisopropylethylamine
<i>i</i>-Pr	Isopropyl
<i>J</i>	Scalar coupling constant (Hz)
λ	Wavelength (nm)
m	Multiplet
MeOH	Methanol
MHz	Megahertz
m/z	Mass to Charge Ratio
NMM	<i>N</i> -Methylmorpholine
NMR	Nuclear Magnetic Resonance
NP	Nanoparticle
PEG	Poly(ethylene) glycol
RT	Room temperature
s	Singlet (NMR)
^tBu	<i>tert</i> -Butyl
TFA	2,2,2-Trifluoroacetic acid
TIS	Triisopropylsilane
TNBS	2,4,6-Trinitrobenzenesulfonic acid
Trt	Trityl (Triphenylmethyl-)

XIII.

REFERENCES

1. Tünde Vig Slenters, PhD dissertation: *Novel silver containing antimicrobial coatings for implant materials: new applications of Ag(I) coordination networks*, **2009**, University of Basel.
2. a) C. Xue, Z. Li, C. A. Mirkin, *small* **2005**, *1*, 513 –516.; b) J. Song, J. Chen, C. M. Klapperich, V. Enga, C. R. Bertozzi, *J. Mater. Chem.*, **2004**, *14*, 2643–2648.
3. D. Bravo, O. Braissant, A. Solokhina, M. Clerc, A. U. Daniels, E. Verrecchia, P. Junier, *FEMS Microbiol. Ecol.*, **2011**, 1–9.
4. a) M. Kahm, G. Hasenbrink, H. L-Fraté, J. Ludwig, M. Kschischo, *J. Stat. Soft.*, **2010**, *33*, 1-21.; b) M. H. Zwietering, I. Jongenburger, F. M. Rombouts, K. V. Riet, *Appl. Environ. Microbiol.* **1990**, *56*, 1875-1881.
5. R. B. Merrifield, *J. Am. Chem. Soc.* **1963**, *85*, 2149.
6. T. Vojkovsky, *Pept. Res.* **1995**, *8*, 236.
7. Novabiochem Catalog **2004.**, W. S. Hancock, J. E. Battersby, D. R. K. Harding, *Analyt. Biochem.* **1975**, *69*, 497.
8. E. Kaiser, R. L. Colescot, C. D. Bossinge, P. I. Cook, *Analyt. Biochem.* **1970**, *34*, 595.
9. Kirsten Belser, PhD dissertation: *Peptid-Metall Wechselwirkungen-Anwendung selektiver Bindung zur Esterhydrolyse und Bildung von Silber-Nanopartikeln*, **2008**, University of Basel.

Curriculum Vitae

Birth 31 January 1976 in Mberengwa (Zimbabwe)
Nationality Zimbabwean
Marital Status Married
Children 2

Education, Qualifications and Research

10/2007 - 10/2011 *University of Basel (Switzerland)*
Doctor of Philosophy (PhD) in Chemistry
Supervisor, Professor Dr. Helma Wennemers

Research, Peptide Control of Noble-Metal Nanoparticle Generation and Stability

09/2006 - 09/2007 *University of Reading in Reading (Great Britain)*
Master of Science (MSc) in Chemical Research
Supervisor, Professor Laurence M. Harwood

Research, Use of Morpholinone Chemistry in the Synthesis of Chiral Amino Acids

10/2005 - 08/2006 *Sprachenzentrum, University of Basel and other language centres in Basel*
Learning German Language

08/2001 - 08/2005 *National University of Science and Technology in Bulawayo (Zimbabwe)*
Bachelor of Science (BSc) in Applied Chemistry

01/1999 - 12/2000 *Bulawayo Polytechnic College in Bulawayo (Zimbabwe)*
National Diploma in Applied Chemical Technology

1984 - 1997 *Mt Selinda High School in Mt Selinda (Zimbabwe)*
School Leaving Certificate

Awards

2002 - 2003 Best Overall Academic Achievement for the Bachelor of Science programme
1999 - 2001 Best Overall Academic Achievement in the Applied Chemical Technology Courses

Research Publications

- Peptide Sequence-Activity Relationships in the Controlled Generation of Stable Silver Nanoparticles in Different Sizes in Solution: Exceptional Antibacterial Activity (*In preparation*)
- Silver Nanoparticle Formation in Different Sizes Induced by Peptides Identified within Split-and-Mix Libraries; *Angew. Chem. Int. Ed.*, **2009**, 48, 3661, K. Belser, T. V. Slenters, **C. Pfumbidzai**, G. Upert, L. Mirolo, K. M. Fromm, H. Wennemers (*qualified as an important scientific paper*)

Invited Oral and Poster Research Presentations at Conferences

2011 Platform of the Swiss Academy of Sciences, Rigi-Workshop in Switzerland
2010 Swiss Chemical Society Fall Meeting, ETH Zürich in Switzerland
National Centre of Competence in Research, University of Basel in Switzerland
2009 Revolutionary Catalysis Meeting, University of Basel in Switzerland
Swiss Nano2009 Workshop on Nanoscience, University of Basel in Switzerland
Bachem Research Sponsors, University of Basel in Switzerland
Swiss Chemical Society Meeting, Ecole Polytechnique Fédérale de Lausanne in Switzerland
2008 Revolutionary Catalysis Meeting, University of Amsterdam in Netherlands

Revolutionary Catalysis Meeting, University of Cambridge in Great Britain

Work Experience

- 08/2003 - 07/2004 *Zimbabwe Pharmaceutical Company in Zimbabwe*
Internship
- 01/2001 - 07/2001 *Rusitu School in Chimanimani (Zimbabwe)*
Teacher of Chemistry and Mathematics
- 06/1999 - 12/1999 *Mutare Board and Paper Mills in Zimbabwe*
Internship
- 1998 *United Nations Organisation (UNO) in Kwekwe (Zimbabwe)*
Polling Assistant

Interests

Reading, Skiing and Hiking (with relatives and friends), Gardening